MULTI-OMICS, EPIGENOMICS AND COMPUTATIONAL ANALYSIS OF NEURODEGENERATIVE DISORDERS

EDITED BY: Manoj Kumar Jaiswal, Deepti Lall and Naveen Kumar Singhal

PUBLISHED IN: Frontiers in Neuroscience

frontiers Research Topics

frontiers

ISSN 1664-8714
ISBN 978-2-88976-691-8
DOI 10.3389/978-2-88976-691-8

About Frontiers

Frontiers is more than just an open-access publisher of scholarly articles: it is a pioneering approach to the world of academia, radically improving the way scholarly research is managed. The grand vision of Frontiers is a world where all people have an equal opportunity to seek, share and generate knowledge. Frontiers provides immediate and permanent online open access to all its publications, but this alone is not enough to realize our grand goals.

Frontiers Journal Series

The Frontiers Journal Series is a multi-tier and interdisciplinary set of open-access, online journals, promising a paradigm shift from the current review, selection and dissemination processes in academic publishing. All Frontiers journals are driven by researchers for researchers; therefore, they constitute a service to the scholarly community. At the same time, the Frontiers Journal Series operates on a revolutionary invention, the tiered publishing system, initially addressing specific communities of scholars, and gradually climbing up to broader public understanding, thus serving the interests of the lay society, too.

Dedication to Quality

Each Frontiers article is a landmark of the highest quality, thanks to genuinely collaborative interactions between authors and review editors, who include some of the world's best academicians. Research must be certified by peers before entering a stream of knowledge that may eventually reach the public - and shape society; therefore, Frontiers only applies the most rigorous and unbiased reviews.
Frontiers revolutionizes research publishing by freely delivering the most outstanding research, evaluated with no bias from both the academic and social point of view. By applying the most advanced information technologies, Frontiers is catapulting scholarly publishing into a new generation.

What are Frontiers Research Topics?

Frontiers Research Topics are very popular trademarks of the Frontiers Journals Series: they are collections of at least ten articles, all centered on a particular subject. With their unique mix of varied contributions from Original Research to Review Articles, Frontiers Research Topics unify the most influential researchers, the latest key findings and historical advances in a hot research area! Find out more on how to host your own Frontiers Research Topic or contribute to one as an author by contacting the Frontiers Editorial Office: frontiersin.org/about/contact

MULTI-OMICS, EPIGENOMICS AND COMPUTATIONAL ANALYSIS OF NEURODEGENERATIVE DISORDERS

Topic Editors:
Manoj Kumar Jaiswal, Icahn School of Medicine at Mount Sinai, United States
Deepti Lall, Cedars Sinai Medical Center, United States
Naveen Kumar Singhal, All India Institute of Medical Sciences, Rishikesh, India

Citation: Jaiswal, M. K., Lall, D., Singhal, N. K., eds. (2022). Multi-omics, Epigenomics and Computational Analysis of Neurodegenerative Disorders. Lausanne: Frontiers Media SA. doi: 10.3389/978-2-88976-691-8

Table of Contents

frontiers | Frontiers in Neuroscience

EDITORIAL
published: 06 July 2022
doi: 10.3389/fnins.2022.930425

Editorial: Multi-omics, Epigenomics, and Computational Analysis of Neurodegenerative Disorders

*Manoj Kumar Jaiswal**

Department of Psychiatry, Icahn School of Medicine at Mount Sinai, New York, NY, United States

Keywords: multi-omics, epigenomics, neurodegeneration, computation, machine learning

Editorial on the Research Topic

Multi-omics, Epigenomics, and Computational Analysis of Neurodegenerative Disorders

With the dawn of multi-omics technologies, integrated with computation and biostatistics, remarkable progress has been made in understanding the pathobiology of neurodegenerative diseases such as Amyotrophic Lateral Sclerosis (ALS), Frontotemporal Dementia (FTD), Alzheimer's disease (AD), Parkinson's Disease (PD), Aging, and others. Multi-omics approaches such as genomic/epigenomic, transcriptomic, proteomic, metabolomics, and miRNAomics, as well as genetic and functional perturbations have changed the experimental modeling of these diseases. For example, in ALS, genomic approaches such as genome wide association studies (GWASs) have led to the discovery of relatively few loci despite 52% heritability estimates (Zhang et al., 2022). However, these changes occur in <10% of ALS patients, and thus, there are likely to be many ALS risk genes yet to be discovered. Similarly, in FTD (Ferrari et al., 2014), AD (Bertram and Tanzi, 2009), PD (Kia et al., 2021), Aging (Walter et al., 2011), and Dementia (Moreno-Grau et al., 2019) GWAS has led to the identification of few candidate genes, novel loci and unique associations, with evidence of disease-associated regulatory changes. Brain region and cell-sub-type-specific (dys)functional multi-omics studies in neurodegenerative diseases, such as RNA-Seq, ChIP-Seq, ATAC-Seq, and Hi-C has fueled genetic discovery in a cell-type dependent manner. For this special Research Topic, we present a compendium of 10 articles, which offer a wide-ranging overview of the different multi-omics pathways and unravel the genomic and transcriptomic alterations in these diseases as well as endeavor to facilitate a better understanding of the mutational landscape of these disorders.

To enable new biomarker discovery in ALS, Dr. Gabriel and colleague examines the whole (unbiased) metabolomics data to study changes in spinal cord regions of two strains of mutant SOD1 mice with fast (129S) or slow (C57BL) disease progression associated with SOD1-G93A ALS transgenic mouse models (Valbuena et al.). The authors show that the C57BL have a more favorable bioenergetic and metabolite profile, including neurotransmitter amino acid metabolism and antioxidant homoeostasis, which were determined to be greatly affected in the thoracic segment. Changes in energy and lipid metabolism were mostly apparent in the lumbar spinal cord and these changes were mainly attributed to background differences between the two strains. Dr. Masashi Aoki's group presents insights into the complexity of multi-omics alteration of motor neurons (MNs) axonal defects in ALS. The authors review the evidence coming from genetic subtypes of ALS and further discuss the potential disease pathways leading to axonal defects (Suzuki et al.). The study by Thompson et al. examines the proteome of ALS and PD patients compared to controls using weighted gene co-expression network analysis (WGCNA) to identify pathways and ontological groupings of interest that differentiate patient groups with particular emphasis

OPEN ACCESS

Edited and reviewed by:
Iliya Lefterov,
University of Pittsburgh, United States

***Correspondence:**
Manoj Kumar Jaiswal
jaiswal.manoj@gmail.com

Specialty section:
This article was submitted to Neurodegeneration, a section of the journal Frontiers in Neuroscience

Received: *27 April 2022*
Accepted: *31 May 2022*
Published: *06 July 2022*

Citation:
Jaiswal MK (2022) Editorial: Multi-omics, Epigenomics, and Computational Analysis of Neurodegenerative Disorders. Front. Neurosci. 16:930425. doi: 10.3389/fnins.2022.930425

on ALS patients. They identify nine co-expression modules, approximately half of which cannot be annotated using Gene Ontology (GO). Among the characterized modules, they found ones associated with intracellular compartments and RNA biology (module 1), the immune system (module 2), which is hypothesized to reflect blood contamination, and axon outgrowth (module 4). They perform paired differential correlation analyses as a more focused correlation approach and find that 11 co-expression modules are altered in ALS, with enrichment in modules 1 and 3, although these modules were without GO enrichment.

In a study on AD, Dr. Andres Kriete's group applied a novel combination of computational strategies to dorsolateral prefrontal cortex RNA-Seq samples from 503 cognitively well-characterized human subjects from the Religious Orders Study/Memory and Aging Project (ROSMAP) and identify 26 distinct modules, encapsulating 4,429 genes (Malamon and Kriete). More specifically, authors organized modules using widely used WGCNA approach and find several gene co-expression modules that become less co-expressed in AD (which they define as "topological erosion"). One of these modules is enriched in genes involved in immune and synaptic system processes. They also report a loss of modular gene expression associated with cognitive decline. Fewer genes remained within statistically preserved modules with the transition from normal cognition through MCI to AD. In addition, they compare SNPs with gene expression from the same donors using expression quantitative trait loci (eQTL) analysis and find that the most significant eQTLs are from the Microtubule Associated Protein Tau (MAPT) locus and the Human Leukocyte Antigen (HLA) complex. Dr. Dhanwani's group carried out a comprehensive study focused on deciphering the role of neuronal antigen specific T cell responses in AD patients and compare these patients with age-matched healthy controls (Dhanwani et al.). The authors have carefully measured T cell responses to several potential antigens and found no differences in the antigen-specific T cell (ASTC) reactivity tested for antigens, relative frequency of major PBMCs subsets, and the expression of genes between AD and healthy controls. Li et al. leveraged several bulk gene expression data sets to identify the association between autophagy-related genes and clinical symptoms of AD using bioinformatics approaches. The study identified 80 autophagy-related genes with differential expression in the brain tissue of patients with AD compared to healthy age-matched control. The expression of a cluster of autophagy-related genes ($n = 16$) correlated with AD clinical symptoms. The authors relate seven autophagy-related proteins that are down-regulated in the brain of AD patients, such as MEF2A and CUX1, with the progression of symptoms of AD patients and focused on the study of MEF2A in detail. A subset of seven autophagy genes were selected as they overlapped two analyzed datasets, and the MEF2A transcription factor was identified as a potential regulator of the expression of the seven genes. MEF2A levels were decreased in AD cases compared to control brain homogenate. Lv et al. describe changes in m6A modifications in the hippocampus of mice harboring a loss-of-function mutation in the gene coding for TYRO Protein Kinase Binding Protein (TYROBP), and serve as a mouse model for Nasu-Hakola disease (NHD). The authors have reported higher levels of total tau, phosphorylated tau, and amyloid β, all of which are correlated with AD and NHD phenotypes. They observe striking reductions in all three RNA methytransferases. Key regulators of the m6A writer machinery (METTL3, METTL14, and WTAP) were also downregulated in terms of relative mRNA and protein levels, contrasting with AD models, while expression of the demethylases FTO and ALKBH5 were largely unchanged.

Tian Tian's group carried out a comprehensive review discussing advances in metabolomics approaches in PD (Zhang et al.). The authors highlight the genetic mutations and mitochondrial dysfunction that occur in patients with mutations and sporadic abnormalities. The authors also described synuclein and parkin gene mutations and functions, as well as concisely recap new metabolomic discoveries in both familial and sporadic PD. Together, this review provides a way forward to advance our current understanding of metabolomics of PD.

David Alan Bennett's group studied four different epigenetic clocks, as calculated on CD4+ cells derived from blood, postmortem DLPFC and PCC samples from participants in the ROSMAP aging study (Grodstein et al.). The authors use Pearson analysis to compare how well four established epigenetic clocks—Horvath, Hannum, PhenoAge, and GrimAge—correlate with chronologic age in ROSMAP subjects with matched CD4+ blood cells from longitudinal blood draws (∼7.5 year interval) and matched DLPFC. The main results reported were that DNAm age estimated from brain samples was consistently lower than age at death, whereas the correlation between DNAm age and chronological age was reasonable. Mean clock age was consistently lower than chronologic age in the brain samples. GrimAge correlated best with $r = 0.92$. Epigenetic age modestly correlated with age in matched blood and brain samples (again GrimAge performed best at $r = 0.76$). Finally, in the oldest-old subjects, these correlations were much weaker.

We recognize that a single collection of articles cannot comprehensively cover the entirety of the extremely broad range of topics that characterize such complex and multifactorial conditions such as neurodegeneration, nor the entire gamut of multiomics modalities. The topics addressed, however, help develop a clear idea, not only of what has been accomplished to date by previous studies, but also of the unmet needs future research should focus on. We are confident that the papers assembled in this Research

Abbreviations: ALS, amyotrophic lateral sclerosis; AD, Alzheimer's disease; ASTC, antigen-specific T cell; PD, Parkinson's disease; FTD, frontotemporal dementia; DEGs, differentially expressed genes; EHR, electronic health records; GO, gene ontology; GWAS, genome-wide association studies; HLA, human leukocyte antigen; KEGG, Kyoto encyclopedia of genes and genomes; eQTL, expression quantitative trait loci; MAPT, microtubule associated protein tau; MNs, motor neurons; NHD, Nasu-Hakola disease; PCA, principal components analysis; ROSMAP, religious orders study/memory and aging project; SOD1, super oxide dismutase 1; TYROBP, TYRO protein kinase binding protein; WGCNA, weighted gene co-expression network analysis; WGS, whole genome sequencing.

Topic will prove useful in spurring and stimulating the future progress.

AUTHOR CONTRIBUTIONS

MKJ conceived, prepared, edited, and approved the article for publication. All contents of this editorial have been solely carried out by MKJ.

ACKNOWLEDGMENTS

The author would like to thank Drs. Pasha Apontes, Ananta Paine, Kenjiro Seki, and his lab colleagues for their comments on the manuscript. The author acknowledges the contributions of all the participating authors, reviewers, and editors for this Research Topic. The author would like to thank Naveen Kumar Singhal and Deepti Lall for their contribution to the Research Topic.

REFERENCES

Bertram, L., and Tanzi, R. E. (2009). Genome-wide association studies in Alzheimer's disease. *Hum. Mol. Genet.* 18, R137–R145. doi: 10.1093/hmg/ddp406

Ferrari, R., Hernandez, D. G., Nalls, M. A., Rohrer, J. D., Ramasamy, A., Kwok, J. B., et al. (2014). Frontotemporal dementia and its subtypes: a genome-wide association study. *Lancet Neurol.* 13, 686–699. doi: 10.1016/S1474-4422(14)70065-1

Kia, D. A., Zhang, D., Guelfi, S., Manzoni, C., Hubbard, L., Reynolds, R. H., et al. (2021). Identification of candidate parkinson disease genes by integrating genome-wide association study, expression, and epigenetic data sets. *JAMA Neurol.* 78, 464–472. doi: 10.1001/jamaneurol.2020.525

Moreno-Grau, S., de Rojas, I., Hernández, I., Quintela, I., Montrreal, L., Alegret, M., et al. (2019). Genome-wide association analysis of dementia and its clinical endophenotypes reveal novel loci associated with Alzheimer's disease and three causality networks: the GR@ACE project. *Alzheimer's Dement.* 15, 1333–1347. doi: 10.1016/j.jalz.2019.06.4950

Walter, S., Atzmon, G., Demerath, E. W., Garcia, M. E., Kaplan, R. C., Kumari, M., et al. (2011). A genome-wide association study of aging. *Neurobiol. Aging* 32, 2109.e2115–2128. doi: 10.1016/j.neurobiolaging.2011.05.026

Zhang, S., Cooper-Knock, J., Weimer, A. K., Shi, M., Moll, T., Marshall, J. N. G., et al. (2022). Genome-wide identification of the genetic basis of amyotrophic lateral sclerosis. *Neuron* 110, 992–1008.e11. doi: 10.1016/j.neuron.2021.12.019

Author Disclaimer: The views expressed in this article are those of the author and do not reflect the official policy or position of the Icahn School of Medicine at Mount Sinai.

Conflict of Interest: The author declares that the research was conducted in the absence of any commercial or financial relationships that could be construed as a potential conflict of interest.

Publisher's Note: All claims expressed in this article are solely those of the authors and do not necessarily represent those of their affiliated organizations, or those of the publisher, the editors and the reviewers. Any product that may be evaluated in this article, or claim that may be made by its manufacturer, is not guaranteed or endorsed by the publisher.

frontiers in Neuroscience

ORIGINAL RESEARCH
published: 10 December 2019
doi: 10.3389/fnins.2019.01276

Spinal Cord Metabolic Signatures in Models of Fast- and Slow-Progressing SOD1^{G93A} Amyotrophic Lateral Sclerosis

Gabriel N. Valbuena[1], Lavinia Cantoni[2], Massimo Tortarolo[3], Caterina Bendotti[3] and Hector C. Keun[1]**

[1] Department of Surgery and Cancer, Imperial College London, London, United Kingdom, [2] Department of Molecular Biochemistry and Pharmacology, Istituto di Ricerche Farmacologiche Mario Negri IRCCS, Milan, Italy, [3] Department of Neuroscience, Istituto di Ricerche Farmacologiche Mario Negri IRCCS, Milan, Italy

OPEN ACCESS

Edited by:
Manoj Kumar Jaiswal, Icahn School of Medicine at Mount Sinai, United States

Reviewed by:
Cassie S. Mitchell, Georgia Institute of Technology, United States
Paul Roy Heath, University of Sheffield, United Kingdom
Bradley J. Turner, Florey Institute of Neuroscience and Mental Health, University of Melbourne, Australia
Gabriela Pintar De Oliveira, Paulista University, Brazil

***Correspondence:**
Caterina Bendotti
caterina.bendotti@marionegri.it
Hector C. Keun
h.keun@imperial.ac.uk

Specialty section:
This article was submitted to Neurodegeneration, a section of the journal Frontiers in Neuroscience

Received: *22 July 2019*
Accepted: *11 November 2019*
Published: *10 December 2019*

Citation:
Valbuena GN, Cantoni L, Tortarolo M, Bendotti C and Keun HC (2019) Spinal Cord Metabolic Signatures in Models of Fast- and Slow-Progressing SOD1^{G93A} Amyotrophic Lateral Sclerosis. Front. Neurosci. 13:1276. doi: 10.3389/fnins.2019.01276

The rate of disease progression in amyotrophic lateral sclerosis (ALS) is highly variable, even between patients with the same genetic mutations. Metabolic alterations may affect disease course variability in ALS patients, but challenges in identifying the preclinical and early phases of the disease limit our understanding of molecular mechanisms underlying differences in the rate of disease progression. We examined effects of SOD1^{G93A} on thoracic and lumbar spinal cord metabolites in two mouse ALS models with different rates of disease progression: the transgenic SOD1^{G93A}-C57BL/6JOlaHsd (C57-G93A, slow progression) and transgenic SOD1^{G93A}-129SvHsd (129S-G93A, fast progression) strains. Samples from three timepoints (presymptomatic, disease onset, and late stage disease) were analyzed using Gas Chromatography-Mass Spectrometry metabolomics. Tissue metabolome differences in the lumbar spinal cord were driven primarily by mouse genetic background, although larger responses were observed in metabolic trajectories after the onset of symptoms. The significantly affected lumbar spinal cord metabolites were involved in energy and lipid metabolism. In the thoracic spinal cord, metabolic differences related to genetic background, background-SOD1 genotype interactions, and longitudinal SOD1^{G93A} effects. The largest responses in thoracic spinal cord metabolic trajectories related to SOD1^{G93A} effects before onset of visible symptoms. More metabolites were significantly affected in the thoracic segment, which were involved in energy homeostasis, neurotransmitter synthesis and utilization, and the oxidative stress response. We find evidence that initial metabolic alterations in SOD1^{G93A} mice confer disadvantages for maintaining neuronal viability under ALS-related stressors, with slow-progressing C57-G93A mice potentially having more favorable spinal cord bioenergetic profiles than 129S-G93A. These genetic

background-associated metabolic differences together with the different early metabolic responses underscore the need to better characterize the impact of germline genetic variation on cellular responses to ALS gene mutations both before and after the onset of symptoms in order to understand their impact on disease development.

Keywords: amyotrophic lateral sclerosis (ALS), SOD1^{G93A} ALS mouse model, metabolism, metabolomics, spinal cord, oxidative stress, TCA cycle, energy metabolism

INTRODUCTION

Amyotrophic lateral sclerosis (ALS) is a rare, fatal neurodegenerative disease characterized by a progressive loss of motor neurons in the spinal cord, brainstem and cerebral cortex. The majority of ALS cases are classified as sporadic (sALS, about 90%) while the remaining 10% are familial (fALS), resulting from inherited mutations in more than 20 genes (Chia et al., 2018). However, we are currently unable to distinguish between the two based on clinical presentation and using existing technologies.

The clinical presentation and course of ALS is markedly heterogeneous. Most ALS patients are only highlighted as probable cases after some aspect of motor function has already been compromised, and their condition would have already deteriorated significantly by the time these diagnoses are confirmed. The rate of disease progression is also highly variable among different patients (Chió et al., 2011; Pupillo et al., 2014; Fournier and Glass, 2015) even between those with the same genetic familial form (Regal et al., 2006). A combination of genetic and environmental or exogenous modifying factors are believed to underlie the variability in disease progression. While there are a number of accurate machine learning models of ALS progression proposed that include rates of decline in functional measures (Kuffner et al., 2015; Westeneng et al., 2018), there are currently no standardized biomarkers or diagnostic protocols at diagnosis to predict how rapidly patients are likely to deteriorate. Together, the inability to identify individuals who will go on to develop ALS ahead of the visible onset of symptoms and the variability of the disease course complicate efforts to study the early stages of the disease in humans, underscoring the need to use animal models to investigate pathogenic mechanisms of the disease.

The transgenic SOD1^{G93A} mouse, expressing ∼20 copies of human SOD1 with the G93A mutation, was developed shortly after SOD1 mutations were first linked to ALS (Gurney et al., 1994). It is currently still the model that best recapitulates several core clinical and neuropathological features of the disease. These mice invariably show progressive hind limb tremor and weakness, locomotor deficits, and paralysis followed by premature death (Bendotti and Carrì, 2004). In these models, extensive motor neuron death in the ventral horn is observed, along with the loss of myelinated axons in the ventral motor roots (Leitner et al., 2009). The mice present with progressive weakness in the hind limb leading to paralysis and death, almost perfectly replicating the disease process in patients (Gurney et al., 1994; Ripps et al., 1995; Wong et al., 1995). These models have been crucial in our understanding of the underlying pathophysiology of ALS (Bento-Abreu et al., 2010), identifying mechanisms linked to motor neuron death such as mitochondrial dysfunction, oxidative stress, protein aggregation, neuroinflammation, and axonal transport defects. Several preclinical trials have been performed in this mouse model, with some interventions successfully delaying the disease course (Carrì et al., 2006; Turner and Talbot, 2008; Mancuso and Navarro, 2015). Unfortunately, these have not led to successful clinical trials in ALS patients (Benatar, 2007; Mitsumoto et al., 2014).

The unpredictable severity of the disease in patients is a key factor in the many failed clinical trials in ALS. This has made it difficult to decipher pathogenesis and to develop effective therapeutic strategies. There is growing evidence indicating that disease severity in humans may be influenced by their genetic background, as seen in mutant SOD1 mice altering the cellular response to mutant SOD1 in a manner that either ameliorates or exacerbates the disease phenotype (Heiman-Patterson et al., 2011). Discovering the molecular mechanisms underlying the variability in the ALS progression may improve our understanding of modifiers of disease development.

In this study, we examined the effects of SOD1^{G93A} on the C57BL/6JOlaHsd (C57) and the 129SvHsd (129S) murine genetic backgrounds, i.e., in the C57-G93A and 129S-G93A strains, two ALS models with major clinical differences as previously described (Pizzasegola et al., 2009). These two transgenic strains have the same copy number of the human mutant SOD1 transgene, contain the same mutation, and express the same amount of mutant SOD1 protein in the spinal cord. However, the transgenic 129S-G93A mice exhibit a much faster rate of disease progression, with mean survival of 129 ± 5 days, compared to the transgenic C57-G93A mice, which have a mean survival of 180 ± 16 days (Pizzasegola et al., 2009). Transcriptome analysis of laser capture microdissected motor neurons from the spinal cord of each line has revealed a marked down regulation at disease onset of genes involved in mitochondrial function, protein degradation, and axonal transport in the fast-progressing transgenic 129S mice (Nardo et al., 2013). The slow-progressing transgenic C57-G93A mice, on the other hand, exhibited an upregulation of genes involved in the regulation of the inflammatory and immune response, supporting a role for genetic modifiers of the disease in determining the severity of disease progression.

Metabolic alterations have been identified as potential factors affecting the variability of the disease course in both ALS patients (Dupuis et al., 2011) and in the fast- and slow-progressing ALS mouse models (Pfohl et al., 2015; Nardo et al., 2016). To verify this hypothesis and identify potential pathways associated with disease progression in SOD1^{G93A} mice, we used Gas

Chromatography-Mass Spectrometry (GC-MS) metabolomics to study metabolic changes in the spinal cord, the key affected tissue in ALS. We studied the slow- and the fast-progressing SOD1^{G93A} ALS mouse models, analyzing samples at three time points: before the appearance of visible symptoms (presymptomatic), at disease onset and at late stage of the disease. We aimed to examine how the metabolic response in the spinal cord evolves over the natural history of the disease, as well as to identify variations in metabolic responses to the mutant SOD1^{G93A} that may direct the two transgenic strains to lead different disease courses.

RESULTS

Principal Component Trajectories of the Thoracic and Lumbar Spinal Cords Metabolomes in the Slow- and Fast-Progressing SOD1^{G93A} Mice

To investigate the dynamic variation in systematic metabolic responses to the mutant SOD1^{G93A}-mediated disease process in the slow- and fast-progressing transgenic mouse strains, the metabolome was measured in the primary affected tissue in ALS, the spinal cord. We examined two spinal cord segments: the lumbar segment (which controls the hindlimbs and is affected earlier in disease) and the thoracic segment (which controls the axial muscles and is affected later in disease progression).

We examined multivariate patterns of metabolite variation and their relationship to disease progression in the spinal cord tissue metabolome by performing a PCA trajectory analysis. For each segment, we performed a principal component analysis (PCA) on the tissue metabolomes from all time points using $\log_{10}$-transformed, mean-centered and UV-scaled data. The principal component analysis describes the main patterns of variation in the metabolome data by calculating a series of principal components (PCs, linear combinations of the original descriptors – in this case the metabolite levels measured) where each PC is orthogonal to each other, allowing systematic variation in the highly multivariate metabolomic data to be summarized in PCs that describe related changes (Wold et al., 1987). The scores of the PCs were then examined to identify the presence of any intrinsic class-related patterns in the data. To visualize the trajectory of the multivariate patterns represented by the PCs over the stages of disease progression studied here, the scores of the principal components examined were averaged for each group of mice at each time point and plotted.

We looked at metabolic trajectories in the original principal components space (examining the scores as calculated in the principal components analysis), to allow for the examination of contributions of genetic background and SOD1 genotype differences to disease-related patterns in the temporal metabolic response. We also compared trajectory geometries between the different mouse genetic backgrounds and SOD1 genotypes by looking at aligned trajectories, where trajectories for all groups are shown to originate from the same starting point (by centering the mean scores of the pre-symptomatic time-points of each group to the origin). Examining the geometry of metabolic trajectories allows us to consider how similar the metabolic responses are between conditions, independent of inherent differences in the initial metabolic state (Keun et al., 2004).

The scale of trajectories were not adjusted for geometric comparisons, as no scalar enlargement or shrinkage of trajectories was observed between mouse backgrounds. This suggests that the overall magnitude of metabolic responses from mutant SOD1^{G93A} and over time are comparable between backgrounds, and that the difference lies more in the directionality of the metabolic response.

An analysis of variance of the linear model relating principal component analysis scores to the three experimental factors SOD1 genotype, background, and disease stage as well as their interactions was performed to determine the percentage of variance explained by each factor in the scores of each principal component. This indicated that variation in the first principal component was dominated by the linear model residuals, indicating that variation in PC1 is not being driven or strongly influenced by our experimental factors. Only small contributions from any of the other experimental factors were seen in PC1 (**Supplementary Figure S1**). As such, we focused the search for trends in metabolic trajectories in the subsequent principal components.

In the lumbar spinal cord, there were pronounced differences in the metabolic profile between the two genetic backgrounds at all time points, with a clear separation between samples from the C57 and 129S mice along the PC2 axis (**Figure 1A**). The loadings show that the top metabolites contributing to PC2 scores are involved in alanine and aspartate metabolism, tyrosine and phenylalanine metabolism, and the malate-aspartate shuttle (**Supplementary Figure S2A**).

Trajectories for the SOD1^{G93A} mice of both backgrounds progressed toward the negative PC3 axis, ending at a comparable level at late stage. The NTG mice, on the other hand, traversed a much more limited distance over the three time points. This difference indicates the presence of a progressive metabolic response to expression of the mutant SOD1^{G93A} protein in the transgenic mice. The metabolites identified in the loadings to have the largest contributions to these effects in PC3 (**Supplementary Figure S2B**) include metabolites involved in central carbon metabolism, alanine, aspartate and glutamine metabolism, and branched chain amino acids.

When we examined the geometry of lumbar spinal cord metabolic trajectories, there were differing responses in the mice with C57 and 129S backgrounds (**Figure 1B**). In the C57 mice, the metabolic trajectories of the NTG and SOD1^{G93A} mice appear to traverse similar directions from the presymptomatic stage to onset, but diverge from each other leading into the late stage. In the 129S background, however, the NTG and SOD1^{G93A} mice exhibited opposing directions of response from the presymptomatic stage to onset.

The largest distance traversed on PC3 was from onset to late stage in both SOD1^{G93A} mice, with metabolic profiles at onset being comparable to their NTG counterparts. This suggests that there are no substantial metabolic changes in the lumbar spinal cord due to the effects of mutant SOD1 expression, and that metabolic responses in this tissue primarily occur in parallel to

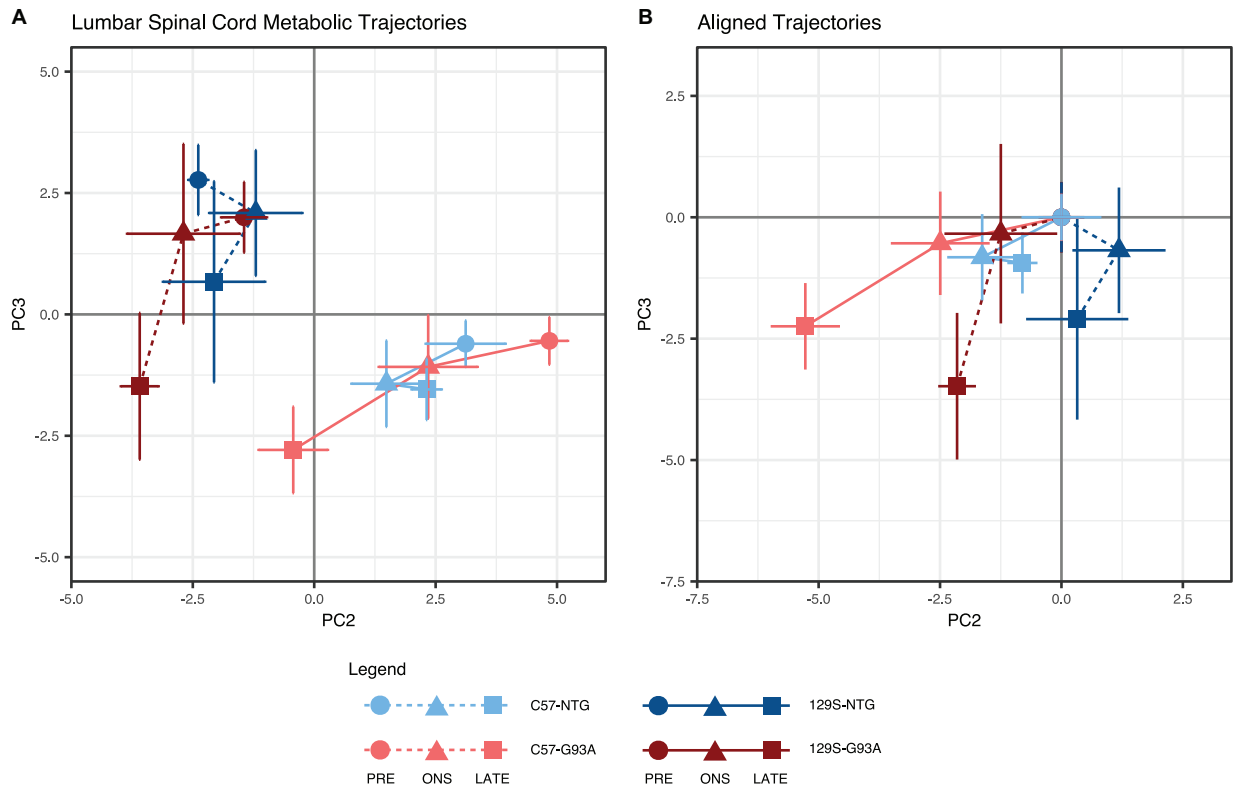

FIGURE 1 | Lumbar spinal cord metabolic trajectories. Figure shows **(A)** metabolic trajectories from a principal components analysis of the lumbar spinal cord metabolome, and **(B)** aligned trajectories, where metabolic trajectories for each mouse background-SOD1 genotype combination are centered to their respective presymptomatic time points. Lumbar spinal cord metabolomes from non-transgenic (NTG) and transgenic human mutant $SOD1^{G93A}$-expressing mice (G93A) in either the slower-progressing C57 background or the faster-progressing 129S background were measured at the presymptomatic stage (PRE), at disease onset (ONS), and at late stage (LATE). We examined the second (PC2) and third (PC3) principal components, which capture variation in the experimental factors being studied (percent contribution to variation of the experimental factors to each principal component are shown in **Supplementary Figure S1A**). The principal component scores for each group are shown as mean ± s.e.m. (n = 5 mice for each group per time point) for each time point.

loss of motor function. Therefore, it is not clear whether they are cause or consequence of the disease, as they may reflect the metabolic state during large-scale motor neuron death. Motor neuron loss is comparable in C57-G93A and 129S-G93A mice (Marino et al., 2015).

In the thoracic spinal cord, we looked at trajectories in the PC2-PC4 space, where the differences between strains are not as pronounced in the NTG mice. A strong effect from mouse background was seen in PC3 (**Supplementary Figure S1B**), with a large positive-negative separation between backgrounds. Metabolic trajectory effects outside of those driven by mouse background were investigated by looking at PC4, which accounts for an almost equivalent proportion of variation in the data (11%) as PC3 (11.7%, **Supplementary Figure S1B**).

Here, the metabolic trajectories for the NTG mice of both backgrounds were clustered around one quadrant of the PCA scores plot (**Figure 2A**). The $SOD1^{G93A}$ mice had similar metabolic profiles to their NTG counterparts at the presymptomatic stage, but traversed away significantly from the NTG space at onset and late stage. Unlike in the lumbar spinal cord, the geometries of metabolic trajectories are much more similar in the thoracic spinal cord (**Figure 2B**). The metabolic trajectories of NTG mice are poorly defined and narrowly localized, while the $SOD1^{G93A}$ mice have well-defined coincident trajectories away from the presymptomatic stage to onset, with divergence from onset to late stage.

The similarity of geometries suggests that the mode of response to $SOD1^{G93A}$ in the thoracic spinal cord is comparable between the two mouse backgrounds. However, both the metabolic profiles and trajectories for the fast progressing 129S-G93A mice are shifted in the same direction as the disease-associated metabolic response. This suggests that in the thoracic spinal cord, the metabolic response to mutant SOD1 is the same, but that the initial metabolic state of the 129S-G93A mice are closer to that of the late disease state. Unlike the lumbar spinal cord, we observe a larger response in the thoracic spinal cord metabolic trajectories of both $SOD1^{G93A}$ mice from the presymptomatic stage to onset, suggesting the presence of early metabolic responses (largely from PC2) that are mobilized in the tissue ahead of the presentation of visible symptoms. From the loadings, the main metabolites contributing to effects in PC2 (**Supplementary Figure S3B**), were amino acid metabolites and metabolites involved in ascorbate metabolism and carnitine synthesis.

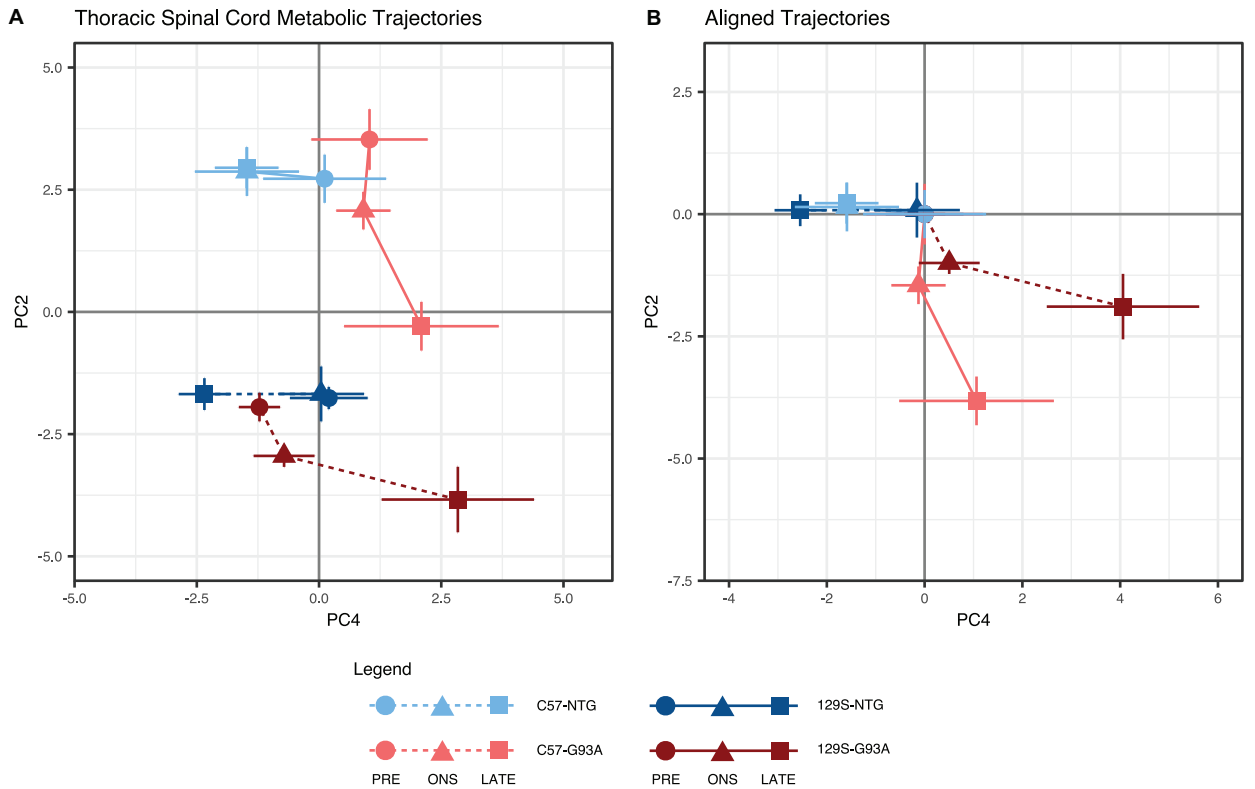

FIGURE 2 | Thoracic spinal cord metabolic trajectories. Figure shows **(A)** metabolic trajectories from a principal components analysis of the thoracic spinal cord metabolome, and **(B)** aligned trajectories, where metabolic trajectories for each mouse background-SOD1 genotype combination are centered to their respective presymptomatic time points. Thoracic spinal cord metabolomes from non-transgenic (NTG) and transgenic human mutant $SOD1^{G93A}$-expressing mice (G93A) in either the slower-progressing C57 background or the faster-progressing 129S background were measured at the presymptomatic stage (PRE), at disease onset (ONS), and at late stage (LATE). We examined the second (PC2) and fourth (PC4) principal components, which capture variation in the experimental factors being studied (percent contribution to variation of the experimental factors to each principal component are shown in **Supplementary Figure S1B**). The principal component scores for each group are shown as mean ± s.e.m. (n = 5 for each group per time point) for each time point.

Metabolic profile separation in the PC4 axis appears to be driven largely by SOD1 genotype, with NTG mice clustering toward the negative PC4 axis and mutant $SOD1^{G93A}$ mice clustered toward the positive PC4 axis (**Figure 2A**). PC4 loadings indicate that the top contributors to variation in this component are neurotransmitters and neurotransmitter metabolites (**Supplementary Figure S3A**). We observe a distinctive disease response for the fast-progressing 129S-G93A mice compared to C57-G93A in terms of effects in this set of metabolites based on scores in PC4.

Effects on Individual Metabolites in the Lumbar Spinal Cord

To evaluate effects on individual metabolites, we used a linear model incorporating effects from the three experimental factors: (1) SOD1 genotype, (2) mouse background, and (3) disease stage, as well as their two-way and three-way interaction effects (see section Materials and Methods).

The largest percent contributions to variance in the metabolites significantly affected in the lumbar spinal cord were effects from mouse background, consistent with the clear clustering by mouse background observed in the metabolic trajectories (**Figure 3A**). There were significant effects from mouse background in 6 metabolites: glyceric acid, 3-hydroxy-3-methylglutaric acid, O-phosphoethanolamine, alpha-ketoglutarate, pantothenic acid, and cholesterol (**Figure 3A**). Significant effects for disease stage were also observed for alpha-ketoglutarate, pantothenic acid, and cholesterol, as well as a significant effect for the interaction between background and disease stage for cholesterol. The only significant effect relating to SOD1 genotype in the lumbar spinal cord was in the interaction between SOD1 genotype and disease stage for fumarate.

The significantly affected metabolites in the lumbar spinal cord are involved in energy and lipid metabolism, with acetyl-CoA as a common node. Pantothenic acid is a key precursor in the synthesis of coenzyme A (CoA). Mitochondrial acetyl-CoA feeds carbon inputs from glycolysis into the TCA cycle, where we find significant effects in alpha-ketoglutarate and fumarate. Cytosolic acetyl-CoA is the ultimate precursor of fatty acids. It is therefore important in lipid metabolism, and there were significant effects in several intermediates: glyceric acid, a metabolite of the glycerol backbone of lipids, O-phosphoethanolamine, which forms the headgroup

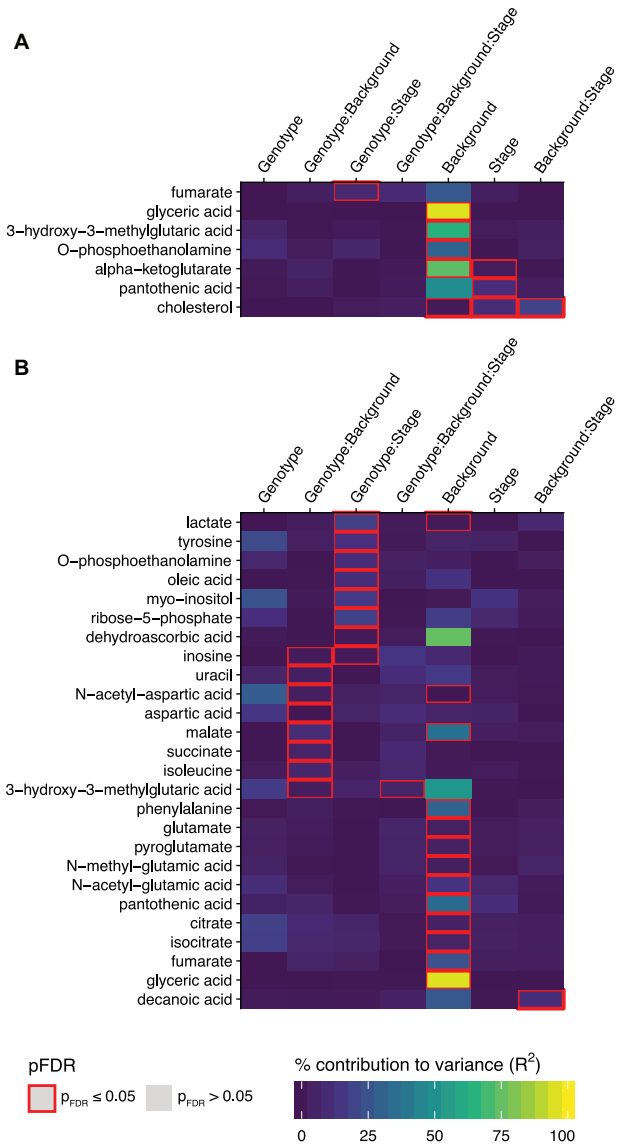

FIGURE 3 | Metabolites with significant associations to SOD1 genotype, mouse background, disease stage, or their two-way and three way interaction effects in the linear model analysis. The percent contribution to variance (R^2) for metabolites with significant associations to any of the three experimental factors SOD1 genotype, mouse background, and disease stage, or their two-way and three-way interaction effects in the linear model analysis (where $p_{FDR} \leq 0.05$) are shown in heatmaps for **(A)** the lumbar spinal cord and **(B)** the thoracic spinal cord. Effects where $p \leq 0.05$ after FDR multiple testing correction are outlined in red ($n = 5$ mice per group for each timepoint).

of PE-lipids, and cholesterol. 3-hydroxy-3-methylglutaric acid is produced from the degradation of leucine to 3-hydroxy-3-methylglutaryl-CoA (HMG-CoA), which can be cleaved into acetoacetate and acetyl-CoA. HMG-CoA is also involved in the synthesis of steroids such as cholesterol, due to its role as precursor in mevalonate synthesis.

There were lower lumbar spinal cord levels of pantothenic acid (**Figure 4A**, $p = 3.22 \times 10^{-9}$, FDR $< 5\%$, t-test comparing levels in C57 with 129S mice), alpha-ketoglutarate (**Figure 4E**, $p = 5.11 \times 10^{-15}$, FDR $< 5\%$) and fumarate (**Figure 4D**, $p = 3.09 \times 10^{-5}$, FDR $< 5\%$) in the 129S mice compared to the C57 mice. This may indicate less efficient TCA cycle activity and reduced CoA biosynthesis in mice with the 129S background. Levels of 3-hydroxy-3-methylglutaric acid in the 129S strain were higher than in the C57 strain (**Figure 4F**, $p = 9.23 \times 10^{-13}$, FDR $< 5\%$), suggesting increased degradation of leucine as an energy compensation mechanism. The levels of O-phosphoethanolamine (**Figure 4C**, $p = 6.10 \times 10^{-6}$, FDR $< 5\%$) and glyceric acid (**Figure 4G**, $p = 3.20 \times 10^{-27}$, FDR $< 5\%$) were also higher in the 129S strain compared to the C57 strain. There were significant effects of background, stage, and their interaction in levels of cholesterol from the linear model (**Figure 3A** and **Supplementary File S1**), with similar levels in C57-NTG and C57-G93A mice that decreased over time (**Figure 4B**), contrasting with lower cholesterol levels in the 129S strain from the presymptomatic stage. Cholesterol levels in the presymptomatic C57 mice were significantly lower than in presymptomatic 129S ($p = 3.554 \times 10^{-4}$).

Overall, the major metabolomic changes in the lumbar spinal cord affected energy and lipid metabolism. These were mainly attributable to the background difference between the C57 and 129S strain, with differences between the transgenic C57-G93A and 129S-G93A mice observable at the presymptomatic stage.

Effects on Individual Metabolites in the Thoracic Spinal Cord

We observed a greater number of significant effects in the thoracic spinal cord. There were significant effects relating to mouse background in 13 metabolites: lactate, N-acetyl-aspartate, malate, phenylalanine, glutamate, pyroglutamate, N-methyl-glutamate, N-acetyl-glutamate, pantothenic acid, citrate, isocitrate, fumarate, and glyceric acid (**Figure 3B**). A significant interaction effect between mouse background and disease stage was also observed for decanoic acid. There were also significant effects for interactions with SOD1 genotype in 15 metabolites. There were significant interaction effects between SOD1 genotype and disease stage for lactate, tyrosine, o-phosphoethanolamine, oleic acid, myo-inositol, ribose-5-phosphate, dehydroascorbic acid, and inosine. Inosine was also found to have significant interaction effects between SOD1 genotype and mouse background, along with uracil, N-acetyl-aspartate, aspartate, malate, succinate, isoleucine and 3-hydroxy-3-methylglutaric acid. Finally, the three-way interaction effect between SOD1 genotype, mouse background, and disease stage was also significant for 3-hydroxy-3-methylglutaric acid.

A number of these metabolites are involved in central carbon metabolism and energy production, like the glycolytic product lactate, the key CoA precursor pantothenic acid, 3-hydroxy-3-methylglutaric acid, and the TCA cycle intermediates citrate, isocitrate, succinate, fumarate and malate. Levels of these metabolites in the NTG mice tend to be higher under the C57 background compared to the 129S ($p < 0.05$ and FDR $< 5\%$ comparing levels in C57 mice to 129S

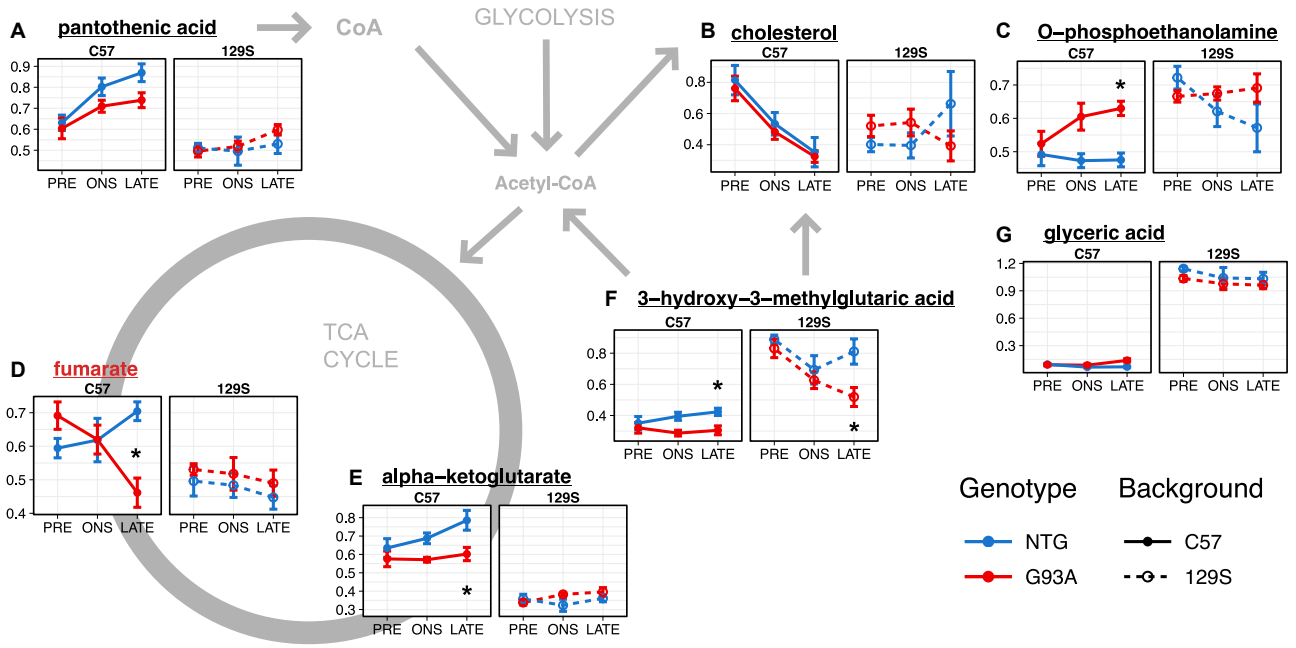

FIGURE 4 | Metabolites with significant effects relating to mouse background or SOD1 genotype in the lumbar spinal cord **(A–G)** are involved in energy metabolism and lipid metabolism. Levels of metabolites with significant effects in the linear model analysis (as indicated in **Figure 3A** and **Supplementary File S1**) are shown as mean ± s.e.m. (n = 5 mice for each group per timepoint) of relative concentration (a.u.). Metabolites with significant effects relating to SOD1 genotype are highlighted with red names, while metabolites with background-related effects are listed in black. Asterisks denote comparisons between NTG and G93A mice where $p < 0.05$ and FDR < 20% from a t-test with Benjamini-Hochberg multiple testing correction (with full statistical results for the two-group comparisons in **Supplementary File S2**).

for fumarate, malate, and pantothenic acid, **Supplementary File S3**) apart from 3-hydroxy-3-methylglutaric acid, where levels were generally higher under the 129S background ($p = 8.11 \times 10^{-11}$, FDR < 5%, **Figure 5I**). This may indicate lower activity of energy metabolism pathways and increased metabolism of leucine to acetyl-CoA that can enter the TCA cycle as a compensatory mechanism in the 129S-NTG mice. Levels of oleic acid (**Figure 5M**) were also markedly higher in the C57 mice compared to 129S ($p = 0.0039$, FDR < 5%).

When we go on to examine the effect of SOD1^{G93A} expression, we find that the two transgenic strains had different responses to mutant SOD1^{G93A} protein expression. Levels of lactate (**Figure 5C**) in SOD1^{G93A} mice were elevated compared to NTG at late stage under both backgrounds ($p = 0.0056$, FDR < 20%). We observed similar changes in thoracic spinal cord levels of 3-hydroxy-3-methylglutaric acid in the two transgenic strains to that in the lumbar spinal cord, with generally lower levels with little temporal variation in SOD1^{G93A} mice compared to NTG under the C57 background ($p = 2.63 \times 10^{-7}$, FDR < 5%, **Figure 5I**) contrasting with a steady decrease over time in the fast-progressing 129S-G93A mice. There were comparable levels of 3-hydroxy-3-methylglutaric acid in the 129S-G93A compared to 129S-NTG at the presymptomatic stage but with markedly lower levels at late stage ($p = 3.06 \times 10^{-4}$, FDR < 20%). Levels of citrate (**Figure 5H**) and isocitrate (**Figure 5L**) were lower in the C57-G93A mice compared to C57-NTG at presymptomatic stage and higher at onset and late stage, but these differences were not statistically significant (**Figure 5**). On the other hand, there were consistently higher levels of citrate ($p = 1.13 \times 10^{-4}$, FDR < 5%) and isocitrate ($p = 1.37 \times 10^{-4}$, FDR < 5%) in 129S-G93A mice compared to 129S-NTG, steadily increasing over time for both genotypes. Levels of succinate, fumarate, and malate tended to be lower in C57-G93A mice compared to C57-NTG, but tended to be higher in 129S-G93A compared to 129S-NTG ($p = 0.0020$ for malate).

The other large group of metabolites showing significant effects in the linear model were amino acids that act as neurotransmitters: aspartate, N-acetyl-aspartate, tyrosine, glutamate, and glutamate metabolites (**Figure 3B**). We observed significantly lower N-acetyl-aspartate levels in C57-G93A mice compared to C57-NTG ($p = 3.32 \times 10^{-4}$, FDR < 5%, **Figure 5N**). There was also a significant decrease in aspartate ($p = 3.30 \times 10^{-4}$, FDR < 20%, **Figure 5J**) and N-acetyl-aspartate ($p = 0.0026$, FDR < 20%, **Figure 5N**) levels of 129S-G93A mice compared to 129S-NTG at late stage, but no significant differences at presymptomatic stage and onset. N-acetyl-glutamate levels were also significantly lower in the 129S mice compared to C57 ($p = 0.0038$, FDR < 5%, **Figure 5T**). Levels of tyrosine tended to be higher in SOD1^{G93A} mice compared to NTG in both strains ($p = 3.20 \times 10^{-4}$, FDR < 5%, in the 129S mice, **Figure 5R**), with marked elevations in the SOD1^{G93A} mice from onset (significant in the 129S mice at onset, $p = 0.0164$, FDR < 20%). We also observed a progressive increase in thoracic spinal cord levels of myo-inositol in SOD1^{G93A} mice of both

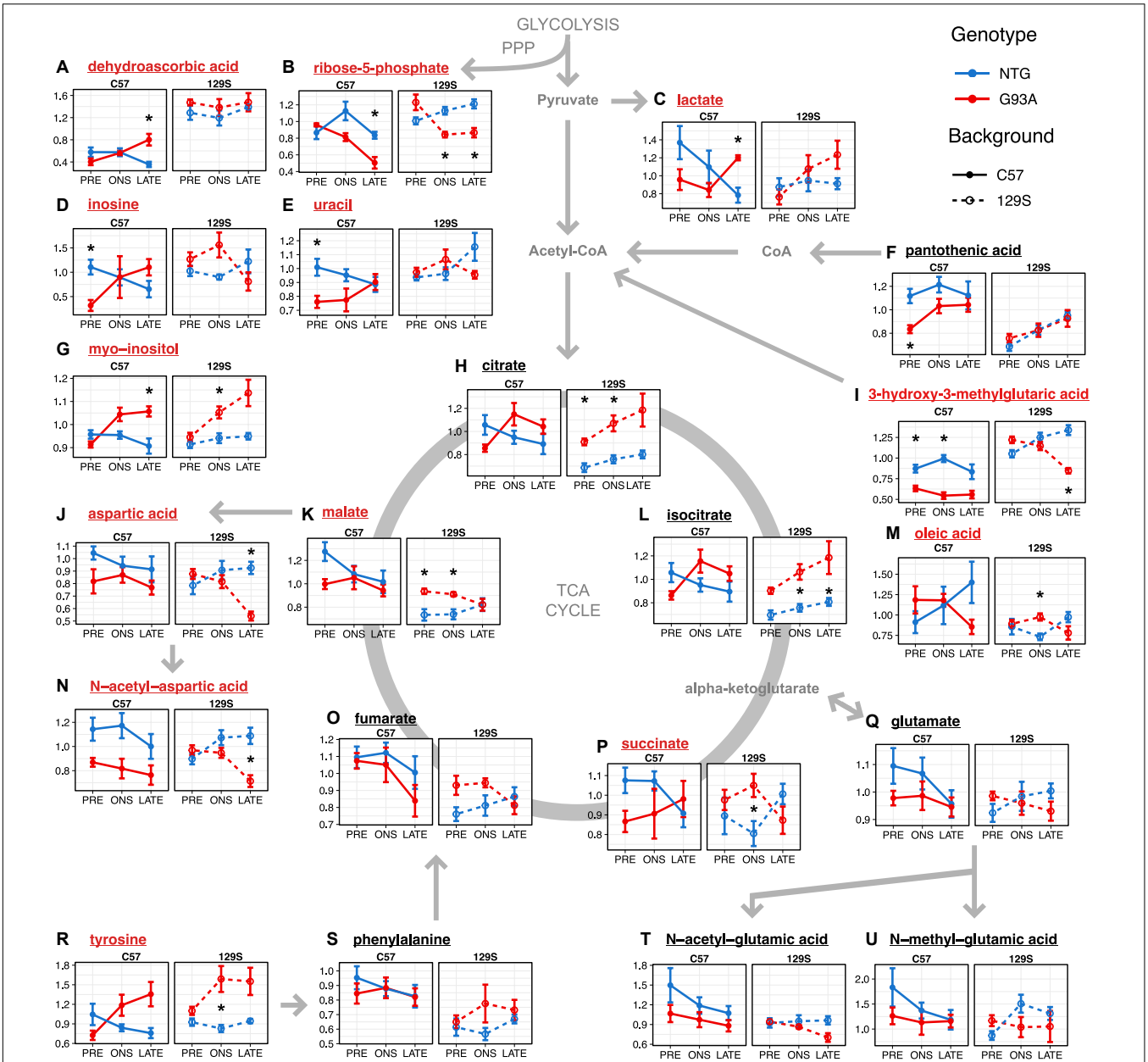

FIGURE 5 | Metabolites involved in energy metabolism, anti-oxidant activity, and neurotransmitter amino acid metabolism **(A–U)** show significant effects in the thoracic spinal cord. Levels of metabolites with significant effects in the linear model analysis (as indicated in **Figure 3B** and **Supplementary File S1**) are shown as mean ± s.e.m. (n = 5 mice for each group per timepoint) of relative concentration (a.u.). Metabolites with significant effects relating to SOD1 genotype are highlighted with red names, while metabolites with background-related effects are listed in black. Asterisks denote comparisons between NTG and G93A mice where $p < 0.05$ and FDR < 20% from a t-test with Benjamini-Hochberg multiple testing correction (with full statistical results for the two-group comparisons in **Supplementary File S2**).

strains (**Figure 5G**), with significant differences between all C57-G93A and all C57-NTG mice ($p = 0.0164$, FDR < 20%), all 129S-G93A and all 129S-NTG mice ($p = 0.0023$, FDR < 5%) and as well between C57-NTG and C57-G93A mice at late stage ($p = 0.0069$, FDR < 20%) and between 129S-NTG and 129S-G93A mice at onset ($p = 0.0111$, FDR < 20%). Inositol has a diverse range of important function in neural tissues, as it is a key osmolyte in the CNS (Fisher et al., 2002) and a precursor for phosphoinositol lipids, which play a prominent role in signal transduction (Fisher et al., 1992) as well as facilitate cellular events such as regulating cell death and survival, membrane trafficking, and maintaining the actin cytoskeleton (Vanhaesebroeck et al., 2001).

The other significantly affected metabolites may indicate the presence of increased oxidative stress. Levels of ribose-5-phosphate (**Figure 5B**), an intermediate of the pentose phosphate pathway, were decreased in the SOD1^{G93A} mice compared

to NTG in both mouse backgrounds at onset (p = 0.0013, FDR < 20% in the 129S mice) and late stage (p = 0.0053, FDR < 20% in C57 mice and p = 0.0023, FDR < 20% in 129S mice). Levels of inosine (**Figure 5D**) and uracil (**Figure 5E**) in NTG mice of both strains appear to be comparable, although levels were increased in 129S-G93A mice compared to C57-G93A mice ($p = 6.07 \times 10^{-4}$, FDR < 5% for uracil). Presymtomatic levels were also lower in C57-G93A mice compared to C57-NTG for inosine (p = 0.0038, FDR < 20%) and uracil (p = 0.0019, FDR < 20%), but no significant difference was seen in 129S mice. The presence of significant responses to $SOD1^{G93A}$ expression in nucleotides may relate to metabolism of uric acid, which can function as an antioxidant (Hooper et al., 1998). There was also a broad increase in dehydroascorbic acid levels in 129S mice compared to C57 regardless of genotype and disease stage ($p = 9.05 \times 10^{-19}$, FDR < 5%, **Figure 5A**), indicating increased oxidation of the antioxidant ascorbic acid or broadly increased antioxidant demand under the 129S background.

Overall, the major metabolic changes in the thoracic spinal cord affected the related pathways of energy metabolism, neurotransmitter amino acid metabolism, and antioxidant homeostasis. Here, we observed effects attributable to the difference in genetic background the two mouse strains, as well as to interactions of $SOD1^{G93A}$ protein expression with mouse genetic background or the stage of disease.

DISCUSSION

Thoracic Spinal Cord Exhibits Large Metabolic Shifts Ahead of the Onset of Symptoms, While the Lumbar Spinal Cord Presents Few Metabolic Changes From Onset

We studied metabolomic changes in the spinal cord of two murine models of fALS with the same genetic trigger (mutant human $SOD1^{G93A}$, expressed in the same amount), but different rates of disease progression. Metabolomic signatures in the spinal cord of these mice might relate to disease severity and help define currently unknown aspects of disease progression variability.

Results show that it is possible to distinguish spinal cord metabolomes in these models by disease stage. In the thoracic spinal cord, metabolomes of $SOD1^{G93A}$ mice exhibited large deviations from their NTG counterparts between the presymptomatic stage and onset, regardless of mouse background. This indicates that the largest metabolic shifts in the thoracic spinal cord happen ahead of the onset of symptoms, and that a metabolic response to mutant SOD1 begins early in the life of the mouse. A greater understanding of early metabolic responses to mutant SOD1 may open possibilities for maintaining motor neurons viability. However, full characterization of these metabolic alterations poses a significant challenge as no clinical or biochemical parameters can conclusively identify early ALS before the presentation of motor symptoms.

It is possible that metabolic responses observed in the thoracic spinal cord may be limited to SOD1-fALS, or even to the subset with $SOD1^{G93A}$, as disease development may vary with the SOD1 mutation present (Andersen et al., 1997). Other SOD1 ALS-related metabolic changes have previously been reported, including differences in cerebrospinal fluid metabolomes with SOD1-fALS patients (Wuolikainen et al., 2012), and neurometabolic changes in cervical spinal cords of asymptomatic mutant SOD1-positive individuals similar to those observed in patients with clinically apparent ALS (Carew et al., 2011). Studies of neonatal high copy number $SOD1^{G93A}$ mice also demonstrate early and widespread abnormal neuronal activity and hyperexcitability (van Zundert et al., 2008).

The thoracic and lumbar spinal cord show similar histopathological changes in ALS patients (Schiffer et al., 1996; Wetts and Vaughn, 1996). A few studies have examined thoracic spinal cord involvement in the murine models. There were degenerative vacuolar changes in thoracic spinal cord motor neurons of the first $SOD1^{G93A}$ mouse line without loss of those cells (Gurney et al., 1994; Chiu et al., 1995). There were no changes in proteasomal activities and no impairment of glucose use rates in the thoracic spinal cord at presymptomatic stage, while significant differences were already apparent in the lumbar tract (Kabashi et al., 2004; Browne et al., 2006). This suggests a slow involvement of the thoracic segment in the disease.

In the lumbar spinal cord, typically the principal region affected in ALS (Chen et al., 2010), the largest metabolic trajectory responses to $SOD1^{G93A}$ expression occur from onset to late stage, with similar metabolic profiles for G93A and NTG mice at presymptomatic stage and onset. The onset of visible symptoms of ALS indicates that a critical mass of motor neurons has already been compromised (Sobue et al., 1983). Histopathological comparison of C57-G93A and 129S-G93A lumbar spinal cords mice showed statistically significant motor neuron loss at onset, and is comparable between the slow-progressing C57-G93A and fast-progressing 129S-G93A (45% vs. 48% motor neuron death), increasing up to 60 and 52% respectively at the late stage (Marino et al., 2015). As such, metabolic effects of $SOD1^{G93A}$ in the lumbar spinal cord may reflect metabolic changes that occur with widespread motor neuron death sufficient to manifest as a motor loss phenotype. It should be emphasized that while the progressive loss of motor neurons from onset to late stage occurs in 2 weeks in fast-progressing mice, a similar loss occurs in 4 weeks in slow-progressing mice. This indicates that some compensatory mechanisms are activated in the motor neurons of slow-progressing mice to keep motor neurons alive for longer.

While we identified relatively few significantly affected metabolites in the lumbar spinal cord, previous work on lumbar motor neuron transcriptomes in the two models we analyze in this study showed a large number of gene expression changes (Nardo et al., 2013). However, those transcriptomes were of a single cell type. As numerous metabolic processes are compartmentalized in the CNS, the analytical approach in the present study examines the metabolome at organ region level which includes contributions from different constituent cell types. In this regard, previous work on the two mouse models studied here show that the environment surrounding the motor

neurons is different, with higher microglia activation in the lumbar spinal cord of the faster-progressing 129S-G93A mice compared to C57-G93A, but similar levels of reactive astrocytosis (Marino et al., 2015; Nardo et al., 2016).

Results in the thoracic spinal cord present the possibility that prophylactic interventions to modify the early metabolic states of individuals susceptible or likely to develop ALS may delay the onset or progression of the disease. Preconditioning with latrepirdine, an adenosine 5′-monophosphate-activated protein kinase (AMPK) activator, delayed the onset of symptoms and extended lifespan in SOD1^{G93A} mice (Coughlan et al., 2015) but did not improve survival in SOD1^{G93A} mice when administered from symptom onset (Tesla et al., 2012). The impact of the presymptomatic metabolic state on disease course is further supported by delayed onset and improved survival with presymptomatic administration of other treatments such as withaferin A (Patel et al., 2015), guanabenz (Wang et al., 2014), and davunetide (Jouroukhin et al., 2012).

Our results introduce key considerations in the design of future spinal cord metabolism studies, as analysis of the thoracic spinal cord may be useful to characterize earlier biochemical abnormalities, while lumbar spinal cord tissue may provide key information on metabolic responses to significant motor neuron loss. Unlike in the lumbar spinal cord (Marino et al., 2015), we only found a significant reduction in the number of thoracic spinal cord motor neurons at the late stage, with no differences between the two mouse strains (**Supplementary Figure S4A**), supporting the later involvement of this region in disease progression in the SOD1^{G93A} mice. However, we observed significant astrogliosis and microgliosis activation in the absence of motor neuron loss in the thoracic segment of both SOD1^{G93A} mouse strains at onset (**Supplementary Figures S4B,C**). Considering that the microglia, but not astrocytes, are already activated at the presymptomatic stage in the lumbar spinal cord without inducing metabolomic changes, we suggest that astrocytosis or other mechanisms are involved in early metabolic abnormalities in the thoracic spinal segment. From this investigation of tissue metabolic changes, a more detailed dissection of these metabolic processes can be initiated, potentially using more advanced analytical techniques to better resolve cell type-specific contributions influencing disease severity.

The Spinal Cord Metabolome Highlights Perturbations in Energy, Neurotransmitter, and Antioxidant Homeostasis Induced by Expression of Mutant SOD1^{G93A}

Levels of intermediates and substrates of glycolysis and the TCA cycle fundamental for energy metabolism were altered in both the lumbar and thoracic spinal cord. This is consistent with the energy imbalance observed in mutant SOD1 mice, with signs of hypermetabolism observed weeks before the onset of symptoms (Dupuis et al., 2004). This has been attributed to abnormalities in muscle energy metabolism (Dupuis et al., 2011) and accompanied by expression of mitochondrial uncoupling proteins in skeletal muscle (Dupuis et al., 2003). However, early dysfunctions in energy metabolism have also been observed in CNS tissue, with abnormal mitochondrial morphology appearing as an early pathogenic feature in mutant SOD1 mice (Wong et al., 1995; Bendotti et al., 2001). Mitochondrial complex I activity was decreased in the SOD1^{G93A} mouse as early as 2 months (Jung et al., 2002), which leads to defects in oxidative phosphorylation and impaired ATP synthesis (Mattiazzi et al., 2002). SOD1^{G93A} mice have exhibited reduced glucose utilization in the brain prior to onset and in the spinal cord as the disease progressed (Browne et al., 2006), and impaired glycolysis in the lumbar spinal cord (Tefera and Borges, 2018). The drop in 3-hydroxy-3-methylglutaric acid levels (indicating increased branched-chain amino acid catabolism) we observe in the SOD1^{G93A} mice suggests decreased glycolysis, as the brain uses ketone as the primary energy source when energy requirements cannot be met by glucose (Kayer, 2006). We previously reported a marked decrease of mitochondrial transcripts and ATP production in the ventral portion of the lumbar spinal cord of 129S-G93A mice compared with C57-G93A at onset (Nardo et al., 2013). The unfavorable mitochondrial metabolic state observed in 129S-G93A mice compared with C57-G93A supports the idea that failing homeostatic regulation of these mechanisms may play a role in accelerating the disease (Irvin et al., 2015).

Furthermore, the metabolism of leucine (precursor of 3-hydroxy-3-methylglutaric acid) and other branched chain amino acids provides additional sources of acetyl-CoA. Breakdown of branched chain amino acids including leucine is increased in SOD1^{G93A} mice spinal cords (Tefera and Borges, 2018) and in SOD1^{G93A} mouse spinal neuron-astrocyte co-cultures (Valbuena et al., 2017).

Levels of amino acids involved in neurotransmission (glutamate and its derivatives, aspartic acid and N-acetyl-aspartic acid) were also perturbed in the thoracic spinal cord, consistent with previous reports both in ALS patients and SOD1^{G93A} fALS models. Decreased levels of aspartate and N-acetyl-aspartic acid have been observed using ^{1}H MRS in patients (Foerster et al., 2013) as well as in SOD1^{G93A} mouse spinal cords and plasma (Niessen et al., 2007; Bame et al., 2014; Tefera and Borges, 2018). Glutamine-glutamate cycle homeostasis was altered in SOD1^{G93A} mouse astrocyte-spinal neuron co-cultures (Valbuena et al., 2017) and neuronal glutamate transfer to astrocytes was reduced in SOD1^{G93A} mouse spinal cords at disease mid-stage (Tefera and Borges, 2018). Glutamate is also essential for the synthesis of GSH, the main CNS antioxidant. Associated impairments in glutamate and GSH metabolism in a SOD1^{G93A} motor neuronal model were restored to control levels by supporting energy metabolism (D'Alessandro et al., 2011). Tyrosine levels, on the other hand, exhibited some of the largest changes and were elevated more quickly in the faster progressing 129S strain compared to the C57. The changes in the neurotransmitter pools will need to be examined in detail, particularly in the context of conflicting evidence on neuronal excitability, with studies demonstrating both hyperexcitability (Kuo et al., 2005; Pieri et al., 2009) and hypoexcitability (Delestree et al., 2014) in mutant SOD1 mouse neurons.

Other metabolic effects may reflect changes in antioxidant homeostasis with SOD1^{G93A} expression. Shifts in levels of nucleotides like inosine and uracil may indicate perturbation in metabolism of uric acid, a scavenger of peroxynitrite (formed when superoxide reacts with nitric oxide) and antioxidant (Hooper et al., 1998). Inosine supplementation increased bioenergetic output from glycolysis in astrocytes with the *C9Orf72* hexanucleotide repeat expansion and increased motor neuron survival in C9Orf72 ALS astrocyte-motor neuron co-cultures (Allen et al., 2019). Peroxynitrite amplifies oxidative damage in mutant SOD1 ALS (Drechsel et al., 2012), and nitrosative stress from SOD1 mutations contribute to protein aggregate formation, a neurotoxic mechanism (Basso et al., 2009). Increased uric acid levels were neuroprotective in a mouse model of multiple sclerosis, where they mitigated CNS tissue damage (Hooper et al., 1998).

The reduced levels of ribose-5-phosphate found with SOD1^{G93A} expression in the thoracic spinal cord are also consistent with increased levels of oxidative stress. This may indicate increased demand for reducing power in the form of NADPH, shifting ribulose-5-phosphate away from ribose-5-phosphate production toward the non-oxidative part of the pentose phosphate pathway, which produces NADPH. Maintenance of NADPH levels is fundamental to maintain GSH in the reduced form. Basal levels of dehydroascorbic acid were higher in the 129S-NTG, suggesting that oxidative stress levels may be higher in this strain and play a role in the faster rate of disease progression. This is supported by evidence that the 129S-NTG mice have higher O_2 consumption and a higher basal metabolic rate than C57-NTG mice (Almind and Kahn, 2004).

Metabolic Responses to Mutant SOD1^{G93A} in the SOD1^{G93A} Transgenic Mice Reflect Differences in Genetic Background Between the Two Strains

Some of the largest effects observed in the spinal cord tissue metabolomes relate to the different genetic background of the two mouse strains. This is the single largest discriminating factor in the lumbar spinal cord, and genetic background-related differences in thoracic spinal cord metabolic profiles are clear in all NTG mice and presymptomatic SOD1^{G93A} mice. These suggest that germline differences in metabolism may contribute to ALS progression differences between the two SOD1^{G93A} strains, as they may affect the capacity of the cell to address toxic impacts of mutant SOD1. This is consistent with the many signs of altered metabolic homeostasis seen in ALS patients (Ngo and Steyn, 2015).

The metabolic states of hyperlipidemia, high cholesterol levels, and type 2 diabetes positively correlated with survival in ALS (Dupuis et al., 2008; Seelen et al., 2014; Kioumourtzoglou et al., 2015) while weight loss associates with poor prognosis (Dupuis et al., 2011). In addition, a range of antecedent diseases have been associated with a delayed ALS onset age but a shorter disease duration (Hollinger et al., 2016). In this context, it is relevant that in wild type mice, the C57 genetic background renders the mice more prone to become obese, insulin resistant, and glucose intolerant and develop diabetes (Almind and Kahn, 2004; Mori et al., 2010). Interestingly, in SOD1^{G93A} mice, the C57 strain exhibits slower disease progression and lower weight loss compared to the 129S (Nardo et al., 2016). The significant associations of glycolysis and TCA cycle metabolites to genetic background we observe indicate impacts on energy and mitochondrial metabolism pathways. Taken together, these suggest that the slow-progressing C57-G93A mice may have a more favorable spinal cord bioenergetic profile than the 129S-G93A. Our study underlines a role for metabolism as a factor in determining disease onset age and survival length. However, further investigation is needed to determine the mechanisms by which these and other metabolic differences that arise due to differences in genetic background impact the severity of disease in ALS.

Thoracic spinal cord metabolomes of presymptomatic 129S-G93A mice appear to be more similar to metabolomes in symptomatic and advanced disease than to presymptomatic C57-G93A mice, indicating that the initial metabolic state under the 129S background may confer disadvantages in maintaining neuronal viability under ALS-related stressors. In instances where basal metabolic states produce similar effects to the response to an ALS mutant gene, a compounding effect may occur that accelerates disease progression. This would be consistent with ALS manifesting according to a liability threshold model, where disease develops when the burden of disease-causing factors crosses a critical threshold (Al-Chalabi and Hardiman, 2013). Analysis of ALS incidence rates indicate that the neurodegenerative process leading to ALS is a multistep process, with a large effect mutation accounting for a greater number of steps (Chió et al., 2018). The remaining steps needed to initiate disease are likely due to exogenous factors, involving an interplay between environmental factors and the genome of individual patients (Chió et al., 2018).

In the analysis of associations to tissue metabolism, we identify a number of metabolites with significant associations to background, stage, SOD1 genotype, or interactions between these factors but with a relatively low corresponding percentage contribution to variation in metabolite tissue levels ($<$10% for some metabolites). This is consistent with observations that contributions to variance in most metabolite levels studied are in the single digit percentages for household effects and significantly associated clinical covariates in families multiplex for coronary artery disease (Shah et al., 2009), for demographic variables (such as age, BMI, sex, ethnicity) in children from 6 european populations (Lau et al., 2018), for BMI in individuals from the TwinsUK and Health Nucleus studies (Cirulli et al., 2019), and for the combined contribution of clinical covariates in individuals from the Framingham study (Rhee et al., 2013). The fractions of variance associated with genetic traits in GWAS studies typically range from 1 to 12% (Gieger et al., 2008; Rhee et al., 2013) or less (Illig et al., 2010). SOD1 is not acting directly to produce metabolites observed in this study in cells, so it is not unreasonable that SOD1 genotype has a similar scale of contribution to variation in individual metabolites.

The significant background–related differences observed for several spinal cord tissue metabolites in the slow-and fast-progressing SOD1^{G93A} mice were seen in a well-defined ALS experimental model in a controlled setting where any environmental factors that may be involved in the disease are significantly reduced. This highlights the potential to identify cellular metabolic pathways that might change the disease course or serve as markers of disease severity in these murine models.

CONCLUSION

This longitudinal study of the spinal cord metabolome in the slow-progressing C57-G93A and the fast-progressing 129S-G93A strain identifies the presence of metabolic responses to SOD1^{G93A} expression before the manifestation of visible symptoms (as seen in thoracic spinal cord tissue), as well as metabolic responses that are pronounced when there is an overt disease phenotype (as seen in the lumbar spinal cord tissue). We found substantial metabolic effects relating to differences in mouse genetic backgrounds, as well as effects that appear to relate mouse background to disease progression. The alterations to metabolite levels observed in the study may indicate changes to neurotransmitter synthesis and utilization, energy homeostasis, and the oxidative stress response. These results indicate a potential role for basal metabolic differences and their alteration of metabolic responses to mutant SOD1^{G93A} expression in influencing the disease severity.

Our investigation of the whole organ metabolome in the thoracic and lumbar segments of the spinal cord of SOD1^{G93A} strains with different disease progression has provided insights into the effect of early metabolic changes and background metabolic differences on variation in ALS disease progression. However, further experimental work is needed to delineate how each background may modify the cell metabolism of the different cell types in the spinal cord as well as their metabolic interplay in ALS. This underscores a need to characterize the impact of germline genetic variation on the cellular response to mutations in ALS genes in early life, to identify cellular processes that may delay the onset or progression of the disease.

MATERIALS AND METHODS

Mouse Models

Female transgenic SOD1^{G93A} mice of the C57BL/6JOlaHsd (C57-G93A) or 129SvHsd (129S-G93A) genetic background and their corresponding non-transgenic (NTG) female littermates (C57-NTG and 129S-NTG respectively) were used in this study. These mouse lines were generated a few years ago from the original B6SJL-TgNSOD-1-SOD1^{G93A} -1Gur line expressing approximately 20 copies of human mutant SOD1 with a Gly93Ala substitution obtained from Jackson Laboratories and then maintained on a C57OlaHsd or 129SvHsd background (for more than 30 or 10 generations, respectively) at Harlan Italy S.R.L. We have focused our investigations on the C57-G93A and the 129S-G93A as we have observed marked differences in disease onset, progression and survival length between these models. The full characterization of the difference in disease onset, progression and survival length between the two SOD1^{G93A} strains with several functional outcome metrics have been detailed in previous publications (Pizzasegola et al., 2009). The age (in weeks, means ± S.D.) of the SOD1^{G93A} mice at the onset of symptoms, paralysis, and survival are shown in **Supplementary Table S3**.

Spinal cords were collected at the presymptomatic stage (at 8 weeks), at disease onset (19 weeks for the C57 strain, and 14 weeks for the 129S strain), and at late stage (21 weeks for the C57 strain, and 16 weeks for the 129S strain). Collection time points for each strain were determined on the basis of motor function analyses (paw grip strength test) and body weight. The progressive impairment of both fore- and hindlimb grip strength is one of the most widely used tests to measure disease progression (Ludolph et al., 2010).

The onset of symptoms was set as the age when the mice showed the first sign of paw grip strength impairment (reduced latency to fall from an inverted grid) and their body weight started to decline. The late stage was set as the point when the mice exhibited a decrease of ∼80% in their latency on the grip strength test and their body weight declined 20% from the initial value.

Mice were maintained at a temperature of 21 ± 1°C with a relative humidity of 55 ± 10% and a 12h light/dark cycle. Food (standard pellets) and water were supplied *ad libitum*. Procedures involving animals and their care were conducted according to the Mario Negri institutional guidelines, which are compliant with national (D.L. no. 116, G.U. suppl. 40, Feb.18, 1992, Circular No.8, G.U., 14 July 1994) and international policies (EEC Council Directive 86/609, OJ L 358, 1 Dec.12, 1987; NIH Guide for the Care and use of Laboratory Animals, U.S. National Research Council, 1996). All experiments and protocols were examined by the Institutional Ethical Committee and authorized by the Italian Ministry of Health. The mice were bred and maintained in a specific pathogen-free environment. Animals with substantial motor impairment had food on the cage bottom and water bottles with long drinking spouts.

Tissue Preparation

Spinal cord tissues were obtained from C57-G93A and 129S-G93A mice and their corresponding age-matched NTG littermates (n = 5 for each group) at the presymptomatic, onset and late stage. Spinal cords were rapidly removed and placed in cold artificial CSF (127 mM NaCl, 1 mM KCl, 1.2 mM KH_2PO_4, 26 mM $NaHCO_3$, 10 mM D-glucose, 2.4 mM $CaCl_2$, 1.3 mM $MgCl_2$) to limit metabolic processes prior to dissection. Tissues were then transferred onto a Petri dish cooled on ice, and the lumbar (L1-L6) and thoracic (T1-T13) segments dissected out and snap frozen in isopentane at −40°C. Tissues were stored at −80°C prior to metabolomic analysis.

Metabolite Extraction

Approximately 25 mg of lumbar and thoracic spinal cord tissue was dissected on dry ice, weighed, and transferred to 2.0 mL screw cap tubes containing 0.1 mm glass beads. Metabolites were then extracted in 80% methanol using a Precellys24 tissue homogenizer operating at 6500 rpm in 2 cycles of 20 s.

The resulting extract was dried down in a vacuum concentrator. Aqueous metabolites were then separated from the dried intracellular extract using a 2:1:3 chloroform:methanol:water extraction method. The aqueous portion of the extract was separated and lyophilized in silanized 1.5 mL glass vials prior to analysis.

Gas Chromatography-Mass Spectrometry Metabolomic Analysis

Spinal cord metabolomes were analyzed in two separate batches, one for each spinal cord segment. Derivatization for GC-MS was carried out by methoximation followed by trimethylsilylation according to the protocol by Kind et al. (2009). Samples were analyzed on an Agilent 7890 gas chromatograph connected to an Agilent 5975 MSD using the FiehnLib settings (Kind et al., 2009) and retention time-locking to myristic acid-d27. GC-MS data were processed by deconvolution using AMDIS with the Fiehn library, followed by integration using GaVIN (Behrends et al., 2011) based on the quantitation ion for each metabolite as taken from the Fiehn library. Metabolite measurements were subjected to a smoothed spline normalization of repeat-injected pooled QC samples prior to further analysis.

Statistical Analysis

Statistical analysis was carried out in R (3.4.3). Principal component analysis was performed on $\log_{10}$-transformed, mean-centered and unit variance (UV)-scaled data using the pcaMethods package. Measures of normality for each metabolite before and after $\log_{10}$-transformation are provided in **Supplementary Table S1** for lumbar spinal cord metabolites and in **Supplementary Table S2** for thoracic spinal cord metabolites.

The effects of experimental factors in our study were tested using a linear model relating tissue metabolite levels or principal components analysis scores to SOD1 genotype, mouse genetic background (strain), disease stage, and the two- and three-way interactions between these factors. The percentage of variance explained by each factor was determined using an ANOVA. The calculated *p*-values were adjusted for multiple comparisons to control the false discovery rate (FDR, Benjamini and Hochberg, 1995). The results of the linear model statistical analyses are provided in **Supplementary File S1**.

Two-group comparisons between NTG and G93A mice for each mouse background and disease stage were tested using a Student's *t*-test, with *p*-values adjusted for multiple comparisons to control the FDR. The results of these statistical comparisons are provided in **Supplementary File S2**. Broader 2-group comparisons looking at larger subgroupings in the sample set (i.e., comparing all C57 with 129S mice, all C57-NTG mice with C57-G93A mice, etc.) were also tested using a Student's *t*-test, with p-values adjusted for multiple comparisons to control the FDR. Comparisons where $p_{FDR} \leq 0.05$ were considered significant. The results of these statistical comparisons are provided in **Supplementary File S3**. Comparisons where $p \leq 0.05$ and FDR $< 20\%$ were considered significant; we have chosen to highlight FDR $< 5\%$ for most comparisons to focus on the most important changes. Summary statistics of metabolite measurements for each group are provided in **Supplementary File S4**.

Immunohistochemistry and Motor Neuron Count

Mice at the onset of the symptoms, under deep anesthesia, were transcardially perfused with PBS followed by 4% PAF solution in PBS. The spinal cord was rapidly removed, post-fixed for 2 h and cryopreserved/dehydrated in 30% sucrose solution overnight before being frozen at −80°C. 10–12 sections of the thoracic spinal cord (segments T5–T8) of 4–5 mice per group were labeled with Neurotrace to detect the Nissl substance of neuronal cells (1:100 for 30 min, Life Technologies). Images were acquired with an Olympus Fluoview confocal microscope and neuron areas were analyzed with free software ImageJ. Only cells with an area $\geq 400\ \mu m^2$ were considered for the quantitative analysis of motor neuron numbers. Data were expressed as mean number of motor neurons per section. Immunofluorescence was evaluated on five coronal thoracic spinal cord section (30 micron thickness) taken one every ten within the T5-T8 segment. After blocking the non-specific binding sites by incubation with a solution containing normal goat serum (NGS 10%) and Triton (0.1%) in PBS 0.01 M, the sections were incubated with the primary antibodies (overnight at 4°C), diluted in a solution containing NGS 1% and Triton 0.1% in PBS 0.01 M: mouse monoclonal anti-GFAP (1:2500, Merk Millipore), rabbit anti-IBA-1 (1:500, Wako). After three washes in PBS 0.01 M, the sections were incubated (1 h at room temperature) with appropriate secondary antibodies conjugated with a fluorophore (Alexa Fluor® Dyes, Life Technologies), diluted (1:500) in a solution containing NGS (1%) in PBS 0.01 M. After 3 washes in PBS 0.01 M, the sections were mounted on glass slides and then covered with coverslips using FluorSaveTM (Calbiochem). Images were acquired with an Olympus Fluoview confocal microscope (20X magnification). The quantification of GFAP and IBA-1 intensity was carried out by determining the mean gray value of fluorescent signals in the gray matter of ventral horns, using the free software ImageJ.

DATA AVAILABILITY STATEMENT

The datasets generated for this study will be made available by the authors on request, without undue reservation, to any qualified researcher.

ETHICS STATEMENT

Procedures involving animals and their care were conducted in accordance with the institutional guidelines at the Mario Negri Institute for Pharmacological Research, which are compliant with national (D.L. no. 116, G.U. suppl. 40, Feb.18, 1992, Circular No.8, G.U., 14 July 1994) and international (EEC Council Directive 86/609, OJ L 358, 1 Dec.12, 1987; NIH Guide for the Care and Use of Laboratory Animals, U.S. National Research Council, 1996) policies. All experiments and protocols were

examined by the Institutional Ethical Committee and authorized by the Italian Ministry of Health.

AUTHOR CONTRIBUTIONS

GV carried out the metabolomics measurements and metabolomic data analysis. MT carried out the tissue collection for analysis. LC contributed to the design, analysis, and interpretation of the study. CB and HK conceived, designed, and coordinated the study. All authors discussed the results, wrote the manuscript, and read and approved the final manuscript.

FUNDING

The research leading to these results received funding from the European Community's Health Seventh Framework Programme (FP7/2007-2013) under Grant Agreement No. 259867 (Euro-MOTOR) and from the "Fondazione Regionale per la Ricerca Biomedica" (TRANS-ALS project).

ACKNOWLEDGMENTS

We acknowledge M. C. Trolese and G. Nardo for their support with the motor neuron counting.

SUPPLEMENTARY MATERIAL

The Supplementary Material for this article can be found online at: https://www.frontiersin.org/articles/10.3389/fnins.2019.01276/full#supplementary-material

FIGURE S1 | Percent contribution to variance of the experimental factors examined in the first 6 principal components of **(A)** lumbar spinal cord and **(B)** thoracic spinal cord metabolic profiles. Effects of the three experimental factors SOD1 genotype, mouse background, and disease stage, as well as their two-way and three-way interaction effects were examined using a linear model.

FIGURE S2 | Lumbar spinal cord principal component analysis loadings for PC2 and PC3.

FIGURE S3 | Thoracic spinal cord principal component analysis loadings for PC4 and PC2.

FIGURE S4 | Neuropathological alterations in the thoracic segment of the spinal cord of two SOD1^{G93A} mouse strains and their respective non-transgenic mice. **(A)** Motor neuron count in thoracic spinal cord at different disease stages. Neurons were labeled with Neurotrace and motor neurons identified by the soma dimension (area $\geq$ 400 μm^2). A slight but not significant decrease in the number of motor neurons was observed in both SOD1^{G93A} mouse strains compared to their respective non-transgenic (NTG) mice at the onset of symptoms (left) while this effect becomes more evident and significant in the late symptomatic stage (right). Quantification of **(B)** GFAP and **(C)** IBA-1 immunostaining in the ventral thoracic spinal cord of both SOD1^{G93A} mouse strains at the onset of the symptoms. In both strains, a marked increase of reactive astrocytosis (GFAP) and microglia (IBA-1) were observed compared to Ntg mice (two-way ANOVA, n = 4-5, $^{*}p < 0.05$, $^{**}p < 0.01$, $^{***}p < 0.001$, and $^{****}p < 0.0001$).

TABLE S1 | Shapiro-Wilk normality test results and skewness measures for the lumbar spinal cord data.

TABLE S2 | Shapiro-Wilk normality test results and skewness measures for the thoracic spinal cord data.

TABLE S3 | Age of mice at different points in the disease course. The onset of symptoms is defined as the time when mice show the first signs of limb muscle force deficit on grip strength (when they fall from the inverted grid before 90 seconds). Paralysis is defined as the time when mice are completely unable to stay on the inverted grid. Survival is defined when mice are not able to right themselves within 10 seconds when laid on their side.

FILE S1 | Results of linear model statistical analysis.

FILE S2 | Results of two-group comparisons (Student's t-test) between NTG and G93A mice for each mouse background and disease stage.

FILE S3 | Results of two-group comparisons (Student's t-test) between larger subgroupings of the sample set.

FILE S4 | Summary statistics of metabolite measurements for each group.

REFERENCES

Al-Chalabi, A., and Hardiman, O. (2013). The epidemiology of ALS: a conspiracy of genes, environment and time. *Nat. Rev. Neurol.* 9, 617–628. doi: 10.1038/nrneurol.2013.203

Allen, S. P., Hall, B., Castelli, L. M., Francis, L., Woof, R., Siskos, A. P., et al. (2019). Astrocyte adenosine deaminase loss increases motor neuron toxicity in amyotrophic lateral sclerosis. *Brain* 142, 586–605. doi: 10.1093/brain/awy353

Almind, K., and Kahn, C. R. (2004). Genetic determinants of energy expenditure and insulin resistance in diet-induced obesity in mice. *Diabetes* 53, 3274–3285. doi: 10.2337/diabetes.53.12.3274

Andersen, P. M., Nilsson, P., Keranen, M. L., Forsgren, L., Hagglund, J., Karlsborg, M., et al. (1997). Phenotypic heterogeneity in motor neuron disease patients with CuZn-superoxide dismutase mutations in scandinavia. *Brain* 120(Pt 10), 1723–1737. doi: 10.1093/brain/120.10.1723

Bame, M., Grier, R. E., Needleman, R., and Brusilow, W. S. (2014). Amino acids as biomarkers in the SOD1(G93A) mouse model of ALS. *Biochim. Biophys. Acta* 1842, 79–87. doi: 10.1016/j.bbadis.2013.10.004

Basso, M., Samengo, G., Nardo, G., Massignan, T., D'Alessandro, G., Tartari, S., et al. (2009). Characterization of detergent-insoluble proteins in ALS indicates a causal link between nitrative stress and aggregation in pathogenesis. *PLoS One* 4:e8130. doi: 10.1371/journal.pone.0008130

Behrends, V., Tredwell, G. D., and Bundy, J. G. (2011). A software complement to AMDIS for processing GC-MS metabolomic data. *Anal. Biochem.* 415, 206–208. doi: 10.1016/j.ab.2011.04.009

Benatar, M. (2007). Lost in translation: treatment trials in the SOD1 mouse and in human ALS. *Neurobiol. Dis.* 26, 1–13. doi: 10.1016/j.nbd.2006.12.015

Bendotti, C., Calvaresi, N., Chiveri, L., Prelle, A., Moggio, M., Braga, M., et al. (2001). Early vacuolization and mitochondrial damage in motor neurons of FALS mice are not associated with apoptosis or with changes in cytochrome oxidase histochemical reactivity. *J. Neurol. Sci.* 191, 25–33. doi: 10.1016/s0022-510x(01)00627-x

Bendotti, C., and Carrì, M. T. (2004). Lessons from models of SOD1-linked familial ALS. *Trends Mol. Med.* 10, 393–400. doi: 10.1016/j.molmed.2004.06.009

Benjamini, Y., and Hochberg, Y. (1995). Controlling the false discovery rate - a practical and powerful approach to multiple testing. *J. R. Stat. Soc. Ser. B Stat. Methodol.* 57, 289–300. doi: 10.1111/j.2517-6161.1995.tb02031.x

Bento-Abreu, A., Van Damme, P., Van Den Bosch, L., and Robberecht, W. (2010). The neurobiology of amyotrophic lateral sclerosis. *Eur. J. Neurosci.* 31, 2247–2265. doi: 10.1111/j.1460-9568.2010.07260.x

Browne, S. E., Yang, L., DiMauro, J. P., Fuller, S. W., Licata, S. C., and Beal, M. F. (2006). Bioenergetic abnormalities in discrete cerebral motor pathways presage spinal cord pathology in the G93A SOD1 mouse model of ALS. *Neurobiol. Dis.* 22, 599–610. doi: 10.1016/j.nbd.2006.01.001

Carew, J. D., Nair, G., Pineda-Alonso, N., Usher, S., Hu, X., and Benatar, M. (2011). Magnetic resonance spectroscopy of the cervical cord in amyotrophic lateral sclerosis. *Amyotroph. Lateral. Scler.* 12, 185–191. doi: 10.3109/17482968.2010.515223

Carrì, M. T., Grignaschi, G., and Bendotti, C. (2006). Targets in ALS: designing multidrug therapies. *Trends Pharmacol. Sci.* 27, 267–273. doi: 10.1016/j.tips.2006.03.009

Chen, H., Guo, Y., Hu, M., Duan, W., Chang, G., and Li, C. (2010). Differential expression and alternative splicing of genes in lumbar spinal cord of an amyotrophic lateral sclerosis mouse model. *Brain Res* 1340, 52–69. doi: 10.1016/j.brainres.2010.03.075

Chia, R., Chió, A., and Traynor, B. J. (2018). Novel genes associated with amyotrophic lateral sclerosis: diagnostic and clinical implications. *Lancet Neurol.* 17, 94–102. doi: 10.1016/S1474-4422(17)30401-5

Chió, A., Calvo, A., Moglia, C., Mazzini, L., Mora, G., and Parals study group. (2011). Phenotypic heterogeneity of amyotrophic lateral sclerosis: a population based study. *J. Neurol. Neurosurg. Psychiatry* 82, 740–746. doi: 10.1136/jnnp.2010.235952

Chió, A., Mazzini, L., D'Alfonso, S., Corrado, L., Canosa, A., Moglia, C., et al. (2018). The multistep hypothesis of ALS revisited: the role of genetic mutations. *Neurology* 91, e635–e642. doi: 10.1212/WNL.0000000000005996

Chiu, A. Y., Zhai, P., Dal Canto, M. C., Peters, T. M., Kwon, Y. W., Prattis, S. M., et al. (1995). Age-dependent penetrance of disease in a transgenic mouse model of familial amyotrophic lateral sclerosis. *Mol. Cell Neurosci.* 6, 349–362. doi: 10.1006/mcne.1995.1027

Cirulli, E. T., Guo, L., Leon Swisher, C., Shah, N., Huang, L., Napier, L. A., et al. (2019). Profound perturbation of the metabolome in obesity is associated with health risk. *Cell Metab.* 48, e482. doi: 10.1016/j.cmet.2018.09.022

Coughlan, K. S., Mitchem, M. R., Hogg, M. C., and Prehn, J. H. (2015). "Preconditioning" with latrepirdine, an adenosine 5'-monophosphate-activated protein kinase activator, delays amyotrophic lateral sclerosis progression in SOD1(G93A) mice. *Neurobiol. Aging* 36, 1140–1150. doi: 10.1016/j.neurobiolaging.2014.09.022

D'Alessandro, G., Calcagno, E., Tartari, S., Rizzardini, M., Invernizzi, R. W., and Cantoni, L. (2011). Glutamate and glutathione interplay in a motor neuronal model of amyotrophic lateral sclerosis reveals altered energy metabolism. *Neurobiol. Dis.* 43, 346–355. doi: 10.1016/j.nbd.2011.04.003

Delestree, N., Manuel, M., Iglesias, C., Elbasiouny, S. M., Heckman, C. J., and Zytnicki, D. (2014). Adult spinal motoneurones are not hyperexcitable in a mouse model of inherited amyotrophic lateral sclerosis. *J. Physiol.* 592, 1687–1703. doi: 10.1113/jphysiol.2013.265843

Drechsel, D. A., Estevez, A. G., Barbeito, L., and Beckman, J. S. (2012). Nitric oxide-mediated oxidative damage and the progressive demise of motor neurons in ALS. *Neurotox. Res.* 22, 251–264. doi: 10.1007/s12640-012-9322-y

Dupuis, L., Corcia, P., Fergani, A., Gonzalez De Aguilar, J. L., Bonnefont-Rousselot, D., Bittar, R., et al. (2008). Dyslipidemia is a protective factor in amyotrophic lateral sclerosis. *Neurology* 70, 1004–1009. doi: 10.1212/01.wnl.0000285080.70324.27

Dupuis, L., di Scala, F., Rene, F., de Tapia, M., Oudart, H., Pradat, P. F., et al. (2003). Up-regulation of mitochondrial uncoupling protein 3 reveals an early muscular metabolic defect in amyotrophic lateral sclerosis. *FASEB J.* 17, 2091–2093. doi: 10.1096/fj.02-1182fje

Dupuis, L., Oudart, H., Rene, F., Gonzalez de Aguilar, J. L., and Loeffler, J. P. (2004). Evidence for defective energy homeostasis in amyotrophic lateral sclerosis: benefit of a high-energy diet in a transgenic mouse model. *Proc. Natl. Acad. Sci. U.S.A.* 101, 11159–11164. doi: 10.1073/pnas.0402026101

Dupuis, L., Pradat, P. F., Ludolph, A. C., and Loeffler, J. P. (2011). Energy metabolism in amyotrophic lateral sclerosis. *Lancet Neurol.* 10, 75–82. doi: 10.1016/S1474-4422(10)70224-6

Fisher, S. K., Heacock, A. M., and Agranoff, B. W. (1992). Inositol lipids and signal transduction in the nervous system: an update. *J. Neurochem.* 58, 18–38. doi: 10.1111/j.1471-4159.1992.tb09273.x

Fisher, S. K., Novak, J. E., and Agranoff, B. W. (2002). Inositol and higher inositol phosphates in neural tissues: homeostasis, metabolism and functional significance. *J. Neurochem.* 82, 736–754. doi: 10.1046/j.1471-4159.2002.01041.x

Foerster, B. R., Pomper, M. G., Callaghan, B. C., Petrou, M., Edden, R. A., Mohamed, M. A., et al. (2013). An imbalance between excitatory and inhibitory neurotransmitters in amyotrophic lateral sclerosis revealed by use of 3-T proton magnetic resonance spectroscopy. *JAMA Neurol.* 70, 1009–1016. doi: 10.1001/jamaneurol.2013.234

Fournier, C., and Glass, J. D. (2015). Modeling the course of amyotrophic lateral sclerosis. *Nat. Biotechnol.* 33, 45–47. doi: 10.1038/nbt.3118

Gieger, C., Geistlinger, L., Altmaier, E., Hrabe de Angelis, M., Kronenberg, F., Meitinger, T., et al. (2008). Genetics meets metabolomics: a genome-wide association study of metabolite profiles in human serum. *PLoS Genet.* 4:e1000282. doi: 10.1371/journal.pgen.1000282

Gurney, M. E., Pu, H., Chiu, A. Y., Dal Canto, M. C., Polchow, C. Y., Alexander, D. D., et al. (1994). Motor neuron degeneration in mice that express a human Cu,Zn superoxide dismutase mutation. *Science* 264, 1772–1775. doi: 10.1126/science.8209258

Heiman-Patterson, T. D., Sher, R. B., Blankenhorn, E. A., Alexander, G., Deitch, J. S., Kunst, C. B., et al. (2011). Effect of genetic background on phenotype variability in transgenic mouse models of amyotrophic lateral sclerosis: a window of opportunity in the search for genetic modifiers. *Amyotroph. Lateral. Scler.* 12, 79–86. doi: 10.3109/17482968.2010.550626

Hollinger, S. K., Okosun, I. S., and Mitchell, C. S. (2016). Antecedent disease and amyotrophic lateral sclerosis: what is protecting whom? *Front. Neurol.* 7:47. doi: 10.3389/fneur.2016.00047

Hooper, D. C., Spitsin, S., Kean, R. B., Champion, J. M., Dickson, G. M., Chaudhry, I., et al. (1998). Uric acid, a natural scavenger of peroxynitrite, in experimental allergic encephalomyelitis and multiple sclerosis. *Proc. Natl. Acad. Sci. U.S.A.* 95, 675–680. doi: 10.1073/pnas.95.2.675

Illig, T., Gieger, C., Zhai, G., Romisch-Margl, W., Wang-Sattler, R., Prehn, C., et al. (2010). A genome-wide perspective of genetic variation in human metabolism. *Nat. Genet.* 42, 137–141. doi: 10.1038/ng.507

Irvin, C. W., Kim, R. B., and Mitchell, C. S. (2015). Seeking homeostasis: temporal trends in respiration, oxidation, and calcium in SOD1 G93A amyotrophic lateral sclerosis mice. *Front. Cell Neurosci.* 9:248. doi: 10.3389/fncel.2015.00248

Jouroukhin, Y., Ostritsky, R., and Gozes, I. (2012). D-NAP prophylactic treatment in the SOD mutant mouse model of amyotrophic lateral sclerosis: review of discovery and treatment of tauopathy. *J. Mol. Neurosci.* 48, 597–602. doi: 10.1007/s12031-012-9882-6

Jung, C., Higgins, C. M., and Xu, Z. (2002). Mitochondrial electron transport chain complex dysfunction in a transgenic mouse model for amyotrophic lateral sclerosis. *J. Neurochem.* 83, 535–545. doi: 10.1046/j.1471-4159.2002.01112.x

Kabashi, E., Agar, J. N., Taylor, D. M., Minotti, S., and Durham, H. D. (2004). Focal dysfunction of the proteasome: a pathogenic factor in a mouse model of amyotrophic lateral sclerosis. *J. Neurochem.* 89, 1325–1335. doi: 10.1111/j.1471-4159.2004.02453.x

Kayer, M. A. (2006). Disorders of ketone production and utilization. *Mol. Genet. Metab.* 87, 281–283. doi: 10.1016/j.ymgme.2006.02.009

Keun, H. C., Ebbels, T. M., Bollard, M. E., Beckonert, O., Antti, H., Holmes, E., et al. (2004). Geometric trajectory analysis of metabolic responses to toxicity can define treatment specific profiles. *Chem. Res. Toxicol.* 17, 579–587. doi: 10.1021/tx034212w

Kind, T., Wohlgemuth, G., Lee, D. Y., Lu, Y., Palazoglu, M., Shahbaz, S., et al. (2009). FiehnLib: mass spectral and retention index libraries for metabolomics based on quadrupole and time-of-flight gas chromatography/mass spectrometry. *Anal. Chem.* 81, 10038–10048. doi: 10.1021/ac9019522

Kioumourtzoglou, M. A., Rotem, R. S., Seals, R. M., Gredal, O., Hansen, J., and Weisskopf, M. G. (2015). Diabetes mellitus, obesity, and diagnosis of amyotrophic lateral sclerosis: a population-based study. *JAMA Neurol.* 72, 905–911. doi: 10.1001/jamaneurol.2015.0910

Kuffner, R., Zach, N., Norel, R., Hawe, J., Schoenfeld, D., Wang, L., et al. (2015). Crowdsourced analysis of clinical trial data to predict amyotrophic lateral sclerosis progression. *Nat. Biotechnol.* 33, 51–57. doi: 10.1038/nbt.3051

Kuo, J. J., Siddique, T., Fu, R., and Heckman, C. J. (2005). Increased persistent Na(+) current and its effect on excitability in motoneurones cultured from mutant SOD1 mice. *J. Physiol.* 563(Pt 3), 843–854. doi: 10.1113/jphysiol.2004.074138

Lau, C. E., Siskos, A. P., Maitre, L., Robinson, O., Athersuch, T. J., Want, E. J., et al. (2018). Determinants of the urinary and serum metabolome in children from six European populations. *BMC Med.* 16:202. doi: 10.1186/s12916-018-1190-8

Leitner, M., Menzies, S., and Lutz, C. (2009). *Working with ALS Mice: Guidelines for Preclinical Testing and Colony Management*. Bar Harbor, ME: The Jackson Laboratory.

Ludolph, A. C., Bendotti, C., Blaugrund, E., Chió, A., Greensmith, L., Loeffler, J. P., et al. (2010). Guidelines for preclinical animal research in ALS/MND: a consensus meeting. *Amyotroph. Lateral. Scler.* 11, 38–45. doi: 10.3109/17482960903545334

Mancuso, R., and Navarro, X. (2015). Amyotrophic lateral sclerosis: current perspectives from basic research to the clinic. *Prog. Neurobiol.* 133, 1–26. doi: 10.1016/j.pneurobio.2015.07.004

Marino, M., Papa, S., Crippa, V., Nardo, G., Peviani, M., Cheroni, C., et al. (2015). Differences in protein quality control correlate with phenotype variability in 2 mouse models of familial amyotrophic lateral sclerosis. *Neurobiol. Aging* 36, 492–504. doi: 10.1016/j.neurobiolaging.2014.06.026

Mattiazzi, M., D'Aurelio, M., Gajewski, C. D., Martushova, K., Kiaei, M., Beal, M. F., et al. (2002). Mutated human SOD1 causes dysfunction of oxidative phosphorylation in mitochondria of transgenic mice. *J. Biol. Chem.* 277, 29626–29633. doi: 10.1074/jbc.M203065200

Mitsumoto, H., Brooks, B. R., and Silani, V. (2014). Clinical trials in amyotrophic lateral sclerosis: why so many negative trials and how can trials be improved? *Lancet Neurol.* 13, 1127–1138. doi: 10.1016/S1474-4422(14)70129-2

Mori, M. A., Liu, M., Bezy, O., Almind, K., Shapiro, H., Kasif, S., et al. (2010). A systems biology approach identifies inflammatory abnormalities between mouse strains prior to development of metabolic disease. *Diabetes* 59, 2960–2971. doi: 10.2337/db10-0367

Nardo, G., Iennaco, R., Fusi, N., Heath, P. R., Marino, M., Trolese, M. C., et al. (2013). Transcriptomic indices of fast and slow disease progression in two mouse models of amyotrophic lateral sclerosis. *Brain* 136(Pt 11), 3305–3332. doi: 10.1093/brain/awt250

Nardo, G., Trolese, M. C., Tortarolo, M., Vallarola, A., Freschi, M., Pasetto, L., et al. (2016). New insights on the mechanisms of disease course variability in ALS from mutant SOD1 mouse models. *Brain Pathol.* 26, 237–247. doi: 10.1111/bpa.12351

Ngo, S. T., and Steyn, F. J. (2015). The interplay between metabolic homeostasis and neurodegeneration: insights into the neurometabolic nature of amyotrophic lateral sclerosis. *Cell Regen* 4:5. doi: 10.1186/s13619-015-0019-6

Niessen, H. G., Debska-Vielhaber, G., Sander, K., Angenstein, F., Ludolph, A. C., Hilfert, L., et al. (2007). Metabolic progression markers of neurodegeneration in the transgenic G93A-SOD1 mouse model of amyotrophic lateral sclerosis. *Eur. J. Neurosci.* 25, 1669–1677. doi: 10.1111/j.1460-9568.2007.05415.x

Patel, P., Julien, J. P., and Kriz, J. (2015). Early-stage treatment with withaferin a reduces levels of misfolded superoxide dismutase 1 and extends lifespan in a mouse model of amyotrophic lateral sclerosis. *Neurotherapeutics* 12, 217–233. doi: 10.1007/s13311-014-0311-0

Pfohl, S. R., Halicek, M. T., and Mitchell, C. S. (2015). Characterization of the contribution of genetic background and gender to disease progression in the SOD1 G93A mouse model of amyotrophic lateral sclerosis: a meta-analysis. *J. Neuromuscul. Dis.* 2, 137–150. doi: 10.3233/JND-140068

Pieri, M., Carunchio, I., Curcio, L., Mercuri, N. B., and Zona, C. (2009). Increased persistent sodium current determines cortical hyperexcitability in a genetic model of amyotrophic lateral sclerosis. *Exp. Neurol.* 215, 368–379. doi: 10.1016/j.expneurol.2008.11.002

Pizzasegola, C., Caron, I., Daleno, C., Ronchi, A., Minoia, C., Carri, M. T., et al. (2009). Treatment with lithium carbonate does not improve disease progression in two different strains of SOD1 mutant mice. *Amyotroph. Lateral. Scler.* 10, 221–228. doi: 10.1080/17482960902803440

Pupillo, E., Messina, P., Logroscino, G., Beghi, E., and Group, S. (2014). Long-term survival in amyotrophic lateral sclerosis: a population-based study. *Ann. Neurol.* 75, 287–297. doi: 10.1002/ana.24096

Regal, L., Vanopdenbosch, L., Tilkin, P., Van den Bosch, L., Thijs, V., Sciot, R., et al. (2006). The G93C mutation in superoxide dismutase 1: clinicopathologic phenotype and prognosis. *Arch. Neurol.* 63, 262–267. doi: 10.1001/archneur.63.2.262

Rhee, E. P., Ho, J. E., Chen, M. H., Shen, D., Cheng, S., Larson, M. G., et al. (2013). A genome-wide association study of the human metabolome in a community-based cohort. *Cell Metab.* 18, 130–143. doi: 10.1016/j.cmet.2013.06.013

Ripps, M. E., Huntley, G. W., Hof, P. R., Morrison, J. H., and Gordon, J. W. (1995). Transgenic mice expressing an altered murine superoxide dismutase gene provide an animal model of amyotrophic lateral sclerosis. *Proc. Natl. Acad. Sci. U.S.A.* 92, 689–693. doi: 10.1073/pnas.92.3.689

Schiffer, D., Cordera, S., Cavalla, P., and Migheli, A. (1996). Reactive astrogliosis of the spinal cord in amyotrophic lateral sclerosis. *J. Neurol. Sci.* 139(Suppl.), 27–33. doi: 10.1016/0022-510x(96)00073-1

Seelen, M., van Doormaal, P. T., Visser, A. E., Huisman, M. H., Roozekrans, M. H., de Jong, S. W., et al. (2014). Prior medical conditions and the risk of amyotrophic lateral sclerosis. *J. Neurol.* 261, 1949–1956. doi: 10.1007/s00415-014-7445-1

Shah, S. H., Hauser, E. R., Bain, J. R., Muehlbauer, M. J., Haynes, C., Stevens, R. D., et al. (2009). High heritability of metabolomic profiles in families burdened with premature cardiovascular disease. *Mol. Syst. Biol.* 5, 258. doi: 10.1038/msb.2009.11

Sobue, G., Sahashi, K., Takahashi, A., Matsuoka, Y., Muroga, T., and Sobue, I. (1983). Degenerating compartment and functioning compartment of motor neurons in ALS: possible process of motor neuron loss. *Neurology* 33, 654–657.

Tefera, T. W., and Borges, K. (2018). Neuronal glucose metabolism is impaired while astrocytic TCA cycling is unaffected at symptomatic stages in the hSOD1(G93A) mouse model of amyotrophic lateral sclerosis. *J. Cereb. Blood Flow Metab.* 39, 1710–1724. doi: 10.1177/0271678X18764775

Tesla, R., Wolf, H. P., Xu, P., Drawbridge, J., Estill, S. J., Huntington, P., et al. (2012). Neuroprotective efficacy of aminopropyl carbazoles in a mouse model of amyotrophic lateral sclerosis. *Proc. Natl. Acad. Sci. U.S.A.* 109, 17016–17021. doi: 10.1073/pnas.1213960109

Turner, B. J., and Talbot, K. (2008). Transgenics, toxicity and therapeutics in rodent models of mutant SOD1-mediated familial ALS. *Prog Neurobiol.* 85, 94–134. doi: 10.1016/j.pneurobio.2008.01.001

Valbuena, G. N., Tortarolo, M., Bendotti, C., Cantoni, L., and Keun, H. C. (2017). Altered metabolic profiles associate with toxicity in SOD1(G93A) astrocyte-neuron co-cultures. *Sci. Rep.* 7:50. doi: 10.1038/s41598-017-00072-4

van Zundert, B., Peuscher, M. H., Hynynen, M., Chen, A., Neve, R. L., Brown, R. H., et al. (2008). Neonatal neuronal circuitry shows hyperexcitable disturbance in a mouse model of the adult-onset neurodegenerative disease amyotrophic lateral sclerosis. *J. Neurosci.* 28, 10864–10874. doi: 10.1523/JNEUROSCI.1340-08.2008

Vanhaesebroeck, B., Leevers, S. J., Ahmadi, K., Timms, J., Katso, R., Driscoll, P. C., et al. (2001). Synthesis and function of 3-phosphorylated inositol lipids. *Annu. Rev. Biochem.* 70, 535–602. doi: 10.1146/annurev.biochem.70.1.535

Wang, L., Popko, B., Tixier, E., and Roos, R. P. (2014). Guanabenz, which enhances the unfolded protein response, ameliorates mutant SOD1-induced amyotrophic lateral sclerosis. *Neurobiol. Dis.* 71, 317–324. doi: 10.1016/j.nbd.2014.08.010

Westeneng, H. J., Debray, T. P. A., Visser, A. E., van Eijk, R. P. A., Rooney, J. P. K., Calvo, A., et al. (2018). Prognosis for patients with amyotrophic lateral sclerosis: development and validation of a personalised prediction model. *Lancet Neurol.* 17, 423–433. doi: 10.1016/S1474-4422(18)30089-9

Wetts, R., and Vaughn, J. E. (1996). Differential vulnerability of two subsets of spinal motor neurons in amyotrophic lateral sclerosis. *Exp. Neurol.* 141, 248–255. doi: 10.1006/exnr.1996.0159

Wold, S., Esbensen, K., and Geladi, P. (1987). Principal component analysis. *Chemometr Intell. Lab. Syst.* 2, 37–52. doi: 10.1016/0169-7439(87)80084-9

Wong, P. C., Pardo, C. A., Borchelt, D. R., Lee, M. K., Copeland, N. G., Jenkins, N. A., et al. (1995). An adverse property of a familial ALS-linked SOD1 mutation causes motor neuron disease characterized by vacuolar degeneration of mitochondria. *Neuron* 14, 1105–1116. doi: 10.1016/0896-6273(95)90259-7

Wuolikainen, A., Andersen, P. M., Moritz, T., Marklund, S. L., and Antti, H. (2012). ALS patients with mutations in the SOD1 gene have an unique metabolomic profile in the cerebrospinal fluid compared with ALS patients without mutations. *Mol. Genet. Metab.* 105, 472–478. doi: 10.1016/j.ymgme.2011.11.201

Conflict of Interest: The authors declare that the research was conducted in the absence of any commercial or financial relationships that could be construed as a potential conflict of interest.

frontiers in Neuroscience

BRIEF RESEARCH REPORT
published: 20 March 2020
doi: 10.3389/fnins.2020.00228

Erosion of Gene Co-expression Networks Reveal Deregulation of Immune System Processes in Late-Onset Alzheimer's Disease

*John Stephen Malamon and Andres Kriete**

Bossone Research Center, School of Biomedical Engineering, Science and Health Systems, Drexel University, Philadelphia, PA, United States

We have applied a novel and integrative analysis framework for next-generation sequencing (NGS) data to 503 human subjects provided by the Religious Orders Study and Memory and Aging Project (ROSMAP) to examine changes in transcriptomic organization and common variants in association with late-onset Alzheimer's disease (LOAD). Our framework identified seven reproducible, co-regulated modules after quality control (QC), clinical segregation, preservation filtering, and functional ontology analysis. These modules were specifically enriched in several innate and adaptive immune system processes, the synaptic vesicle cycle, and Hippo signaling. Topological and functional erosion of these modules due to shedding of genes and loss of in-module connectivity was diagnostic of disease progression. Perturbation analysis revealed that only 1% of eQTLs overlapped genes participating in these co-regulated modules. Common variants nevertheless identified components of the immune systems like human leukocyte antigen (HLA) complex and microtubule-associated protein tau (MAPT) regions in association with LOAD. Our results implicate microglial function, adaptive immune response, and the structural degeneration of neurons as contributors to the transcriptional deregulation observed along with common genetic variants in the progression of LOAD.

Keywords: Alzheimer's, networks, immune system, synapses, functional, eQTL, WGCNA

OPEN ACCESS

Edited by:
Naveen Kumar Singhal, All India Institute of Medical Sciences, Rishikesh, India

Reviewed by:
Romina Vuono, University of Kent, United Kingdom
Jeremy Miller, Allen Institute for Brain Science, United States

***Correspondence:**
Andres Kriete
ak3652@drexel.edu

Specialty section:
This article was submitted to Neurodegeneration, a section of the journal Frontiers in Neuroscience

Received: *06 September 2019*
Accepted: *02 March 2020*
Published: *20 March 2020*

Citation:
Malamon JS and Kriete A (2020) Erosion of Gene Co-expression Networks Reveal Deregulation of Immune System Processes in Late-Onset Alzheimer's Disease. Front. Neurosci. 14:228. doi: 10.3389/fnins.2020.00228

INTRODUCTION

Late-onset Alzheimer's disease (LOAD) is a complex condition involving tau protein aggregates or tauopathy, amyloid and lipid processing, aging, immune system response, metabolism, lysosomal processing, and cerebrovascular health (Rogers et al., 1988; Braak et al., 2011; Jevtic et al., 2017; Wang et al., 2017). Progress in understanding and describing this large and diverse set of biological systems is in part determined by our ability to fully integrate clinical neuropathological data with comprehensive models that combine several modes of next-generation sequencing (NGS) data. To this end, we have applied our novel and integrative analysis framework to 503 subjects (305 cases/198 controls) provided by the Religious Orders Study and Memory and Aging Project (ROSMAP) study (Bennett et al., 2012) to develop a detailed landscape of the genetic and regulatory systems involved in LOAD, specifically with respect to clinical scores. Our study

accomplished the following four objectives: (1) identified changes in transcriptional organization in association with clinical phenotypes; (2) characterized the systematic transcriptomic and functional changes accompanying LOAD through clinical segregation co-expression analysis; (3) identified common genomic loci involved in LOAD; and (4) tested the relationship between predicted expression quantitative trait loci (eQTLs) and systematic changes in gene expression.

One of the core elements of our approach is a weighted gene co-expression analysis (WGCNA), enabling the classification and identification of highly correlated and connected modules of genes grouped by co-expression (Zhang and Horvath, 2005; Langfelder and Horvath, 2008). Network modules can be described as series of interrelated nodes and edges. Here, nodes are messenger RNA (mRNA) transcripts. Edges represent the correlation coefficients between two or more given nodes, where degrees are the number of edges shared by nodes. Genes usually have many regulators, so we chose a hierarchical co-expression model. Our combined approach increases specificity by reducing large co-expression networks to only functionally significant and highly reproducible modules. Functional significance is defined as the Gene Ontology biological process *p*-value and reproducibility is defined as the module preservation Z-score (Langfelder et al., 2011). Co-expression analysis has been successfully applied in Alzheimer's disease (AD), incorporating clinical scores and differential expression to identify co-regulated modules changing with disease in an "all-in-one" analytical design (Miller et al., 2008; Liang et al., 2018; Meng and Mei, 2019). However, the common approach to co-expression modeling does not include clinical segregation analysis. Here we provide clinical segregation for three groups: no cognitive impairment (NCI), mild cognitive impairment (MCI), and AD subjects. Additionally, strong genetic associations have been observed in LOAD (Naj et al., 2011; Lambert et al., 2013; Sims et al., 2017) along with systematic changes in gene expression profiles and transcriptional organization (Miller et al., 2008, 2010; Zhang et al., 2013; Ramasamy et al., 2014). Therefore, we hypothesize that genetic variation should account for changes in gene expression observed in transcriptomic analyses. We systematically tested the relationship between predicted eQTLs and transcriptomic organization to show underlying perturbations in gene networks that can partially account for changes observed in co-expression analyses.

METHODS

The Accelerating Medicines Partnership (AMP) provides a variety of multi-platform next-generation sequence (NGS), clinical, and other –omics data. We selected all subjects from the ROSMAP study with overlapping clinical, RNA-seq, and DNA-seq data from the prefrontal cortex from a total of 503 elderly individuals varying from cognitively healthy to diagnosed AD (Bennett et al., 2012; De Jager et al., 2018). All subjects reported race as Caucasian. According to study details, RNA was extracted from the gray matter of the dorsolateral prefrontal cortex and quantified using the NanoDrop spectrophotometer.;101-bp paired-end, Illumina HiSeq reads were aligned to the human reference genome 19 (hg19). Genotype data were generated using the Affymetrix GeneChip 6.0 platform and filtered based on the following quality control (QC) criteria: genotype call rate less than 99%, minor allele frequency (MAF) less than 2%, and a Hardy–Weinberg equilibrium threshold below 1%. A total of 619,377 single nucleotide polymorphisms (SNPs) passed QC and were used in this analysis.

Analysis Framework

Our analytical framework was previously introduced (Malamon and Kriete, 2018) and extended here to include additional features, such as clinical segregation, module preservation, gene set, and functional enrichment analyses (see **Supplementary Figure 1** for workflow diagram and full description of methods). This workflow consists of four main components: QC, co-expression modeling, functional enrichment, and eQTL analysis. We perform a comprehensive, three-tiered QC process to normalize and reduce the RNA-seq dataset to the 20,000 most informationally dense and connected transcripts. Co-expression networks are constructed using the WGCNA toolkit (Langfelder and Horvath, 2008). Next, we apply WGCNA's module preservation testing procedure to measure statistical reproducibility in all modules. We exclude all modules with preservation Z-scores below 10 standard deviations. Higher Z-scores signify modules that reoccur despite changing input conditions. These become candidate modules. Functional term and enrichment analyses are performed on all candidate modules. Gene set enrichment analysis (GSEA) (Subramanian et al., 2005) was used to examine larger functional network trends and reproduce candidate modules and genes. We provide a novel approach leveraging clinical segregation co-expression analysis to examine and compare alterations in network and module structure and organization with disease progression. For segregation analysis, QC, co-expression modeling, and functional enrichment were repeated for all clinical subgroups. Finally, genome-wide association (GWA) and perturbation analyses were performed. GWA provides all genomic loci (SNPs) predicted in association with disease status. eQTL analysis provides the predicted effects of SNPs on gene expression. Perturbation analysis was performed by overlapping co-expression module genes with eQTLs.

Clinical Segregation Analysis

Figure 1 outlines our clinical segregation protocol, which was designed to assess how transcriptomic differences are presented in clinical subgroups. We segregated samples by extracting sample data based on COGDX and CERAD scores and processing each group independently in WGCNA (see **Supplementary Table 1** for clinical definitions and **Supplementary Figure 2** for data plot). COGDX collapses 19 different neuropsychological tests into a single "Global Cognitive Score" (De Jager et al., 2018). The CERAD protocol provides neuropathological classifications for disease based on a wide variety of life-style, neuropsychological, and cognitive tests (Mirra et al., 1991). For COGDX, we segregated samples leaving 167 subjects with NCI, 131 subjects with MCI, and 205 subjects

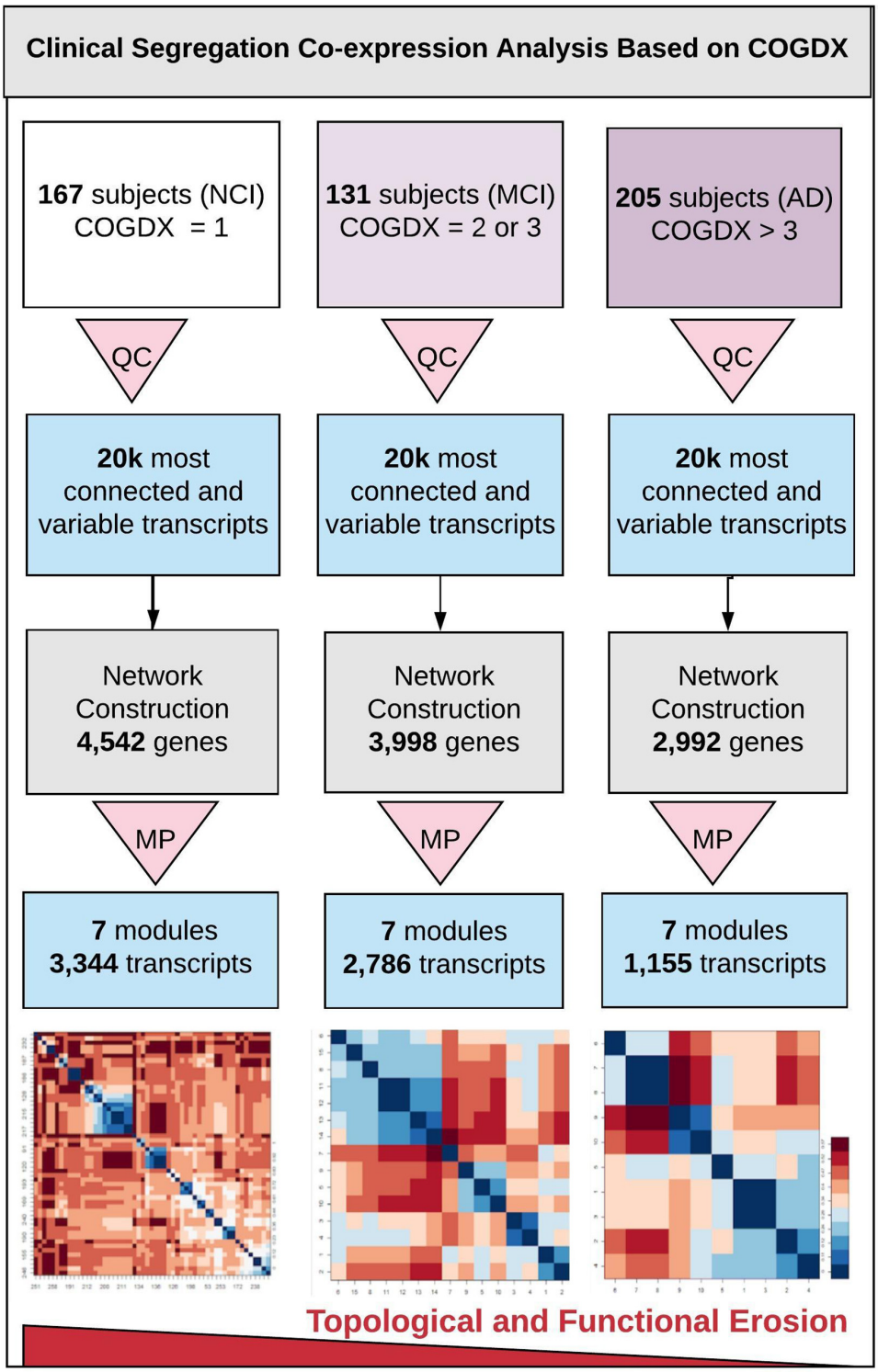

FIGURE 1 | Overview of clinical segregation co-expression analysis. An outline of our novel approach for independently analyzing and comparing co-expression networks and module characteristics in regard of clinical disease progression scores. The three vertical lanes represent COGDX segregation for three different cognitive scores (NCI, MCI, and AD) as defined in **Supplementary Table 1**. All subgroups were processed independently. First, quality control (QC) was applied to each set to retain only the 20,000 most informationally dense and variable transcripts. Next, networks were constructed with identical modeling parameters for all three subgroups. Module preservation (MP) testing was used to filter modules to only those that were highly reproducible (Z-score $>$ 10), leaving seven modules. Within these modules, we observed a significant loss in the total transcripts classified, within-module connectivity, and functional term enrichment in association with disease progression. Heatmap tiles in the bottom lane refer to functionally significant GO biological process terms.

with an Alzheimer's diagnosis (AD). For CERAD, we segregated samples leaving 130 subjects with no AD (CERAD_1), 226 subjects with possible or probable AD (CERAD_2), and 147 subjects with confirmed AD (CERAD_3). We independently processed and analyzed all six clinical subgroups using WGCNA with the same network parameters for all experiments.

RESULTS

Network Construction

We calculated the transcriptomic network's total connectivity using the median-based bi-weight mid-correlation, which is more accurate than Pearson's method for gene co-expression modeling (Zheng et al., 2014). Raising the soft-threshold to a power of 6 produced an overall R^2 value of 0.895, as seen in **Supplementary Figure 3**. Note that the R^2 value rises sharply and quickly flattens out with a slope of −1.080 at just six iterations. WGCNA was used to construct the initial co-expression network (**Supplementary Figure 4**) using all 503 subjects. Careful consideration was used in selecting the criteria for module identification, also known as branch trimming. We identified 26 distinct modules, totaling 4,429 transcripts with an average of 201 genes per module. Modules contain directionally signed groups of genes. In other words, genes in the same module are co-expressed in the same direction and well correlated with one another. We selected to lean on the side of specificity by not partitioning around medoids, leaving a total of 15,571 (77.85%) transcripts out of modules (unclassified), as indicated in gray (**Supplementary Figure 4**). Overall, the dendrogram shows clean, distinct clustering with sufficient levels of local dissimilarity. WGCNA arbitrarily assigns module names by color, i.e., gray and magenta. **Supplementary Figure 5** shows all module-to-module and module-to-eigentrait (eigenvector of clinical metric) correlations for each of the four clinical NP traits. **Supplementary Spreadsheet S1** contains all co-expressed genes grouped by module.

Clinical Segregation and Module Preservation Analysis

To investigate network and module characteristics with respect to disease progression, we segregated samples according to COGDX and CERAD scores and analyzed each of the six clinical subgroups independently in WGCNA. Clinical subgroups were assigned according to **Supplementary Table 1**. For example, subjects with COGDX scores of 0 or 1 were assigned to the NCI group. For COGDX, we uniquely classified 4,542, 3,998, and 2,992 genes for the NCI, MCI, and AD groups, respectively. For CERAD, we uniquely classified 3,426, 3,957, and 3,991 genes for the CERAD_1, CERAD_2, and CERAD_3 groups, respectively. WGCNA's *module preservation* function allowed us to accurately measure module reproducibility through permutation testing. We calculated module preservation Z-statistics using 200 permutations for all six subgroups. See **Supplementary Figure 6** for preservation statistics. Modules with Z-scores above 10 are not obtained by random chance and can be reliably reproduced (Langfelder et al., 2011; Li et al., 2015). A total of seven candidate modules (**Table 1**) survived preservation testing. Segregation by COGDX showed increased reproducibility and stability in module preservation over segregation based on CERAD assessment scores; therefore, we selected COGDX modules for further analysis.

Functional Enrichment of Co-expression Modules

Biologically relevant, functional pathways should be reproducible and overlap known LOAD pathologies. To this end, we queried the GO database to examine the functional ontologies of the seven candidate modules. **Table 1** provides statistically significant biological process terms involving known LOAD pathologies. The "magenta" module, which showed the strongest functional association, was well-correlated with COGDX and highly enriched with many immune-related genes including ABI3, APBB1IP, CD33, CD86, DOCK2, human leukocyte antigen (HLA)-DRA, HLA-DMB, MS4A4A, MS4A6A, MS4A7A, TREM2, and TYROBP. Other "magenta" GO terms include "complement pathway," "cytokine signaling," "neutrophil degranulation," and "Toll-Like receptor activation." Additional modules involving the immune system included the "turquoise" and "brown" modules, which were both enriched for the "regulation of complement activation." A GO "cellular components" query revealed the "dendrite membrane" as significant for the "yellow" module (p-value = 3.73E-06). This observation is consistent with the "biological process" query results, which provided several synaptic processes including "neuronal projection," "vesicle cycle," and "synaptic maintenance." The "blue" module was functionally enriched for genes in the Hippo signaling pathway, including AMOT, FAT4, LAT2, TJP1, TJP2, STK3, and YAP1. "Fatty acid oxidation" was also significant for the "blue" module. Additionally, cell-specific enrichment was performed on all seven modules (Uhlen et al., 2015; Kuleshov et al., 2016; Lachmann et al., 2018). See **Supplementary Table 2** for results.

Organizational Changes in Immune Module

Figure 2 shows the erosion of the "magenta" module by comparing the network characteristics of the three co-expression networks segregated by COGDX. "Magenta" contained 191, 145, and 99 genes for NCI, MCI, and AD, respectively (**Figure 2A**) and shared 86 genes across all clinical groups. The mean intramodular degrees for the NCI, MCI, and AD subgroups provided in **Figure 2B** were 47.13, 39.27, and 31.27, respectively. The "blue" module shared 85 genes in all three subgroups with 859, 693, and 222 genes, respectively. The mean intramodular degrees for each subgroup were 409.32, 341.86, and 127.42 for the "blue" module. The "yellow" module shared 27 genes with 859, 693, and 222 genes, respectively. The mean intramodular degrees for "yellow" were 90.48, 74.69, and 12.66, respectively (p-value = 2.2E-16). Similar trends were observed in the other four modules. ANOVA and Bartlett's test for heteroscedasticity were performed for all transcripts by COGDX subgroup revealing a significant (p-value < 0.05) increase in the expression of 22 "magenta," 31 "yellow," and 70 "blue" genes. Heteroscedasticity was significant

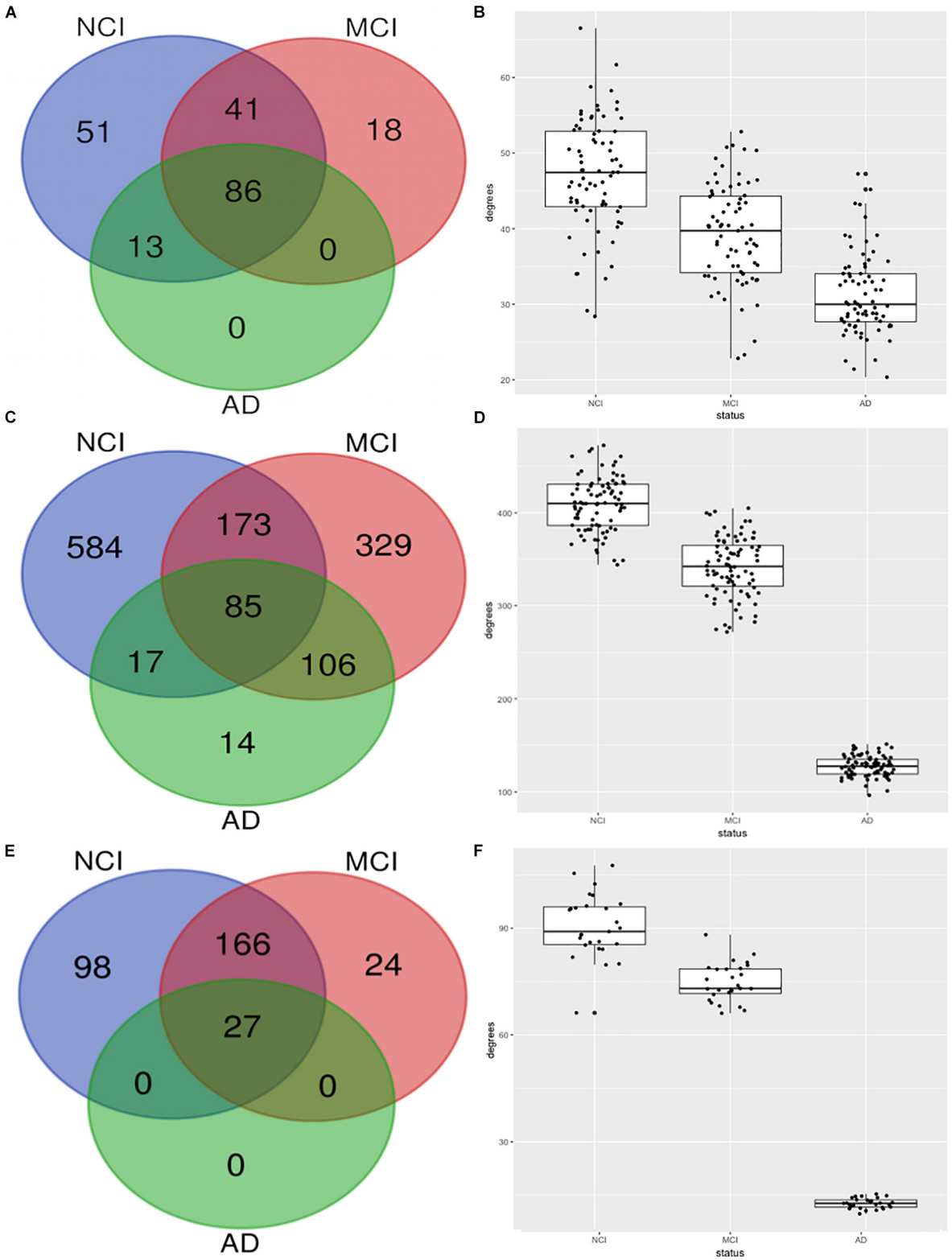

FIGURE 2 | Erosion of nodes and edges for top three functional modules by CODGX segregation. **(A)** Venn diagram of genes in the immune-enriched module (magenta) for the three COGDX subgroups, NCI, MCI, and AD. **(B)** Boxplots with the number of intramodular connections (degrees) grouped by COGDX. **(C)** Venn diagram for "blue" module (Hippo Signaling). **(D)** Boxplots of degrees grouped by COGDX for "blue" module. **(E)** Venn diagram for "yellow" module (synaptic vesicle cycle). **(F)** Boxplots of degrees grouped by COGDX for the "yellow" module.

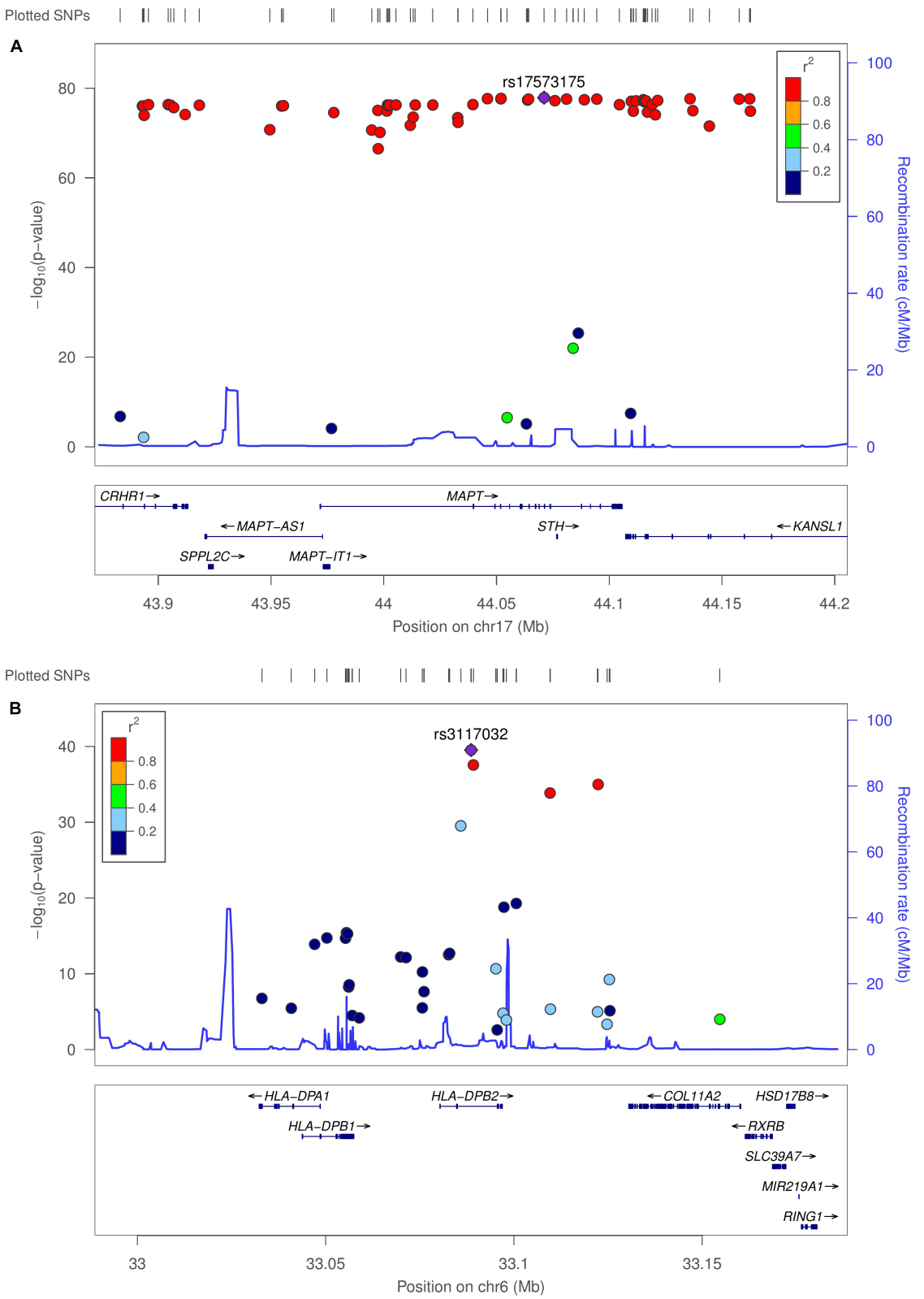

FIGURE 3 | Genome-wide association plots for eQTL analysis. Regional association plots for MAPT and HLA-DPB2 regions. **(A)** Recombination rates (cM/Mb) (right vertical axis) and $-\log_{10}$ (*p*-value) (left vertical axis) for SNPs with linkage peaks in blue for the MAPT and **(B)** HLA-DPB2 regions. SNPs are colored by the linkage disequilibrium correlation coefficient (R^2). Genetic linkage data were provided by the International HapMap Project.

TABLE 1 | Statistically significant functional terms for seven well-preserved modules sorted by adjusted *p*-value.

Module name	# of genes			Highest fold enrichment ontology term	Fold enrichment	Lowest *p*-value	Adjusted *p*-value
	NCI	MCI	AD				
Magenta	191	145	99	Regulation of T cell activation via T cell receptor contact with antigen bound to MHC molecule on antigen presenting cell	>100	Immune system process	1.80E-40
Yellow	291	217	27	Regulation of synaptic vesicle cycle	12.67	Modulation of chemical synaptic transmission	1.32E-14
Blue	859	693	222	Hippo signaling	9.74	Regulation of cell signaling	2.69E-14
Turquoise	1305	992	429	Regulation of complement activation	6.26	Cellular component organization or biogenesis	1.47E-08
Green	66	168	54	Phospholipid dephosphorylation	12.64	Cellular protein metabolic process	1.67E-07
Red	181	65	129	Regulation of synapse organization	5.23	Chemical synaptic transmission	5.11E-05
Brown	451	506	195	Regulation of complement activation	8.86	Humoral immune response	1.60E-04

NCI, MCI, and AD columns provide the number of module genes by COGDX subgroup. GO's DAVID functional analysis results are provided for seven modules. Highest fold enrichment and lowest p-value (Bonferroni adjusted) are provided in the fifth and seventh columns with the predicted biological process.

(p-value < 0.001) for 36, 48, and 74 genes, respectively. These data provide supporting evidence for the deregulation of gene networks in these three modules. **Supplementary Spreadsheet S2** contains all ANOVA and Bartlett's testing results.

Gene Set Enrichment Analysis

The Broad Institute's GSEA toolkit was used to identify disease-associated pathways via the KEGG biological pathway database (Kanehisa and Goto, 2000; Kanehisa et al., 2016, 2017). We performed a pre-ranked analysis with 10,000 permutations to discover differences in functional gene networks with regard to disease status. **Supplementary Figure 7** provides the top and bottom five KEGG pathways sorted by p-value. The top five most significant (p-value $<$ 1.5E-03) pathways positively enriched or under-represented in cases contained several immune-related genes also observed in co-expression modeling, including HLA-DRA, HLA-DMB, and CD86. Interestingly, cases exhibited deregulation in many immune system-related genes, which is consistent with the shedding of co-expressed genes revealed in the previous section. Negative enrichment scores denote an overrepresentation of pathway gene expression in cases. "*Alzheimer's, Parkinson's, and Huntington's disease*" pathways showed high overrepresentation in cases.

Transcription Factor Analysis

Finally, we asked whether transcription factors may be influential for the observed changes in modules. Transcription factor binding site interrogation was performed using human single-site analysis (oPOSSUM) (Ho Sui et al., 2005) carried out at 8-bit minimum specificity, 40% conservation cutoff, 5,000 bp upstream/downstream the transcription start site, 85% matrix threshold, against a background of 24,752 genes. "Magenta" genes were highly enriched (p-value < 0.001) for the SPI1 and Interferon Regulatory Factor 8 (IRF8) transcription factor binding motif. Genes with SP1 binding site were also enriched in genes lost from "magenta" and included CD4, CYBA, HAMP, HCST, HLA-DMA, IL18, TLR10, and TREM2. Genes with PPARG:RXRA binding site included CD4, CYBA, HAMP, HCST, HLA-DMA, IL18, TLR10, and TREM2.

Expression Quantitative Trait Locus Analysis

We used MatrixEQTL (Shabalin, 2012) to test the linear associations between changes in gene expression and genotype for the same 503 individuals used in co-expression modeling. Interestingly, 90% of the top 100 eQTLs (sorted by adjusted p-value) occurred in the microtubule-associated protein tau (MAPT) region. Several HLA loci were statistically significant, including HLA-A, HLA-C, HLA-DOB, HLA-DP1, HLA-DRB1, and HLA-DRB5. Allele-specific changes in expression were observed not only on MAPT but also on MAPT-AS1, CRHR1, KANSL1-AS1, LRRC37A2, MAPK8IP1P1, and MAPK8IP1P2. Regional association plots for the MAPT and HLA-DPB2 regions were generated using LocusZoom (Pruim et al., 2010), provided in **Figure 3**. Linkage data were provided by the International HapMap Project (The International HapMap Consortium, 2003). **Supplementary Figures 8–10** provide genome-wide association and box-plots of gene expression by genotype for four MAPT and four HLA-region SNPs identified in eQTL analysis. **Supplementary Spreadsheet S3** contains all significant eQTLs with SNP (rsID), location, and p-value.

Perturbation Testing

To determine specific sources of genetic variation and their effects on the transcriptome, we overlapped all predicted eQTLs with all genes classified in co-expression modeling. Less than 1% of eQTLs (N = 5,392 gene/SNP pairs) across the 522 genes overlapped genes identified in co-expression network modules. We observed no discernable pattern in eQTLs and classified genes. Although observed differences in co-expression based on segregation are largely unexplained by individual eQTLs, functional ontology and transcription factor enrichment analysis provided polymorphisms in multiple genes sharing the

transcription factor IRF motifs M08887 and M00972, which regulate many HLA genes.

DISCUSSION

Our analysis revealed several key functional domains and pathways through which systematic deregulation occurs in LOAD. Co-expressed transcripts, transcription factors, and genomic loci were statistically significant contributors to LOAD progression via deregulation along several immune system pathways. In segregation co-expression analysis, we observed a substantial reduction in the organizational structure of several well-preserved, functional modules, as indicated by fewer classified genes and lower intramodular connectivity in MCI and AD subjects as compared to controls. In the course of this experiment, we improved specificity in detecting functionally relevant co-expression modules in a complex disease through rigorous QC protocols and data reduction schemes, namely, module preservation testing. This is significant because co-expression analyses produce very large networks with dozens of modules. This much data can be cumbersome and difficult to interpret. Network module erosion and gene shedding were observed in the microglia ("magenta"), synaptic ("yellow"), and Hippo signaling ("blue") modules.

We chose to make the "magenta" module the focus of this discussion based on two statistical facts: (1) it was the most statistically significant module in functional gene enrichment analysis (**Table 1**) and (2) this module has been observed before in a similar study. Zhang et al. (2013) identified a module ("light cyan") containing 537 genes in the human prefrontal cortex which were highly associated (p-value = 2.1e-87) with the same immune-related GO terms. Remarkably, 98 "light cyan" genes overlapped our "magenta" module. Assuming a hypergeometric distribution, the probability of identifying the same 98 genes from a total gene pool of 20,000 is 3.54e-129. We initially hypothesized that co-expression analysis would reveal cell-specific expression modules. Co-expression segregation analysis allowed us to compare specific changes in network and module organization.

The "magenta" module contained genes such as ABI3, CD33, MS4A46, MS4A6S, TREM2, and TYROBP, which have been previously linked to AD through protein-coding mutations (Naj et al., 2011; Sims et al., 2017) and are all critical to microglial activation and response (Satoh et al., 2017). Microglia are the principal innate immune cells of the brain and ingest and degrade amyloid plaques (Koenigsknecht-Talboo and Landreth, 2005). Segregation analysis based on COGDX showed that CD33 and TREM2 were co-expressed in NCI and MCI subjects but not in AD subjects, and CD4 was only co-expressed in the MCI module. CD33 and CD4 are associated with reactive microglia and have been linked to AD (Griciuc et al., 2013). TREM2 is activated by ligand binding and increases Aß clearance through the apoptosis-related phosphatidylinositol-3 kinase (PI3K) signaling pathway, while activating CD33 attenuates the innate immune response and Aß clearance. CD33 and TREM2 showed high heteroskedasticity in AD subjects and have been suggested as cross-talking Alzheimer's genes (Chan et al., 2015). Taken together, our data suggest that CD33 and TREM2 co-regulation are important to maintaining healthy brain aging. ANOVA analysis of the "magenta" module showed increased expression in many genes including IL10RA and CD37. CD37 is activated by Aβ and mediates both humoral and cellular immune responses (van Spriel et al., 2004, 2009). This module also included HLA-DMA, HLA-DMB, and HLA-DRA.

Since the purpose of this study was to compare normal brain aging with AD, underlying aging pathways were not directly assessed. However, we noticed an interesting overlap with previous findings in a WGCNA study on the aging of the prefrontal cortex (Hu et al., 2018). Hu et al. reported a module enriched in the synaptic vesicle cycle function associated with brain aging progression. This module ("blue") overlaps with the enrichment of our "yellow" module defined here. Within the GO term "synaptic vesicle cycle," seven genes (AP2M1, ATP6V0D1, DNM1, RAB3A, STX1A, UNC13A, and VAMP2), involved in vesicle transport, endocytosis, and exocytosis, are shared between both studies. The difference in platforms and sample sizes makes this similarity remarkable, suggesting a further manifestation of synaptic dysfunction and impaired cognition in LOAD. The "blue" module was significantly enriched for Hippo signaling, which not only has implications on cell growth and autophagy but also the immune system (Zhang et al., 2018). Aß has been shown to initiate nuclear pro-apoptotic transcription factors in the Hippo signaling pathway, resulting in neuronal death (Sanphui and Biswas, 2013).

Our second motivation for the study was to examine the common genetic variants associated with LOAD. LOAD is likely influenced by the interaction of many polygenic, low- and moderate-effect variants. In our study, less than 1% of eQTLs overlapped genes classified in co-expression modeling. Of course, this did not directly explain changes in coexpression; however, eQTL analysis provided perturbations in multiple, functionally related genes (HLA-A, HLA-C, HLA-DOB, HLA-DP1, HLA-DRB1, and HLA-DRB5), all sharing transcription factor motif IRF. Interferon-regulatory factors modulate the interferon system in innate and adaptive immunity, and INF-γ induces differential expression of MHC class II HLA-DR and HLA-DP genes (Helbig et al., 1991). IFN-γ is expressed by infiltrating Th1 cells, resident microglia, and neurons and has been implicated in the development of AD and systemic autoimmunity. IFN-γ signaling is known to adversely affect AD pathologies and cognitive function (Mastrangelo et al., 2009; Monteiro et al., 2016). Activation of microglia by INF-γ inhibits Aβ clearance (Bate et al., 2006; Browne et al., 2013). HLA region eQTLs and changes in IFN-γ signaling can partially explain transcriptomic immune deregulation observed in cases.

The high concentration of eQTLs in the MAPT region highlights the impact of genetic variation on disease risk not only through MAPT haplotypes but also in several neighboring genes. MAPT pathologies provide a mechanistic link between the immune system and neurodegeneration involving microglia activation (Bhaskar et al., 2010). Splice-variants of MAPT-AS1 actively suppress MAPT translation (Coupland et al., 2016) and could prove to be a useful therapeutic target by reducing hyperphosphorylated tau levels. KANSL1 is critical to

brain development (Koolen et al., 1993) and has been linked to AD (Jun et al., 2016). Corticotropin Releasing Hormone Receptor 1 (CRHR1) agonists have been shown to increase Aβ production (Futch et al., 2017). Determining the precise nature of the relationship between genetic variation and the expression of MAPT region genes will undoubtedly provide additional insights into tauopathy and thus LOAD risk.

Immune network architectures account for desirable immune system properties such as inducibility, adaptability, and robustness (Schrom et al., 2017). Data segregation combined with co-expression analysis sheds light onto these processes in LOAD, revealing adaptations during disease onset and erosion of networks in the later stages. Observed increases in transcriptional heterogeneity resemble observations in Parkinson's disease (Mar et al., 2011), but can only partially account for module erosion since many highly variable genes are still present in the AD modules. Taken together, this study provides insights into a complex and dynamic landscape of genetic and regulatory processes centered around innate and adaptive immune system function. Systematic reductions in co-regulated genes and intramodular connectivity were diagnostic of increasing variability in several critical LOAD pathologies, including neuroinflammation, adaptive immunity, synaptic loss, and apoptosis. We propose that a reduction in regulatory and compensatory systems could also account for decreased robustness during disease progression, but the underlying mechanisms and the combined role of genetic variants are far from clear. This study highlights the adequacy of combining multi-omics NGS data types with longitudinal clinical and other developing, deep-phenotype data to decipher the complex molecular dynamics underlying complex diseases like LOAD.

DATA AVAILABILITY STATEMENT

All data analyzed were obtained from the Accelerating Medicines Partnership for Alzheimer's Disease (AMP-AD) Data Portal and can be accessed at https://www.synapse.org/#!Synapse:syn2580853/wiki/409844.

AUTHOR CONTRIBUTIONS

JM performed co-expression, functional, GSEA, and eQTL analyses. AK performed TF analysis and supervised the study. JM and AK analyzed the functional outcomes and wrote the manuscript.

FUNDING

The study was supported in part by a Drexel Areas of Research Excellence (DARE) initiative on Cell2Society Aging Research (AK).

ACKNOWLEDGMENTS

We thank the many people who have contributed in myriad ways to the ROSMAP and Accelerating Medicines Partnership. We would also like to sincerely thank Drs. Ahmet Sacan and Catherine von Reyn (Drexel University's School of Biomedical Engineering, Science and Health Systems), Dr. Daniel Marenda (Drexel University's Department of Biology), and Dr. Peter Clark (University of Pennsylvania's School of Medicine) for their advisement on this study.

SUPPLEMENTARY MATERIAL

The Supplementary Material for this article can be found online at: https://www.frontiersin.org/articles/10.3389/fnins.2020.00228/full#supplementary-material

REFERENCES

Bate, C., Kempster, S., Last, V., and Williams, A. (2006). Interferon-gamma increases neuronal death in response to amyloid-beta1-42. *J. Neuroinflammation* 3:7.

Bennett, D. A., Schneider, J. A., Arvanitakis, Z., and Wilson, R. S. (2012). Overview and findings from the religious orders study. *Curr. Alzheimer Res.* 9, 628–645. doi: 10.2174/156720512801322573

Bhaskar, K., Konerth, M., Kokiko-Cochran, O. N., Cardona, A., Ransohoff, R. M., and Lamb, B. T. (2010). Regulation of tau pathology by the microglial fractalkine receptor. *Neuron* 68, 19–31. doi: 10.1016/j.neuron.2010.08.023

Braak, H., Thal, D. R., Ghebremedhin, E., and Del Tredici, K. (2011). Stages of the pathologic process in Alzheimer disease: age categories from 1 to 100 years. *J. Neuropathol. Exp. Neurol.* 70, 960–969. doi: 10.1097/NEN.0b013e318232a379

Browne, T. C., McQuillan, K., McManus, R. M., O'Reilly, J. A., Mills, K. H., and Lynch, M. A. (2013). IFN-gamma Production by amyloid beta-specific Th1 cells promotes microglial activation and increases plaque burden in a mouse model of Alzheimer's disease. *J. Immunol.* 190, 2241–2251. doi: 10.4049/jimmunol.1200947

Chan, G., White, C. C., Winn, P. A., Cimpean, M., Replogle, J. M., Glick, L. R., et al. (2015). CD33 modulates TREM2: convergence of Alzheimer loci. *Nat. Neurosci.* 18, 1556–1558. doi: 10.1038/nn.4126

Coupland, K. G., Kim, W. S., Halliday, G. M., Hallupp, M., Dobson-Stone, C., and Kwok, J. B. (2016). Role of the long non-coding RNA MAPT-AS1 in regulation of microtubule associated protein Tau (MAPT) expression in Parkinson's disease. *PLoS One* 11:e0157924. doi: 10.1371/journal.pone.0157924

De Jager, P. L., Ma, Y., McCabe, C., Xu, J., Vardarajan, B. N., Felsky, D., et al. (2018). A multi-omic atlas of the human frontal cortex for aging and Alzheimer's disease research. *Sci. Data* 5:180142. doi: 10.1038/sdata.2018.142

Futch, H. S., Croft, C. L., Truong, V. Q., Krause, E. G., and Golde, T. E. (2017). Targeting psychologic stress signaling pathways in Alzheimer's disease. *Mol. Neurodegener.* 12:49. doi: 10.1186/s13024-017-0190-z

Griciuc, A., Serrano-Pozo, A., Parrado, A. R., Lesinski, A. N., Asselin, C. N., Mullin, K., et al. (2013). Alzheimer's disease risk gene CD33 inhibits microglial uptake of amyloid beta. *Neuron* 78, 631–643. doi: 10.1016/j.neuron.2013.04.014

Helbig, H., Kittredge, K. L., Palestine, A. G., Coca-Prados, M., and Nussenblatt, R. B. (1991). Gamma-interferon induces differential expression of HLA-DR, -DP and -DQ in human ciliary epithelial cells. *Graefes Arch. Clin. Exp. Ophthalmol.* 229, 191–194. doi: 10.1007/bf00170556

Ho Sui, S. J., Mortimer, J. R., Arenillas, D. J., Brumm, J., Walsh, C. J., Kennedy, B. P., et al. (2005). oPOSSUM: identification of over-represented transcription

factor binding sites in co-expressed genes. *Nucleic Acids Res.* 33, 3154–3164. doi: 10.1093/nar/gki624

Hu, Y., Zhao, T., Zang, T., Zhang, Y., and Cheng, L. (2018). Identification of Alzheimer's disease-related genes based on data integration method. *Front. Genet.* 9:703. doi: 10.3389/fgene.2018.00703

Jevtic, S., Sengar, A. S., Salter, M. W., and McLaurin, J. (2017). The role of the immune system in Alzheimer disease: etiology and treatment. *Ageing Res. Rev.* 40, 84–94. doi: 10.1016/j.arr.2017.08.005

Jun, G., Ibrahim-Verbaas, C. A., Vronskaya, M., Lambert, J. C., Chung, J., Naj, A. C., et al. (2016). A novel Alzheimer disease locus located near the gene encoding Tau protein. *Mol. Psychiatry* 21, 108–117. doi: 10.1038/mp.2015.23

Kanehisa, M., Furumichi, M., Tanabe, M., Sato, Y., and Morishima, K. (2017). KEGG: new perspectives on genomes, pathways, diseases and drugs. *Nucleic Acids Res.* 45, D353–D361. doi: 10.1093/nar/gkw1092

Kanehisa, M., and Goto, S. (2000). KEGG: Kyoto encyclopedia of genes and genomes. *Nucleic Acids Res.* 28, 27–30. doi: 10.1093/nar/28.1.27

Kanehisa, M., Sato, Y., Kawashima, M., Furumichi, M., and Tanabe, M. (2016). KEGG as a reference resource for gene and protein annotation. *Nucleic Acids Res.* 44, D457–D462. doi: 10.1093/nar/gkv1070

Koenigsknecht-Talboo, J., and Landreth, G. E. (2005). Microglial phagocytosis induced by fibrillar beta-amyloid and IgGs are differentially regulated by proinflammatory cytokines. *J. Neurosci.* 25, 8240–8249. doi: 10.1523/JNEUROSCI.1808-05.2005

Koolen, D. A., Morgan, A., and de Vries, B. B. A. (1993). "Koolen-de vries syndrome," in *GeneReviews((R))*, eds M. P. Adam, H. H. Ardinger, R. A. Pagon, S. E. Wallace, L. J. H. Bean, K. Stephens, et al. (Seattle, WA: OMIM).

Kuleshov, M. V., Jones, M. R., Rouillard, A. D., Fernandez, N. F., Duan, Q., Wang, Z., et al. (2016). Enrichr: a comprehensive gene set enrichment analysis web server 2016 update. *Nucleic Acids Res.* 44, W90–W97. doi: 10.1093/nar/gkw377

Lachmann, A., Torre, D., Keenan, A. B., Jagodnik, K. M., Lee, H. J., Wang, L., et al. (2018). Massive mining of publicly available RNA-seq data from human and mouse. *Nat. Commun.* 9:1366. doi: 10.1038/s41467-018-03751-6

Lambert, J. C., Ibrahim-Verbaas, C. A., Harold, D., Naj, A. C., Sims, R., Bellenguez, C., et al. (2013). Meta-analysis of 74,046 individuals identifies 11 new susceptibility loci for Alzheimer's disease. *Nat. Genet.* 45, 1452–1458. doi: 10.1038/ng.2802

Langfelder, P., and Horvath, S. (2008). WGCNA: an R package for weighted correlation network analysis. *BMC Bioinformatics* 9:559. doi: 10.1186/1471-2105-9-559

Langfelder, P., Luo, R., Oldham, M. C., and Horvath, S. (2011). Is my network module preserved and reproducible? *PLoS Comput. Biol.* 7:e1001057. doi: 10.1371/journal.pcbi.1001057

Li, B., Zhang, Y., Yu, Y., Wang, P., Wang, Y., Wang, Z., et al. (2015). Quantitative assessment of gene expression network module-validation methods. *Sci. Rep.* 5:15258. doi: 10.1038/srep15258

Liang, J. W., Fang, Z. Y., Huang, Y., Liuyang, Z. Y., Zhang, X. L., Wang, J. L., et al. (2018). Application of weighted gene co-expression network analysis to explore the key genes in Alzheimer's disease. *J. Alzheimers Dis.* 65, 1353–1364. doi: 10.3233/JAD-180400

Malamon, J. S., and Kriete, A. (2018). Integrated systems approach reveals sphingolipid metabolism pathway dysregulation in association with late-onset Alzheimer's Disease. *Biology* 7:16. doi: 10.3390/biology7010016

Mar, J. C., Matigian, N. A., Mackay-Sim, A., Mellick, G. D., Sue, C. M., Silburn, P. A., et al. (2011). Variance of gene expression identifies altered network constraints in neurological disease. *PLoS Genet.* 7:e1002207. doi: 10.1371/journal.pgen.1002207

Mastrangelo, M. A., Sudol, K. L., Narrow, W. C., and Bowers, W. J. (2009). Interferon-{gamma} differentially affects Alzheimer's disease pathologies and induces neurogenesis in triple transgenic-AD mice. *Am. J. Pathol.* 175, 2076–2088. doi: 10.2353/ajpath.2009.090059

Meng, G., and Mei, H. (2019). Transcriptional dysregulation study reveals a core network involving the progression of Alzheimer's disease. *Front. Aging Neurosci.* 11:101. doi: 10.3389/fnagi.2019.00101

Miller, J. A., Horvath, S., and Geschwind, D. H. (2010). Divergence of human and mouse brain transcriptome highlights Alzheimer disease pathways. *Proc. Natl. Acad. Sci. U.S.A.* 107, 12698–12703. doi: 10.1073/pnas.0914257107

Miller, J. A., Oldham, M. C., and Geschwind, D. H. (2008). A systems level analysis of transcriptional changes in Alzheimer's disease and normal aging. *J. Neurosci.* 28, 1410–1420. doi: 10.1523/JNEUROSCI.4098-07.2008

Mirra, S. S., Heyman, A., McKeel, D., Sumi, S. M., Crain, B. J., Brownlee, L. M., et al. (1991). The consortium to establish a registry for Alzheimer's disease (CERAD). Part II. Standardization of the neuropathologic assessment of Alzheimer's disease. *Neurology* 41, 479–486. doi: 10.1212/wnl.41.4.479

Monteiro, S., Ferreira, F. M., Pinto, V., Roque, S., Morais, M., de Sa-Calcada, D., et al. (2016). Absence of IFN-gamma promotes hippocampal plasticity and enhances cognitive performance. *Transl. Psychiatry* 6:e707. doi: 10.1038/tp.2015.194

Naj, A. C., Jun, G., Beecham, G. W., Wang, L. S., Vardarajan, B. N., Buros, J., et al. (2011). Common variants at MS4A4/MS4A6E, CD2AP, CD33 and EPHA1 are associated with late-onset Alzheimer's disease. *Nat. Genet.* 43, 436–441. doi: 10.1038/ng.801

Pruim, R. J., Welch, R. P., Sanna, S., Teslovich, T. M., Chines, P. S., Gliedt, T. P., et al. (2010). LocusZoom: regional visualization of genome-wide association scan results. *Bioinformatics* 26, 2336–2337. doi: 10.1093/bioinformatics/btq419

Ramasamy, A., Trabzuni, D., Guelfi, S., Varghese, V., Smith, C., Walker, R., et al. (2014). Genetic variability in the regulation of gene expression in ten regions of the human brain. *Nat. Neurosci.* 17, 1418–1428. doi: 10.1038/nn.3801

Rogers, J., Luber-Narod, J., Styren, S. D., and Civin, W. H. (1988). Expression of immune system-associated antigens by cells of the human central nervous system: relationship to the pathology of Alzheimer's disease. *Neurobiol. Aging* 9, 339–349. doi: 10.1016/s0197-4580(88)80079-4

Sanphui, P., and Biswas, S. C. (2013). FoxO3a is activated and executes neuron death via Bim in response to beta-amyloid. *Cell Death Dis.* 4:e625. doi: 10.1038/cddis.2013.148

Satoh, J. I., Kino, Y., Yanaizu, M., Tosaki, Y., Sakai, K., Ishida, T., et al. (2017). Microglia express ABI3 in the brains of Alzheimer's disease and Nasu-Hakola disease. *Intractable Rare Dis. Res.* 6, 262–268. doi: 10.5582/irdr.2017.01073

Schrom, E., Prada, J. M., and Graham, A. L. (2017). Immune signaling networks: sources of robustness and constrained evolvability during coevolution. *Mol. Biol. Evol.* 35, 676–687. doi: 10.1093/molbev/msx321

Shabalin, A. A. (2012). Matrix eQTL: ultra fast eQTL analysis via large matrix operations. *Bioinformatics* 28, 1353–1358. doi: 10.1093/bioinformatics/bts163

Sims, R., van der Lee, S. J., Naj, A. C., Bellenguez, C., Badarinarayan, N., Jakobsdottir, J., et al. (2017). Rare coding variants in PLCG2, ABI3, and TREM2 implicate microglial-mediated innate immunity in Alzheimer's disease. *Nat. Genet.* 49, 1373–1384. doi: 10.1038/ng.3916

Subramanian, A., Tamayo, P., Mootha, V. K., Mukherjee, S., Ebert, B. L., Gillette, M. A., et al. (2005). Gene set enrichment analysis: a knowledge-based approach for interpreting genome-wide expression profiles. *Proc. Natl. Acad. Sci. U.S.A.* 102, 15545–15550. doi: 10.1073/pnas.0506580102

The International HapMap Consortium, (2003). The International HapMap Project. *Nature* 426, 789–796. doi: 10.1038/nature02168

Uhlen, M., Fagerberg, L., Hallstrom, B. M., Lindskog, C., Oksvold, P., Mardinoglu, A., et al. (2015). Proteomics. Tissue-based map of the human proteome. *Science* 347:1260419. doi: 10.1126/science.1260419

van Spriel, A. B., Puls, K. L., Sofi, M., Pouniotis, D., Hochrein, H., Orinska, Z., et al. (2004). A regulatory role for CD37 in T cell proliferation. *J. Immunol.* 172, 2953–2961. doi: 10.4049/jimmunol.172.5.2953

van Spriel, A. B., Sofi, M., Gartlan, K. H., van der Schaaf, A., Verschueren, I., Torensma, R., et al. (2009). The tetraspanin protein CD37 regulates IgA responses and anti-fungal immunity. *PLoS Pathog.* 5:e1000338. doi: 10.1371/journal.ppat.1000338

Wang, J., Gu, B. J., Masters, C. L., and Wang, Y. J. (2017). A systemic view of Alzheimer disease - insights from amyloid-beta metabolism beyond the brain. *Nat. Rev. Neurol.* 13:703. doi: 10.1038/nrneurol.2017.147

Zhang, B., Gaiteri, C., Bodea, L. G., Wang, Z., McElwee, J., Podtelezhnikov, A. A., et al. (2013). Integrated systems approach identifies genetic nodes and networks in late-onset Alzheimer's disease. *Cell* 153, 707–720. doi: 10.1016/j.cell.2013.03.030

Zhang, B., and Horvath, S. (2005). A general framework for weighted gene co-expression network analysis. *Stat. Appl. Genet. Mol. Biol.* 4:Article17. doi: 10.2202/1544-6115.1128

Zhang, Y., Zhang, H., and Zhao, B. (2018). Hippo signaling in the immune system. *Trends Biochem. Sci.* 43, 77–80. doi: 10.1016/j.tibs.2017.11.009

Zheng, C. H., Yuan, L., Sha, W., and Sun, Z. L. (2014). Gene differential coexpression analysis based on biweight correlation and maximum clique. *BMC Bioinformatics* 15(Suppl. 15):S3. doi: 10.1186/1471-2105-15-S15-S3

Conflict of Interest: The authors declare that the research was conducted in the absence of any commercial or financial relationships that could be construed as a potential conflict of interest.

frontiers in Neuroscience

REVIEW
published: 25 March 2020
doi: 10.3389/fnins.2020.00194

Omics Approach to Axonal Dysfunction of Motor Neurons in Amyotrophic Lateral Sclerosis (ALS)

Naoki Suzuki[1,2], Tetsuya Akiyama[1], Hitoshi Warita[1] and Masashi Aoki[1]**

[1] Department of Neurology, Tohoku University School of Medicine, Sendai, Japan, [2] Department of Neurology, Shodo-kai Southern Tohoku General Hospital, Miyagi, Japan

Amyotrophic lateral sclerosis (ALS) is an intractable adult-onset neurodegenerative disease that leads to the loss of upper and lower motor neurons (MNs). The long axons of MNs become damaged during the early stages of ALS. Genetic and pathological analyses of ALS patients have revealed dysfunction in the MN axon homeostasis. However, the molecular pathomechanism for the degeneration of axons in ALS has not been fully elucidated. This review provides an overview of the proposed axonal pathomechanisms in ALS, including those involving the neuronal cytoskeleton, cargo transport within axons, axonal energy supply, clearance of junk protein, neuromuscular junctions (NMJs), and aberrant axonal branching. To improve understanding of the global changes in axons, the review summarizes omics analyses of the axonal compartments of neurons *in vitro* and *in vivo*, including a motor nerve organoid approach that utilizes microfluidic devices developed by this research group. The review also discusses the relevance of intra-axonal transcription factors frequently identified in these omics analyses. Local axonal translation and the relationship among these pathomechanisms should be pursued further. The development of novel strategies to analyze axon fractions provides a new approach to establishing a detailed understanding of resilience of long MN and MN pathology in ALS.

Keywords: amyotrophic lateral sclerosis (ALS), omics analysis, axonal dysfunction, local translation, axon branching, motor nerve organoid, human induced pluripotent stem cell (hiPSC)-derived motor neuron

OPEN ACCESS

Edited by:
Manoj Kumar Jaiswal, Icahn School of Medicine at Mount Sinai, United States

Reviewed by:
Philip Van Damme, KU Leuven, Belgium
Ludo M. Van Den Bosch, KU Leuven, Belgium
Masahisa Katsuno, Nagoya University Hospital, Japan

****Correspondence:***
Naoki Suzuki
naoki@med.tohoku.ac.jp
Masashi Aoki
aokim@med.tohoku.ac.jp

Specialty section:
This article was submitted to Neurodegeneration, a section of the journal Frontiers in Neuroscience

Received: *28 November 2019*
Accepted: *24 February 2020*
Published: *25 March 2020*

Citation:
Suzuki N, Akiyama T, Warita H and Aoki M (2020) Omics Approach to Axonal Dysfunction of Motor Neurons in Amyotrophic Lateral Sclerosis (ALS). Front. Neurosci. 14:194. doi: 10.3389/fnins.2020.00194

INTRODUCTION

Amyotrophic lateral sclerosis (ALS) is a devastating adult-onset neurodegenerative disorder (Brown and Al-Chalabi, 2017). Both the upper and lower motor neurons (MNs) are affected, such that the disorder is characterized by muscle weakness with spasticity and atrophy. Approximately 10% of ALS occurrence is familial (Ghasemi and Brown, 2018). Since the identification in 1993 (Rosen et al., 1993) of *copper/zinc superoxide dismutase 1* (*SOD1*) in ALS patients with an autosomal dominant trait in 1993 (Aoki et al., 1993), more than 25 genes have been reported as causative genes of familial ALS (Maday et al., 2014; De Vos and Hafezparast, 2017; Ghasemi and Brown, 2018; Cook and Petrucelli, 2019).

The pathomechanisms of ALS have been examined using familial ALS models. Intracellular generation of reactive oxygen species production (Borchelt et al., 1994; Wiedau-Pazos et al., 1996; Howland et al., 2002) and unfolded protein response/endoplasmic reticulum (ER) stress

(Kikuchi et al., 2006; Kieran et al., 2007; Urushitani et al., 2008) have been inferred from the discovery of SOD1 as a factor. A cell non-autonomous effect (Boillee et al., 2006; Di Giorgio et al., 2007; Nagai et al., 2007; Yamanaka et al., 2008; de Boer et al., 2014) has also been examined in mutant *SOD1*-transgenic mouse and cellular models. Mutations in the RNA-binding protein (RBP) *TAR DNA-binding protein* (*TARDBP* encoding TDP-43) can result in ALS (Kabashi et al., 2008; Rutherford et al., 2008), and cytoplasmic TDP-43 inclusions have been reported in over 90% of cases of sporadic ALS (Mackenzie et al., 2010). In 2009, *fused in sarcoma* (*FUS*) was determined in 2009 to be the causative gene of ALS (Kwiatkowski et al., 2009; Vance et al., 2009). FUS and TDP-43 have similar structural characteristics, including an RNA recognition motif (RRM), a nuclear export signal (NES), a nuclear localization signal (NLS), and prion-like domains (PrLDs) (Kapeli et al., 2017). The C-terminal NLS site regulates the nucleocytoplasmic localization of FUS and is a hotspot for mutations in familial ALS (Kwiatkowski et al., 2009; Vance et al., 2009; Suzuki et al., 2010; Nishiyama et al., 2017). Abnormal phase separation of FUS is involved in this pathomechanism (Guo et al., 2018; Hofweber et al., 2018; Qamar et al., 2018). NLS mutations impair the nuclear import of FUS, and the level of mislocalized cytoplasmic FUS is correlated to the severity of the clinical ALS phenotypes (Dormann et al., 2010). In addition, recent reports have demonstrated that the abnormal NLS function results in the aberrant accumulation of mutant FUS in the cytoplasm (Ichiyanagi et al., 2016; Guo et al., 2018; Hofweber et al., 2018; Qamar et al., 2018; Yoshizawa et al., 2018). Previous studies have found that the toxic gain of function occurring with mutant *FUS* is crucial for neurodegeneration (Scekic-Zahirovic et al., 2016; Sharma et al., 2016; Shiihashi et al., 2016).

A hexanucleotide repeat expansion in *chromosome 9 open reading frame 72* (*C9orf72*) (DeJesus-Hernandez et al., 2011; Renton et al., 2011) is the most common cause of ALS when examined in Western countries (Balendra and Isaacs, 2018). Loss of function of C9ORF72 (Burberry et al., 2016; O'Rourke et al., 2016), toxic gain of function of C9ORF72 due to repeat RNA (Peters et al., 2015; Jiang et al., 2016), and toxic gain of function due to proteins with dipeptide repeats resulting from repeat-associated non-ATG translation (Mori et al., 2013; Kwon et al., 2014; Mizielinska et al., 2014; Wen et al., 2014; Chew et al., 2015) have been suggested as disease mechanisms.

These findings are mainly focused on the event in the cytoplasm of MNs. Actually, long axons, which have lengths of up to 100 cm in humans, are characteristic of MN morphology, and connect the soma of MNs to the skeletal muscles. In ALS, MNs are dysfunctional due to axonal degeneration (Ferraiuolo et al., 2011), that occurs prior to the motor phenotype in ALS (Fischer et al., 2004; Roy et al., 2005). Consistent with this observation, transgenic models of ALS also demonstrate abnormal axons and other degenerative processes, followed by the death of MNs (Armstrong and Drapeau, 2013; Tian et al., 2016; Fujimori, 2018). Other studies have revealed that axonal damage occurs earlier than the death of cell bodies and subsequent symptoms in patients; such symptoms become apparent only after the loss of many MNs (Dadon-Nachum et al., 2011).

Various reviews have described the physiological and pathological features of neuronal axons, including cargo transport within axons, local translation, and the axonal transcriptome (Jung et al., 2012; Maday et al., 2014; Batista and Hengst, 2016; Neto et al., 2016; Brady and Morfini, 2017; De Vos and Hafezparast, 2017). However, because primary neurons from patients cannot be easily obtained and because axons produce low sample yields and are difficult to culture, the details of the pathological mechanisms of ALS remain unclear. To further elucidate the resilience and pathomechanisms in MN axons, this review summarizes omics analyses of the axon compartment using microfluidic devices and *ex vivo* samples. Intra-axonal transcription and local axonal translation are the mechanisms of ALS emerging in the field, as discussed in the following.

ACCUMULATING EVIDENCE OF AXONAL DYSFUNCTION IN ALS

The global pathomechanisms of axons in ALS are considered next, in an overview of the current knowledge of axonal events in MNs. This section classifies the pathomechanisms of axonal dysfunction into six subsections, including neuronal cytoskeleton, cargo transport within axons, axonal energy supply, clearance of junk protein, neuromuscular junctions (NMJs), and aberrant axonal branching (**Figure 1**). As mentioned in the introduction, an increasing number of genes have been found as causative or associated genes for ALS. Evidence of axon pathomechanisms from the genetics of ALS is also accumulating (**Table 1**). These mechanisms are explained in each subsection.

Neuronal Cytoskeleton

The axon can be visualized as a railway, and the electric signal should be transferred from one train terminal station (the cell body) to another terminal station (the skeletal muscle). Mutations in genes associated with microtubules have been identified as the causative events in ALS.

Several variants of the gene encoding α-tubulin, *TUBA4A*, destabilize the microtubule network and reduce the repolymerization capability of this network (Smith et al., 2014). A missense mutation in the *tubulin-specific chaperone E* gene, causing MN degeneration in the progressive motor neuronopathy model mouse, ends in microtubule and axonal defects similar to those induced by the ALS-linked *TUBA4A* variation in patients (Bommel et al., 2002; Martin et al., 2002).

Mutations in *profilin 1* (*PFN1*) can also lead to familial ALS. PFN1 converts monomeric actin to filamentous actin. Ubiquitinated aggregates are present in cells that express mutant *PFN1*, and many of these aggregates include TDP-43, which is associated with ALS (Wu et al., 2012). Such cells also have lower levels of bound actin and block axon growth. Primary MNs that harbor mutant *PFN1* have a lower ratio of monomeric to filamentous actin and smaller growth cones. The PFN1 transgenic mouse has also been observed to recapitulate the phenotype of MN disease (Fil et al., 2017).

NIMA (never in mitosis gene A)-related kinase 1 (NEK1) has been linked to cilia formation, microtubule stability, and

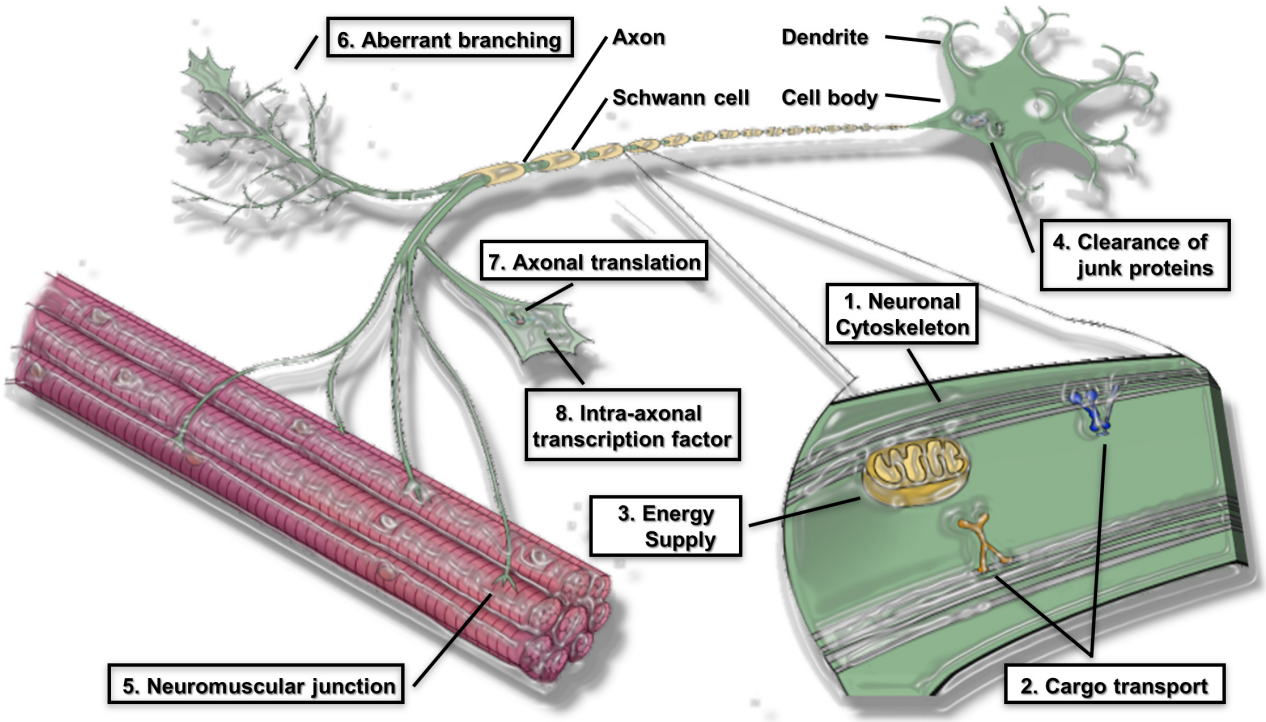

FIGURE 1 | Proposed pathomechanism of ALS in axon compartments. (1) Neuronal cytoskeleton; (2) cargo transport within axons; (3) axonal energy supply; (4) clearance of junk protein; (5) Neuromuscular junction (NMJs); (6) aberrant axonal branching; (7) Axonal translation; (8) Intra-axonal transcription factors are prominent features of the proposed pathomechanism.

neuronal morphology (Thiel et al., 2011). The *NEK1* gene was identified as a susceptibility factor for ALS (Brenner et al., 2016; Kenna et al., 2016). Using *in vivo* imaging, axonal degeneration was identified as an early event in the *SOD1* and *C9ORF72* repeat expansion mouse models of ALS (Tian et al., 2016). Neurofilament L transcripts are reduced in ALS (Bergeron et al., 1994). Neurofilaments are also found in a spheroid structure (large axonal swelling) (Corbo and Hays, 1992). Neurofilament light (NFL) and phosphorylated neurofilament heavy (pNFH) are also known as biomarkers for ALS (Brettschneider et al., 2006; Steinacker et al., 2016).

Thus, a dysfunctional cytoskeleton plays a role in ALS pathogenesis.

Cargo Transport Within Axons

Maintenance of the function and structure of all types of cells in mammals requires the intracellular transport of cargo. This transport is especially important in neurons because of their axonal and cell body polarization (De Vos and Hafezparast, 2017). Proteins and mRNA, as well as organelles, are generally synthesized in the soma and transported along the axon. Proper transport is required for the distribution of this cargo at the right time and place in the axon. Using electron microscopy of autopsy samples from ALS cases, defects in the cargo transport within axon transport in ALS have been observed. The studies of this transport defect revealed that the proximal axons of large MNs harbor abnormal accumulation of mitochondria, phosphorylated neurofilaments, and lysosomes (Hirano et al., 1984a,b; Okada et al., 1995; Rouleau et al., 1996). In addition, spheroids present in the axons contain different types of vesicles, lysosomes, mitochondria, neurofilaments, and microtubules (De Vos and Hafezparast, 2017). The accumulation of phosphorylated neurofilaments at the initial segment of MN axons is a major pathological characteristic of ALS (Ackerley et al., 2004; Brady and Morfini, 2017).

Aberrant cargo transport within axons occurs early in ALS disease progression (Williamson and Cleveland, 1999; De Vos et al., 2007). For example, an altered transport of mitochondria in axons has been demonstrated in two different mutant *SOD1*-G93A transgenic mouse models of ALS (Magrane et al., 2014). The slow anterograde transport of cytoskeletal components is decreased during the months prior to the initial neurodegeneration in mutant *SOD1*-G37R transgenic mice, a change that has been exhibited using metabolic labeling studies (Williamson and Cleveland, 1999). In mutant *SOD1*-G93A transgenic mouse models, inhibiting p38 MAPK α rescues retrograde cargo transport defects within axons (Gibbs et al., 2018).

TDP-43 functions as an mRNA transporter across the axonal cytoskeleton, and ALS-related mutations in TDP-43 alter this transport function (Alami et al., 2014). Mitotracker and Lysotracker experiments in *FUS*-mutant iPSC-derived MNs have demonstrated that defects in the cargo transport within axons can be rescued by histone deacetylase 6 inhibition (Guo et al., 2017).

TABLE 1 | Motor neuron disease-associated mutations and axonal pathology.

Disease	Gene	Protein	Axonal pathology
ALS1	SOD1	Superoxide dismutase 1	Impaired transport of mitochondria, microtubule stability, modulation of motor proteins via p38 MAP kinase etc.
ALS2	ALS2	Alsin	Impaired endocytic trafficking, signaling endosomes
ALS5/SPG11	SPG11	Spatacsin	Axonal destabilization, reduced tubulin acetylation, reduced anterograde vesicle transport
ALS6	FUS	FUS	Defective transport of mitochondria, aberrant microtubule acetylation, NMJ deformity, aberrant axon branching, Fos-B overexpression
ALS8	VAPB	Vesicle-associated membrane protein-associated protein B	Impaired transport of mitochondria and vesicles
ALS10	TARDBP	TAR DNA-binding protein 43	Defective transport of mitochondria and mRNP granules; reduced expression of dynactin 1; aberrant microtubule stability/acetylation
ALS17	CHMP2B	Charged multivesicular body protein 2B	Impaired endocytic trafficking, signaling endosomes
ALS12	OPTN	optineurin	Progressive dysmyelination and axonal degeneration through engagement of necroptotic machinery in the CNS, including RIPK1
ALS18	PFN1	Profilin I	Decreased bound actin levels and can inhibit axon outgrowth. Primary motor neurons expressing mutant PFN1 display smaller
ALS22	TUBA4A	Tubulin, alpha 4a	Destabilization of microtubules, general transport defect
ALS23	ANXA11	annexin AII	Molecular tether between lysosomes and RNA granules in axon
ALS25/SPGIO	KIF5A	Kinesin heavy chain	Reduced kinesin-1 mediated transport, impaired neurofilament transport
FALS/HMN7B/ Perry syndrome	DCTN1	Dynactin 1 (p150, glued homolog, Drosophila)	Altered axonal transport and vesicle trafficking, impaired signaling endosome trafficking
FTDALS1	C9orf72	C90RF72	Defective transport of mitochondria
SPG4	SPAST	Spastin	Destabilization of microtubules, impaired transport of mitochondria and vesicles
SPG30	KIF1A	Kinesin Family Member 1A	Reduced kinesin-3 mediated transport
SBMA	AR	Androgen receptor	Defective retrograde and anterograde transport, modulation of motor proteins via JNK

Modified from Maday et al. (2014); De Vos and Hafezparast (2017), and Ghasemi and Brown (2018). Also refer to OMIM (https://www.omim.org/) as of June 2019.

Mutations in the genes that code for the motor protein dynactin (*DCTN1*) (Puls et al., 2003) have been identified in the genetic analyses of familial ALS. Mutant dynactin binds weakly to microtubules, compared with the binding of wild-type proteins. ALS and slowly progressing, autosomal dominant, distal hereditary motor neuropathy in vocal paresis (HMN7B) are due to loss-of-function mutations in *DCTN1* (Puls et al., 2003; Munch et al., 2004; Yan et al., 2015). DCTN1 expression is also found to be downregulated in ALS-derived autopsy samples (Jiang et al., 2005).

Kinesin family member 5A (*KIF5A*) is a newly identified gene that plays a role in ALS (Brenner et al., 2018; Nicolas et al., 2018). Mutations that occur in the N-terminal motor domain of KIF5A cause an autosomal dominant type of hereditary spastic paraplegia known as spastic paraplegia (SPG)10, as well as Charcot–Marie–Tooth disease type 2 (Fichera et al., 2004). In contrast, mutations associated with ALS are mainly found in the C-terminal domain, which is important for binding cargo. Patients with loss-of-function *KIF5A* mutations have longer survival times than those with typical ALS (Brenner et al., 2018; Nicolas et al., 2018). Mutations in *KIF5A*, as well as *KIF1A*, which are loss-of-function mutations, are present in the motor or neck domains (Ebbing et al., 2008; Citterio et al., 2015).

In addition to MNs, mature sensory axons also possess a complex series of mRNA. A microtubule-stabilizing agent, paclitaxel, which impairs cargo transport within axons, results in sensory neuropathy (Gumy et al., 2011). Defects in the cargo transport within axons are common to various neurodegenerative diseases. Impaired cargo transport in axons can cause neurodegeneration (Millecamps and Julien, 2013).

Axonal Energy Supply

The mitochondria play an important role in meeting the axonal energy demand as they generate ATP through oxidative phosphorylation (Chamberlain and Sheng, 2019). Following their synthesis in the cell body, the mitochondria enter the axon where they undergo robust trafficking and accumulate at the nodes of Ranvier to meet metabolic needs (Zhang et al., 2012). Disruption of the mitochondrial activity, transport proteins, and microtubule association likely leads to dysfunctional mitochondrial transport in neurodegenerative diseases. Energy deficits in injured axons are caused by damage to the mitochondria following damage to axons, a decrease in mitochondrial transport in axons of mature neurons, and an increased energy consumption (Zhou et al., 2016). During regeneration, the axons adapt to this increased energy demand by changing the dynamics of the mitochondria (Kiryu-Seo and Kiyama, 2019). Mutations in *RAPGEF2* mutations impair microtubule stability and the mitochondria distribution in axons (Heo et al., 2018). Reduction in mitochondrial Rho GTPase 1 (Miro 1), the outer mitochondrial membrane protein, leads to anterograde axonal transport defects (Moller et al., 2017). The imbalance between mitochondrial fission and fusion leads to abnormal mitochondrial morphology, underlies axonal damage, and is

a potential therapeutic target for treating SPG15 and SPG48 (Denton et al., 2018). The ER and mitochondria form complex sites of interactions known as mitochondria-associated membranes (Gentile et al., 2019). Decreased ER-mitochondria association can occur as a result of loss-of-function mutations in *SIGMAR1*, leading to impaired retrograde transport and, ultimately, to axonal degeneration and MN death (Bernard-Marissal et al., 2015; Watanabe et al., 2016).

Astrocytes and oligodendrocytes may meet the axonal energy demand (Kang et al., 2010; Lee et al., 2012; Morrison et al., 2013). A deficiency in monocarboxylate transporter 1 (MCT1) was observed in oligodendroglia in the ventral cord of *SOD1* transgenic mice and in the motor cortex of ALS patients (Kang et al., 2013; Philips et al., 2013). The removal of the *SOD1* mutation from oligodendroglial precursor cells was observed to result in marked attenuation of the progression of the disease (Kang et al., 2013). Reducing the expression of *MCT1* in oligodendroglia is the pathomechanism involving the energy supply that contributes to MN degeneration in ALS.

Clearance of Junk Protein

The ubiquitin proteasome and autophagy clearance systems are significant homeostatic processes engaged in eliminating defective organelles and aggregated proteins throughout the life span of the neuron. Impairment of the ubiquitin proteasome degradation system in MNs has been reported to replicate the ALS phenotype in mice (Tashiro et al., 2012). Mice with MN-specific, conditional knockout of the proteasome subunit *Rpt3* exhibit locomotor dysfunction, progressive MN loss, and gliosis (Tashiro et al., 2012). Constitutive autophagy in neurons also maintains cellular homeostasis by balancing the synthesis and degradation of proteins, particularly within the distal axonal processes (Maday and Holzbaur, 2016). Several genes, such as *valosin-containing protein*, are involved in the protein degradation process (Johnson et al., 2010).

What about in the axon fraction? Disruption of the endosomal-lysosomal system due to ALS2/Alsin loss exacerbates the phenotype of *SOD1*-H46R transgenic mice by accelerating the accumulation of misfolded proteins and immature vesicles in the spinal cord (Hadano et al., 2010). In the early symptomatic and even presymptomatic *SOD1*-H46R transgenic mice, degenerating and swollen spinal axons with the accumulation of autophagosome-like vesicles have been observed (Hadano et al., 2010). A recent study also reported impairment of the degradation of autophagic vacuoles that engulf damaged mitochondria from distal axons in the *SOD1*-G93A transgenic mouse model (Xie et al., 2015). The clearance of dysfunctional mitochondria from axons may be mediated by syntaphilin, a mitochondria-anchoring protein, which is expressed at high levels in the early disease stages of ALS in MNs (Lin et al., 2017). *FUS* mutation causes axonal retention of the FUS protein prior to its aggregation, which is caused by poly(ADP-ribose) polymerase-dependent DNA response signaling (Naumann et al., 2018). The authors of this review also observed the accumulation of mutant FUS protein in the neurites of *FUS*-mutant induced pluripotent stem cell (iPSC)-derived MNs (Akiyama et al., 2019).

Optineurin (*OPTN*) mutations are implicated in both familial and sporadic ALS (Maruyama et al., 2010). OPTN binds to ubiquitin and regulates NFκB activation and apoptosis (Nakazawa et al., 2016). OPTN is also involved in several selective autophagy processes regulated by TBK1 (Li et al., 2016). Receptor-interacting kinase (RIPK) 1-dependent signaling is suppressed by OPTN through the regulation of its turnover (Ito et al., 2016). OPTN loss leads to progressive demyelination and axonal degeneration through the activation of necroptotic machinery in the central nervous system (CNS) (Ito et al., 2016). These observations suggest that RIPK1 and RIPK3 are significant in the process of progressive axonal degeneration.

A novel variant in *UBQLN4* compromises motor axon morphogenesis in zebrafish, impairing the proteasomal function (Edens et al., 2017; Morrice et al., 2018). Based on these reports, the clearance of junk protein is important in the compartment of the MN axon.

NMJs

Amyotrophic lateral sclerosis can be redefined as a distal axonopathy disease, because many molecular changes influencing MN degeneration occur at the NMJ (Moloney et al., 2014). The NMJ is a highly specialized synapse, that controls signals between muscles and nerves for skeletal muscle function. Neuromuscular remodeling precedes loss of the motor unit in the mutant *SOD1*-G37R transgenic mouse model (Martineau et al., 2018).

Certain molecules, including galectin-1 (Ferraiuolo et al., 2007; Plachta et al., 2007), CD44 (Schmidt et al., 2011), and amyloid precursor protein (Bryson et al., 2012), affect the function of NMJ. Axon guidance molecules affecting the stability of the cytoskeleton, such as Semaphorin 3A (Venkova et al., 2014), Ephrin A4 (Takata et al., 2013), and Nogo-A (Pradat et al., 2007), have been reported to alter the function of the NMJ in the early stage of ALS. The loss of mitofusin 2 in neurons causes NMJ dysfunction, whereas the upregulation of mitofusin 2 ameliorates the phenotype of mutant *SOD1*-G93A transgenic mice (Wang et al., 2018).

The expression of mutant *FUS* or *FUS* knockdown in zebrafish results in the impairment of motor activity and reduces quantal transmission at NMJs, indicating loss and gain of function of FUS (Armstrong and Drapeau, 2013). These changes in FUS culminate in presynaptic dysfunction at the NMJ (Armstrong and Drapeau, 2013). There is evidence that FUS plays multiple roles in the nucleus and axonal compartments involved in NMJ maintenance and axonal transport (Schoen et al., 2015; So et al., 2018). FUS mediates the regulation of acetylcholine receptor transcription at NMJ and is dysregulated in ALS (Picchiarelli et al., 2019).

C9ORF72 was identified on the presynaptic side where the protein interacts with Rab3 protein family members, suggesting that it has a role in the regulation of synaptic vesicle functions as a guanine nucleotide exchange factor (Frick et al., 2018).

In *Drosophila*, the protein Arc1 is a component of the capsid-like structures that bind *DARC1* mRNA in neurons. These capsids are included in the extracellular vesicles that are transferred across the NMJ from MNs to the muscle cells (Ashley et al., 2018).

The transport of mRNA across the NMJ via these retrovirus-like capsids and extracellular vesicles is required for synaptic plasticity (Ashley et al., 2018). Dipeptide repeat proteins related to C9ORF72 spread between cells *in vitro* and *in vivo* (Westergard et al., 2016). Tau is another protein that is transported from donor cells to recipient cells through the cell culture medium (Wu et al., 2016b). Evidence suggests that the mechanism of pathogenic molecular transfer, termed the prion hypothesis, may be activated in the extracellular space and across the NMJ synapses during degeneration of the motor cortex with centrifugal spreading (Furukawa et al., 2011; Nonaka et al., 2013; Porta et al., 2018).

Aberrant Axonal Branching

Axonal branching is a fundamental mechanism of nervous system neuroplasticity (Menon and Gupton, 2018). Accumulating evidence suggests that aberrant axonal branching is involved in the pathomechanisms of ALS.

Overexpression of mutant human *TARDBP* in zebrafish embryos induces a phenotype that includes shorter MN axons, premature and increased branching, and abnormal swimming (Kabashi et al., 2010). On the other hand, overexpression of progranulin rescues mutant *TARDBP*-induced aberrant axonal branching and short axonal outgrowth (Laird et al., 2010).

Injection of morpholino antisense oligonucleotides to inhibit the translation of target mRNA and to knock down *SMN* in zebrafish embryos significantly increases MN branching (McWhorter et al., 2003). C9ORF72 modulates the activity of the small GTPases, resulting in increased activity of LIM kinases 1 and 2 and regulation of axonal actin dynamics (Sivadasan et al., 2016). Various actin isoforms are expressed in primary mouse MNs, and their transcripts have been observed to be translocated into axons (Moradi et al., 2017). It is proposed that short hairpin RNA-mediated depletion of α-*actin* reduces axonal filopodia dynamics and disrupts collateral branch formation in developing MNs (Moradi et al., 2017).

Temporary overexpression of human cyclin-F (*CCNF)* in zebrafish embryos increases the levels of cleaved caspase-3 and cell death in the spinal cord. The mutant *CCNF* zebrafish also developed an MN axonopathy, which consists of shortened primary MN axons and an increased frequency of aberrant axonal branching (Hogan et al., 2017).

A recent study reported that MNs cultured from mutant *SOD1*-G93A transgenic mouse models exhibit enhanced axonal outgrowth and dendritic branching (Osking et al., 2019). As the level of branching does not correlate with the severity of the disease, in this study, the authors concluded that axonal branching does not affect the disease process. Increased synaptic activity or branching is considered desirable in the field of psychiatric disease (Shao et al., 2019). The authors of the present review identified aberrant axonal branching in *FUS*-mutant iPSC-derived MNs (Akiyama et al., 2019). The sensory axons branching in the presence of nerve growth factor (NGF) can be observed at sites marked by stalled mitochondria. NGF promotes branching through the generation of ATP and active axonal translation of mRNA (Spillane et al., 2013). The mechanism underlying mitochondrial stalling and growth factor distribution in MNs requires examination.

The meaning of axonal branching might be different in each stage of the development (Jung et al., 2012). In the embryonic stage, axon pathfinding and synaptic formation are important. However, in the developed stage, aberrant axon branching might have a disadvantage in terms of normal function of signal transmission. The significance of aberrant axonal branching in the neurodegenerative model *in vivo* has not yet been elucidated.

OMICS PROFILING OF THE AXONAL COMPARTMENT

The previous section provided an overview of the important pathomechanisms of MN axons. These pathomechanisms have been found to influence each other and cannot be entirely separated. This section reviews the omics analysis of the axon compartment in order to obtain an overall understanding of this complex process occurring in an important region of the neuron.

Lessons From Different Nervous Systems

The rationale for conducting omics analysis of the axon compartment is as follows (**Table 2**). Surprisingly complex, constantly changing transcriptomes are present in mature axons. Thus, axonal mRNA localization is likely to be tightly regulated and to play multiple roles. The ribosomal protein S6 has been observed with immunoelectron microscopy in the axons of embryonic sympathetic and hippocampal neurons grown *in vitro* (Tcherkezian et al., 2010), indicating that local mRNA translation also occurs in growing axons. Further, the local translation of proteins from mRNAs selectively transported from the soma to the synaptic terminal appears to be involved in the regulation of axon outgrowth and regeneration (Zheng et al., 2001; Taylor et al., 2009).

Elucidation of what features of axonal function require local translation and determination of the mRNAs that mediate these functions have induced intriguing challenges in the field of axonal biology (Deglincerti and Jaffrey, 2012; Jung et al., 2012). Assessment of the axonal transcriptome using microarray studies has identified important axonal mRNAs and has demonstrated the complexity and dynamic nature of the axonal transcriptome (Zivraj et al., 2010; Gumy et al., 2011).

In a pioneering study involving omics analysis in axons, more than 200 different mRNAs were identified with cDNA microarray analysis in axons derived from rat with injured sensory neurons (Willis et al., 2007). Proteins involved in the transcription, synthesis of proteins, intracellular transport, calcium metabolism, mitochondrial functions, and cytoskeletal functions were identified in the study (Willis et al., 2007). The report raised several important questions regarding axonal translation (Deglincerti and Jaffrey, 2012), including the question of why transcripts for nuclear proteins are localized to distal axons.

Using a microfluidic chamber enabling the isolation of axons without contamination with non-axonal material, mRNA has

TABLE 2 | Omics analyses of the axon compartment in *in vivo*, *ex vivo,* and *in vitro* models of several types of nervous systems.

Disease modeling	System	Cell resource	*Vivo/Vitro*	Methodology	Analysis	Core result	References
ALS	Motor	Human iPS-derived motor neuron	*in vitro*	Separating axon using microfluidics (Jiksak Bioengineering)	RNA sequencing	Increased level of Fos-B mRNA, the binding target of FUS, in FUS-mutant MNs. While Fos-B reduction using si-RNA or an inhibitor ameliorated the observed aberrant axon branching, Fos-B overexpression resulted in aberrant axon branching even in zebrafish model.	Akiyama et al., 2019
ALS	Motor	Mouse and human stem cell-derived spinal motor axons	*in vitro*	Microfluidics	RNA sequencing	Identified 3,500–5,000 transcripts in mouse and human stem cell-derived spinal motor axons, most of which are required for oxidative energy production and ribogenesis. Axons contained transcription factor mRNAs, e.g., Ybx1, with implications for local functions. In SOD1G93A mutant, identifying 121 ALS-dysregulated transcript, including Nrp1, Dbn1, and Nek1, a known ALS-causing gene.	Nijssen et al., 2018
No	Motor	hiPSC-derived motor neuron	*in vitro*	Permeable inserts culture device	RNA sequencing	Discriminate axonal and somatodendritic compartments	Maciel et al., 2018
No	Retina	Retinal ganglion cells (RGCs) exit from the eye primordia from Xenopus laevis embryos	*Ex vivo*	Axon grow through the 1 μm pores of the transfilter on the Boyden chamber	Pulsed stable isotope labeling of amino acids in cell culture (pSILAC) with ultrasensitive sample preparation technology termed single-pot solid-phase-enhanced sample preparation (SP3)	Axons stimulated by different cues (netrin-1, BDNF, Sema3A) showed distinct signatures with over 100 different nascent protein species	Cagnetta et al., 2018
ALS	Spinal	Dissociated spinal cord culture from ICR mice at E12.5	*Ex vivo*	Modified boyden chamber membrane culture system	RNA sequencing	Elavl2 and miR-146a, miR-126-5p, miR-99a are shared in axons of lentiviral overexpression of both p.A315T TARDBP and p.G93A SOD1 mutants.	Rotem et al., 2017
No	Neuron	Differentiated neurons from human ESC	*in vitro*	Microfluidics	Microarray	Confirmed the presence of two well characterized axonal mRNAs in model organisms, β-actin and GAP43, within hESC-neuron projections. oxytocin mRNA localized to these human projections and confirmed its localization using RNA-FISH.	Bigler et al., 2017
No	Motor	Isolated motor neuron from E12.5 CD-1 mouse spinal cord using p75NTR antibody panning	*Ex vivo*	Xona microfluidics, SND 150 chamber	RNA sequencing	Double-random priming transcriptome methods enable to serially diluted total RNA down to 10 pg	Briese et al., 2016
No	Retina	Retinal ganglion cells (RGCs) of mouse	*in vivo*	Axonal translatome using Axon-TRAP-RiboTag mouse and IP of ribosome mRNAs	*in vivo* axonal translatome	The embryonic to postnatal axonal translatome comprises an evolving subset of enriched genes with axon-specific roles, suggesting distinct steps in axon wiring, such as elongation, pruning, and synaptogenesis. Adult axons have a complex translatome with strong links to axon survival, neurotransmission and neurodegenerative disease.	Shigeoka et al., 2016

TABLE 2 | Continued

Disease modeling	System	Cell resource	*Vivo/Vitro*	Methodology	Analysis	Core result	References
SMA	Motor	Isolated motor neuron from E12.5 CD-1 mouse spinal cord using p75NTR antibody panning	*Ex vivo*	Xona microfluidics, SND 150 chamber	Microarray	Knockdown of SMN, the protein deficient in spinal muscular atrophy, produced a large number of transcript alterations in both compartments. Transcripts associated with axon growth and synaptic activity were down-regulated on the axonal side of smn- deficient motor neurons.	Saal et al., 2014
No	Retina	DRG explants dissected from embryonic (E16) and adult (3–5 mo old) from Sprague Dawley rats	*Ex vivo*	Compartmentalized chamber to isolate mRNA from pure embryonic and adult sensory axons devoid of non-neuronal or cell body contamination	Genome-wide microarray	Tubulin-beta3 (Tubb3) mRNA is present only in embryonic axons, with Tubb3 locally synthesized in axons of embryonic, but not adult neurons where it is transported	Gumy et al., 2011
No	Retina	Retinal ganglion cell (RGC) axons of two vertebrate species, mouse and Xenopus	*Ex vivo*	Laser capture microdissection (LCM) to isolate the growth cones	Coupled with unbiased genomewide microarray profiling.	Many presynaptic protein mRNAs are present exclusively in old growth cones. ome receptor transcripts (e.g., EphB4), present exclusively in old growth cones, were equally abundant in young and old cell bodies.	Zivraj et al., 2010
No	Cortical	Cortical and hippocampal dissociated neurons from embryonic Sprague Dawley rats at E18	*Ex vivo*	Microfluidic chamber with microgrooves (7.5 μm wide, 3 μm high)	Microarray	Axonal transcripts are enriched for protein translational machinery, transport, cytoskeleton, and mitochondrial maintenance.	Taylor et al., 2009
No	Motor	Primary DRG cultures from L4-5 were prepared from Sprague Dawley rats that had been injury conditioned 7 days before by sciatic nerve crush at midthigh level	*Ex vivo*	Dissociated DRGs were plated into tissue culture inserts containing porous membranes (8-μm pores). Axons were isolated after 16-20 h in culture by scraping away the cellular content from the upper or lower membrane surfaces	cDNA microarray	Neurotrophins (nerve growth factor, brainderived neurotrophic factor, and neurotrophin-3) regulate axonal mRNA levels and use distinct downstream signals to localize individual mRNAs.	Willis et al., 2007

been purified from mature CNS axons (Taylor et al., 2009). The same study also described the localization of catenin-β1 and neurexin-3 mRNA with fluorescence *in situ* hybridization in the axonal compartment (Taylor et al., 2009). The somatodendritic compartments are enriched in transcripts with postsynaptic functions and in nuclear non-coding RNAs such as *7SK*, whereas transcripts related to translation such as*7SL*, the cytoplasmic non-coding RNA, are upregulated in the compartment of the axon fraction (Briese et al., 2016).

Transcriptome-wide analyses have revealed numerous transcripts encoding transmembrane or secreted proteins, which comprise about 13% of the total mRNAs found in growth cones (Zivraj et al., 2010). Transcripts present in axons encode many transmembrane proteins, such as integrins and protocadherins, which are cell adhesion molecules, and EphB4 and Nrp2, which are guidance receptors (Zivraj et al., 2010). Thus, local translation may change the cell adhesion capacity of axons and allow axons to respond to extracellular signaling molecules (Gumy et al., 2011). Axons also contain transcripts that code for secreted proteins, including semaphorin and ephrin, which are guidance molecules; BMP1, CTGF, and FGF, which are growth factors; and collagen and TIMP3, which compose and regulate the extracellular matrix. Thus, it is expected that local translation probably plays a role in the regulation of extracellular components by affecting proteins that are secreted from growth cones (Deglincerti and Jaffrey, 2012). Axons also contain structures that resemble the ER and Golgi. Specific labeling of the ER and Golgi exhibits irregular, punctate staining along the axon, suggesting that axon-specific versions of these organelles may be present in nerve terminals (Merianda et al., 2009).

The development of compartmentalization has enabled the examination of axon pathology in MN diseases. The knockdown of *SMN*, which encodes the protein that is deficient in spinal muscular atrophy (SMA), was shown to produce numerous transcript alterations in both axon and somatic compartments of the microarray (Saal et al., 2014). Transcripts associated with axon growth and synaptic activity are downregulated on the axonal side of *SMN*-deficient MNs. Improvements in the handling of small quantities of RNA have led to further progress in this field (Briese et al., 2016).

Evaluation of cultured spinal cord neurons grown with a compartmented platform and subjected to next-generation sequencing technology revealed that mRNAs and miRNAs are differentially expressed in the somatic compared with the axonal neuronal compartments (Rotem et al., 2017). In axons with lentiviral overexpression of p.A315T *TARDBP* or p.G93A *SOD1* mutants, *Elavl2*, *miR-146a*, *miR-126-5p*, and *miR-99a* are commonly expressed. Examination of the local transcriptome revealed that the most abundant mRNAs within human embryonic stem cell-derived neuronal projections are functionally similar to the rat axonal transcriptome of cortical neurons (Bigler et al., 2017).

The use of microfluidic technology has been particularly useful in neuroscience research. Microfluidic platforms have allowed researchers to address specific questions related to axonal guidance, synapse formation, and cargo transport within axons, and led to the development of three-dimensional (3D) CNS models for pharmacological testing and drug screening (Neto et al., 2016). Human iPSC-derived MNs grown in a culture device with permeable inserts were observed to produce large amounts of enriched axonal material that can be harvested for RNA isolation and sequencing (Maciel et al., 2018). Transcriptome profiling has revealed axonal and somatodendritic compartment-specific expression.

Recently, Nijissen and colleagues developed a refined method named Axon-seq, combining microfluidics, RNA sequencing, and bioinformatics analysis (Nijssen et al., 2018). These results demonstrated that the transcriptome of the axon compartment is quite different from that of the soma and includes a smaller number of mRNAs. They identified up to 5,000 mRNAs in mouse and human stem cell-derived MN axons; the functions of the majority of these are oxidative energy and ribosome production. Axons contain transcription factor mRNAs, implicating local functions. Investigation into the response of degenerated ALS motor axons to the *SOD1*-G93A mutation identified 121 ALS-dysregulated transcripts. Among these, *Nrp1* and *Dbn1* are involved in axonal function, and *Nek1* is a known ALS-causative gene (Brenner et al., 2016; Kenna et al., 2016; Nijssen et al., 2018). Axon-seq is an advanced technique for sequencing the RNA in axons, and thus can provide enhanced knowledge about peripheral nerve biology to explain the vulnerability/resilience of MN (Nijssen et al., 2017; Allodi et al., 2019) and to identify the treatment of MN diseases.

Development of a Microfluidic Device for Larger-Scale Omics Analysis

Despite the improvement offered by the microfluidic device, harvesting a sufficient volume of lysate from the axon compartment remains challenging. In the process of improving the dimensions of the well and materials, a novel microfluidic device was developed by the authors of this study (**Table 3**). The device enabled comparison of two sets of isogenic *FUS*-mutant iPSC-derived MNs generated using genome editing technology (Joung and Sander, 2013; Okano and Yamanaka, 2014), and provided observations of increased branching in *FUS*-mutant MN axons compared with those in isogenic controls (Akiyama et al., 2019). This phenotype was confirmed using other ALS-causative mutations, including *SOD1* and *TARDBP*. Combining this innovative microfluidic device (Kawada et al., 2017) with hiPSC-derived MN organoids further revealed the entire *in vitro* profile of the human MN axons. This technique identified increased *Fos-B* mRNA as a binding partner of FUS and as a causative event for aberrant axon morphology both *in vitro* and *in vivo*.

Morphological changes in MN axon branching have been found to precede MN death in the mutant *SOD1*-G93A transgenic mouse model (Tian et al., 2016), and abnormal neural branching has been detected in zebrafish that overexpress mutant *FUS* (Armstrong and Drapeau, 2013). Improvements in axon morphology following suppression of abnormally upregulated *Fos-B* in *FUS* mutants suggested a novel therapeutic candidate for *FUS*-mutant ALS.

TABLE 3 | Comparison of our microfluidic devices with those of previous studies.

	Neuron device	Modified boyden	Nerve organoid device
Company	Xona Microfluidics	Corning	Jiksak Bioengineering
Dimension	2 D	2 D	3 D (axon bundle)
Cell type	Primary mouse motor neuron	Primary mouse motor neuron	iPSCs derived motor neuron
Pore size	1∼3 um	3 um	150∼200 um
Axon length	150 um	NA	10,000 μm (1 cm)
Retrievable neurons	∼10*3	5 × 10*5	10*4-
RNA	20 pg-	0.3 ng/μl	12 ng (l ng/μl) -
References	Briese et al., 2016; Bigler et al., 2017; Nijssen et al., 2018, etc.	Rotem et al., 2017; Maciel et al., 2018, etc.	Akiyama et al., 2019; Kawada et al., 2017

Previous studies have also reported that upregulation of *Fos-B* mRNA is associated with increases in spines (Lafragette et al., 2017; Cahill et al., 2018) and growth cones (Anastasiadou and Knoll, 2016). δ*Fos-B* modulates immature spines of the nucleus accumbens in a model of drug addiction (Grueter et al., 2013). Certain chemical stimulators such as kainic acid lead to neurodegeneration via upregulated expression of immediate early genes, including that of *Fos-B* (Pereno et al., 2011). The hyperexcitability hypothesis is a major theme in proposing the pathomechanism of ALS (Wainger et al., 2014). A recent report of activator protein-1 (AP-1) and MN degeneration in the mutant *SOD1*-G93A transgenic mouse model has attracted attention (Bhinge et al., 2017). Additionally, the suppression of dual leucine zipper kinase, the upstream signal protein for c-Jun (AP-1 family member), may become a therapeutic target for ALS (Bhinge et al., 2017). Although substantial differences have been reported in *SOD1*-ALS compared with *FUS*-ALS and *TARDBP*-ALS (Fujimori, 2018), *SOD1*-, *TARDBP*-, and *FUS*-mutant MNs have common features, suggesting a role for AP-1 in the neurodegeneration observed in ALS. The Fos-B protein accumulates abnormally in the MNs of ALS patients, including in sporadic cases. Thus, Fos-B appears to be a potential therapeutic target molecule.

The novel microfluidic device described in the preceding paragraph comprises a large canal that enables the collection of sufficient samples of isolated MN axons for RNA sequencing (Kawada et al., 2017). This device has proven useful in visualizing the global profile of the axon compartment. Although other types of microfluidic devices, some of which are specific to cell fraction analysis, are available on the market (Briese et al., 2016; Rotem et al., 2017), they are typically restricted by the limited amount of specimen obtained (**Table 3**). As only a very small amount of specimen can be analyzed, variation in conditions, such as cell purity and culture procedures, may influence the results. Kawada's microfluidic device enables analysis with fewer technical biases because it involves the collection of large amounts of macroscopically observable axon bundles. RNA profiles from the axon samples have reproduced the previously reported profiles of the MN axon (Briese et al., 2016; Rotem et al., 2017), justifying the methodology of this novel device. Furthermore, the data obtained may provide important resources for the subcellular fractional analysis of stem cell-derived MN axons.

Are These mRNAs Translated in Axons?

An important question is whether these mRNAs are translated in axons or transported to the nucleus/cell body. The importance of axonal translation for CNS maintenance is under debate (Spaulding and Burgess, 2017). Several types of mature polarized cells utilize asymmetrical mRNA localization as a means of synaptic communication with other types of cells (Xing and Bassell, 2013). *In vivo*, the longest axons, such as those of mature sensory and motor peripheral neurons, rely most strongly on mRNA transport and local translation to maintain homeostasis.

Upregulation of ribosome synthesis in axons has been found to occur early in the pathogenesis of both mutant *SOD1*-G93A transgenic mouse models and human ALS autopsy samples, which suggests the involvement of Schwann cells in ALS pathology and in aberrant axonal RNA metabolism (Verheijen et al., 2014). Gene expression analyses of the anterior branch of human obturator MNs biopsied from patients with ALS demonstrated upregulation of a cluster of genes that play important roles in biological processes involving RNA processing and protein metabolism (Riva et al., 2016).

Direct evidence for neurodegeneration has been obtained from the observation of mRNA transport dysregulation due to mutations in the RBP SMN1, which causes SMA (Wang et al., 2016b). SMN is present ubiquitously, and its deletion is lethal. However, MNs are more sensitive to SMN reduction than other cell types, possibly because reduced SMN decreases the axonal localization of several mRNAs (Rage et al., 2013) and inhibits the activity of the mammalian target of rapamycin in axons (Kye et al., 2014). An additional role for SMN is in the regulation of axonal localization and local translation of *growth-associated protein 43* (*GAP43*) mRNA in growth cones (Fallini et al., 2016). The overexpression of two mRNA-binding proteins, HuD and IGF2 mRNA-binding protein 1, restores the mRNA and protein levels of GAP43 and has been shown to rescue the axon outgrowth defects in the neurons of an SMA patient (Fallini et al., 2016).

In previous studies, protein interaction screening intended to elucidate *FUS*-mutant phenotypes also identified several molecules that interact with FUS, including SMN (Yamazaki et al., 2012; Groen et al., 2013). Aberrant distribution of SMN in cytosolic FUS accumulations induces SMN reduction in axons. Accumulation of mutant human FUS induces an integrated stress response and reduces protein synthesis in nearby axons (Lopez-Erauskin et al., 2018).

Non-nuclear pools of splicing factor, proline-glutamine rich (SFPQ) are essential for normal motor development via local mRNA maintenance or processing, and the coiled-coil domain

of SFPQ is required for axonal localization (Thomas-Jinu et al., 2017). The RBPs modulate nuclear processing, intracellular transport, and local translation of target mRNAs for an accurate spatial and temporal gene expression. SFPQ functions as an RBP because it binds to and modulates numerous neuronal mRNAs, including in cells, such as dorsal root ganglion neurons. SFPQ, which has been identified by subcellular compartmentalization analysis (Cosker et al., 2016; Takeuchi et al., 2018), has been found to orchestrate spatial gene expression, which is essential for axonal viability.

Local translation is also involved in several neurodevelopmental disorders (Batista and Hengst, 2016). Local translation defects are associated with fragile X mental retardation and autism spectrum disorders (Kelleher and Bear, 2008). Fragile X mental retardation protein, which is present in dendritic spines, growth cones, and axons, modulates plasticity (Bassell and Warren, 2008) and the presynaptic proteome (Christie et al., 2009; Akins et al., 2012). In mouse brain slices, loss of the fragile X mental retardation protein was found to perturb the development of presynaptic nerve terminals (Hanson and Madison, 2007).

Degeneration of motor axons results from mutations in various tRNA synthetases, which is consistent with the notion that local translation of transported mRNA is necessary for axonal homeostasis (He et al., 2015; Storkebaum, 2016). Recently, cytoplasmic polyadenylation element-binding protein 4 was found to orchestrate the dysregulation of mRNA expression in autism (Parras et al., 2018). Identification of a master regulator of RNA metabolism would be beneficial in understanding and treating for both diseases that affect MNs and psychiatric diseases.

Nascent chain tracking is a novel technique for visualizing local translation. This method uses multi-epitope tags and antibody-based fluorescent probes to quantify the dynamics of protein synthesis at the level of individual mRNAs (Morisaki et al., 2016). Due to its sensitivity and versatility, nascent chain tracking is a useful tool for quantifying mRNA translation kinetics. Synaptic activity can induce mRNA localization and the local translation of β-actin, which stabilizes expanding synapses at dendritic spines (Wu et al., 2016a; Yoon et al., 2016). Real-time visualization of mRNA translation in the axonal compartment is an innovative method enabling analysis of axonal pathology *in vivo* (Wang et al., 2016a; Yan et al., 2016). The inducible fluorescent probe can be regulated in time and space in neurons and is used to examine the maturation of miRNA. The local maturation of miRNA by synaptic stimulation results in a spatially restricted protein synthesis reduction from the mRNA (Sambandan et al., 2017). The proteomics approach described in a later section adds to the understanding of the global change of nascent proteins produced in the axon fraction.

Role of Intra-Axonal Transcription Factors

Why transcripts for nuclear proteins are localized to the distal axons is a big question raised by the omics analysis. Fos-B, a mediator of abnormal axonal branching in *FUS*-mutated MNs, is a transcription factor. Another research group also reported dysregulated transcription factors in ALS MNs (Nijssen et al., 2018). In determining the role of transcription factors in the axon compartment, a comprehensive transcription of the action fraction has identified mRNAs encoding a larger amount of transcription factors and co-factors (Ji and Jaffrey, 2014). One example is that of axonal STAT3, which is translated locally, activated upon nerve injury, and is transported retrogradely with dynein and importin α5, modulating the survival of peripheral sensory neurons (Ben-Yaakov et al., 2012). Recently, *Tp53inp2* was reported to be an atypical mRNA regulating axon growth by enhancing the NGF-TrkA pathway independently with translation (Crerar et al., 2019). Importantly, data have indicated that axonal degeneration shared early molecular change in the neurodegenerative process of neurological disorders in aged populations (Dadon-Nachum et al., 2011; Tagliaferro and Burke, 2016; Salvadores et al., 2017).

In the brain of a person with Alzheimer's disease, inhibition of local translation of *Atf4* mRNA overproduction eliminates amyloid β-induced cell loss (Baleriola et al., 2014; Peng et al., 2016). *Atf4* mRNA translation is controlled by phosphorylation of elongation initiation factor 2a, pivotal for an integrated stress response (Batista and Hengst, 2016). The role of axonal transcription factors in relation to translated proteins and non-translated RNA requires further elucidation.

Interaction Among the Mechanisms Already Described

The hallmark feature in the majority of autopsy cases of ALS is nuclear depletion and cytoplasmic accumulation of TDP-43 in degenerated neurons (Kim and Taylor, 2017). Thus, dysfunctional trafficking between the nucleus and cytoplasm likely plays a role in the pathology of ALS (Nedelsky and Taylor, 2019) and may also be important in normal physiological aging, Huntington's disease, and Alzheimer's disease (Nedelsky and Taylor, 2019). RBPs with prion-like domains (PrLDs) undergo liquid-liquid phase separation to form functional liquids, which can be converted into abnormal hydrogels that contain pathological fibrils that are often seen in neurodegenerative diseases. TDP-43, FUS, heterogeneous nuclear ribonucleoprotein A1 (hnRNPA1), and hnRNPA2 are nuclear RBPs with PrLDs that are incorrectly sent to cytoplasmic inclusions in neurodegenerative diseases. Mutations in PrLDs increase the rate of fibril formation and initiate disease (Guo et al., 2018). Karyopherin-β2, also known as transportin-1, binds the proline-tyrosine NLS and then blocks and reverses FUS, TATA-box-binding protein associated factor (TAF) 15, Ewing sarcoma RBP1 (EWSR1), hnRNPA1, and hnRNPA2 fibril formation. Importin-α and karyopherin-β1 also block and reverse TDP-43 fibril formation. Phase separation, like stress granule formation, is an emerging property of proteins containing PrLD such as FUS (Guo et al., 2018; Hofweber et al., 2018; Qamar et al., 2018; Yoshizawa et al., 2018). T-cell-restricted intracellular antigen-1 (TIA1) mutations were found to delay stress granule disassembly and to promote

the accumulation of granules harboring TDP-43 (Mackenzie et al., 2017). *C. elegans* TIAR-2/TIA protein functions cell autonomously to inhibit axon regeneration (Andrusiak et al., 2019). One of the important roles of phase separation is transcription enhancement (Sabari et al., 2018), which might be related to local translation/transcription. The association between axonal dysfunction and these cytoplasmic events, including phase separation, has not yet been elucidated.

There is emerging evidence of interactions among different processes of axonal pathology in ALS. Annexin A11 (ANXA11), a phosphoinositide-binding protein associated with the RNA granule, has the role of a molecular tether between lysosomes and RNA granules. Such tethering is impaired by the ALS-associated *ANXA11* mutation (Smith et al., 2017; Liao et al., 2019). Late endosome bearing mRNA encoding mitochondrial functional molecules stops at mitochondria and these mRNAs are translated on Rab7a endosomes locally in the axon (Cioni et al., 2019).

In summary, exactly how these complex mechanisms are influenced by each other is still unknown. There is a need for understanding how cytoskeletons are maintained, and how molecules are transported/metabolized/synthesized, or abolished when unnecessary. Elucidating the interaction of these mechanisms might answer the vital question of why MNs are vulnerable in ALS.

Advanced Omics Analysis and Further Consideration

Conducting a comprehensive analysis of the newly produced proteome from limited samples of subcellular compartments that are uncontaminated by the somatodendrite remains a major technical problem (Eichelbaum and Krijgsveld, 2014). Stable isotope labeling of amino acids in cell culture (SILAC) has been combined with single-well solid phase-enhanced sample prep. Using this method, the newly produced proteome of isolated retinal axons was obtained rapidly (in approximately 5 min) (Cagnetta et al., 2018). Treating axons treated with stimuli such as netrin-1, brain-derived neurotropic factor, and Sema3A, has demonstrated distinct proteomes with more than 100 different nascent proteins. Compartment analysis using pulsed SILAC may be applied to ALS cells with a sophisticated culture device.

Using an axon-TRAP-RiboTag approach in mice, the dynamic translatome of axons in the retina *in vivo* matches the subcellular function (Shigeoka et al., 2016). The translatome of the embryonic and postnatal axons includes a changing, enriched set of genes with axon-specific roles. Thus, specific steps in axon wiring, such as axon growth, elimination of unnecessary axons, and synaptogenesis, may be present. Adult axons harbor a complicated translatome that plays a role in axon survival, neurotransmission, and neurodegenerative diseases. Mating of several ALS mouse models can help in precisely understanding mRNA dysregulation. Further transcriptome and proteome analyses using labeled growth cones of single projections in the mouse cerebral cortex *in vivo* may also be of use (Poulopoulos et al., 2019). Spatial transcriptomics is another method for elucidating gene expression in the mouse spinal cord over the disease course, and in postmortem tissue from patients with ALS (Maniatis et al., 2019). Another important approach is the single-cell transcriptomics of nerve organoids *in vitro* (Quadrato et al., 2017); pseudo-time analysis or single-cell trajectory analysis can help establish the relationship between the cause and effect of the transcriptome of the organoids (Xiang et al., 2017; Klaus et al., 2019). Sophisticated neuromuscular co-culture organoids would be beneficial for these studies.

Stimulated Raman scattering microscopy is a new technique for chemical imaging that can be used to map the distribution of various molecules–including lipids, proteins, and nucleic acids–in live cells and tissues, as determined by their intrinsic molecular vibration (Freudiger et al., 2008). The authors of this review used this type of imaging to visualize peripheral degeneration in several ALS mouse models and human postmortem tissue (Tian et al., 2016). Non-labeled live imaging of motor axons may assist in monitoring the time course of axonal pathology *in vivo*.

In clinical settings, the strength-duration time constant, which represents the hyperexcitability of an MN axon, is significantly increased in patients (Kanai et al., 2006, 2012; Geevasinga et al., 2015). Hyperexcitability is thought to be the target of MN death in ALS (Wainger et al., 2014). In cell culture settings, the shortened isoform of TDP-43 is upregulated by neuronal hyperactivation (Weskamp et al., 2019). The role of these short isoform of TDP-43, which might be the product of dysregulation of RNA metabolism, should be considered in the axon fraction. Recent studies have revealed the importance of stathmin-2 (STMN2), a regulator of microtubule stability, in the pathomechanism of *TARDBP* mutation (Klim et al., 2019; Melamed et al., 2019). The expression of a microtubule regulator, *STMN2*, is decreased following *TARDBP* knockdown, when TDP-43 is mis-localized, and in MNs from patients and the spinal cord of postmortem samples. The reduced function of TDP-43 results in the loss of STMN2 due to altered splicing. This is functionally important, as STMN2 is necessary for the outgrowth and regeneration of MN axons. Post-translational STMN2 stabilization rescues neurite outgrowth and axon regeneration deficits by TDP-43 depletion (Klim et al., 2019). A reduction in TDP-43 inhibits axonal regeneration of iPSC-derived MNs, whereas rescue of the expression of STMN2 restores the axonal regeneration capacity (Melamed et al., 2019). The effect of the short form of TDP-43 or cryptic exons under the control of TDP-43 (Ling et al., 2015) should be examined in the axon fraction.

CONCLUDING REMARKS

As described in the preceding section, advanced omics approaches, *in vivo* analysis, and axon–cytoplasmic interactions should be examined as the next steps in investigating axonal pathology in neurodegenerative disease research. The novel concept of microfluidic devices, including the nerve organoid device presented by the authors of this review, should be applied to other neuron types, co-culture systems,

or proteomics analyses using human pluripotent cells, because this technique may help elucidate the resilience of long MN and the pathomechanism of ALS.

AUTHOR CONTRIBUTIONS

NS, TA, and MA prepared the manuscript. All authors read, revised, and approved the final version of the manuscript.

FUNDING

This work was supported by funding from Grant-in-Aid for Young Scientists (A) (15H05667), Grant-in-Aid for Scientific Research (C) (18K07519), and Grant-in-Aid for Scientific Research (B) (16H05318) from Japanese Ministry of Education, Culture, Sports, Science and Technology; the Research Project for Practical Applications of Regenerative Medicine from the Japan Agency for Medical Research and Development (AMED) (Grant number 19bm0804003h0003); Japan Intractable Diseases (Nanbyo) Research Foundation, the Kanae Foundation for the Promotion of Medical Science, and "Inochi-no-Iro" ALS research grant.

ACKNOWLEDGMENTS

The authors thank H. Okano, T. Fujii, J. Kawada, S. Mitsuzawa, and K. Eggan for the excellent comments, Y. Akiyama for the illustrations. The authors also would like to thank Enago (www.enago.jp) for the English language review.

REFERENCES

Ackerley, S., Grierson, A. J., Banner, S., Perkinton, M. S., Brownlees, J., Byers, H. L., et al. (2004). p38alpha stress-activated protein kinase phosphorylates neurofilaments and is associated with neurofilament pathology in amyotrophic lateral sclerosis. *Mol. Cell. Neurosci.* 26, 354–364. doi: 10.1016/j.mcn.2004.02.009

Akins, M. R., Leblanc, H. F., Stackpole, E. E., Chyung, E., and Fallon, J. R. (2012). Systematic mapping of fragile X granules in the mouse brain reveals a potential role for presynaptic FMRP in sensorimotor functions. *J. Comp. Neurol.* 520, 3687–3706. doi: 10.1002/cne.23123

Akiyama, T., Suzuki, N., Ishikawa, M., Fujimori, K., Sone, T., Kawada, J., et al. (2019). Aberrant axon branching via Fos-B dysregulation in FUS-ALS motor neurons. *EBiomedicine* 45, 362–378. doi: 10.1016/j.ebiom.2019.06.013

Alami, N. H., Smith, R. B., Carrasco, M. A., Williams, L. A., Winborn, C. S., Han, S. S. W., et al. (2014). Axonal transport of TDP-43 mRNA granules is impaired by ALS-causing mutations. *Neuron* 81, 536–543. doi: 10.1016/j.neuron.2013.12.018

Allodi, I., Nijssen, J., Benitez, J. A., Schweingruber, C., Fuchs, A., Bonvicini, G., et al. (2019). Modeling motor neuron resilience in ALS using stem cells. *Stem Cell Rep.* 12, 1329–1341. doi: 10.1016/j.stemcr.2019.04.009

Anastasiadou, S., and Knoll, B. (2016). The multiple sclerosis drug fingolimod (FTY720) stimulates neuronal gene expression, axonal growth and regeneration. *Exp. Neurol.* 279, 243–260. doi: 10.1016/j.expneurol.2016.03.012

Andrusiak, M. G., Sharifnia, P., Lyu, X., Wang, Z., Dickey, A. M., Wu, Z., et al. (2019). Inhibition of axon regeneration by liquid-like TIAR-2 granules. *Neuron* 104, 290–304.e8. doi: 10.1016/j.neuron.2019.07.004

Aoki, M., Ogasawara, M., Matsubara, Y., Narisawa, K., Nakamura, S., Itoyama, Y., et al. (1993). Mild ALS in Japan associated with novel SOD mutation. *Nat. Genet.* 5, 323–324. doi: 10.1038/ng1293-323

Armstrong, G. A., and Drapeau, P. (2013). Loss and gain of FUS function impair neuromuscular synaptic transmission in a genetic model of ALS. *Hum. Mol. Genet.* 22, 4282–4292. doi: 10.1093/hmg/ddt278

Ashley, J., Cordy, B., Lucia, D., Fradkin, L. G., Budnik, V., and Thomson, T. (2018). Retrovirus-like gag protein Arc1 binds RNA and traffics across synaptic boutons. *Cell* 172, 262–274.e11. doi: 10.1016/j.cell.2017.12.022

Balendra, R., and Isaacs, A. M. (2018). *C9orf72*-mediated ALS and FTD: multiple pathways to disease. *Nat. Rev. Neurol.* 14, 544–558. doi: 10.1038/s41582-018-0047-2

Baleriola, J., Walker, C. A., Jean, Y. Y., Crary, J. F., Troy, C. M., Nagy, P. L., et al. (2014). Axonally synthesized ATF4 transmits a neurodegenerative signal across brain regions. *Cell* 158, 1159–1172. doi: 10.1016/j.cell.2014.07.001

Bassell, G. J., and Warren, S. T. (2008). Fragile X syndrome: loss of local mRNA regulation alters synaptic development and function. *Neuron* 60, 201–214. doi: 10.1016/j.neuron.2008.10.004

Batista, A. F., and Hengst, U. (2016). Intra-axonal protein synthesis in development and beyond. *Int. J. Dev. Neurosci.* 55, 140–149. doi: 10.1016/j.ijdevneu.2016.03.004

Ben-Yaakov, K., Dagan, S. Y., Segal-Ruder, Y., Shalem, O., Vuppalanchi, D., Willis, D. E., et al. (2012). Axonal transcription factors signal retrogradely in lesioned peripheral nerve. *EMBO J.* 31, 1350–1363. doi: 10.1038/emboj.2011.494

Bergeron, C., Beric-Maskarel, K., Muntasser, S., Weyer, L., Somerville, M. J., and Percy, M. E. (1994). Neurofilament light and polyadenylated mRNA levels are decreased in amyotrophic lateral sclerosis motor neurons. *J. Neuropathol. Exp. Neurol.* 53, 221–230. doi: 10.1097/00005072-199405000-00002

Bernard-Marissal, N., Medard, J. J., Azzedine, H., and Chrast, R. (2015). Dysfunction in endoplasmic reticulum-mitochondria crosstalk underlies SIGMAR1 loss of function mediated motor neuron degeneration. *Brain* 138, 875–890. doi: 10.1093/brain/awv008

Bhinge, A., Namboori, S. C., Zhang, X., Vandongen, A. M. J., and Stanton, L. W. (2017). Genetic correction of SOD1 mutant iPSCs reveals ERK and JNK activated AP1 as a driver of neurodegeneration in amyotrophic lateral sclerosis. *Stem Cell Rep.* 8, 856–869. doi: 10.1016/j.stemcr.2017.02.019

Bigler, R. L., Kamande, J. W., Dumitru, R., Niedringhaus, M., and Taylor, A. M. (2017). Messenger RNAs localized to distal projections of human stem cell derived neurons. *Sci. Rep.* 7:611. doi: 10.1038/s41598-017-00676-w

Boillee, S., Yamanaka, K., Lobsiger, C. S., Copeland, N. G., Jenkins, N. A., Kassiotis, G., et al. (2006). Onset and progression in inherited ALS determined by motor neurons and microglia. *Science* 312, 1389–1392. doi: 10.1126/science.1123511

Bommel, H., Xie, G., Rossoll, W., Wiese, S., Jablonka, S., Boehm, T., et al. (2002). Missense mutation in the *tubulin-specific chaperone E (Tbce)* gene in the mouse mutant progressive motor neuronopathy, a model of human motoneuron disease. *J. Cell Biol.* 159, 563–569. doi: 10.1083/jcb.200208001

Borchelt, D. R., Lee, M. K., Slunt, H. S., Guarnieri, M., Xu, Z. S., Wong, P. C., et al. (1994). Superoxide dismutase 1 with mutations linked to familial amyotrophic lateral sclerosis possesses significant activity. *Proc. Natl. Acad. Sci. U.S.A.* 91, 8292–8296. doi: 10.1073/pnas.91.17.8292

Brady, S. T., and Morfini, G. A. (2017). Regulation of motor proteins, axonal transport deficits and adult-onset neurodegenerative diseases. *Neurobiol. Dis.* 105, 273–282. doi: 10.1016/j.nbd.2017.04.010

Brenner, D., Muller, K., Wieland, T., Weydt, P., Bohm, S., Lule, D., et al. (2016). NEK1 mutations in familial amyotrophic lateral sclerosis. *Brain* 139:e28.

Brenner, D., Yilmaz, R., Muller, K., Grehl, T., Petri, S., Meyer, T., et al. (2018). Hot-spot KIF5A mutations cause familial ALS. *Brain* 141, 688–697. doi: 10.1093/brain/awx370

Brettschneider, J., Petzold, A., Sussmuth, S. D., Ludolph, A. C., and Tumani, H. (2006). Axonal damage markers in cerebrospinal fluid are increased in ALS. *Neurology* 66, 852–856. doi: 10.1212/01.wnl.0000203120.85850.54

Briese, M., Saal, L., Appenzeller, S., Moradi, M., Baluapuri, A., and Sendtner, M. (2016). Whole transcriptome profiling reveals the RNA content of motor axons. *Nucleic Acids Res.* 44:e33. doi: 10.1093/nar/gkv1027

Brown, R. H. Jr., and Al-Chalabi, A. (2017). Amyotrophic lateral sclerosis. *N. Engl. J. Med.* 377:1602.

Bryson, J. B., Hobbs, C., Parsons, M. J., Bosch, K. D., Pandraud, A., Walsh, F. S., et al. (2012). Amyloid precursor protein (APP) contributes to pathology in the SOD1(G93A) mouse model of amyotrophic lateral sclerosis. *Hum. Mol. Genet.* 21, 3871–3882. doi: 10.1093/hmg/dds215

Burberry, A., Suzuki, N., Wang, J. Y., Moccia, R., Mordes, D. A., Stewart, M. H., et al. (2016). Loss-of-function mutations in the *C9ORF72* mouse ortholog cause fatal autoimmune disease. *Sci. Transl. Med.* 8:347ra93. doi: 10.1126/scitranslmed.aaf6038

Cagnetta, R., Frese, C. K., Shigeoka, T., Krijgsveld, J., and Holt, C. E. (2018). Rapid cue-specific remodeling of the nascent axonal proteome. *Neuron* 99, 29–46.e4. doi: 10.1016/j.neuron.2018.06.004

Cahill, M. E., Walker, D. M., Gancarz, A. M., Wang, Z. J., Lardner, C. K., Bagot, R. C., et al. (2018). The dendritic spine morphogenic effects of repeated cocaine use occur through the regulation of serum response factor signaling. *Mol. Psychiatry* 23, 1474–1486. doi: 10.1038/mp.2017.116

Chamberlain, K. A., and Sheng, Z. H. (2019). Mechanisms for the maintenance and regulation of axonal energy supply. *J. Neurosci. Res.* 97, 897–913. doi: 10.1002/jnr.24411

Chew, J., Gendron, T. F., Prudencio, M., Sasaguri, H., Zhang, Y. J., Castanedes-Casey, M., et al. (2015). Neurodegeneration. *C9ORF72* repeat expansions in mice cause TDP-43 pathology, neuronal loss, and behavioral deficits. *Science* 348, 1151–1154. doi: 10.1126/science.aaa9344

Christie, S. B., Akins, M. R., Schwob, J. E., and Fallon, J. R. (2009). The FXG: a presynaptic fragile X granule expressed in a subset of developing brain circuits. *J. Neurosci.* 29, 1514–1524. doi: 10.1523/JNEUROSCI.3937-08.2009

Cioni, J. M., Lin, J. Q., Holtermann, A. V., Koppers, M., Jakobs, M. A. H., Azizi, A., et al. (2019). Late endosomes act as mRNA translation platforms and sustain mitochondria in axons. *Cell* 176, 56–72.e15. doi: 10.1016/j.cell.2018.11.030

Citterio, A., Arnoldi, A., Panzeri, E., Merlini, L., D'angelo, M. G., Musumeci, O., et al. (2015). Variants in *KIF1A* gene in dominant and sporadic forms of hereditary spastic paraparesis. *J. Neurol.* 262, 2684–2690. doi: 10.1007/s00415-015-7899-9

Cook, C., and Petrucelli, L. (2019). Genetic convergence brings clarity to the enigmatic red line in ALS. *Neuron* 101, 1057–1069. doi: 10.1016/j.neuron.2019.02.032

Corbo, M., and Hays, A. P. (1992). Peripherin and neurofilament protein coexist in spinal spheroids of motor neuron disease. *J. Neuropathol. Exp. Neurol.* 51, 531–537. doi: 10.1097/00005072-199209000-00008

Cosker, K. E., Fenstermacher, S. J., Pazyra-Murphy, M. F., Elliott, H. L., and Segal, R. A. (2016). The RNA-binding protein SFPQ orchestrates an RNA regulon to promote axon viability. *Nat. Neurosci.* 19, 690–696. doi: 10.1038/nn.4280

Crerar, H., Scott-Solomon, E., Bodkin-Clarke, C., Andreassi, C., Hazbon, M., Logie, E., et al. (2019). Regulation of NGF signaling by an axonal untranslated mRNA. *Neuron* 102, 553–563.e8. doi: 10.1016/j.neuron.2019.02.011

Dadon-Nachum, M., Melamed, E., and Offen, D. (2011). The "dying-back" phenomenon of motor neurons in ALS. *J. Mol. Neurosci.* 43, 470–477. doi: 10.1007/s12031-010-9467-1

de Boer, A. S., Koszka, K., Kiskinis, E., Suzuki, N., Davis-Dusenbery, B. N., and Eggan, K. (2014). Genetic validation of a therapeutic target in a mouse model of ALS. *Sci. Transl. Med.* 6:248ra104. doi: 10.1126/scitranslmed.3009351

De Vos, K. J., Chapman, A. L., Tennant, M. E., Manser, C., Tudor, E. L., Lau, K. F., et al. (2007). Familial amyotrophic lateral sclerosis-linked SOD1 mutants perturb fast axonal transport to reduce axonal mitochondria content. *Hum. Mol. Genet.* 16, 2720–2728. doi: 10.1093/hmg/ddm226

De Vos, K. J., and Hafezparast, M. (2017). Neurobiology of axonal transport defects in motor neuron diseases: opportunities for translational research? *Neurobiol. Dis.* 105, 283–299. doi: 10.1016/j.nbd.2017.02.004

Deglincerti, A., and Jaffrey, S. R. (2012). Insights into the roles of local translation from the axonal transcriptome. *Open Biol.* 2:120079. doi: 10.1098/rsob.120079

DeJesus-Hernandez, M., Mackenzie, I. R., Boeve, B. F., Boxer, A. L., Baker, M., Rutherford, N. J., et al. (2011). Expanded GGGGCC hexanucleotide repeat in noncoding region of *C9ORF72* causes chromosome 9p-linked FTD and ALS. *Neuron* 72, 245–256. doi: 10.1016/j.neuron.2011.09.011

Denton, K., Mou, Y., Xu, C. C., Shah, D., Chang, J., Blackstone, C., et al. (2018). Impaired mitochondrial dynamics underlie axonal defects in hereditary spastic paraplegias. *Hum. Mol. Genet.* 27, 2517–2530. doi: 10.1093/hmg/ddy156

Di Giorgio, F. P., Carrasco, M. A., Siao, M. C., Maniatis, T., and Eggan, K. (2007). Non-cell autonomous effect of glia on motor neurons in an embryonic stem cell-based ALS model. *Nat. Neurosci.* 10, 608–614. doi: 10.1038/nn1885

Dormann, D., Rodde, R., Edbauer, D., Bentmann, E., Fischer, I., Hruscha, A., et al. (2010). ALS-associated fused in sarcoma (FUS) mutations disrupt Transportin-mediated nuclear import. *EMBO J.* 29, 2841–2857. doi: 10.1038/emboj.2010.143

Ebbing, B., Mann, K., Starosta, A., Jaud, J., Schols, L., Schule, R., et al. (2008). Effect of spastic paraplegia mutations in KIF5A kinesin on transport activity. *Hum. Mol. Genet.* 17, 1245–1252. doi: 10.1093/hmg/ddn014

Edens, B. M., Yan, J., Miller, N., Deng, H. X., Siddique, T., and Ma, Y. C. (2017). A novel ALS-associated variant in *UBQLN4* regulates motor axon morphogenesis. *eLife* 6:e25453. doi: 10.7554/eLife.25453

Eichelbaum, K., and Krijgsveld, J. (2014). Rapid temporal dynamics of transcription, protein synthesis, and secretion during macrophage activation. *Mol. Cell. Proteomics* 13, 792–810. doi: 10.1074/mcp.M113.030916

Fallini, C., Donlin-Asp, P. G., Rouanet, J. P., Bassell, G. J., and Rossoll, W. (2016). Deficiency of the survival of motor neuron protein impairs mRNA localization and local translation in the growth cone of motor neurons. *J. Neurosci.* 36, 3811–3820. doi: 10.1523/JNEUROSCI.2396-15.2016

Ferraiuolo, L., Heath, P. R., Holden, H., Kasher, P., Kirby, J., and Shaw, P. J. (2007). Microarray analysis of the cellular pathways involved in the adaptation to and progression of motor neuron injury in the SOD1 G93A mouse model of familial ALS. *J. Neurosci.* 27, 9201–9219. doi: 10.1523/jneurosci.1470-07.2007

Ferraiuolo, L., Kirby, J., Grierson, A. J., Sendtner, M., and Shaw, P. J. (2011). Molecular pathways of motor neuron injury in amyotrophic lateral sclerosis. *Nat. Rev. Neurol.* 7, 616–630. doi: 10.1038/nrneurol.2011.152

Fichera, M., Lo Giudice, M., Falco, M., Sturnio, M., Amata, S., Calabrese, O., et al. (2004). Evidence of kinesin heavy chain (KIF5A) involvement in pure hereditary spastic paraplegia. *Neurology* 63, 1108–1110. doi: 10.1212/01.wnl.0000138731.60693.d2

Fil, D., Deloach, A., Yadav, S., Alkam, D., Macnicol, M., Singh, A., et al. (2017). Mutant Profilin1 transgenic mice recapitulate cardinal features of motor neuron disease. *Hum. Mol. Genet.* 26, 686–701. doi: 10.1093/hmg/ddw429

Fischer, L. R., Culver, D. G., Tennant, P., Davis, A. A., Wang, M., Castellano-Sanchez, A., et al. (2004). Amyotrophic lateral sclerosis is a distal axonopathy: evidence in mice and man. *Exp. Neurol.* 185, 232–240. doi: 10.1016/j.expneurol.2003.10.004

Freudiger, C. W., Min, W., Saar, B. G., Lu, S., Holtom, G. R., He, C., et al. (2008). Label-free biomedical imaging with high sensitivity by stimulated Raman scattering microscopy. *Science* 322, 1857–1861. doi: 10.1126/science.1165758

Frick, P., Sellier, C., Mackenzie, I. R. A., Cheng, C. Y., Tahraoui-Bories, J., Martinat, C., et al. (2018). Novel antibodies reveal presynaptic localization of C9orf72 protein and reduced protein levels in *C9orf72* mutation carriers. *Acta Neuropathol. Commun.* 6:72. doi: 10.1186/s40478-018-0579-0

Fujimori, K. (2018). Modeling sporadic ALS in iPSC-derived motor neurons identifies a potential therapeutic agent. *Nat. Med.* 24, 1579–1589. doi: 10.1038/s41591-018-0140-5

Furukawa, Y., Kaneko, K., Watanabe, S., Yamanaka, K., and Nukina, N. (2011). A seeding reaction recapitulates intracellular formation of sarkosyl-insoluble transactivation response element (TAR) DNA-binding protein-43 inclusions. *J. Biol. Chem.* 286, 18664–18672. doi: 10.1074/jbc.M111.231209

Geevasinga, N., Menon, P., Howells, J., Nicholson, G. A., Kiernan, M. C., and Vucic, S. (2015). Axonal ion channel dysfunction in *C9orf72* familial amyotrophic lateral sclerosis. *JAMA Neurol.* 72, 49–57. doi: 10.1001/jamaneurol.2014.2940

Gentile, F., Scarlino, S., Falzone, Y. M., Lunetta, C., Tremolizzo, L., Quattrini, A., et al. (2019). The peripheral nervous system in amyotrophic lateral sclerosis: opportunities for translational research. *Front. Neurosci.* 13:601. doi: 10.3389/fnins.2019.00601

Ghasemi, M., and Brown, R. H. Jr. (2018). Genetics of amyotrophic lateral sclerosis. *Cold Spring Harb. Perspect. Med.* 8:a024125. doi: 10.1101/cshperspect.a024125

Gibbs, K. L., Kalmar, B., Rhymes, E. R., Fellows, A. D., Ahmed, M., Whiting, P., et al. (2018). Inhibiting p38 MAPK alpha rescues axonal retrograde transport defects in a mouse model of ALS. *Cell Death Dis.* 9:596. doi: 10.1038/s41419-018-0624-8

Groen, E. J., Fumoto, K., Blokhuis, A. M., Engelen-Lee, J., Zhou, Y., Van Den Heuvel, D. M., et al. (2013). ALS-associated mutations in FUS disrupt the

axonal distribution and function of SMN. *Hum. Mol. Genet.* 22, 3690–3704. doi: 10.1093/hmg/ddt222

Grueter, B. A., Robison, A. J., Neve, R. L., Nestler, E. J., and Malenka, R. C. (2013). FosB differentially modulates nucleus accumbens direct and indirect pathway function. *Proc. Natl. Acad. Sci. U.S.A.* 110, 1923–1928. doi: 10.1073/pnas.1221742110

Gumy, L. F., Yeo, G. S., Tung, Y. C., Zivraj, K. H., Willis, D., Coppola, G., et al. (2011). Transcriptome analysis of embryonic and adult sensory axons reveals changes in mRNA repertoire localization. *RNA* 17, 85–98. doi: 10.1261/rna.2386111

Guo, L., Kim, H. J., Wang, H., Monaghan, J., Freyermuth, F., Sung, J. C., et al. (2018). Nuclear-import receptors reverse aberrant phase transitions of RNA-binding proteins with prion-like domains. *Cell* 173, 677–692.e20. doi: 10.1016/j.cell.2018.03.002

Guo, W., Naujock, M., Fumagalli, L., Vandoorne, T., Baatsen, P., Boon, R., et al. (2017). HDAC6 inhibition reverses axonal transport defects in motor neurons derived from FUS-ALS patients. *Nat. Commun.* 8:861. doi: 10.1038/s41467-017-00911-y

Hadano, S., Otomo, A., Kunita, R., Suzuki-Utsunomiya, K., Akatsuka, A., Koike, M., et al. (2010). Loss of ALS2/Alsin exacerbates motor dysfunction in a SOD1-expressing mouse ALS model by disturbing endolysosomal trafficking. *PLoS One* 5:e9805. doi: 10.1371/journal.pone.0009805

Hanson, J. E., and Madison, D. V. (2007). Presynaptic FMR1 genotype influences the degree of synaptic connectivity in a mosaic mouse model of fragile X syndrome. *J. Neurosci.* 27, 4014–4018. doi: 10.1523/jneurosci.4717-06.2007

He, W., Bai, G., Zhou, H., Wei, N., White, N. M., Lauer, J., et al. (2015). CMT2D neuropathy is linked to the neomorphic binding activity of glycyl-tRNA synthetase. *Nature* 526, 710–714. doi: 10.1038/nature15510

Heo, K., Lim, S. M., Nahm, M., Kim, Y. E., Oh, K. W., Park, H. T., et al. (2018). A *de novo RAPGEF2* variant identified in a sporadic amyotrophic lateral sclerosis patient impairs microtubule stability and axonal mitochondria distribution. *Exp. Neurobiol.* 27, 550–563. doi: 10.5607/en.2018.27.6.550

Hirano, A., Donnenfeld, H., Sasaki, S., and Nakano, I. (1984a). Fine structural observations of neurofilamentous changes in amyotrophic lateral sclerosis. *J. Neuropathol. Exp. Neurol.* 43, 461–470. doi: 10.1097/00005072-198409000-00001

Hirano, A., Nakano, I., Kurland, L. T., Mulder, D. W., Holley, P. W., and Saccomanno, G. (1984b). Fine structural study of neurofibrillary changes in a family with amyotrophic lateral sclerosis. *J. Neuropathol. Exp. Neurol.* 43, 471–480. doi: 10.1097/00005072-198409000-00002

Hofweber, M., Hutten, S., Bourgeois, B., Spreitzer, E., Niedner-Boblenz, A., Schifferer, M., et al. (2018). Phase separation of FUS is suppressed by its nuclear import receptor and arginine methylation. *Cell* 173, 706–719.e13. doi: 10.1016/j.cell.2018.03.004

Hogan, A. L., Don, E. K., Rayner, S. L., Lee, A., Laird, A. S., Watchon, M., et al. (2017). Expression of ALS/FTD-linked mutant CCNF in zebrafish leads to increased cell death in the spinal cord and an aberrant motor phenotype. *Hum. Mol. Genet.* 26, 2616–2626. doi: 10.1093/hmg/ddx136

Howland, D. S., Liu, J., She, Y., Goad, B., Maragakis, N. J., Kim, B., et al. (2002). Focal loss of the glutamate transporter EAAT2 in a transgenic rat model of SOD1 mutant-mediated amyotrophic lateral sclerosis (ALS). *Proc. Natl. Acad. Sci. U.S.A.* 99, 1604–1609. doi: 10.1073/pnas.032539299

Ichiyanagi, N., Fujimori, K., Yano, M., Ishihara-Fujisaki, C., Sone, T., Akiyama, T., et al. (2016). Establishment of in vitro FUS-associated familial amyotrophic lateral sclerosis model using human induced pluripotent stem cells. *Stem Cell Rep.* 6, 496–510. doi: 10.1016/j.stemcr.2016.02.011

Ito, Y., Ofengeim, D., Najafov, A., Das, S., Saberi, S., Li, Y., et al. (2016). RIPK1 mediates axonal degeneration by promoting inflammation and necroptosis in ALS. *Science* 353, 603–608. doi: 10.1126/science.aaf6803

Ji, S. J., and Jaffrey, S. R. (2014). Axonal transcription factors: novel regulators of growth cone-to-nucleus signaling. *Dev. Neurobiol.* 74, 245–258. doi: 10.1002/dneu.22112

Jiang, J., Zhu, Q., Gendron, T. F., Saberi, S., Mcalonis-Downes, M., Seelman, A., et al. (2016). Gain of toxicity from ALS/FTD-linked repeat expansions in *C9ORF72* is alleviated by antisense oligonucleotides targeting GGGGCC-containing RNAs. *Neuron* 90, 535–550. doi: 10.1016/j.neuron.2016.04.006

Jiang, Y. M., Yamamoto, M., Kobayashi, Y., Yoshihara, T., Liang, Y., Terao, S., et al. (2005). Gene expression profile of spinal motor neurons in sporadic amyotrophic lateral sclerosis. *Ann. Neurol.* 57, 236–251. doi: 10.1002/ana.20379

Johnson, J. O., Mandrioli, J., Benatar, M., Abramzon, Y., Van Deerlin, V. M., Trojanowski, J. Q., et al. (2010). Exome sequencing reveals VCP mutations as a cause of familial ALS. *Neuron* 68, 857–864. doi: 10.1016/j.neuron.2010.11.036

Joung, J. K., and Sander, J. D. (2013). TALENs: a widely applicable technology for targeted genome editing. *Nat. Rev. Mol. Cell Biol.* 14, 49–55. doi: 10.1038/nrm3486

Jung, H., Yoon, B. C., and Holt, C. E. (2012). Axonal mRNA localization and local protein synthesis in nervous system assembly, maintenance and repair. *Nat. Rev. Neurosci.* 13, 308–324. doi: 10.1038/nrn3210

Kabashi, E., Lin, L., Tradewell, M. L., Dion, P. A., Bercier, V., Bourgouin, P., et al. (2010). Gain and loss of function of ALS-related mutations of TARDBP (TDP-43) cause motor deficits in vivo. *Hum. Mol. Genet.* 19, 671–683. doi: 10.1093/hmg/ddp534

Kabashi, E., Valdmanis, P. N., Dion, P., Spiegelman, D., Mcconkey, B. J., Vande Velde, C., et al. (2008). TARDBP mutations in individuals with sporadic and familial amyotrophic lateral sclerosis. *Nat. Genet.* 40, 572–574. doi: 10.1038/ng.132

Kanai, K., Kuwabara, S., Misawa, S., Tamura, N., Ogawara, K., Nakata, M., et al. (2006). Altered axonal excitability properties in amyotrophic lateral sclerosis: impaired potassium channel function related to disease stage. *Brain* 129, 953–962. doi: 10.1093/brain/awl024

Kanai, K., Shibuya, K., Sato, Y., Misawa, S., Nasu, S., Sekiguchi, Y., et al. (2012). Motor axonal excitability properties are strong predictors for survival in amyotrophic lateral sclerosis. *J. Neurol. Neurosurg. Psychiatry* 83, 734–738. doi: 10.1136/jnnp-2011-301782

Kang, S. H., Fukaya, M., Yang, J. K., Rothstein, J. D., and Bergles, D. E. (2010). NG2+ CNS glial progenitors remain committed to the oligodendrocyte lineage in postnatal life and following neurodegeneration. *Neuron* 68, 668–681. doi: 10.1016/j.neuron.2010.09.009

Kang, S. H., Li, Y., Fukaya, M., Lorenzini, I., Cleveland, D. W., Ostrow, L. W., et al. (2013). Degeneration and impaired regeneration of gray matter oligodendrocytes in amyotrophic lateral sclerosis. *Nat. Neurosci.* 16, 571–579. doi: 10.1038/nn.3357

Kapeli, K., Martinez, F. J., and Yeo, G. W. (2017). Genetic mutations in RNA-binding proteins and their roles in ALS. *Hum. Genet.* 136, 1193–1214. doi: 10.1007/s00439-017-1830-7

Kawada, J., Kaneda, S., Kirihara, T., Maroof, A., Levi, T., Eggan, K., et al. (2017). Generation of a motor nerve organoid with human stem cell-derived neurons. *Stem Cell Rep.* 9, 1441–1449. doi: 10.1016/j.stemcr.2017.09.021

Kelleher, R. J. III, and Bear, M. F. (2008). The autistic neuron: troubled translation? *Cell* 135, 401–406. doi: 10.1016/j.cell.2008.10.017

Kenna, K. P., Van Doormaal, P. T., Dekker, A. M., Ticozzi, N., Kenna, B. J., Diekstra, F. P., et al. (2016). NEK1 variants confer susceptibility to amyotrophic lateral sclerosis. *Nat. Genet.* 48, 1037–1042. doi: 10.1038/ng.3626

Kieran, D., Woods, I., Villunger, A., Strasser, A., and Prehn, J. H. (2007). Deletion of the BH3-only protein puma protects motoneurons from ER stress-induced apoptosis and delays motoneuron loss in ALS mice. *Proc. Natl. Acad. Sci. U.S.A.* 104, 20606–20611. doi: 10.1073/pnas.0707906105

Kikuchi, H., Almer, G., Yamashita, S., Guegan, C., Nagai, M., Xu, Z., et al. (2006). Spinal cord endoplasmic reticulum stress associated with a microsomal accumulation of mutant superoxide dismutase-1 in an ALS model. *Proc. Natl. Acad. Sci. U.S.A.* 103, 6025–6030. doi: 10.1073/pnas.0509227103

Kim, H. J., and Taylor, J. P. (2017). Lost in transportation: nucleocytoplasmic transport defects in ALS and other neurodegenerative diseases. *Neuron* 96, 285–297. doi: 10.1016/j.neuron.2017.07.029

Kiryu-Seo, S., and Kiyama, H. (2019). Mitochondrial behavior during axon regeneration/degeneration in vivo. *Neurosci. Res.* 139, 42–47. doi: 10.1016/j.neures.2018.08.014

Klaus, J., Kanton, S., Kyrousi, C., Ayo-Martin, A. C., Di Giaimo, R., Riesenberg, S., et al. (2019). Altered neuronal migratory trajectories in human cerebral organoids derived from individuals with neuronal heterotopia. *Nat. Med.* 25, 561–568. doi: 10.1038/s41591-019-0371-0

Klim, J. R., Williams, L. A., Limone, F., Guerra San Juan, I., Davis-Dusenbery, B. N., Mordes, D. A., et al. (2019). ALS-implicated protein TDP-43 sustains levels of STMN2, a mediator of motor neuron growth and repair. *Nat. Neurosci.* 22, 167–179. doi: 10.1038/s41593-018-0300-4

Kwiatkowski, T. J. Jr., Bosco, D. A., Leclerc, A. L., Tamrazian, E., Vanderburg, C. R., Russ, C., et al. (2009). Mutations in the FUS/TLS gene on chromosome

16 cause familial amyotrophic lateral sclerosis. *Science* 323, 1205–1208. doi: 10.1126/science.1166066

Kwon, I., Xiang, S., Kato, M., Wu, L., Theodoropoulos, P., Wang, T., et al. (2014). Poly-dipeptides encoded by the *C9orf72* repeats bind nucleoli, impede RNA biogenesis, and kill cells. *Science* 345, 1139–1145. doi: 10.1126/science.1254917

Kye, M. J., Niederst, E. D., Wertz, M. H., Goncalves Ido, C., Akten, B., Dover, K. Z., et al. (2014). SMN regulates axonal local translation via miR-183/mTOR pathway. *Hum. Mol. Genet.* 23, 6318–6331. doi: 10.1093/hmg/ddu350

Lafragette, A., Bardo, M. T., Lardeux, V., Solinas, M., and Thiriet, N. (2017). Reduction of cocaine-induced locomotor effects by enriched environment is associated with cell-specific accumulation of DeltaFosB in striatal and cortical subregions. *Int. J. Neuropsychopharmacol.* 20, 237–246. doi: 10.1093/ijnp/pyw097

Laird, A. S., Van Hoecke, A., De Muynck, L., Timmers, M., Van Den Bosch, L., Van Damme, P., et al. (2010). Progranulin is neurotrophic in vivo and protects against a mutant TDP-43 induced axonopathy. *PLoS One* 5:e13368. doi: 10.1371/journal.pone.0013368

Lee, Y., Morrison, B. M., Li, Y., Lengacher, S., Farah, M. H., Hoffman, P. N., et al. (2012). Oligodendroglia metabolically support axons and contribute to neurodegeneration. *Nature* 487, 443–448. doi: 10.1038/nature11314

Li, F., Xie, X., Wang, Y., Liu, J., Cheng, X., Guo, Y., et al. (2016). Structural insights into the interaction and disease mechanism of neurodegenerative disease-associated optineurin and TBK1 proteins. *Nat. Commun.* 7:12708. doi: 10.1038/ncomms12708

Liao, Y. C., Fernandopulle, M. S., Wang, G., Choi, H., Hao, L., Drerup, C. M., et al. (2019). RNA granules hitchhike on lysosomes for long-distance transport, using annexin A11 as a molecular tether. *Cell* 179, 147–164.e20. doi: 10.1016/j.cell.2019.08.050

Lin, M. Y., Cheng, X. T., Xie, Y., Cai, Q., and Sheng, Z. H. (2017). Removing dysfunctional mitochondria from axons independent of mitophagy under pathophysiological conditions. *Autophagy* 13, 1792–1794. doi: 10.1080/15548627.2017.1356552

Ling, J. P., Pletnikova, O., Troncoso, J. C., and Wong, P. C. (2015). TDP-43 repression of nonconserved cryptic exons is compromised in ALS-FTD. *Science* 349, 650–655. doi: 10.1126/science.aab0983

Lopez-Erauskin, J., Tadokoro, T., Baughn, M. W., Myers, B., Mcalonis-Downes, M., Chillon-Marinas, C., et al. (2018). ALS/FTD-linked mutation in FUS suppresses intra-axonal protein synthesis and drives disease without nuclear loss-of-function of FUS. *Neuron* 100, 816–830.e7. doi: 10.1016/j.neuron.2018.09.044

Maciel, R., Bis, D. M., Rebelo, A. P., Saghira, C., Zuchner, S., and Saporta, M. A. (2018). The human motor neuron axonal transcriptome is enriched for transcripts related to mitochondrial function and microtubule-based axonal transport. *Exp. Neurol.* 307, 155–163. doi: 10.1016/j.expneurol.2018.06.008

Mackenzie, I. R., Nicholson, A. M., Sarkar, M., Messing, J., Purice, M. D., Pottier, C., et al. (2017). TIA1 mutations in amyotrophic lateral sclerosis and frontotemporal dementia promote phase separation and alter stress granule dynamics. *Neuron* 95, 808–816.e9. doi: 10.1016/j.neuron.2017.07.025

Mackenzie, I. R., Rademakers, R., and Neumann, M. (2010). TDP-43 and FUS in amyotrophic lateral sclerosis and frontotemporal dementia. *Lancet Neurol.* 9, 995–1007. doi: 10.1016/S1474-4422(10)70195-2

Maday, S., and Holzbaur, E. L. (2016). Compartment-specific regulation of autophagy in primary neurons. *J. Neurosci.* 36, 5933–5945. doi: 10.1523/JNEUROSCI.4401-15.2016

Maday, S., Twelvetrees, A. E., Moughamian, A. J., and Holzbaur, E. L. (2014). Axonal transport: cargo-specific mechanisms of motility and regulation. *Neuron* 84, 292–309. doi: 10.1016/j.neuron.2014.10.019

Magrane, J., Cortez, C., Gan, W. B., and Manfredi, G. (2014). Abnormal mitochondrial transport and morphology are common pathological denominators in SOD1 and TDP43 ALS mouse models. *Hum. Mol. Genet.* 23, 1413–1424. doi: 10.1093/hmg/ddt528

Maniatis, S., Aijo, T., Vickovic, S., Braine, C., Kang, K., Mollbrink, A., et al. (2019). Spatiotemporal dynamics of molecular pathology in amyotrophic lateral sclerosis. *Science* 364, 89–93. doi: 10.1126/science.aav9776

Martin, N., Jaubert, J., Gounon, P., Salido, E., Haase, G., Szatanik, M., et al. (2002). A missense mutation in *Tbce* causes progressive motor neuronopathy in mice. *Nat. Genet.* 32, 443–447. doi: 10.1038/ng1016

Martineau, E., Di Polo, A., Vande Velde, C., and Robitaille, R. (2018). Dynamic neuromuscular remodeling precedes motor-unit loss in a mouse model of ALS. *eLife* 7:e41973. doi: 10.7554/eLife.41973

Maruyama, H., Morino, H., Ito, H., Izumi, Y., Kato, H., Watanabe, Y., et al. (2010). Mutations of optineurin in amyotrophic lateral sclerosis. *Nature* 465, 223–226. doi: 10.1038/nature08971

McWhorter, M. L., Monani, U. R., Burghes, A. H., and Beattie, C. E. (2003). Knockdown of the survival motor neuron (Smn) protein in zebrafish causes defects in motor axon outgrowth and pathfinding. *J. Cell Biol.* 162, 919–931.

Melamed, Z., Lopez-Erauskin, J., Baughn, M. W., Zhang, O., Drenner, K., Sun, Y., et al. (2019). Premature polyadenylation-mediated loss of stathmin-2 is a hallmark of TDP-43-dependent neurodegeneration. *Nat. Neurosci.* 22, 180–190. doi: 10.1038/s41593-018-0293-z

Menon, S., and Gupton, S. (2018). Recent advances in branching mechanisms underlying neuronal morphogenesis. *F1000Res.* 7:F1000 Faculty Rev-1779.

Merianda, T. T., Lin, A. C., Lam, J. S., Vuppalanchi, D., Willis, D. E., Karin, N., et al. (2009). A functional equivalent of endoplasmic reticulum and Golgi in axons for secretion of locally synthesized proteins. *Mol. Cell. Neurosci.* 40, 128–142. doi: 10.1016/j.mcn.2008.09.008

Millecamps, S., and Julien, J. P. (2013). Axonal transport deficits and neurodegenerative diseases. *Nat. Rev. Neurosci.* 14, 161–176. doi: 10.1038/nrn3380

Mizielinska, S., Gronke, S., Niccoli, T., Ridler, C. E., Clayton, E. L., Devoy, A., et al. (2014). *C9orf72* repeat expansions cause neurodegeneration in *Drosophila* through arginine-rich proteins. *Science* 345, 1192–1194. doi: 10.1126/science.1256800

Moller, A., Bauer, C. S., Cohen, R. N., Webster, C. P., and De Vos, K. J. (2017). Amyotrophic lateral sclerosis-associated mutant SOD1 inhibits anterograde axonal transport of mitochondria by reducing Miro1 levels. *Hum. Mol. Genet.* 26, 4668–4679. doi: 10.1093/hmg/ddx348

Moloney, E. B., De Winter, F., and Verhaagen, J. (2014). ALS as a distal axonopathy: molecular mechanisms affecting neuromuscular junction stability in the presymptomatic stages of the disease. *Front. Neurosci.* 8:252. doi: 10.3389/fnins.2014.00252

Moradi, M., Sivadasan, R., Saal, L., Luningschror, P., Dombert, B., Rathod, R. J., et al. (2017). Differential roles of alpha-, beta-, and gamma-actin in axon growth and collateral branch formation in motoneurons. *J. Cell Biol.* 216, 793–814. doi: 10.1083/jcb.201604117

Mori, K., Weng, S. M., Arzberger, T., May, S., Rentzsch, K., Kremmer, E., et al. (2013). The *C9orf72* GGGGCC repeat is translated into aggregating dipeptide-repeat proteins in FTLD/ALS. *Science* 339, 1335–1338. doi: 10.1126/science.1232927

Morisaki, T., Lyon, K., Deluca, K. F., Deluca, J. G., English, B. P., Zhang, Z., et al. (2016). Real-time quantification of single RNA translation dynamics in living cells. *Science* 352, 1425–1429. doi: 10.1126/science.aaf0899

Morrice, J. R., Gregory-Evans, C. Y., and Shaw, C. A. (2018). Modeling environmentally-induced motor neuron degeneration in zebrafish. *Sci. Rep.* 8:4890. doi: 10.1038/s41598-018-23018-w

Morrison, B. M., Lee, Y., and Rothstein, J. D. (2013). Oligodendroglia: metabolic supporters of axons. *Trends Cell Biol.* 23, 644–651. doi: 10.1016/j.tcb.2013.07.007

Munch, C., Sedlmeier, R., Meyer, T., Homberg, V., Sperfeld, A. D., Kurt, A., et al. (2004). Point mutations of the p150 subunit of dynactin (DCTN1) gene in ALS. *Neurology* 63, 724–726. doi: 10.1212/01.wnl.0000134608.83927.b1

Nagai, M., Re, D. B., Nagata, T., Chalazonitis, A., Jessell, T. M., Wichterle, H., et al. (2007). Astrocytes expressing ALS-linked mutated SOD1 release factors selectively toxic to motor neurons. *Nat. Neurosci.* 10, 615–622. doi: 10.1038/nn1876

Nakazawa, S., Oikawa, D., Ishii, R., Ayaki, T., Takahashi, H., Takeda, H., et al. (2016). Linear ubiquitination is involved in the pathogenesis of optineurin-associated amyotrophic lateral sclerosis. *Nat. Commun.* 7:12547. doi: 10.1038/ncomms12547

Naumann, M., Pal, A., Goswami, A., Lojewski, X., Japtok, J., Vehlow, A., et al. (2018). Impaired DNA damage response signaling by FUS-NLS mutations leads to neurodegeneration and FUS aggregate formation. *Nat. Commun.* 9:335. doi: 10.1038/s41467-017-02299-1

Nedelsky, N. B., and Taylor, J. P. (2019). Bridging biophysics and neurology: aberrant phase transitions in neurodegenerative disease. *Nat. Rev. Neurol.* 15, 272–286. doi: 10.1038/s41582-019-0157-5

Neto, E., Leitao, L., Sousa, D. M., Alves, C. J., Alencastre, I. S., Aguiar, P., et al. (2016). Compartmentalized microfluidic platforms: the unrivaled breakthrough of in vitro tools for neurobiological research. *J. Neurosci.* 36, 11573–11584. doi: 10.1523/jneurosci.1748-16.2016

Nicolas, A., Kenna, K. P., Renton, A. E., Ticozzi, N., Faghri, F., Chia, R., et al. (2018). Genome-wide analyses identify KIF5A as a novel ALS gene. *Neuron* 97, 1268–1283.e6. doi: 10.1016/j.neuron.2018.02.027

Nijssen, J., Aguila, J., Hoogstraaten, R., Kee, N., and Hedlund, E. (2018). Axon-Seq decodes the motor axon transcriptome and its modulation in response to ALS. *Stem Cell Rep.* 11, 1565–1578. doi: 10.1016/j.stemcr.2018.11.005

Nijssen, J., Comley, L. H., and Hedlund, E. (2017). Motor neuron vulnerability and resistance in amyotrophic lateral sclerosis. *Acta Neuropathol.* 133, 863–885. doi: 10.1007/s00401-017-1708-8

Nishiyama, A., Niihori, T., Warita, H., Izumi, R., Akiyama, T., Kato, M., et al. (2017). Comprehensive targeted next-generation sequencing in Japanese familial amyotrophic lateral sclerosis. *Neurobiol. Aging* 53, e191–e194. doi: 10.1016/j.neurobiolaging.2017.01.004

Nonaka, T., Masuda-Suzukake, M., Arai, T., Hasegawa, Y., Akatsu, H., Obi, T., et al. (2013). Prion-like properties of pathological TDP-43 aggregates from diseased brains. *Cell Rep.* 4, 124–134. doi: 10.1016/j.celrep.2013.06.007

Okada, Y., Yamazaki, H., Sekine-Aizawa, Y., and Hirokawa, N. (1995). The neuron-specific kinesin superfamily protein *KIF1A* is a unique monomeric motor for anterograde axonal transport of synaptic vesicle precursors. *Cell* 81, 769–780. doi: 10.1016/0092-8674(95)90538-3

Okano, H., and Yamanaka, S. (2014). iPS cell technologies: significance and applications to CNS regeneration and disease. *Mol. Brain* 7:22. doi: 10.1186/1756-6606-7-22

O'Rourke, J. G., Bogdanik, L., Yanez, A., Lall, D., Wolf, A. J., Muhammad, A. K., et al. (2016). *C9orf72* is required for proper macrophage and microglial function in mice. *Science* 351, 1324–1329. doi: 10.1126/science.aaf1064

Osking, Z., Ayers, J. I., Hildebrandt, R., Skruber, K., Brown, H., Ryu, D., et al. (2019). ALS-linked SOD1 mutants enhance neurite outgrowth and branching in adult motor neurons. *iScience* 11, 294–304. doi: 10.1016/j.isci.2018.12.026

Parras, A., Anta, H., Santos-Galindo, M., Swarup, V., Elorza, A., Nieto-Gonzalez, J. L., et al. (2018). Autism-like phenotype and risk gene mRNA deadenylation by CPEB4 mis-splicing. *Nature* 560, 441–446. doi: 10.1038/s41586-018-0423-5

Peng, Y., Kim, M. J., Hullinger, R., O'riordan, K. J., Burger, C., Pehar, M., et al. (2016). Improved proteostasis in the secretory pathway rescues Alzheimer's disease in the mouse. *Brain* 139, 937–952. doi: 10.1093/brain/awv385

Pereno, G. L., Balaszczuk, V., and Beltramino, C. A. (2011). Kainic acid-induced early genes activation and neuronal death in the medial extended amygdala of rats. *Exp. Toxicol. Pathol.* 63, 291–299. doi: 10.1016/j.etp.2010.02.001

Peters, O. M., Cabrera, G. T., Tran, H., Gendron, T. F., Mckeon, J. E., Metterville, J., et al. (2015). Human *C9ORF72* hexanucleotide expansion reproduces RNA foci and dipeptide repeat proteins but not neurodegeneration in BAC transgenic mice. *Neuron* 88, 902–909. doi: 10.1016/j.neuron.2015.11.018

Philips, T., Bento-Abreu, A., Nonneman, A., Haeck, W., Staats, K., Geelen, V., et al. (2013). Oligodendrocyte dysfunction in the pathogenesis of amyotrophic lateral sclerosis. *Brain* 136, 471–482. doi: 10.1093/brain/aws339

Picchiarelli, G., Demestre, M., Zuko, A., Been, M., Higelin, J., Dieterle, S., et al. (2019). FUS-mediated regulation of acetylcholine receptor transcription at neuromuscular junctions is compromised in amyotrophic lateral sclerosis. *Nat. Neurosci.* 22, 1793–1805. doi: 10.1038/s41593-019-0498-9

Plachta, N., Annaheim, C., Bissiere, S., Lin, S., Ruegg, M., Hoving, S., et al. (2007). Identification of a lectin causing the degeneration of neuronal processes using engineered embryonic stem cells. *Nat. Neurosci.* 10, 712–719. doi: 10.1038/nn1897

Porta, S., Xu, Y., Restrepo, C. R., Kwong, L. K., Zhang, B., Brown, H. J., et al. (2018). Patient-derived frontotemporal lobar degeneration brain extracts induce formation and spreading of TDP-43 pathology in vivo. *Nat. Commun.* 9:4220. doi: 10.1038/s41467-018-06548-9

Poulopoulos, A., Murphy, A. J., Ozkan, A., Davis, P., Hatch, J., Kirchner, R., et al. (2019). Subcellular transcriptomes and proteomes of developing axon projections in the cerebral cortex. *Nature* 565, 356–360. doi: 10.1038/s41586-018-0847-y

Pradat, P. F., Bruneteau, G., Gonzalez De Aguilar, J. L., Dupuis, L., Jokic, N., Salachas, F., et al. (2007). Muscle Nogo-A expression is a prognostic marker in lower motor neuron syndromes. *Ann. Neurol.* 62, 15–20. doi: 10.1002/ana.21122

Puls, I., Jonnakuty, C., Lamonte, B. H., Holzbaur, E. L., Tokito, M., Mann, E., et al. (2003). Mutant dynactin in motor neuron disease. *Nat. Genet.* 33, 455–456.

Qamar, S., Wang, G., Randle, S. J., Ruggeri, F. S., Varela, J. A., Lin, J. Q., et al. (2018). FUS phase separation is modulated by a molecular chaperone and methylation of arginine cation-pi interactions. *Cell* 173, 720–734.e15. doi: 10.1016/j.cell.2018.03.056

Quadrato, G., Nguyen, T., Macosko, E. Z., Sherwood, J. L., Min Yang, S., Berger, D. R., et al. (2017). Cell diversity and network dynamics in photosensitive human brain organoids. *Nature* 545, 48–53. doi: 10.1038/nature22047

Rage, F., Boulisfane, N., Rihan, K., Neel, H., Gostan, T., Bertrand, E., et al. (2013). Genome-wide identification of mRNAs associated with the protein SMN whose depletion decreases their axonal localization. *RNA* 19, 1755–1766. doi: 10.1261/rna.040204.113

Renton, A. E., Majounie, E., Waite, A., Simon-Sanchez, J., Rollinson, S., Gibbs, J. R., et al. (2011). A hexanucleotide repeat expansion in *C9ORF72* is the cause of chromosome 9p21-linked ALS-FTD. *Neuron* 72, 257–268. doi: 10.1016/j.neuron.2011.09.010

Riva, N., Clarelli, F., Domi, T., Cerri, F., Gallia, F., Trimarco, A., et al. (2016). Unraveling gene expression profiles in peripheral motor nerve from amyotrophic lateral sclerosis patients: insights into pathogenesis. *Sci. Rep.* 6:39297. doi: 10.1038/srep39297

Rosen, D. R., Siddique, T., Patterson, D., Figlewicz, D. A., Sapp, P., Hentati, A., et al. (1993). Mutations in Cu/Zn superoxide dismutase gene are associated with familial amyotrophic lateral sclerosis. *Nature* 362, 59–62.

Rotem, N., Magen, I., Ionescu, A., Gershoni-Emek, N., Altman, T., Costa, C. J., et al. (2017). ALS along the axons - expression of coding and noncoding RNA differs in axons of ALS models. *Sci. Rep.* 7:44500. doi: 10.1038/srep44500

Rouleau, G. A., Clark, A. W., Rooke, K., Pramatarova, A., Krizus, A., Suchowersky, O., et al. (1996). SOD1 mutation is associated with accumulation of neurofilaments in amyotrophic lateral sclerosis. *Ann. Neurol.* 39, 128–131.

Roy, S., Zhang, B., Lee, V. M., and Trojanowski, J. Q. (2005). Axonal transport defects: a common theme in neurodegenerative diseases. *Acta Neuropathol.* 109, 5–13. doi: 10.1007/s00401-004-0952-x

Rutherford, N. J., Zhang, Y. J., Baker, M., Gass, J. M., Finch, N. A., Xu, Y. F., et al. (2008). Novel mutations in TARDBP (TDP-43) in patients with familial amyotrophic lateral sclerosis. *PLoS Genet.* 4:e1000193. doi: 10.1371/journal.pgen.1000193

Saal, L., Briese, M., Kneitz, S., Glinka, M., and Sendtner, M. (2014). Subcellular transcriptome alterations in a cell culture model of spinal muscular atrophy point to widespread defects in axonal growth and presynaptic differentiation. *RNA* 20, 1789–1802. doi: 10.1261/rna.047373.114

Sabari, B. R., Dall'agnese, A., Boija, A., Klein, I. A., Coffey, E. L., Shrinivas, K., et al. (2018). Coactivator condensation at super-enhancers links phase separation and gene control. *Science* 361:eaar3958. doi: 10.1126/science.aar3958

Salvadores, N., Sanhueza, M., Manque, P., and Court, F. A. (2017). Axonal degeneration during aging and its functional role in neurodegenerative disorders. *Front. Neurosci.* 11:451. doi: 10.3389/fnins.2017.00451

Sambandan, S., Akbalik, G., Kochen, L., Rinne, J., Kahlstatt, J., Glock, C., et al. (2017). Activity-dependent spatially localized miRNA maturation in neuronal dendrites. *Science* 355, 634–637. doi: 10.1126/science.aaf8995

Scekic-Zahirovic, J., Sendscheid, O., El Oussini, H., Jambeau, M., Sun, Y., Mersmann, S., et al. (2016). Toxic gain of function from mutant FUS protein is crucial to trigger cell autonomous motor neuron loss. *EMBO J.* 35, 1077–1097. doi: 10.15252/embj.201592559

Schmidt, N., Akaaboune, M., Gajendran, N., Martinez-Pena, Y., Valenzuela, I., Wakefield, S., et al. (2011). Neuregulin/ErbB regulate neuromuscular junction development by phosphorylation of alpha-dystrobrevin. *J. Cell Biol.* 195, 1171–1184. doi: 10.1083/jcb.201107083

Schoen, M., Reichel, J. M., Demestre, M., Putz, S., Deshpande, D., Proepper, C., et al. (2015). Super-resolution microscopy reveals presynaptic localization of the ALS/FTD related protein FUS in hippocampal neurons. *Front. Cell. Neurosci.* 9:496. doi: 10.3389/fncel.2015.00496

Shao, Z., Noh, H., Bin Kim, W., Ni, P., Nguyen, C., Cote, S. E., et al. (2019). Dysregulated protocadherin-pathway activity as an intrinsic defect in induced pluripotent stem cell-derived cortical interneurons from subjects with schizophrenia. *Nat. Neurosci.* 22, 229–242. doi: 10.1038/s41593-018-0313-z

Sharma, A., Lyashchenko, A. K., Lu, L., Nasrabady, S. E., Elmaleh, M., Mendelsohn, M., et al. (2016). ALS-associated mutant FUS induces selective motor neuron degeneration through toxic gain of function. *Nat. Commun.* 7:10465. doi: 10.1038/ncomms10465

Shigeoka, T., Jung, H., Jung, J., Turner-Bridger, B., Ohk, J., Lin, J. Q., et al. (2016). Dynamic axonal translation in developing and mature visual circuits. *Cell* 166, 181–192. doi: 10.1016/j.cell.2016.05.029

Shiihashi, G., Ito, D., Yagi, T., Nihei, Y., Ebine, T., and Suzuki, N. (2016). Mislocated FUS is sufficient for gain-of-toxic-function amyotrophic lateral sclerosis phenotypes in mice. *Brain* 139, 2380–2394. doi: 10.1093/brain/aww161

Sivadasan, R., Hornburg, D., Drepper, C., Frank, N., Jablonka, S., Hansel, A., et al. (2016). *C9ORF72* interaction with cofilin modulates actin dynamics in motor neurons. *Nat. Neurosci.* 19, 1610–1618. doi: 10.1038/nn.4407

Smith, B. N., Ticozzi, N., Fallini, C., Gkazi, A. S., Topp, S., Kenna, K. P., et al. (2014). Exome-wide rare variant analysis identifies TUBA4A mutations associated with familial ALS. *Neuron* 84, 324–331. doi: 10.1016/j.neuron.2014.09.027

Smith, B. N., Topp, S. D., Fallini, C., Shibata, H., Chen, H. J., Troakes, C., et al. (2017). Mutations in the vesicular trafficking protein annexin A11 are associated with amyotrophic lateral sclerosis. *Sci. Transl. Med.* 9:eaad9157. doi: 10.1126/scitranslmed.aad9157

So, E., Mitchell, J. C., Memmi, C., Chennell, G., Vizcay-Barrena, G., Allison, L., et al. (2018). Mitochondrial abnormalities and disruption of the neuromuscular junction precede the clinical phenotype and motor neuron loss in hFUSWT transgenic mice. *Hum. Mol. Genet.* 27, 463–474. doi: 10.1093/hmg/ddx415

Spaulding, E. L., and Burgess, R. W. (2017). Accumulating evidence for axonal translation in neuronal homeostasis. *Front. Neurosci.* 11:312. doi: 10.3389/fnins.2017.00312

Spillane, M., Ketschek, A., Merianda, T. T., Twiss, J. L., and Gallo, G. (2013). Mitochondria coordinate sites of axon branching through localized intra-axonal protein synthesis. *Cell Rep.* 5, 1564–1575. doi: 10.1016/j.celrep.2013.11.022

Steinacker, P., Feneberg, E., Weishaupt, J., Brettschneider, J., Tumani, H., Andersen, P. M., et al. (2016). Neurofilaments in the diagnosis of motoneuron diseases: a prospective study on 455 patients. *J. Neurol. Neurosurg. Psychiatry* 87, 12–20. doi: 10.1136/jnnp-2015-311387

Storkebaum, E. (2016). Peripheral neuropathy via mutant tRNA synthetases: inhibition of protein translation provides a possible explanation. *Bioessays* 38, 818–829. doi: 10.1002/bies.201600052

Suzuki, N., Aoki, M., Warita, H., Kato, M., Mizuno, H., Shimakura, N., et al. (2010). FALS with FUS mutation in Japan, with early onset, rapid progress and basophilic inclusion. *J. Hum. Genet.* 55, 252–254. doi: 10.1038/jhg.2010.16

Tagliaferro, P., and Burke, R. E. (2016). Retrograde axonal degeneration in Parkinson disease. *J. Parkinsons Dis.* 6, 1–15. doi: 10.3233/JPD-150769

Takata, M., Tanaka, H., Kimura, M., Nagahara, Y., Tanaka, K., Kawasaki, K., et al. (2013). Fasudil, a rho kinase inhibitor, limits motor neuron loss in experimental models of amyotrophic lateral sclerosis. *Br. J. Pharmacol.* 170, 341–351. doi: 10.1111/bph.12277

Takeuchi, A., Iida, K., Tsubota, T., Hosokawa, M., Denawa, M., Brown, J. B., et al. (2018). Loss of Sfpq causes long-gene transcriptopathy in the brain. *Cell Rep.* 23, 1326–1341. doi: 10.1016/j.celrep.2018.03.141

Tashiro, Y., Urushitani, M., Inoue, H., Koike, M., Uchiyama, Y., Komatsu, M., et al. (2012). Motor neuron-specific disruption of proteasomes, but not autophagy, replicates amyotrophic lateral sclerosis. *J. Biol. Chem.* 287, 42984–42994. doi: 10.1074/jbc.M112.417600

Taylor, A. M., Berchtold, N. C., Perreau, V. M., Tu, C. H., Li Jeon, N., and Cotman, C. W. (2009). Axonal mRNA in uninjured and regenerating cortical mammalian axons. *J. Neurosci.* 29, 4697–4707. doi: 10.1523/JNEUROSCI.6130-08.2009

Tcherkezian, J., Brittis, P. A., Thomas, F., Roux, P. P., and Flanagan, J. G. (2010). Transmembrane receptor DCC associates with protein synthesis machinery and regulates translation. *Cell* 141, 632–644. doi: 10.1016/j.cell.2010.04.008

Thiel, C., Kessler, K., Giessl, A., Dimmler, A., Shalev, S. A., Von Der Haar, S., et al. (2011). NEK1 mutations cause short-rib polydactyly syndrome type Majewski. *Am. J. Hum. Genet.* 88, 106–114. doi: 10.1016/j.ajhg.2010.12.004

Thomas-Jinu, S., Gordon, P. M., Fielding, T., Taylor, R., Smith, B. N., Snowden, V., et al. (2017). Non-nuclear pool of splicing factor SFPQ regulates axonal transcripts required for normal motor development. *Neuron* 94, 322–336.e5. doi: 10.1016/j.neuron.2017.03.026

Tian, F., Yang, W., Mordes, D. A., Wang, J. Y., Salameh, J. S., Mok, J., et al. (2016). Monitoring peripheral nerve degeneration in ALS by label-free stimulated Raman scattering imaging. *Nat. Commun.* 7:13283. doi: 10.1038/ncomms13283

Urushitani, M., Ezzi, S. A., Matsuo, A., Tooyama, I., and Julien, J. P. (2008). The endoplasmic reticulum-Golgi pathway is a target for translocation and aggregation of mutant superoxide dismutase linked to ALS. *FASEB J.* 22, 2476–2487. doi: 10.1096/fj.07-092783

Vance, C., Rogelj, B., Hortobagyi, T., De Vos, K. J., Nishimura, A. L., Sreedharan, J., et al. (2009). Mutations in FUS, an RNA processing protein, cause familial amyotrophic lateral sclerosis type 6. *Science* 323, 1208–1211. doi: 10.1126/science.1165942

Venkova, K., Christov, A., Kamaluddin, Z., Kobalka, P., Siddiqui, S., and Hensley, K. (2014). Semaphorin 3A signaling through neuropilin-1 is an early trigger for distal axonopathy in the SOD1G93A mouse model of amyotrophic lateral sclerosis. *J. Neuropathol. Exp. Neurol.* 73, 702–713. doi: 10.1097/NEN.0000000000000086

Verheijen, M. H., Peviani, M., Hendricusdottir, R., Bell, E. M., Lammens, M., Smit, A. B., et al. (2014). Increased axonal ribosome numbers is an early event in the pathogenesis of amyotrophic lateral sclerosis. *PLoS One* 9:e87255. doi: 10.1371/journal.pone.0087255

Wainger, B. J., Kiskinis, E., Mellin, C., Wiskow, O., Han, S. S., Sandoe, J., et al. (2014). Intrinsic membrane hyperexcitability of amyotrophic lateral sclerosis patient-derived motor neurons. *Cell Rep.* 7, 1–11. doi: 10.1016/j.celrep.2014.03.019

Wang, C., Han, B., Zhou, R., and Zhuang, X. (2016a). Real-time imaging of translation on single mRNA transcripts in live cells. *Cell* 165, 990–1001. doi: 10.1016/j.cell.2016.04.040

Wang, E. T., Taliaferro, J. M., Lee, J. A., Sudhakaran, I. P., Rossoll, W., Gross, C., et al. (2016b). Dysregulation of mRNA localization and translation in genetic disease. *J. Neurosci.* 36, 11418–11426. doi: 10.1523/jneurosci.2352-16.2016

Wang, L., Gao, J., Liu, J., Siedlak, S. L., Torres, S., Fujioka, H., et al. (2018). Mitofusin 2 regulates axonal transport of calpastatin to prevent neuromuscular synaptic elimination in skeletal muscles. *Cell Metab.* 28, 400–414.e8. doi: 10.1016/j.cmet.2018.06.011

Watanabe, S., Ilieva, H., Tamada, H., Nomura, H., Komine, O., Endo, F., et al. (2016). Mitochondria-associated membrane collapse is a common pathomechanism in SIGMAR1- and SOD1-linked ALS. *EMBO Mol. Med.* 8, 1421–1437. doi: 10.15252/emmm.201606403

Wen, X., Tan, W., Westergard, T., Krishnamurthy, K., Markandaiah, S. S., Shi, Y., et al. (2014). Antisense proline-arginine RAN dipeptides linked to *C9ORF72*-ALS/FTD form toxic nuclear aggregates that initiate in vitro and in vivo neuronal death. *Neuron* 84, 1213–1225. doi: 10.1016/j.neuron.2014.12.010

Weskamp, K., Tank, E. M., Miguez, R., Mcbride, J. P., Gomez, N. B., White, M., et al. (2019). Shortened TDP43 isoforms upregulated by neuronal hyperactivity drive TDP43 pathology in ALS. *J. Clin. Invest.* 130, 1139–1155. doi: 10.1172/JCI130988

Westergard, T., Jensen, B. K., Wen, X., Cai, J., Kropf, E., Iacovitti, L., et al. (2016). Cell-to-cell transmission of dipeptide repeat proteins linked to *C9orf72*-ALS/FTD. *Cell Rep.* 17, 645–652. doi: 10.1016/j.celrep.2016.09.032

Wiedau-Pazos, M., Goto, J. J., Rabizadeh, S., Gralla, E. B., Roe, J. A., Lee, M. K., et al. (1996). Altered reactivity of superoxide dismutase in familial amyotrophic lateral sclerosis. *Science* 271, 515–518.

Williamson, T. L., and Cleveland, D. W. (1999). Slowing of axonal transport is a very early event in the toxicity of ALS-linked SOD1 mutants to motor neurons. *Nat. Neurosci.* 2, 50–56. doi: 10.1038/4553

Willis, D. E., Van Niekerk, E. A., Sasaki, Y., Mesngon, M., Merianda, T. T., Williams, G. G., et al. (2007). Extracellular stimuli specifically regulate localized

levels of individual neuronal mRNAs. *J. Cell Biol.* 178, 965–980. doi: 10.1083/jcb.200703209

Wu, B., Eliscovich, C., Yoon, Y. J., and Singer, R. H. (2016a). Translation dynamics of single mRNAs in live cells and neurons. *Science* 352, 1430–1435. doi: 10.1126/science.aaf1084

Wu, C. H., Fallini, C., Ticozzi, N., Keagle, P. J., Sapp, P. C., Piotrowska, K., et al. (2012b). Mutations in the profilin 1 gene cause familial amyotrophic lateral sclerosis. *Nature* 488, 499–503. doi: 10.1038/nature11280

Wu, J. W., Hussaini, S. A., Bastille, I. M., Rodriguez, G. A., Mrejeru, A., Rilett, K., et al. (2016b). Neuronal activity enhances tau propagation and tau pathology in vivo. *Nat. Neurosci.* 19, 1085–1092. doi: 10.1038/nn.4328

Xiang, Y., Tanaka, Y., Patterson, B., Kang, Y. J., Govindaiah, G., Roselaar, N., et al. (2017). Fusion of regionally specified hPSC-derived organoids models human brain development and interneuron migration. *Cell Stem Cell* 21, 383–398.e7. doi: 10.1016/j.stem.2017.07.007

Xie, Y., Zhou, B., Lin, M. Y., Wang, S., Foust, K. D., and Sheng, Z. H. (2015). Endolysosomal deficits augment mitochondria pathology in spinal motor neurons of asymptomatic fALS mice. *Neuron* 87, 355–370. doi: 10.1016/j.neuron.2015.06.026

Xing, L., and Bassell, G. J. (2013). mRNA localization: an orchestration of assembly, traffic and synthesis. *Traffic* 14, 2–14. doi: 10.1111/tra.12004

Yamanaka, K., Chun, S. J., Boillee, S., Fujimori-Tonou, N., Yamashita, H., Gutmann, D. H., et al. (2008). Astrocytes as determinants of disease progression in inherited amyotrophic lateral sclerosis. *Nat. Neurosci.* 11, 251–253. doi: 10.1038/nn2047

Yamazaki, T., Chen, S., Yu, Y., Yan, B., Haertlein, T. C., Carrasco, M. A., et al. (2012). FUS-SMN protein interactions link the motor neuron diseases ALS and SMA. *Cell Rep.* 2, 799–806. doi: 10.1016/j.celrep.2012.08.025

Yan, S., Guo, C., Hou, G., Zhang, H., Lu, X., Williams, J. C., et al. (2015). Atomic-resolution structure of the CAP-Gly domain of dynactin on polymeric microtubules determined by magic angle spinning NMR spectroscopy. *Proc. Natl. Acad. Sci. U.S.A.* 112, 14611–14616. doi: 10.1073/pnas.1509852112

Yan, X., Hoek, T. A., Vale, R. D., and Tanenbaum, M. E. (2016). Dynamics of translation of single mRNA molecules in vivo. *Cell* 165, 976–989. doi: 10.1016/j.cell.2016.04.034

Yoon, Y. J., Wu, B., Buxbaum, A. R., Das, S., Tsai, A., English, B. P., et al. (2016). Glutamate-induced RNA localization and translation in neurons. *Proc. Natl. Acad. Sci. U.S.A.* 113, E6877–E6886.

Yoshizawa, T., Ali, R., Jiou, J., Fung, H. Y. J., Burke, K. A., Kim, S. J., et al. (2018). Nuclear import receptor inhibits phase separation of FUS through binding to multiple sites. *Cell* 173, 693–705.e22. doi: 10.1016/j.cell.2018.03.003

Zhang, C. L., Rodenkirch, L., Schultz, J. R., and Chiu, S. Y. (2012). A novel method to study the local mitochondrial fusion in myelinated axons in vivo. *J. Neurosci. Methods* 207, 51–58. doi: 10.1016/j.jneumeth.2012.03.013

Zheng, J. Q., Kelly, T. K., Chang, B., Ryazantsev, S., Rajasekaran, A. K., Martin, K. C., et al. (2001). A functional role for intra-axonal protein synthesis during axonal regeneration from adult sensory neurons. *J. Neurosci.* 21, 9291–9303. doi: 10.1523/jneurosci.21-23-09291.2001

Zhou, B., Yu, P., Lin, M. Y., Sun, T., Chen, Y., and Sheng, Z. H. (2016). Facilitation of axon regeneration by enhancing mitochondrial transport and rescuing energy deficits. *J. Cell Biol.* 214, 103–119. doi: 10.1083/jcb.201605101

Zivraj, K. H., Tung, Y. C., Piper, M., Gumy, L., Fawcett, J. W., Yeo, G. S., et al. (2010). Subcellular profiling reveals distinct and developmentally regulated repertoire of growth cone mRNAs. *J. Neurosci.* 30, 15464–15478. doi: 10.1523/JNEUROSCI.1800-10.2010

Conflict of Interest: The authors declare that the research was conducted in the absence of any commercial or financial relationships that could be construed as a potential conflict of interest.

The reviewer MK declared a past co-authorship with the authors NS and MA to the handling Editor.

frontiers in Neuroscience

ORIGINAL RESEARCH
published: 27 August 2020
doi: 10.3389/fnins.2020.00874

T Cell Responses to Neural Autoantigens Are Similar in Alzheimer's Disease Patients and Age-Matched Healthy Controls

Rekha Dhanwani[1], John Pham[1], Ashmitaa Logandha Ramamoorthy Premlal[1], April Frazier[1], Atul Kumar[2], Maria Elena Pero[2,3], Francesca Bartolini[2], Juliana Rezende Dutra[4], Karen S. Marder[4], Bjoern Peters[1,5], David Sulzer[6,7], Alessandro Sette[1,5] and Cecilia S. Lindestam Arlehamn[1]**

[1] Division of Vaccine Discovery, La Jolla Institute for Immunology, La Jolla, CA, United States, [2] Department of Pathology and Cell Biology, Columbia University, New York, NY, United States, [3] Department of Veterinary Medicine and Animal Production, University of Naples Federico II, Naples, Italy, [4] Department of Neurology, Columbia University Irving Medical Center, New York, NY, United States, [5] Department of Medicine, University of California, San Diego, La Jolla, CA, United States, [6] Department of Neurology, New York State Psychiatric Institute, Columbia University, New York, NY, United States, [7] Department of Psychiatry and Pharmacology, New York State Psychiatric Institute, Columbia University, New York, NY, United States

OPEN ACCESS

Edited by:
Manoj Kumar Jaiswal, Icahn School of Medicine at Mount Sinai, United States

Reviewed by:
Sudhanshu P. Raikwar, University of Missouri, United States
Raj N. Kalaria, Newcastle University, United Kingdom

***Correspondence:**
Alessandro Sette
alex@lji.org
Cecilia S. Lindestam Arlehamn
cecilia@lji.org

Specialty section:
This article was submitted to Neurodegeneration, a section of the journal Frontiers in Neuroscience

Received: *26 May 2020*
Accepted: *27 July 2020*
Published: *27 August 2020*

Citation:
Dhanwani R, Pham J, Premlal ALR, Frazier A, Kumar A, Pero ME, Bartolini F, Dutra JR, Marder KS, Peters B, Sulzer D, Sette A and Lindestam Arlehamn CS (2020) T Cell Responses to Neural Autoantigens Are Similar in Alzheimer's Disease Patients and Age-Matched Healthy Controls. Front. Neurosci. 14:874. doi: 10.3389/fnins.2020.00874

Alzheimer's disease (AD), a chronic multifactorial and complex neurodegenerative disorder is a leading cause of dementia. Recently, neuroinflammation has been hypothesized as a contributing factor to AD pathogenesis. The role of adaptive immune responses against neuronal antigens, which can either confer protection or induce damage in AD, has not been fully characterized. Here, we measured T cell responses to several potential antigens of neural origin including amyloid precursor protein (APP), amyloid beta (Aβ), tau, α-synuclein, and transactive response DNA binding protein (TDP-43) in patients with AD and age-matched healthy controls (HC). Antigen-specific T cell reactivity was detected for all tested antigens, and response to tau-derived epitopes was particularly strong, but no significant differences between individuals with AD and age-matched HC were identified. We also did not observe any correlation between the antigen-specific T cell responses and clinical variables including age, gender, years since diagnosis and cognitive score. Additionally, further characterization did not reveal any differences in the relative frequency of major Peripheral Blood Mononuclear Cells (PBMC) subsets, or in the expression of genes between AD patients and HC. These observations have not identified a key role of neuronal antigen-specific T cell responses in AD.

Keywords: Alzheimer's disease, neurodegenration, autoimmunity, T cell responses, transcriptomics, neuroantigens

INTRODUCTION

Alzheimer's disease (AD) is a neurodegenerative disorder associated with the progressive loss of structure and function in neurons, leading to dementia and affecting predominantly elderly individuals. The disease is characterized by extracellular plaques that consist of amyloid beta peptides (Aβ) that is produced from the amyloid precursor protein (APP) and neurofibrillary

tangles that consist of hyperphosphorylated tau (Grundke-Iqbal et al., 1986; Butterfield and Boyd-Kimball, 2004).

Aggregation or misfolding of autoantigens expressed in the brain, such as Aβ (Finder and Glockshuber, 2007), α-synuclein (Paleologou et al., 2005), tau (Honson and Kuret, 2008), and transactive response DNA binding protein (TDP-43) (Cook et al., 2008; Guo et al., 2011; Herman et al., 2011; Jiang et al., 2016), could render susceptibility to adaptive T cell responses and are associated with Parkinson's disease (PD), AD, and amyotrophic lateral sclerosis (ALS). The role of T cell autoimmunity has been studied in various animal models (Wong et al., 2002; Bloom et al., 2005; Janus and Welzl, 2010; Dawson et al., 2018), but less frequently in humans (Sulzer et al., 2017; Lodygin et al., 2019).

There are, however, increasing reasons to speculate that T cell responses in neurodegenerative diseases, including AD, are mounted against aggregated or misfolded neural proteins (Mietelska-Porowska and Wojda, 2017). Some studies have shown increased infiltration of T cells in response to inflammatory signals in the brains of AD patients (Itagaki et al., 1988; Pirttila et al., 1992; Merlini et al., 2018). It is also speculated that neuroinflammation is not the only source of neurodegeneration in the AD brain. The AD induced neurodegeneration could emerge due to multi−faceted interactions between inflammation and other processes such as NFT formation, Aβ deposition, glutamate excitotoxicity, reactive oxygen intermediate toxicity, and/or other mechanisms that induce neuronal death in the AD cortex (Cooper et al., 2000). However, the functional role and reactivity of the CNS infiltrating T cells have not been determined, in part due to limited sample availability. An alternative approach is to study T cell responses in PBMCs that can help better understand the role of adaptive immune responses in AD in more accessible samples. This approach was recently successful in characterizing the role of T cells in AD (Monsonego et al., 2003; Gate et al., 2020), as well as Parkinson's disease (PD), another important neurodegenerative disorder (Sulzer et al., 2017; Lindestam Arlehamn et al., 2019, 2020).

In addition to self-antigens implicated in the pathogenesis of neurodegenerative diseases, some microbes like *Bordetella pertussis* (PT) and herpesviruses have also been hypothesized to be associated with the development of AD (Lin et al., 2002; Rubin and Glazer, 2017; Allnutt et al., 2020). Therefore, characterizing neural and microbial antigen-specific T cell responses in peripheral T cells from individuals with AD may help untangle the complex concept of autoimmunity in neurodegeneration and establish a correlation between T cell reactivity and disease progression.

Here, to assess the potential involvement of peripheral T cells in AD, we performed a range of immunological assays in individuals with AD and age-matched HC. Specifically, we (i) compared the relative frequency of major PBMC cell subsets, (ii) characterized T cell responses to proteins involved in neurodegeneration such as Aβ, APP, tau, α-synuclein, TDP-43, PT, and Epstein-Barr virus and cytomegalovirus (EBV/CMV), (iii) correlated antigen-specific reactivity with demographic and clinical variables including age, gender, time since diagnosis and cognitive score, and (iv) conducted a transcriptomic analysis of PBMC, CD4 memory and CD8 memory T cells to assess differential expression of genes in AD compared to HC. In summary, these analyses revealed no statistically significant differences between the populations of AD patients and age-matched HC.

RESULTS

Relative Frequency of Major PBMC Subsets in AD Compared to Age-Matched HC

We previously described the establishment of a flow cytometry panel designed to quantitate the relative frequency of major PBMC subsets in order to examine potential differences as a function of disease states (Burel et al., 2017). Here, we utilized this panel to specifically examine whether differences in lymphocyte subsets could be associated with AD. We first analyzed the relative frequency of major PBMC subsets, i.e., monocytes, NK cells, B cells, T cells, and CD4 and CD8 memory T cells, in 27 AD and 30 age-matched HC by flow cytometric analysis (gating strategy in **Supplementary Figure S1**). In general, the frequency of all PBMC subsets was remarkably similar between AD and HC (**Figure 1**). The only significant difference observed was related to the frequency of the T_{EMRA} subset of CD4 memory T cells, which was found to be decreased in AD patients.

Cytokine Responses to Neural and Microbial Antigens in AD and Age-Matched HC

Aβ, α-synuclein, tau and TDP-43 have been implicated in AD and other forms of dementia, as well as in PD (Paleologou et al., 2005; Finder and Glockshuber, 2007; Cook et al., 2008; Honson and Kuret, 2008; Guo et al., 2011; Herman et al., 2011; Jiang et al., 2016). We examined whether T cell reactivity against these proteins could be detected and, if so, whether differences existed between AD patients and age-matched HC. Accordingly, PBMCs were stimulated for 2 weeks *in vitro* with peptide pools representing the different proteins. The APP pool corresponded to 153 peptides, while the amyloid beta-42 (Aβ) pool encompassed 9 peptides. The previously described α-syn epitope and tau peptide pools consisted of 11 and 70 peptides, respectively (Sulzer et al., 2017; Lindestam Arlehamn et al., 2019). We also studied a TDP-43 peptide pool which is composed of 82 peptides. We further measured cytokine responses against pertussis (PT) and EBV/CMV peptide pools (Bancroft et al., 2016; Dan et al., 2016; Tian et al., 2017; da Silva Antunes et al., 2018).

After 2 weeks, cultures were harvested and stimulated with the relevant antigen used in establishing the cultures, or PHA as a control, in a triple-color IFNγ, IL-5, and IL-10 Fluorospot assay. While T cell reactivity was detected for all tested antigens, no significant differences in total response magnitude (**Figure 2A**) or specific cytokines (**Figure 3**) were observed between AD patients and age-matched HC.

Additionally, due to the difference in ethnicity between AD and HC cohorts (**Table 1**), we also analyzed our data excluding

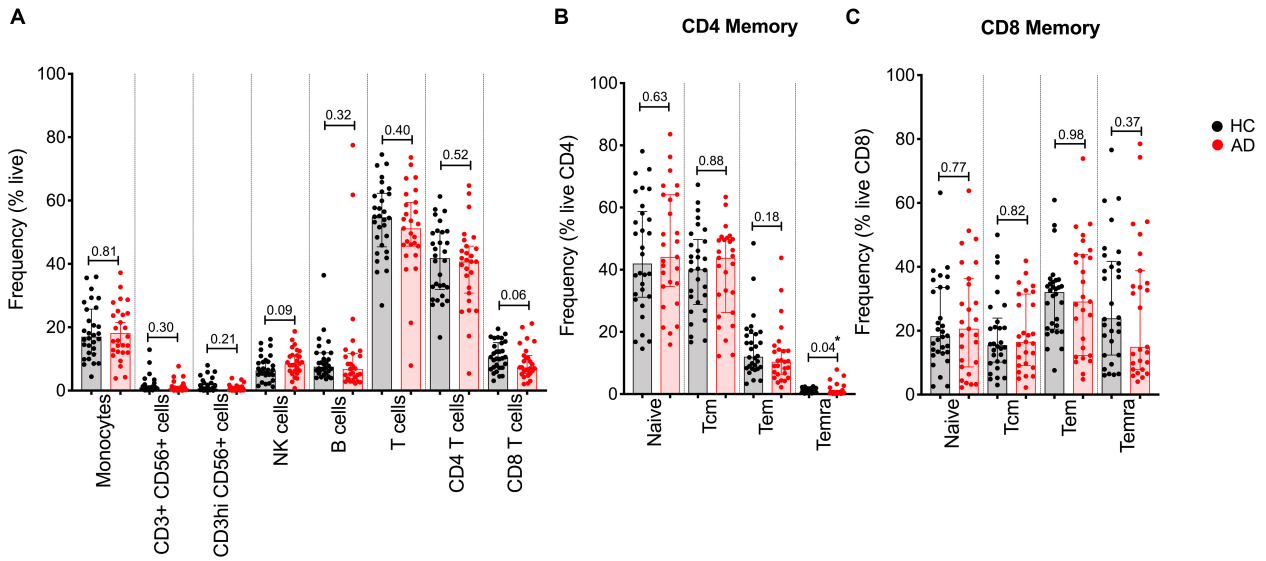

FIGURE 1 | Relative frequency of different cell subsets in HC and AD. **(A)** Frequency of major PBMC subsets in AD (red bars and circles) and age-matched HC (black bar and circles). **(B)** CD4 memory and **(C)** CD8 memory T cells were further evaluated for frequency of naïve, effector memory (T_{em}), central memory (T_{cm}), and T_{EMRA} populations. Each point represents a donor. Median ± interquartile range is displayed. Two-tailed Mann–Whitney test. Cells were gated according to the gating strategy in **Supplementary Figure S1**.

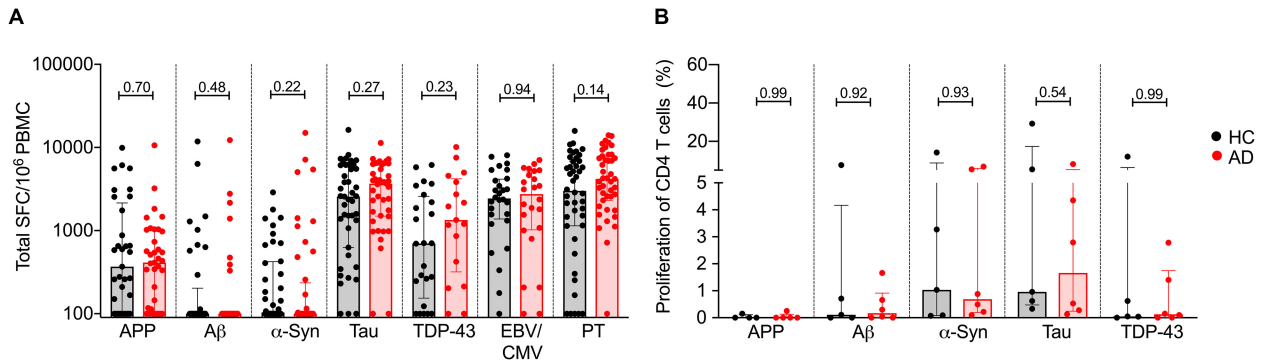

FIGURE 2 | T cell reactivity to APP, Aβ, α-synuclein, tau, TDP-43, EBV/CMV, and PT in AD and age-matched HC. **(A)** Magnitude of total response (sum of IFNγ, IL-5, and IL-10) in HC (black bar and circles) and AD (red bar and circles) to APP (HC, n = 33; AD n = 37), Aβ (HC, n = 37; AD, n = 37), α-syn (HC, n = 40; AD, n = 44), tau (HC, n = 43; AD n = 41), TDP-43 (HC, n = 24; AD, n = 17), EBV/CMV (HC, n = 28; AD, n = 24), and PT (HC, n = 44; AD, n = 43). Each dot represents a subject. Median ± interquartile range is shown. Two-tailed Mann–Whitney test. **(B)** Proliferation of CD4 T cells in AD (n = 6) and HC (n = 6). % of proliferated $CD4^{++}$ T cell (CFSE-ve) population in DMSO stimulated condition was subtracted from antigen stimulated condition. Median ± interquartile range is displayed. Each point represents a subject. Two-tailed Mann–Whitney test.

non-Caucasian subjects and found no significant difference in T cell reactivity between AD and HC, with the exception of PT reactivity. PT-specific T cell responses were higher in AD as compared to HC (**Supplementary Figure S2**). A trend for higher PT-specific T cell reactivity was also observed in the entire cohort (**Figure 2**).

We have previously described higher magnitude of responses against tau as compared to α-syn in individuals with PD and HC (Lindestam Arlehamn et al., 2019). Notably, the magnitude of cytokine responses against APP, Aβ and α-syn were weaker than that observed against tau, EBV/CMV and PT. This suggests that these antigens are less immunogenic.

Proliferative Responses in AD and Age-Matched HC

We next sought to confirm these findings using an alternative readout, namely a proliferative assay that was recently described as a means to detect β-synuclein T cell reactivity in multiple sclerosis and PD patients (Lodygin et al., 2019). Accordingly, we determined the frequency of proliferating $CD4^+$ T cells in response to the same antigens, in a subset of 6 AD and 6 HC. The PBMCs were stained with CFSE, stimulated with the respective antigens and cultured for 11 days. After 11 days, cells were stained with CD3, CD4, and CD8 antibodies, and the percentage of $CD4^+$ T cell proliferation

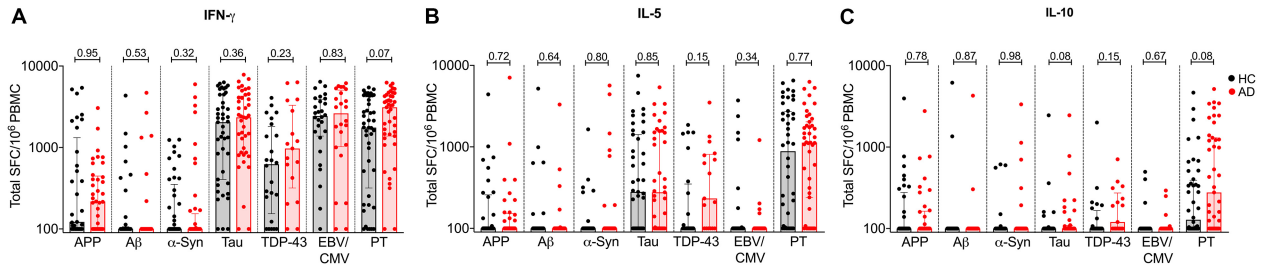

FIGURE 3 | Individual cytokine responses to APP, Aβ, α-synuclein, tau, TDP-43, EBV/CMV, and PT in AD and age-matched HC **(A)** IFNγ, **(B)** IL-5, and **(C)** IL-10. Each symbol represents a subject. HC is represented in black bar and circles and AD is represented in red bar and circles. Median ± interquartile range is shown.

was measured (gating strategy in **Supplementary Figure S3**). Utilizing this alternative readout, no difference was observed in the percentage of proliferating $CD4^+$ T cells between AD and HC (**Figure 2B**).

Correlations Between Antigen Specific T Cell Reactivity, Sex, and Clinical Variables

In a recent study (Lindestam Arlehamn et al., 2020), the T cell reactivity to α-synuclein was related to early diagnoses of PD, suggesting that correlational studies may help establish a link with disease progression. To investigate whether any such relationships exists in AD, we examined the possible correlations between antigen specific T cell reactivity and clinical variables such as gender, age, time since diagnosis and cognitive score. First, we compared the magnitude and frequency of antigen-specific T cell responses as a function of sex and found no significant difference in the T cell responses of males and females with AD as compared to age-matched HC (**Figure 4**).

Next, we examined whether antigen-specific T cell reactivity correlated with clinical variables relevant to AD patients: age, years since diagnosis and cognitive function (the Montreal Cognitive Assessment; MoCA) (Davis et al., 2015). Unlike Parkinson's disease, where a strong positive correlation was established between T cell reactivity to α-syn and clinical variables including age and time since diagnosis (Lindestam Arlehamn et al., 2020), no correlation was detected in AD patients between antigen-specific T cell reactivity and clinical parameters (**Figure 5**).

TABLE 1 | Characteristics of the subjects enrolled in the study.

Characteristics and demographics	AD	HC
Total subjects enrolled	51	53
Median age (range), yr	69, (52–89)	68, (56–92)
Male, % (n)	51% (26)	43% (23)
Caucasian, % (n)	65% (33)	92.5% (49)
Median years since diagnosis, (range), yr	4, (0.5–11)	NA
Median MoCA[a] (range)	18 (8–26)	28 (24–30)
Median MMSE[b] (range)	22 (16–28)	30 (29–30)

[a]*MoCA collected at CUMC only.* [b]*MMSE collected at PrecisionMed only.*

Transcriptional Profiling of PBMCs, CD4, and CD8 Memory T Cells in AD and HC

Finally, we examined whether differences between individuals with AD and HC could be detected at the level of gene expression in different cell populations. PBMCs, CD4 memory, and CD8 memory T cells from the CUMC cohort were sorted (gating strategy in **Supplementary Figure S1**) and RNA was extracted as described in the methods section. Principal component analysis (PCA) of the 1000 most variable genes revealed that PBMCs, CD4 memory and CD8 memory T cells formed distinct clusters, as expected (**Figure 6A**). This cell subset clustering was also evident when the 100 most variable genes were considered (**Figure 6B** and **Supplementary Table S1**). Next, we performed a pairwise analysis to identify any differentially expressed (DE) genes between AD and HC in PBMCs, CD4 memory and CD8 memory T cells. At a cut-off of $\log_2$ fold change >0.5 and p_{adj} less than 0.05, PBMCs had no differences in patterns of gene expression between AD and HC (0 DE genes), and only two genes each were differentially expressed in CD4 memory (GNAL and KIF18B) and CD8 memory (RPL10P6 and PRAM1) T cells (**Figure 6C**). Moreover, we exclusively looked into differential expression of miRNAs due to their wide implication in AD pathogenesis (Cosin-Tomas et al., 2017; Hara et al., 2017; Kumar and Reddy, 2018; Moradifard et al., 2018; Angelucci et al., 2019). However, as shown in **Supplementary Figure S4**, there were no miRNAs that were differentially expressed between AD and HC subjects in either of the cell subsets tested in this study, reflecting the lack of differences observed in the overall DEseq analysis.

DISCUSSION

We investigated autoreactivity of T cells against antigens that have been associated with AD, specifically Aβ, APP, α-synuclein, tau and TDP-43. To do so, peripheral T cells of AD patients and age-matched HC were systematically compared for differences in the frequency of T cell subsets, cytokine responses, proliferative capacity and differential gene expression signatures.

We chose these targets because they are proteins that accumulate in association with several neurodegenerative diseases, including AD, and are subject to post-translational modifications in the course of disorders that may produce neoantigens. Pathological manifestations are characterized by

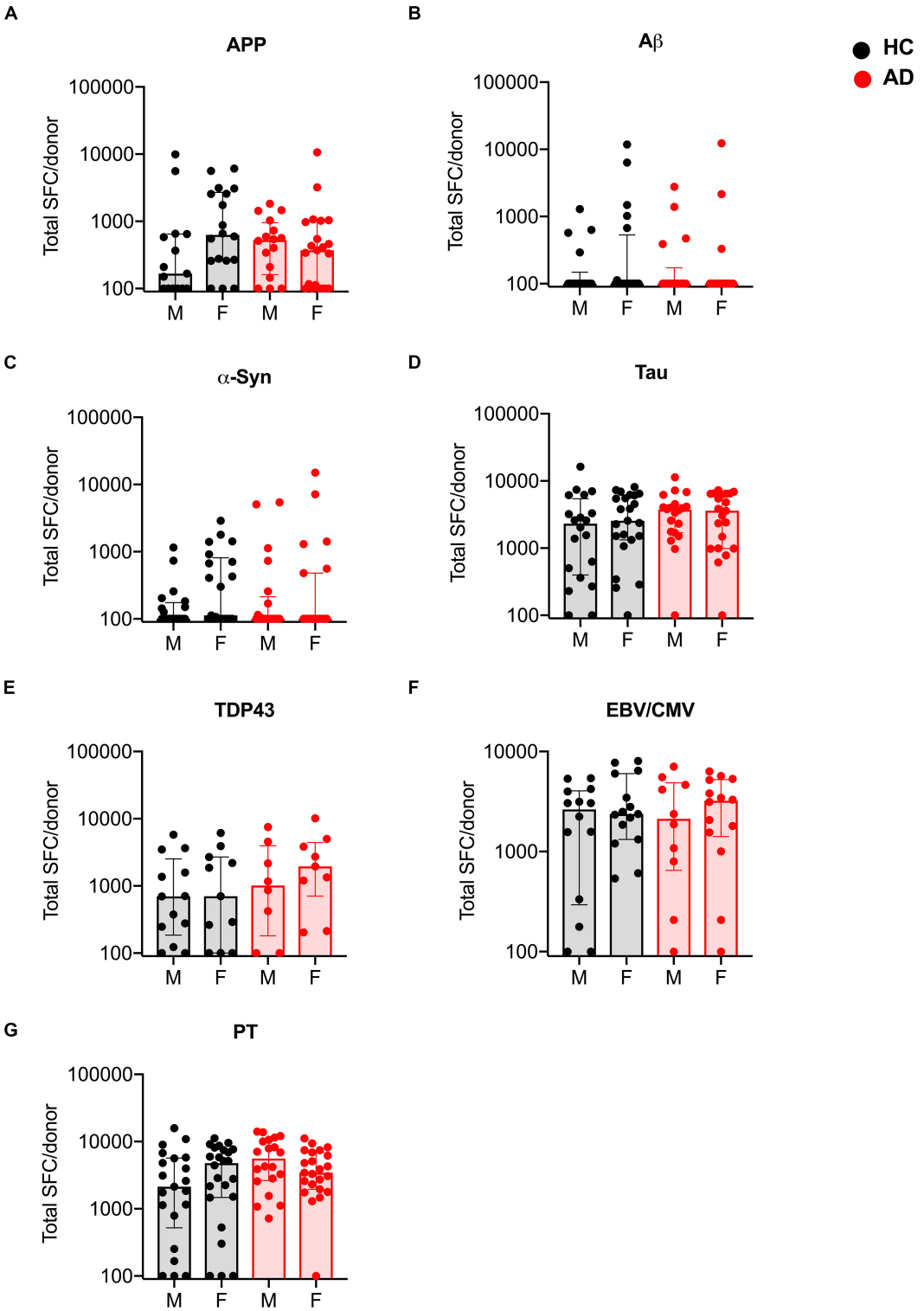

FIGURE 4 | Magnitude of T cell responses to specific antigens in males and females with AD and age-matched HC. **(A)** APP (HC males *n* = 15, females *n* = 18; AD males *n* = 16, females *n* = 21) **(B)** Aβ (HC males *n* = 18, females *n* = 20; AD males *n* = 18, females *n* = 19) **(C)** α-synuclein (HC males *n* = 20, females *n* = 21; AD males *n* = 21, females *n* = 23) **(D)** tau (HC males *n* = 20, females *n* = 23; AD males *n* = 20, females *n* = 21) **(E)** TDP-43 (HC males *n* = 13, females *n* = 11; AD males *n* = 8, females *n* = 9) **(F)** EBV/CMV (HC males *n* = 14, females *n* = 15; AD males *n* = 10, females *n* = 14) **(G)** PT (HC males *n* = 21, females *n* = 24; AD males *n* = 20, females *n* = 23). Each dot represents a donor. Black dot (within gray bar) represents HC and red dot (within red bar) represents AD. Median with interquartile range is displayed.

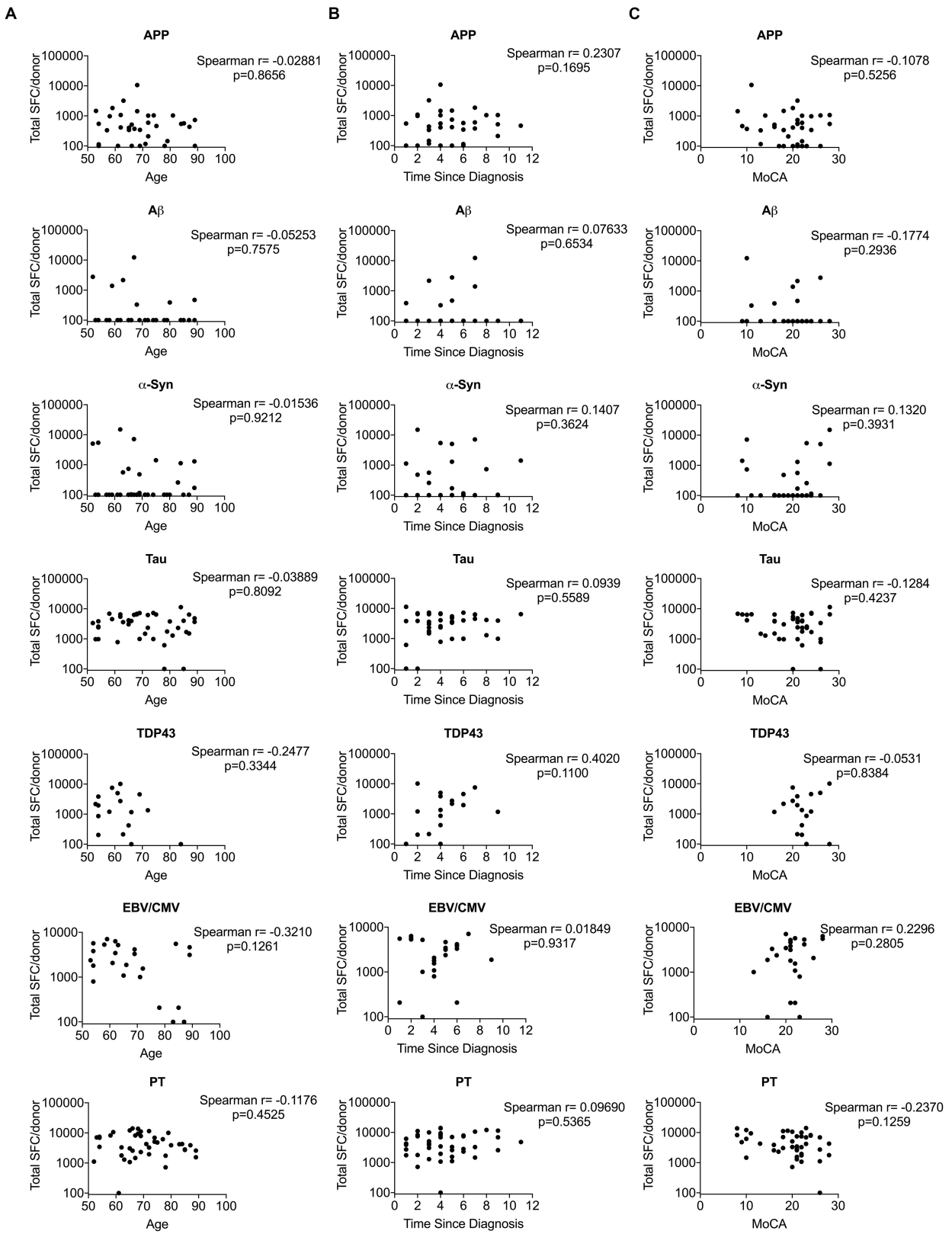

FIGURE 5 | Correlation between T cell reactivity to different antigens and clinical variables. **(A)** Age vs. T cell reactivity. **(B)** Time since diagnosis vs. T cell reactivity **(C)** MoCA vs. T cell reactivity. *X*-axis in panels **(A–C)** represent clinical variables age, time since diagnosis and MoCA, respectively and *Y*-axis represents T cell reactivity. Each dot represents a donor. Non-parametric Spearman test was performed.

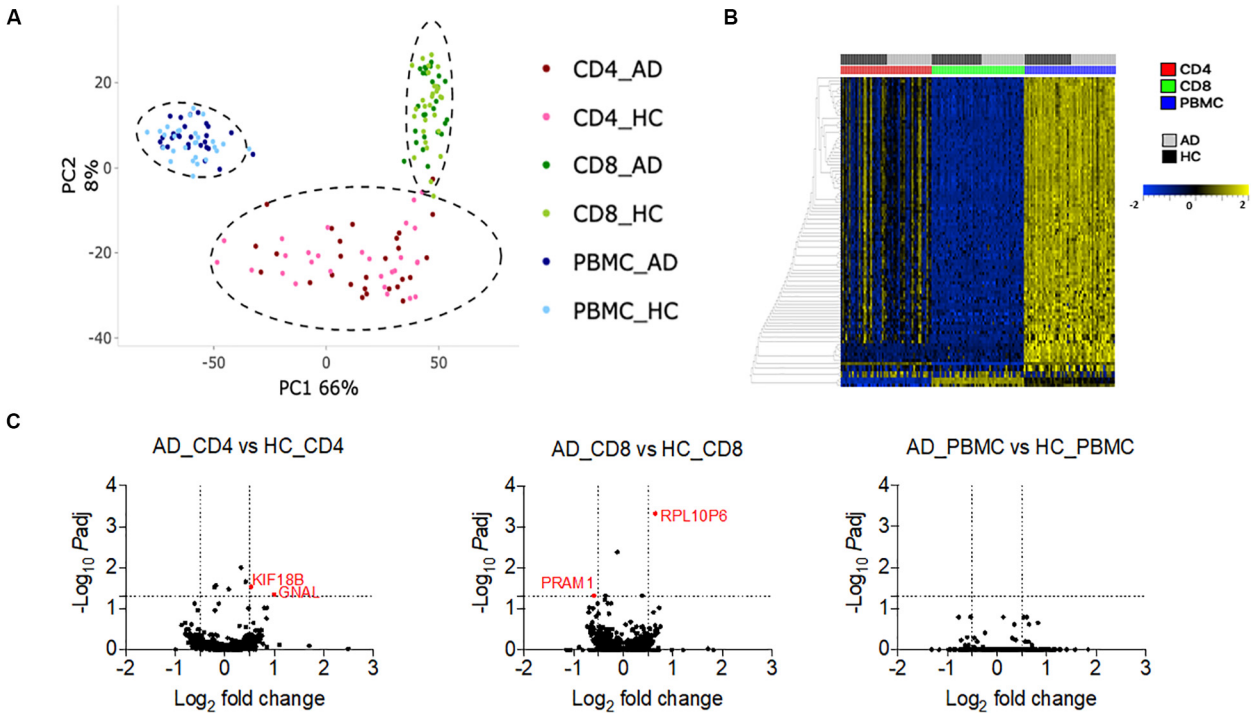

FIGURE 6 | Transcriptomic profile of PBMC, CD4 memory and CD8 memory T cells in AD and HC **(A)**. PCA analysis of gene expression data from PBMC (HC n = 28 and AD n = 27), CD4 memory (HC n = 28 and AD n = 27), and CD8 memory (HC n = 30 and AD n = 26) T cells of HC and AD **(B)**. Heat map of the top 100 variable genes in PBMC, CD4 memory, and CD8 memory T cells **(C)**. Volcano plots show $\log_2$ fold change vs. $-\log_{10}$ p_{adj} value for the comparison between AD and HC PBMC, AD, and HC CD4 memory and AD and HC CD8 memory T cells. Dotted lines indicate the cut off limit of $\log_2$ fold change (on x-axis) and $-\log_{10}$ p_{adj} (on y-axis). Because most of the genes are non-significant, they fall on the axis. The genes with $\log_2$ fold change greater than 0.5 or less than –0.5 and adjusted p-Value less than 0.05 are considered significant and are represented in red.

the immune system's failure to clear the deposited aggregated proteins (Irvine et al., 2008). This pathological presentation is attributed to a combination of molecular and environmental factors, such as aging and genetics (Cacabelos et al., 2005). At the molecular level, the neurodegenerative diseases are characterized by the accumulation of protein fragments that cluster together, producing toxic effects on neurons and disrupting cell to cell communication.

Several research groups have reported the presence of autoantibodies against a variety of molecules in AD (Du et al., 2001; Rosenmann et al., 2006; Dodel et al., 2011). Natural autoantibodies are produced under physiological conditions to clear dead cells or toxic autoantigens and thereby dampen inflammatory signals. This feature of natural autoantibodies highlights their potential role in conferring protection against the progression of AD (Du et al., 2001; Weksler et al., 2002; Brettschneider et al., 2005; Britschgi et al., 2009; Dodel et al., 2011; Qu et al., 2014). Moreover, some autoantibodies have also emerged as potential biomarkers for AD. However, with the exception of some reports (Monsonego et al., 2003; Gate et al., 2020), the role of aberrant T cell responses that equally contribute to driving autoimmunity in AD has not been well characterized. Thus, addressing the potential role of autoreactive T cells in AD might improve our understanding of neurodegenerative diseases and offer novel avenues of therapeutic intervention.

Here, multiple approaches of investigating T cell reactivity to the various antigens revealed no difference between AD and age-matched healthy controls except near significant increase in IFNγ and IL-10 response to PT in AD patients. This is in agreement with the recent hypothesis that B. pertussis plays a role in the etiology of AD (Rubin and Glazer, 2017). Our findings are consistent with reports of increased T cell reactivity to Aβ in older humans and patients with AD compared to healthy young adults, but no difference in T cell reactivity between healthy older humans and AD (Giubilei et al., 2003; Monsonego et al., 2003). Additionally, no difference was observed in the frequency of various cell subsets, except for CD4 T_{EMRA} subset. A previous study (Richartz-Salzburger et al., 2007) reported only slight increase in circulating $CD4^+$ T cells and a decreased frequency of $CD3^+$ T cells, $CD8^+$ T cells, and $CD19^+$ cells in AD compared to healthy controls. Furthermore, recently an increase in $CD3^+CD8^+CD45RA^+CD27^-$ TEMRA T cells was reported in mild cognitive impairment (MCI) or AD patients (Gate et al., 2020). In our cohort there was no significant difference in the frequency of this cell subset. Other studies have also reported differences in various immune cell subsets such as decreased T cell numbers and changes in the CD4 T cell compartment (Pellicano et al., 2012; Busse et al., 2017). The discrepancies of the different studies could be related to differences in several factors such as T cell stimulation methodology, sample size, drugs

used by patients for disease management and/or in the criteria used to define AD subjects. Our flow cytometry panels did not include in-depth analysis of Tregs, and different subsets of Tregs were recently found to be decreased in AD patients compared to HC (Ciccocioppo et al., 2019). Different miRNAs have previously been identified in serum, plasma, CSF, or brain as differentially regulated or expressed between AD and age-matched HC (Cosin-Tomas et al., 2017; Hara et al., 2017; Kumar and Reddy, 2018; Moradifard et al., 2018; Angelucci et al., 2019). No studies have so far shown differentially expressed miRNAs in these cohorts in peripheral T cell subsets or PBMCs. Future studies can confirm whether differences in other cell subsets, such as specifically Treg subsets, immune parameters, or miRNA expression in these cell subsets exist between AD and HC.

Because it is well-known that aging alters the components of innate and adaptive immunity we included age-matched healthy controls in this study. Age-related irreversible alterations correlate with a general increase in propensity to autoimmunity (Maletto et al., 1994; Simon et al., 2015), which may affect antigen-specific T cell responses. The increase in autoimmunity with age was recently supported by our study in Parkinson's disease where α-syn-specific T cell responses increase as a function of age (Lindestam Arlehamn et al., 2020). One caveat of our study is that the AD and HC cohorts were not matched for race. However, no differences were detected between race-matched AD and HC cohorts. Moreover, if race influences the immunological responses measured we would have expected to see more differences rather than fewer.

Our findings suggest a difference in the disease pathology of PD and AD. PD is associated with an increase in T cell reactivity to α-synuclein (Sulzer et al., 2017; Lindestam Arlehamn et al., 2020). These increased T cell responses to α-synuclein are negatively correlated with time since PD diagnosis (Lindestam Arlehamn et al., 2020). For AD however, with the exception of a minor decrease in the CD4 T_{EMRA} cell population in AD, no difference in T cell reactivity between AD and HC was noted, and no correlation could be established between T cell reactivity and clinical variables, which is in agreement with a previous study (Giubilei et al., 2003). This may reflect a fundamental difference between PD and AD, with T cells and associated inflammation playing a key role in PD, but not AD. In that respect, it is noteworthy that PD incidence is increased in association with other inflammatory autoimmune diseases such as IBD, and that anti-TNF treatment is associated with a reduction in PD incidence (Peter et al., 2018), while no such effect has been reported in the case of AD.

In conclusion, this study highlights a clear difference between the role of T cell mediated immunity in PD and AD. However, the lack of evidence for differential T cell recognition of the antigens we studied in AD does not rule out that other proteins or the same proteins with different post-translational modifications may show differential response. There may further be different forms or stages of AD where such differences could occur. Hence, further studies deconvoluting the autoantigens at the epitope level, including of CNS infiltrating cells, and investigating the role of post-translationally autoantigen modifications such as acetylation and phosphorylation might reveal differences in T cell reactivity between AD and healthy controls providing detailed insights on AD associated autoimmune responses.

MATERIALS AND METHODS

Ethics Statement

All participants provided written informed consent for participation in the study. Ethical approval was obtained from the Institutional review boards at the La Jolla Institute for Immunology (LJI; protocol number VD-155) and the Columbia University Medical Center (CUMC; protocol number IRB-AAAQ9714).

Study Subjects

We recruited a total of 104 individuals diagnosed with AD ($n = 51$) and age-matched healthy subjects ($n = 53$) in this study. The subjects were recruited from two sites: 66 subjects from Alzheimer's Disease Research Center at Columbia University Medical Center (CUMC) (AD $n = 33$ and HC $n = 33$) and 38 subjects from a San Diego-based Contract Research Organization, PrecisionMed (AD $n = 18$ and HC $n = 20$). The characteristics of the enrolled subjects are detailed in **Table 1**.

Subjects recruited at CUMC were diagnosed by neurologists according to the National Institute of Aging and Alzheimer's Association criteria (McKhann et al., 2011). Fifteen AD subjects had neuropsychological testing only and 18 AD subjects had neuropsychological testing and combinations of positive biomarkers including SPECT scan ($n = 6$), FDG PET scan ($n = 4$), CSF ($n = 3$), or amyloid scan ($n = 7$). They were all followed for at least 2 consecutive visits. Eleven AD subjects started having cognitive symptoms before age 65, and were thus early onset AD. 33 HC subjects were evaluated for at least 2 consecutive years with a normal neurophysiological testing. The neurophysiological testing comprised of MMSE, MoCA, digit forward and backward, logical memory, selective reminding test, fluency (phonemic and semantic), multilingual naming test, global deficit score and neuropsychiatric inventory questionnaire. Some HC were also screened for the same biomarkers as the AD patients. They were all negative, CSF scan was performed in 7 individuals, and amyloid scan in 10.

At PrecisionMed, AD subjects were diagnosed according to NINCDS-ADRDA criteria (McKhann et al., 1984) by a neurologist or internist. The subjects underwent MRI/CT to rule out other causes of cognitive decline and those that were diagnosed with AD exhibited MMSE score ≤ 26, deficit in two or more areas of cognition, progressive worsening of memory and other cognitive functions along with any of other supportive parameters like progressive deterioration of specific cognitive function such as language (aphasia), motor skills (apraxia) and perceptions (agnosia), impaired activities of daily living and altered patterns of behavior, associated symptoms of depression, insomnia, incontinence, delusions, illusions, hallucinations, catastrophic verbal, emotional, or physical outbursts, sexual disorders, and weight loss, plateaus in the course of progression of the illness and /or seizures at advance stage. Of the 18 AD subjects, 14 were homozygous for APOE ε3, three subjects

expressed APOE ε2/ε3, and one expressed APOE ε3/ε4. The HC were self-reported and had MMSE of ≥29.

Neither of the cohorts included neuropathological confirmation of AD, hence it is possible that some individuals may present mixed pathology of AD and other forms of dementia, such as limbic-predominant age-related TDP-43 encephalopathy (LATE), as LATE can mimic AD presentation. However, clinical and imaging or biological tools were used to try to minimize this risk. Moreover, LATE primarily affects older individuals (>80yo). In the CUMC cohort, 10 out of 33 AD subjects were older than 80 years, and all of them had clinical presentation and neuropsychological testing suggestive of AD. In the PrecisionMed cohort, one AD subject was above 80 years.

Another neurological condition that is characterized by deposits of Aβ peptide in the vessels is cerebral amyloid angiopathy (CAA). The deposits in CAA are biochemically similar to the material comprising senile plaques in AD, however subjects with a MRI suggestive of CAA (multiple hemorrhages; single lobar, cortical or cortical-subcortical hemorrhage; superficial siderosis) were not enrolled in this study.

Generation of Peptide Pools

Peptides for all the antigens tested in the study were synthesized by A&A, LLC (San Diego) on a small scale (1 mg/ml). The APP peptide pool (total of 153 peptides, 15-mers overlapping by 10 residues spanning the entire protein sequence), Aβ (9 15-mer peptides spanning the Aβ-42 peptide), α-syn epitope pool (total of 11 peptides) (Sulzer et al., 2017), tau (total of 70 peptides) (Lindestam Arlehamn et al., 2019), TDP-43 peptide pool (total of 82 peptides, 15-mers overlapping by 10 residues spanning the entire protein sequence), pertussis (PT) (total of 132 peptides) (Bancroft et al., 2016; da Silva Antunes et al., 2018), and EBV/CMV pool (total of 270 peptides) (Dan et al., 2016; Tian et al., 2017) were synthesized and then reconstituted in DMSO. The individual peptides were then pooled, lyophilized and reconstituted at a concentration of 1 mg/ml. The peptide pools were tested at a final concentration of 2 or 5 ug/ml.

Isolation of PBMCs

Whole blood was collected in EDTA vacutainers and PBMCs were isolated by density gradient centrifugation with Ficoll-Paque plus (GE #17144003). Briefly, blood was spun at 1850 rpm for 15 min with brakes off to remove plasma. Blood was then diluted with RPMI and 35 ml of blood was gently layered on 15 ml Ficoll-Paque plus and centrifuged at 1850 rpm for 25 min with brakes off. The cells at the interface were collected, washed with RPMI, counted and cryopreserved in 90% v/v FBS and 10 % v/v DMSO and stored in liquid nitrogen.

Fluorospot Assay

Peripheral blood mononuclear cells were thawed and stimulated for 2 weeks *in vitro* at $2x10^6$ cells per well in a 24-well plate with APP, amyloid beta (Aβ), α-syn, tau, TDP-43, pertussis (PT), or EBV/CMV pools. PHA was used as control. Cells were fed with 10 U/ml recombinant IL-2 at an interval of 4 days. After 2 weeks of culture, cells were harvested and T cell responses to specific antigens were measured by IFNγ, IL-5, and IL-10 Fluorospot assay. Plates (Mabtech, Nacka Strand, Sweden) were coated overnight at 4°C with an antibody mixture of mouse anti-human IFNγ clone (clone 1-D1K), mouse anti-human IL-5 (clone TRFK5), and mouse anti-human IL-10 (clone 9D7). Briefly, 100,000 cells were plated in each well of the pre-coated Immobilon-FL PVDF 96 well plates (Mabtech), stimulated with the respective antigen at the respective concentration of 5 μg/ml and incubated at 37°C in a humidified CO_2 incubator for 20−24 h. Cells stimulated with each antigen was also stimulated with 10 μg/ml PHA that served as a positive control. In order to assess nonspecific cytokine production, cells were also stimulated with DMSO at the corresponding concentration present in the peptide pools. All conditions were tested in triplicates. After incubation, cells were removed, plates were washed six times with 200 μl PBS/0.05% Tween 20 using an automated plate washer. After washing, 100 μl of an antibody mixture containing IFNγ (7-B6-1-FS-BAM), IL-5 (5A10-WASP), and IL-10 (12G8-biotin) prepared in PBS with 0.1% BSA was added to each well and plates were incubated for 2 h at room temperature. The plates were again washed six times as described above and incubated with diluted fluorophores (anti-BAM-490, anti-WASP-640, and SA-550) for 1 h at room temperature. After incubation, the plates were again washed as described above and incubated with a fluorescence enhancer for 15 min. Finally, the plates were blotted dry and spots were counted by computer-assisted image analysis (AID iSpot, AID Diagnostica GMBH, Strassberg, Germany). The responses were considered positive if they met all three criteria (i) the net spot forming cells per 10^6 PBMC were ≥100 (ii) the stimulation index ≥2, and (iii) $p \leq 0.05$ by Student's *t*-test or Poisson distribution test.

Proliferation Assay

Peripheral blood mononuclear cells were thawed in RPMI supplemented with 5% human serum (Gemini Bio-Products, West Sacramento, CA), 1% Glutamax (Gibco, Waltham, MA, United States), 1% penicillin/streptomycin (Omega Scientific, Tarzana, CA, United States), and 50 U/ml Benzonase (Millipore Sigma, Burlington, MA, United States). The cells were then washed and viable cells were counted using the trypan blue dye exclusion method. Viable cells were labeled with 5-chloromethylfluorescein diacetate (CFSE) at a concentration of 10 uM by incubating the cells suspended in 1 ml of PBS with CFSE at 37°C for 10−12 min. The labeled cells were then washed twice with 20% FBS prepared in PBS and spun at 2500 rpm for 5 min. Cells were then resuspended and cultured for 11 days in RPMI media supplemented with 5% human Ab serum, Glutamax and penicillin/streptomycin in the presence of APP, amyloid beta, α-syn, tau, TDP-43, EBV/CMV and PT peptide pools. After 4 days of culture cells were supplemented with 10 U/ml recombinant IL-2 and on day 8, cells were again stimulated with peptide pools. On day 11, cells were stained with a mix of anti-CD3-AF700 (clone UCHT1, BD pharmigen), anti-CD4-APC ef 780 (clone RPA-T4, eBiosciences) and anti-CD8a-BV650 (clone RPA-T8, Biolegend). The percentage of proliferating CD3+ CD4+ T cells was used a read out. The samples were acquired on BD LSR I flow cytometer (BD Biosciences, San Jose, CA). The percentage of proliferating CD3+ CD4+CFSE-T cells to

each antigen was calculated by subtracting the background values (as determined from DMSO stimulated control) using FlowJo X Software (FlowJo LLC, Ashland, OR, United States). The gating strategy is shown in **Supplementary Figure S3**.

Flow Cytometry

Cryopreserved PBMCs were thawed in RPMI supplemented with 5% human serum (Gemini Bio-Products, West Sacramento, CA, United States), 1% Glutamax (Gibco, Waltham, MA, United States), 1% penicillin/streptomycin (Omega Scientific, Tarzana, CA, United States), and 50 U/ml Benzonase (Millipore Sigma, Burlington, MA, United States). Cells were then washed and counted. 1 million cells were then blocked in 10% FBS for 10 min at 4°C. After blocking, cells were stained with a combination of APCef780 conjugated anti-CD4 (clone RPA-T4, eBiosciences), AF700 conjugated anti-CD3 (clone UCHT1, BD Pharmigen), BV650 conjugated anti-CD8a (clone RPA-T8, Biolegend), PECy7 conjugated anti-CD19 (clone HIB19, TONBO), APC conjugated anti-CD14 (clone 61D3, TONBO), PerCPCy5.5 conjugated anti-CCR7 (clone G043H7, Biolegend), PE conjugated anti-CD56 (eBiosciences), FITC conjugated anti-CD25 (clone M-A251, BD Pharmigen), eF450 conjugated anti-CD45RA (clone HI100, eBiosciences) and eF506 live dead aqua dye (eBiosciences) for 30 min at 4°C. Cells were then washed twice and acquired or sorted on a BD FACSAria flow cytometer (BD Biosciences, San Jose, CA) to measure the frequency of different cell subsets. The gating strategy is shown in **Supplementary Figure S1**.

RNA Extraction and cDNA Library Preparation

A total of 100,000 PBMCs, CD4 or CD8 memory T cells were sorted and collected in Trizol in a 1.5 ml tube. Memory T cells were sorted based on CD45RA and CCR7 expression (**Supplementary Figure S1**), where $CD45RA^{-}CCR7^{+}$ Tcm, $CD45RA^{-}CCR7^{-}$ Tem, and $CD45RA^{+}CCR7^{-}$ Temra cells were included and $CD45RA^{+}CCR7^{+}$ naïve T cells were excluded. Tubes were vortexed, spun and stored at −80°C until processed. RNA was extracted using miRNeasy Micro Kit (Qiagen) on a Qiacube. Purified total RNA was amplified following the smart-seq2 protocol. cDNA was purified using AMPure XP beads, and barcoded Illumina sequencing libraries were generated, loaded and sequenced on the Illumina sequencing platform HiSeq 2500.

RNAseq Analysis

Samples were sequenced using Hiseq 2500 (Illumina) to obtain 50 bp single reads. The paired-end reads that passed Illumina filters were filtered for reads aligning to tRNA, rRNA, adapter sequences, and spike-in controls. The reads were then aligned to GRCh38 reference genome and Gencode v27 annotations, which includes protein coding genes as well as pseudogenes, lncRNAs, and miRNAs, using STAR (v2.6.1c) (Dobin et al., 2013). DUST scores were calculated with PRINSEQ Lite (v 0.20.3) (Schmieder and Edwards, 2011) and low-complexity reads (DUST > 4) were removed from the BAM files. The alignment results were parsed via the SAMtools (Li et al., 2009) to generate SAM files. Read counts of each genomic feature were obtained with the featureCounts program (v1.6.5) (Liao et al., 2014). After removing absent features (zero counts in all samples), the raw counts were then imported to R/Bioconductor package DESeq2 (Love et al., 2014) to identify differentially expressed genes among samples. *P*-values for differential expression were calculated using the Wald test for differences between the base means of two conditions. These *p*-Values are then corrected for multiple tests using the Benjamini Hochberg algorithm (Benjamini and Hochberg, 1995) to control the false discovery rate. We considered genes differentially expressed between two groups of samples when the DESeq2 analysis resulted in an adjusted *P*-value of <0.05 and the absolute value of the log fold-change in gene expression was greater than 0.5. Variance stabilizing transformation (DESeq2 1.26.0) was applied on the read counts for all samples. Since there were samples from multiple mapping runs, an adjustment for batch effects using the outcome of interest as the disease state was performed using ComBat (sva 3.34.0). A principal components analysis was performed on the top 1000 variable genes using the prcomp function in the stats v3.6.3 library under R v3.6.3. The RNA-seq dataset analyzed as part of this study have been deposited in the NCBI Gene Expression Omnibus (GEO) database with the primary accession number GSE153104.

Statistics

Statistical analyses were performed using GraphPad Prism version 8.1.1. Data were analyzed using non-parametric statistical tests. Mann—Whitney two-tailed test was performed to compare T cell responses to all the antigens and frequency of cell subsets in AD and HC. Spearman test was performed to check the significance of correlation between T cell responses and clinical variables.

DATA AVAILABILITY STATEMENT

The RNA-seq dataset analyzed as part of this study have been deposited in the NCBI Gene Expression Omnibus (GEO) database with the primary accession number GSE153104.

ETHICS STATEMENT

The studies involving human participants were reviewed and approved by the La Jolla Institute for Immunology (LJI; protocol number VD-155) and the Columbia University Medical Center (CUMC; protocol number IRB-AAAQ9714). The patients/participants provided their written informed consent to participate in this study.

AUTHOR CONTRIBUTIONS

RD, BP, DS, AS, and CL designed and directed the study. RD and JP performed the experiments and analyzed the data.

RD and AP analyzed the RNA-seq data. FB, MP, and AK provided the crucial reagents. JD and KM recruited the participants and performed the clinical evaluations. AF maintained the patient data, records, and assisted in participant recruitment. RD, DS, AS, and CL wrote the manuscript. All authors read, edited, and approved the manuscript.

FUNDING

The Illumina HiSeq 2500 sequencer was purchased through NIH S10ODO16262. This study was supported by the NIH NINDS R01 NS095435 (AS and DS), the JPB Foundation (DS), NIH/NIA R01AG050658 (FB), and NIH/NIA P30 AG066462 (KM).

ACKNOWLEDGMENTS

We would like to thank the AD and HC subjects for participating and donating the samples to this study. We would also like to thank the Flow Cytometry core, Next-Generation sequencing core and Bioinformatic core facilities of La Jolla Institute of Immunology for their services.

SUPPLEMENTARY MATERIAL

The Supplementary Material for this article can be found online at: https://www.frontiersin.org/articles/10.3389/fnins.2020.00874/full#supplementary-material

REFERENCES

Allnutt, M. A., Johnson, K., Bennett, D. A., Connor, S. M., Troncoso, J. C., Pletnikova, O., et al. (2020). Human Herpesvirus 6 detection in Alzheimer's disease cases and controls across multiple cohorts. *Neuron* 105, 1027–1035.e2. doi: 10.1016/j.neuron.2019.12.031

Angelucci, F., Cechova, K., Valis, M., Kuca, K., Zhang, B., and Hort, J. (2019). MicroRNAs in Alzheimer's disease: diagnostic markers or therapeutic agents? *Front. Pharmacol.* 10:665. doi: 10.3389/fphar.2019.00665

Bancroft, T., Dillon, M. B., da Silva Antunes, R., Paul, S., Peters, B., Crotty, S., et al. (2016). Th1 versus Th2 T cell polarization by whole-cell and acellular childhood pertussis vaccines persists upon re-immunization in adolescence and adulthood. *Cell Immunol.* 304-305, 35–43. doi: 10.1016/j.cellimm.2016.05.002

Benjamini, Y., and Hochberg, Y. (1995). Controlling the false discovery rate: a practical and powerful approach to multiple testing. *J. R. Stat. Soc. Ser. B* 57, 289–300.

Bloom, F. E., Reilly, J. F., Redwine, J. M., Wu, C. C., Young, W. G., and Morrison, J. H. (2005). Mouse models of human neurodegenerative disorders: requirements for medication development. *Arch. Neurol.* 62, 185–187. doi: 10.1001/archneur.62.2.185

Brettschneider, S., Morgenthaler, N. G., Teipel, S. J., Fischer-Schulz, C., Burger, K., Dodel, R., et al. (2005). Decreased serum amyloid beta(1-42) autoantibody levels in Alzheimer's disease, determined by a newly developed immuno-precipitation assay with radiolabeled amyloid beta(1-42) peptide. *Biol. Psychiatry* 57, 813–816. doi: 10.1016/j.biopsych.2004.12.008

Britschgi, M., Olin, C. E., Johns, H. T., Takeda-Uchimura, Y., LeMieux, M. C., Rufibach, K., et al. (2009). Neuroprotective natural antibodies to assemblies of amyloidogenic peptides decrease with normal aging and advancing Alzheimer's disease. *Proc. Natl. Acad. Sci. U.S.A.* 106, 12145–12150. doi: 10.1073/pnas.0904866106

Burel, J. G., Qian, Y., Lindestam Arlehamn, C., Weiskopf, D., Zapardiel-Gonzalo, J., Taplitz, R., et al. (2017). An integrated workflow to assess technical and biological variability of cell population frequencies in human peripheral blood by flow cytometry. *J. Immunol.* 198, 1748–1758. doi: 10.4049/jimmunol.1601750

Busse, M., Michler, E., von Hoff, F., Dobrowolny, H., Hartig, R., Frodl, T., et al. (2017). Alterations in the peripheral immune system in dementia. *J. Alzheimers Dis.* 58, 1303–1313. doi: 10.3233/JAD-161304

Butterfield, D. A., and Boyd-Kimball, D. (2004). Amyloid beta-peptide(1-42) contributes to the oxidative stress and neurodegeneration found in Alzheimer disease brain. *Brain Pathol.* 14, 426–432. doi: 10.1111/j.1750-3639.2004.tb00087.x

Cacabelos, R., Fernandez-Novoa, L., Lombardi, V., Kubota, Y., and Takeda, M. (2005). Molecular genetics of Alzheimer's disease and aging. *Methods Find Exp. Clin. Pharmacol.* 27(Suppl A), 1–573.

Ciccocioppo, F., Lanuti, P., Pierdomenico, L., Simeone, P., Bologna, G., Ercolino, E., et al. (2019). The characterization of regulatory T-cell profiles in Alzheimer's disease and multiple sclerosis. *Sci. Rep.* 9:8788. doi: 10.1038/s41598-019-45433-3

Cook, C., Zhang, Y. J., Xu, Y. F., Dickson, D. W., and Petrucelli, L. (2008). TDP-43 in neurodegenerative disorders. *Expert Opin Biol. Ther.* 8, 969–978. doi: 10.1517/14712598.8.7.969

Cooper, N. R., Kalaria, R. N., McGeer, P. L., and Rogers, J. (2000). Key issues in Alzheimer's disease inflammation. *Neurobiol. Aging* 21, 451–453. doi: 10.1016/s0197-4580(00)00148-2

Cosin-Tomas, M., Antonell, A., Llado, A., Alcolea, D., Fortea, J., Ezquerra, M., et al. (2017). Plasma miR-34a-5p and miR-545-3p as early biomarkers of Alzheimer's disease: potential and limitations. *Mol. Neurobiol.* 54, 5550–5562. doi: 10.1007/s12035-016-0088-8

da Silva Antunes, R., Babor, M., Carpenter, C., Khalil, N., Cortese, M., Mentzer, A. J., et al. (2018). Th1/Th17 polarization persists following whole-cell pertussis vaccination despite repeated acellular boosters. *J. Clin. Invest.* 128, 3853–3865. doi: 10.1172/JCI121309

Dan, J. M., Lindestam Arlehamn, C. S., Weiskopf, D., da Silva Antunes, R., Havenar-Daughton, C., Reiss, S. M., et al. (2016). A cytokine-independent approach to identify antigen-specific human germinal center T follicular helper cells and rare antigen-specific CD4+ T cells in blood. *J. Immunol.* 197, 983–993. doi: 10.4049/jimmunol.1600318

Davis, D. H., Creavin, S. T., Yip, J. L., Noel-Storr, A. H., Brayne, C., and Cullum, S. (2015). Montreal cognitive assessment for the diagnosis of Alzheimer's disease and other dementias. *Cochrane Database Syst. Rev.* 2015:CD010775. doi: 10.1002/14651858.CD010775.pub2

Dawson, T. M., Golde, T. E., and Lagier-Tourenne, C. (2018). Animal models of neurodegenerative diseases. *Nat. Neurosci.* 21, 1370–1379. doi: 10.1038/s41593-018-0236-8

Dobin, A., Davis, C. A., Schlesinger, F., Drenkow, J., Zaleski, C., Jha, S., et al. (2013). STAR: ultrafast universal RNA-seq aligner. *Bioinformatics* 29, 15–21. doi: 10.1093/bioinformatics/bts635

Dodel, R., Balakrishnan, K., Keyvani, K., Deuster, O., Neff, F., Andrei-Selmer, L. C., et al. (2011). Naturally occurring autoantibodies against beta-amyloid: investigating their role in transgenic animal and in vitro models of Alzheimer's disease. *J. Neurosci.* 31, 5847–5854. doi: 10.1523/JNEUROSCI.4401-10.2011

Du, Y., Dodel, R., Hampel, H., Buerger, K., Lin, S., Eastwood, B., et al. (2001). Reduced levels of amyloid beta-peptide antibody in Alzheimer disease. *Neurology* 57, 801–805. doi: 10.1212/wnl.57.5.801

Finder, V. H., and Glockshuber, R. (2007). Amyloid-beta aggregation. *Neurodegener Dis.* 4, 13–27. doi: 10.1159/000100355

Gate, D., Saligrama, N., Leventhal, O., Yang, A. C., Unger, M. S., Middeldorp, J., et al. (2020). Clonally expanded CD8 T cells patrol the cerebrospinal fluid in Alzheimer's disease. *Nature* 577, 399–404. doi: 10.1038/s41586-019-1895-7

Giubilei, F., Antonini, G., Montesperelli, C., Sepe-Monti, M., Cannoni, S., Pichi, A., et al. (2003). T cell response to amyloid-beta and to mitochondrial antigens

in Alzheimer's disease. *Dement. Geriatr. Cogn. Disord.* 16, 35–38. doi: 10.1159/000069991

Grundke-Iqbal, I., Iqbal, K., Tung, Y. C., Quinlan, M., Wisniewski, H. M., and Binder, L. I. (1986). Abnormal phosphorylation of the microtubule-associated protein tau (tau) in Alzheimer cytoskeletal pathology. *Proc. Natl. Acad. Sci. U.S.A.* 83, 4913–4917. doi: 10.1073/pnas.83.13.4913

Guo, W., Chen, Y., Zhou, X., Kar, A., Ray, P., Chen, X., et al. (2011). An ALS-associated mutation affecting TDP-43 enhances protein aggregation, fibril formation and neurotoxicity. *Nat. Struct. Mol. Biol.* 18, 822–830. doi: 10.1038/nsmb.2053

Hara, N., Kikuchi, M., Miyashita, A., Hatsuta, H., Saito, Y., Kasuga, K., et al. (2017). Serum microRNA miR-501-3p as a potential biomarker related to the progression of Alzheimer's disease. *Acta Neuropathol. Commun.* 5:10. doi: 10.1186/s40478-017-0414-z

Herman, A. M., Khandelwal, P. J., Stanczyk, B. B., Rebeck, G. W., and Moussa, C. E. (2011). beta-amyloid triggers ALS-associated TDP-43 pathology in AD models. *Brain Res.* 1386, 191–199. doi: 10.1016/j.brainres.2011.02.052

Honson, N. S., and Kuret, J. (2008). Tau aggregation and toxicity in tauopathic neurodegenerative diseases. *J. Alzheimers Dis.* 14, 417–422. doi: 10.3233/jad-2008-14409

Irvine, G. B., El-Agnaf, O. M., Shankar, G. M., and Walsh, D. M. (2008). Protein aggregation in the brain: the molecular basis for Alzheimer's and Parkinson's diseases. *Mol. Med.* 14, 451–464. doi: 10.2119/2007-00100.Irvine

Itagaki, S., McGeer, P. L., and Akiyama, H. (1988). Presence of T-cytotoxic suppressor and leucocyte common antigen positive cells in Alzheimer's disease brain tissue. *Neurosci. Lett.* 91, 259–264.

Janus, C., and Welzl, H. (2010). Mouse models of neurodegenerative diseases: criteria and general methodology. *Methods Mol. Biol.* 602, 323–345. doi: 10.1007/978-1-60761-058-8_19

Jiang, L. L., Zhao, J., Yin, X. F., He, W. T., Yang, H., Che, M. X., et al. (2016). Two mutations G335D and Q343R within the amyloidogenic core region of TDP-43 influence its aggregation and inclusion formation. *Sci. Rep.* 6:23928. doi: 10.1038/srep23928

Kumar, S., and Reddy, P. H. (2018). MicroRNA-455-3p as a potential biomarker for Alzheimer's disease: an update. *Front. Aging Neurosci.* 10:41. doi: 10.3389/fnagi.2018.00041

Li, H., Handsaker, B., Wysoker, A., Fennell, T., Ruan, J., Homer, N., et al. (2009). The sequence alignment/map format and SAMtools. *Bioinformatics* 25, 2078–2079. doi: 10.1093/bioinformatics/btp352

Liao, Y., Smyth, G. K., and Shi, W. (2014). featureCounts: an efficient general purpose program for assigning sequence reads to genomic features. *Bioinformatics* 30, 923–930. doi: 10.1093/bioinformatics/btt656

Lin, W. R., Wozniak, M. A., Cooper, R. J., Wilcock, G. K., and Itzhaki, R. F. (2002). Herpesviruses in brain and Alzheimer's disease. *J. Pathol.* 197, 395–402. doi: 10.1002/path.1127

Lindestam Arlehamn, C. S., Dhanwani, R., Pham, J., Kuan, R., Frazier, A., Rezende Dutra, J., et al. (2020). alpha-Synuclein-specific T cell reactivity is associated with preclinical and early Parkinson's disease. *Nat. Commun.* 11:1875. doi: 10.1038/s41467-020-15626-w

Lindestam Arlehamn, C. S., Pham, J., Alcalay, R. N., Frazier, A., Shorr, E., Carpenter, C., et al. (2019). Widespread tau-specific CD4 T cell reactivity in the general population. *J. Immunol.* 203, 84–92. doi: 10.4049/jimmunol.1801506

Lodygin, D., Hermann, M., Schweingruber, N., Flugel-Koch, C., Watanabe, T., Schlosser, C., et al. (2019). beta-synuclein-reactive T cells induce autoimmune CNS grey matter degeneration. *Nature* 566, 503–508. doi: 10.1038/s41586-019-0964-2

Love, M. I., Huber, W., and Anders, S. (2014). Moderated estimation of fold change and dispersion for RNA-seq data with DESeq2. *Genome Biol.* 15:550. doi: 10.1186/s13059-014-0550-8

Maletto, B., Gruppi, A., and Pistoresi-Palencia, M. C. (1994). Aging: the cellular immune response against autologous and foreign antigens is affected before the humoral response. *Immunol. Lett.* 40, 243–250.

McKhann, G., Drachman, D., Folstein, M., Katzman, R., Price, D., and Stadlan, E. M. (1984). Clinical diagnosis of Alzheimer's disease: report of the NINCDS-ADRDA work group under the auspices of department of health and human services task force on Alzheimer's disease. *Neurology* 34, 939–944. doi: 10.1212/wnl.34.7.939

McKhann, G. M., Knopman, D. S., Chertkow, H., Hyman, B. T., Jack, C. R. Jr., Kawas, C. H., et al. (2011). The diagnosis of dementia due to Alzheimer's disease: recommendations from the National Institute on Aging-Alzheimer's association workgroups on diagnostic guidelines for Alzheimer's disease. *Alzheimers Dement.* 7, 263–269. doi: 10.1016/j.jalz.2011.03.005

Merlini, M., Kirabali, T., Kulic, L., Nitsch, R. M., and Ferretti, M. T. (2018). Extravascular CD3+ T cells in brains of alzheimer disease patients correlate with tau but not with amyloid pathology: an immunohistochemical study. *Neurodegener. Dis.* 18, 49–56. doi: 10.1159/000486200

Mietelska-Porowska, A., and Wojda, U. (2017). T lymphocytes and inflammatory mediators in the interplay between brain and blood in Alzheimer's disease: potential pools of new biomarkers. *J. Immunol. Res.* 2017:4626540. doi: 10.1155/2017/4626540

Monsonego, A., Zota, V., Karni, A., Krieger, J. I., Bar-Or, A., Bitan, G., et al. (2003). Increased T cell reactivity to amyloid beta protein in older humans and patients with Alzheimer disease. *J. Clin. Invest.* 112, 415–422. doi: 10.1172/JCI18104

Moradifard, S., Hoseinbeyki, M., Ganji, S. M., and Minuchehr, Z. (2018). Analysis of microRNA and gene expression profiles in Alzheimer's disease: a meta-analysis approach. *Sci. Rep.* 8:4767. doi: 10.1038/s41598-018-20959-0

Paleologou, K. E., Irvine, G. B., and El-Agnaf, O. M. (2005). Alpha-synuclein aggregation in neurodegenerative diseases and its inhibition as a potential therapeutic strategy. *Biochem. Soc. Trans.* 33(Pt 5), 1106–1110. doi: 10.1042/BST20051106

Pellicano, M., Larbi, A., Goldeck, D., Colonna-Romano, G., Buffa, S., Bulati, M., et al. (2012). Immune profiling of Alzheimer patients. *J. Neuroimmunol.* 242, 52–59. doi: 10.1016/j.jneuroim.2011.11.005

Peter, I., Dubinsky, M., Bressman, S., Park, A., Lu, C., Chen, N., et al. (2018). Anti-tumor necrosis factor therapy and incidence of parkinson disease among patients with inflammatory bowel disease. *JAMA Neurol.* 75, 939–946. doi: 10.1001/jamaneurol.2018.0605

Pirttila, T., Mattinen, S., and Frey, H. (1992). The decrease of CD8-positive lymphocytes in Alzheimer's disease. *J. Neurol. Sci.* 107, 160–165. doi: 10.1016/0022-510x(92)90284-r

Qu, B. X., Gong, Y., Moore, C., Fu, M., German, D. C., Chang, L. Y., et al. (2014). Beta-amyloid auto-antibodies are reduced in Alzheimer's disease. *J. Neuroimmunol.* 274, 168–173. doi: 10.1016/j.jneuroim.2014.06.017

Richartz-Salzburger, E., Batra, A., Stransky, E., Laske, C., Kohler, N., Bartels, M., et al. (2007). Altered lymphocyte distribution in Alzheimer's disease. *J. Psychiatr. Res.* 41, 174–178. doi: 10.1016/j.jpsychires.2006.01.010

Rosenmann, H., Meiner, Z., Geylis, V., Abramsky, O., and Steinitz, M. (2006). Detection of circulating antibodies against tau protein in its unphosphorylated and in its neurofibrillary tangles-related phosphorylated state in Alzheimer's disease and healthy subjects. *Neurosci. Lett.* 410, 90–93. doi: 10.1016/j.neulet.2006.01.072

Rubin, K., and Glazer, S. (2017). The pertussis hypothesis: *Bordetella pertussis* colonization in the pathogenesis of Alzheimer's disease. *Immunobiology* 222, 228–240. doi: 10.1016/j.imbio.2016.09.017

Schmieder, R., and Edwards, R. (2011). Quality control and preprocessing of metagenomic datasets. *Bioinformatics* 27, 863–864. doi: 10.1093/bioinformatics/btr026

Simon, A. K., Hollander, G. A., and McMichael, A. (2015). Evolution of the immune system in humans from infancy to old age. *Proc. Biol. Sci.* 282:20143085. doi: 10.1098/rspb.2014.3085

Sulzer, D., Alcalay, R. N., Garretti, F., Cote, L., Kanter, E., Agin-Liebes, J., et al. (2017). T cells from patients with Parkinson's disease recognize alpha-synuclein peptides. *Nature* 546, 656–661. doi: 10.1038/nature22815

Tian, Y., Babor, M., Lane, J., Schulten, V., Patil, V. S., Seumois, G., et al. (2017). Unique phenotypes and clonal expansions of human CD4 effector memory T cells re-expressing CD45RA. *Nat. Commun.* 8:1473. doi: 10.1038/s41467-017-01728-5

Weksler, M. E., Relkin, N., Turkenich, R., LaRusse, S., Zhou, L., and Szabo, P. (2002). Patients with Alzheimer disease have lower levels of serum anti-amyloid peptide antibodies than healthy elderly individuals. *Exp. Gerontol.* 37, 943–948. doi: 10.1016/s0531-5565(02)00029-3

Wong, P. C., Cai, H., Borchelt, D. R., and Price, D. L. (2002). Genetically engineered mouse models of neurodegenerative diseases. *Nat. Neurosci.* 5, 633–639. doi: 10.1038/nn0702-633

Conflict of Interest: The authors declare that the research was conducted in the absence of any commercial or financial relationships that could be construed as a potential conflict of interest.

frontiers in Neuroscience

CORRECTION
published: 13 January 2021
doi: 10.3389/fnins.2020.641809

Corrigendum: T Cell Responses to Neural Autoantigens Are Similar in Alzheimer's Disease Patients and Age-Matched Healthy Controls

Rekha Dhanwani[1], John Pham[1], Ashmitaa Logandha Ramamoorthy Premlal[1], April Frazier[1], Atul Kumar[2], Maria Elena Pero[2,3], Francesca Bartolini[2], Juliana Rezende Dutra[4], Karen S. Marder[4], Bjoern Peters[1,5], David Sulzer[6,7], Alessandro Sette[1,5] and Cecilia S. Lindestam Arlehamn[1]**

[1] Division of Vaccine Discovery, La Jolla Institute for Immunology, La Jolla, CA, United States, [2] Department of Pathology and Cell Biology, Columbia University, New York, NY, United States, [3] Department of Veterinary Medicine and Animal Production, University of Naples Federico II, Naples, Italy, [4] Department of Neurology, Columbia University Irving Medical Center, New York, NY, United States, [5] Department of Medicine, University of California, San Diego, La Jolla, CA, United States, [6] Department of Neurology, New York State Psychiatric Institute, Columbia University, New York, NY, United States, [7] Department of Psychiatry and Pharmacology, New York State Psychiatric Institute, Columbia University, New York, NY, United States

Keywords: Alzheimer's disease, neurodegenration, autoimmunity, T cell responses, transcriptomics, neuroantigens

OPEN ACCESS

Approved by:
Frontiers Editorial Office, Frontiers Media SA, Switzerland

***Correspondence:**
Alessandro Sette
alex@lji.org
Cecilia S. Lindestam Arlehamn
cecilia@lji.org

Specialty section:
This article was submitted to Neurodegeneration, a section of the journal Frontiers in Neuroscience

Received: *15 December 2020*
Accepted: *16 December 2020*
Published: *13 January 2021*

Citation:
Dhanwani R, Pham J, Premlal ALR, Frazier A, Kumar A, Pero ME, Bartolini F, Dutra JR, Marder KS, Peters B, Sulzer D, Sette A and Lindestam Arlehamn CS (2021) Corrigendum: T Cell Responses to Neural Autoantigens Are Similar in Alzheimer's Disease Patients and Age-Matched Healthy Controls. Front. Neurosci. 14:641809. doi: 10.3389/fnins.2020.641809

A Corrigendum on

T Cell Responses to Neural Autoantigens Are Similar in Alzheimer's Disease Patients and Age-Matched Healthy Controls

by Dhanwani, R., Pham, J., Premlal, A. L. R., Frazier, A., Kumar, A., Pero, M. E., et al. (2020). Front. Neurosci. 14:874. doi: 10.3389/fnins.2020.00874

In the original article, we neglected to include the funder NIH/NIA, P30 AG066462 to KM.

The authors apologize for this error and state that this does not change the scientific conclusions of the article in any way. The original article has been updated.

frontiers in Neuroscience

ORIGINAL RESEARCH
published: 07 January 2021
doi: 10.3389/fnins.2020.555307

Characteristics of Epigenetic Clocks Across Blood and Brain Tissue in Older Women and Men

Francine Grodstein[1,2†], Bernardo Lemos[3†], Lei Yu[1,4], Artemis Iatrou[1], Philip L. De Jager[5] and David A. Bennett[1,4]*

[1] Rush Alzheimer's Disease Center, Rush University Medical Center, Chicago, IL, United States, [2] Department of Internal Medicine, Rush University Medical Center, Chicago, IL, United States, [3] Department of Environmental Health, Harvard TH Chan School of Public Health, Boston, MA, United States, [4] Department of Neurological Sciences, Rush University Medical Center, Chicago, IL, United States, [5] Department of Neurology and Taub Institute for Research on Alzheimer's Disease and the Aging Brain, Center for Translational and Computational Neuroimmunology, Columbia University Irving Medical Center, New York, NY, United States

Epigenetic clocks are among the most promising biomarkers of aging. It is particularly important to establish biomarkers of brain aging to better understand neurodegenerative diseases. To advance application of epigenetic clocks—which were largely created with DNA methylation levels in blood samples—for use in brain, we need clearer evaluation of epigenetic clock behavior in brain, including direct comparisons of brain specimens with blood, a more accessible tissue for research. We leveraged data from the Religious Orders Study and Rush Memory and Aging Project to examine three established epigenetic clocks (Horvath, Hannum, PhenoAge clocks) and a newer clock, trained in cortical tissue. We calculated each clock in three different specimens: (1) antemortem CD4+ cells derived from blood (n = 41); (2) postmortem dorsolateral prefrontal cortex (DLPFC, n = 730); and (3) postmortem posterior cingulate cortex (PCC, n = 186), among older women and men, age 66–108 years at death. Across all clocks, epigenetic age calculated from blood and brain specimens was generally lower than chronologic age, although differences were smallest for the Cortical clock when calculated in the brain specimens. Nonetheless, we found that Pearson correlations of epigenetic to chronologic ages in brain specimens were generally reasonable for all clocks; correlations for the Horvath, Hannum, and PhenoAge clocks largely ranged from 0.5 to 0.7 (all $p < 0.0001$). The Cortical clock outperformed the other clocks, reaching a correlation of 0.83 in the DLFPC ($p < 0.0001$) for epigenetic vs. chronologic age. Nonetheless, epigenetic age was quite modestly correlated across blood and DLPFC in 41 participants with paired samples [Pearson r from 0.21 (p = 0.2) to 0.32 (p = 0.05)], indicating that broader research in neurodegeneration may benefit from clocks using CpG sites better conserved across blood and brain. Finally, in analyses stratified by sex, by pathologic diagnosis of Alzheimer disease, and by clinical diagnosis of Alzheimer dementia, correlations of epigenetic to chronologic age remained consistently high across all groups. Future research in brain aging will benefit from epigenetic clocks constructed in brain specimens, including exploration of any advantages of focusing on CpG sites conserved across brain and other tissue types.

Keywords: dementia, epigenetics, aging, neurology, biomarkers

OPEN ACCESS

Edited by:
Manoj Kumar Jaiswal, Icahn School of Medicine at Mount Sinai, United States

Reviewed by:
Scott Edward Counts, Michigan State University, United States
Nicola J. Armstrong, Murdoch University, Australia
Morgan Levine, Yale University, United States

****Correspondence:***
Francine Grodstein
francine_grodstein@rush.edu

† These authors have contributed equally to this work

Specialty section:
This article was submitted to Neurodegeneration, a section of the journal Frontiers in Neuroscience

Received: *24 April 2020*
Accepted: *09 December 2020*
Published: *07 January 2021*

Citation:
Grodstein F, Lemos B, Yu L, Iatrou A, De Jager PL and Bennett DA (2021) Characteristics of Epigenetic Clocks Across Blood and Brain Tissue in Older Women and Men. Front. Neurosci. 14:555307. doi: 10.3389/fnins.2020.555307

INTRODUCTION

Chronologic age is the strongest risk factor for many chronic diseases; however, disease risk is heterogeneous within age groups, likely due, in part, to variation in "biologic age." Substantial research has explored biomarkers of aging (Jylhava et al., 2017), which are critical tools for predicting disease risk, assessing mechanisms underlying aging processes, and developing interventions to delay aging-associated declines in health. Epigenetic modifications are a hallmark of aging, and epigenetic clocks are among the most promising biomarkers of aging to date (Jylhava et al., 2017). However, the majority of research establishing the relevance of epigenetic clocks has largely focused on their relations with overall longevity (Fransquet et al., 2019). In the US, heart disease and cancer mortality, primary causes of death, have decreased (Siegel et al., 2018; Shah et al., 2019) while deaths due to Alzheimer dementia and related dementias have increased 145% over the last 20 years (Alzheimer's Association, 2019); other neurodegenerative diseases are increasing as well (e.g., Parkinson Disease; Marras et al., 2018). Thus, establishing effective biomarkers of brain aging is particularly important for improving public health in the coming decades, and eventually reducing neurodegenerative diseases of aging.

Epigenetic dysregulation has been clearly implicated in brain aging and neurologic diseases (Klein et al., 2016). In initial evidence, several epigenetic clocks were well-correlated with chronologic age when measured in brain tissue (Lu et al., 2017), and in limited existing research, the Religious Orders Study (ROS) and the Rush Memory and Aging Project (MAP) reported that some epigenetic clocks assessed in brain tissue appear modestly associated with neurodegenerative pathology (Levine et al., 2015, 2018). In a small number of studies, epigenetic age measured in blood has also been related to clinical neurologic outcomes (Marioni et al., 2015; Horvath et al., 2016; Chuang et al., 2017; Raina et al., 2017). However, clearer understanding of epigenetic clock behavior in brain is needed to advance applications of these clocks for brain health.

Specifically, growing research indicates that epigenetic clocks, most of which were built with data across the lifespan and relatively few in the oldest age ranges, may become less accurate at the advanced ages at which many neurodegenerative diseases manifest (Armstrong et al., 2017; El Khoury et al., 2019; Shireby et al., 2020). In particular, at the oldest ages—ranging up to supercentenarians (Horvath et al., 2015)—epigenetic age estimates for many of the clocks appear consistently lower than chronologic age. Thus, additional examination of clock behavior at more extreme older ages is needed, especially if the trajectory of biological age may not be linear in advanced age. Further, direct comparisons are needed of epigenetic clock behavior in brain specimens compared to more accessible tissue (e.g., blood). Initial evidence, including in ROS and MAP, has suggested that DNA methylation (DNAm) states do not appear correlated in blood vs. brain specimens (Lunnon et al., 2014; Yu et al., 2016). Nonetheless, this work has examined hundreds of thousands of CpG sites simultaneously, and may not apply to the more focused signatures provided by epigenetic clocks.

Thus, we leveraged the data from the Religious Orders Study and the Rush Memory and Aging Project to examine inter-relations of four different epigenetic clocks measured in three different specimens: (1) antemortem $CD4^+$ cells derived from blood (two measures, on average 7.5 years apart); (2) postmortem dorsolateral prefrontal cortex (DLPFC); and (3) postmortem posterior cingulate cortex (PCC), among older women and men, age 66–108 years at death. We chose to focus here on a range of different epigenetic clocks: the Horvath clock, developed across multiple tissues (Horvath, 2013); the Hannum clock, trained in blood samples (Hannum et al., 2013); the PhenoAge clock, developed with biomarkers of aging as the dependent variable rather than age (Levine et al., 2018); and a new clock trained in cortical tissue (Cortical clock; Shireby et al., 2020).

MATERIALS AND METHODS

Study Populations

The Religious Orders Study (Bennett et al., 2018) was initiated in 1994, and includes older priests, nuns and brothers from across the United States, free of known dementia at the time of enrollment. Participants agreed to annual neurological exams, neuropsychological testing, and blood draw, and signed an informed consent and Anatomic Gift Act to donate their brains at death. Over 1,468 participants completed a baseline evaluation. The follow-up rate and autopsies exceed 90%. The Rush Memory and Aging Project (Bennett et al., 2018) was established in 1997 with virtually identical design and data collection, and includes older men and women from across the Chicago metropolitan area, without known dementia at enrollment; over 2,170 participants completed a baseline evaluation to date. The follow-up rate exceeds 90% and the autopsy rate exceeds 80%. ROSMAP data can be requested at www.radc.rush.edu.

For the work described here, we leveraged DNA methylation profiling previously completed in stored peripheral blood samples collected from participants at cohort baseline and again proximate to death, as well as from frozen DLPFC and PCC tissue. The average postmortem interval was approximately 9 h.

Assessment of DNA Methylation States and Epigenetic Clocks

First, DNAm was profiled in a set of 41 matched blood samples and DLPFC specimens. The blood DNAm was profiled in $CD4^+$ T cells isolated from frozen peripheral blood mononuclear cells (PBMCs). For the original research, we had been interested in $CD4^+$ lymphocytes because they represent a single cell type related to immune function. As previously described (De Jager et al., 2014), the PBMCs were washed with RPMI1640 medium to remove Dimethyl sulfoxide (DMSO) exposure. $CD4^+$ T-cells were isolated using magnetic-activated cell sorting (MACS) and reached the purity of at least 95% as assessed by flow cytometry. Blood DNA isolation was performed using AllPrep DNA/RNA Micro kit, according to manufacturer's instructions.

In the DLPFC, 100 mg frozen sections were thawed on ice, with the gray matter dissected from the white matter. The Qiagen QIAamp DNA mini protocol was used for DNA isolation, as

previously published (De Jager et al., 2014). In the blood and DLPFC, DNA methylation profiles were generated using the Illumina Infinium HumanMethylation450 platform. Details on the processing and quality control pipelines have been previously described in detail (De Jager et al., 2014; Yu et al., 2016). After processing, data on 420,132 CpG sites were retained across the 22 autosomes. At each site, DNAm level was presented as a beta value, that is, the ratio of the methylated probe intensity to the sum of methylated and unmethylated probe intensities. The values ranged from 0 to 1, where a larger value indicates higher methylation.

In more recent work with the larger set of DLPFC specimens (n = 730) and the PCC (n = 186), processing methods were updated. Thus, the data presented for the blood and matched DLPFC maintain the original pipelines, while the data presented for the full set of 730 DLPFC and the 186 PCC utilize the updated pipelines. For the PCC, we also updated to the Infinium MethylationEPIC array. For the full set of DLPFC and PCC, the raw signal intensities were imported into the R statistical environment with functions from the methylumi package and further processed with the wateRmelon package. The pipeline for quality control was generally consistent for the HumanMethylation450 and the MethylationEPIC arrays. Initial quality control assessment was performed using functions in the methylumi package to exclude samples with inefficient bisulfite conversion (<90%) as well as outliers. Further preprocessing was conducted using the wateRmelon package by applying a p-filter. Probes having more than 1% of samples with a detection p-value greater than 0.05 and a beadcount lower than 3 in more than 5% of samples were excluded. Finally, the filtered data were normalized with "dasen." Non-CpG SNP (Single Nucleotide Polymorphism) probes, probes that had been reported to contain common (MAF > 5%) SNPs in the CG or single base extension position, or probes that were non-specific or mismapped, were flagged and disregarded in the evaluation of our results. The resulting datasets for analysis here consisted of 730 samples with 423,841 probes each for the DLPFC, and 186 samples with 810,015 probes each for the PCC. Adequate information for probes relevant to the four clocks was available after all processing.

We used open source software at https://dnamage.genetics.ucla.edu/home_ to calculate three epigenetic clocks in the blood samples, DLPFC, and PCC: Horvath clock (Horvath, 2013), Hannum clock (Hannum et al., 2013), and PhenoAge clock (Levine et al., 2018). The Horvath clock is a pan-tissue clock, originally constructed utilizing CpG sites across 51 human cell types and tissues. The clock was designed by regressing DNAm states on chronologic age and using elastic net regression to identify a prediction model; it combines information from 353 CpG sites to calculate epigenetic age. The Hannum clock was developed similarly, by regressing DNAm states on chronologic age, although only in peripheral blood samples, and includes 71 CpG sites. The PhenoAge clock was created in blood samples, but regressed DNAm states on clinical biomarkers rather than on chronologic age; it incorporate 513 CpG sites. The Cortical clock was calculated using publically available code provided by the authors[1].

Populations for Analysis

For examining epigenetic clocks in the $CD4^+$ cells, we leveraged information from 41 ROS or MAP participants, who also had archived DLPFC. The 41 participants were identified from a subset of those who provided annual blood, and had samples from baseline and proximate to death (mean = 7.5 years of follow-up). For further examination focused in the DLPFC, we used 730 specimens that were part of previous research on DNAm and neurodegeneration; analyses of the Cortical clock in DLPFC excluded 88 specimens, which had been part of the original training set for the Cortical clock. Finally, for the PCC, 186 samples were available at the time we conducted these analyses. For examining correlations across tissues, we examined 41 participants with both blood samples and DLPFC, as well as 90 women and men who had information on epigenetic clocks in both DLPFC and PCC. No participant had DNAm profiles across all three specimens.

Statistical Analysis

First, we examined the Pearson correlations of each epigenetic clock, in each specimen type, to chronologic age at specimen collection. In addition, since previous research (Armstrong et al., 2017; El Khoury et al., 2019; Shireby et al., 2020) has noted that epigenetic clock age often underestimates chronologic age in older age groups, we created quintiles of chronologic age, and then examined the difference of epigenetic and chronologic age separately within each quintile, for each clock. These age group analyses were conducted in the DLPFC and PCC specimens, due to the larger sample sizes available.

Next, we considered the correlations of epigenetic clock ages across the two timepoints within the $CD4^+$ cells, as well as clock ages across the 41 matched $CD4^+$ and DLPFC, and across the 90 matched DLPFC and PCC. To understand how the various clocks relate to each other, within each specimen, we also compared epigenetic clock ages across the four clocks (e.g., correlation of the Horvath to Hannum clock within baseline blood samples). To help evaluate the difference between epigenetic and chronologic age, we also calculated the residuals from regressing epigenetic age on chronologic age for each specimen type (which has been termed "age acceleration"). Analyses separately examined both epigenetic age and epigenetic age acceleration.

Finally, we considered how key factors such as sex, Alzheimer disease (AD) neuropathology, and clinical health status may affect clock behavior. We conducted analyses of the correlation of epigenetic to chronologic age separately according to: sex (male/female); pathologic diagnosis of Alzheimer disease (yes/no); and clinical diagnosis of Alzheimer dementia (yes/no). Ascertainment of and pathologic AD was identified using the NIA/Reagan criteria, and clinical Alzheimer dementia was assessed by experienced clinicians, using cognitive and clinical data, as previously described (McKhann et al., 1984; National Institute on Aging Reagan Institute Working Group

[1]https://github.com/gemmashireby/CorticalClock

on Diagnostic Criteria for the Neuropathological Assessment of Alzheimer's Disease, 1997; Bennett et al., 2006). These subgroup analyses included only DLPFC and PCC, due to the larger sample sizes available in these specimens.

RESULTS

Chronologic age was approximately 81 years (standard deviation, SD, 6.2) at the baseline blood collection, 89 years (SD 4.7) at the second blood collection proximate to death, and nearly 90 years (SD 4.9) in the matched postmortem DLPFC ($n = 41$). For the full set of brain specimens, mean age at death was 88.0 (SD 6.7) in those with DLPFC ($n = 730$) and 90.0 (SD 6.0) years in those with PCC ($n = 186$) (**Table 1**). Approximately 2/3 of participants were female. Clinical diagnosis of Alzheimer dementia as of death was common, ranging from approximately half of participants with a blood sample, to approximately one-third of those with PCC specimens. Pathologic diagnosis of AD was highly prevalent—60% of participants with a blood sample and over 70% of those with brain specimens.

Across virtually all specimen types, mean epigenetic age was lower than mean chronologic age (**Table 1**). In the blood samples, the PhenoAge and Cortical clocks produced the largest differences between mean chronologic and epigenetic ages. Specifically, mean PhenoAge was 59.8 (SD 8.8) in the baseline blood samples and 63.8 (SD 8.1) in the blood proximate to death; Cortical age was 50.3 (SD 8.1) in the baseline blood and 53.4 (SD 7.9) in the blood proximate to death. Interestingly, in the blood samples, mean Hannum clock age was closest to chronologic age (baseline blood collection: mean Hannum age = 70.1, SD 6.8; blood proximate to death: mean = 73.6, SD 6.5), likely because the Hannum clock was originally constructed in peripheral blood. Finally, we could consider change in epigenetic clock age over time within the two paired blood samples; as expected, the average epigenetic age was greater in the second than the first blood sample for all four clocks. Nonetheless, the difference in mean epigenetic age over the two timepoints was approximately 3–5 years across all four clocks, while the corresponding change in chronologic age was 7.5 years.

In the brain specimens (**Table 1**), mean Cortical age was closest to mean chronologic age (DLPFC: mean Cortical age = 86.5, SD 6.0; PCC: mean = 95.9, SD 5.2). Further, mean Cortical age in the PCC was greater than chronologic age, while clock age was lower than chronologic age for all the other clocks. In particular, PhenoAge was substantially younger than chronologic age in the brain specimens, with a mean of 1.6 (SD 5.8) in DLPFC and 12.1 (SD 4.3) in PCC.

To more closely examine differences between epigenetic and chronologic ages in the brain specimens, we divided the population into quintiles of age, and constructed boxplots of "delta age" by subtracting chronologic from epigenetic age (**Figure 1**); thus, negative values of delta age indicate that epigenetic age is younger than chronologic age. In DLPFC, for the Horvath, Hannum, and PhenoAge clocks, within every quintile of age, the median delta age as well as the upper 25th percentile of the distribution were all negative (**Figure 1**). However, of these three clocks, the smallest delta ages were consistently observed for the Horvath multi-tissue clock. Yet, for the Cortical clock, median delta age was positive (median = 0.7 years) in the youngest quintile of age, and the cutpoints for the upper 25th percentile of the distribution were positive through the youngest three quintiles of age. Thus, Cortical clock was the only one which did not largely underestimate chronologic age at the younger ages in this sample. Nonetheless, across all four clocks, median delta age became larger and more negative with each older age group. For example, in the oldest quintile of age, median delta age was 12.1 years, 37.3, 92.3, and 4.2 for the Horvath, Hannum,

TABLE 1 | Characteristics of participants: Religious Orders Study and Memory and Aging Project.

	Populations for analysis, according to specimen types[a]				
	Baseline blood	**Blood proximate to death**	**DLPFC with matched blood**	**All DLPFC[b]**	**PCC**
N	41	41	41	730	186
Chronologic Age (mean, SD)	81.2 (6.2)	88.7 (4.7)	89.6 (4.9)	88.0 (6.7)	90.0 (6.0)
Female (%)	66%	66%	66%	64%	66%
Clinical Alzheimer Dementia	0	54%	54%	42%	33%
Pathologic Alzheimer Disease	n/a	73%	73%	60%	60%
Epigenetic Age (Mean, SD, range)					
Horvath clock	64.6 (8.4) Range:52.4,87.8	67.6 (7.2) Range:49.7,90.4	69.3 (5.3) Range: 59.6,82.6	79.7 (6.3) Range:60.8,103.5	71.3 (3.9) Range:56.4,82.6
Hannum clock	70.1 (6.8) Range:57.2,88.3	73.6 (6.5) Range:54.4,87.8	51.4 (3.3) Range:43.8,59.5	57.0 (3.2) Range:44.8,66.4	59.1 (2.5) Range:49.3,64.4
PhenoAge clock	59.8 (8.8) Range:39.0,87.5	63.8 (8.1) Range:43.7,80.9	4.5 (5.4) Range:-6.4,23.4	1.6 (5.8) Range:-16.9,24.7	12.1 (4.3) Range:1.5,39.7
Cortical clock	50.3 (8.1) Range:27.9,65.4	53.4 (7.9) Range:39.2,71.3	79.5 (5.6) Range:70.6,94.8	87.3 (5.6) Range:65.0,102	95.9 (5.2) Range:79.1,124

[a]*DLPFC, dorsolateral prefrontal cortex; PCC, posterior cingulate cortex.* [b]*For analyses of the Cortical clock in the set of all DLPFC, we excluded 88 specimens which had been part of the original training set for this clock, thus, n = 642 for the Cortical clock.*

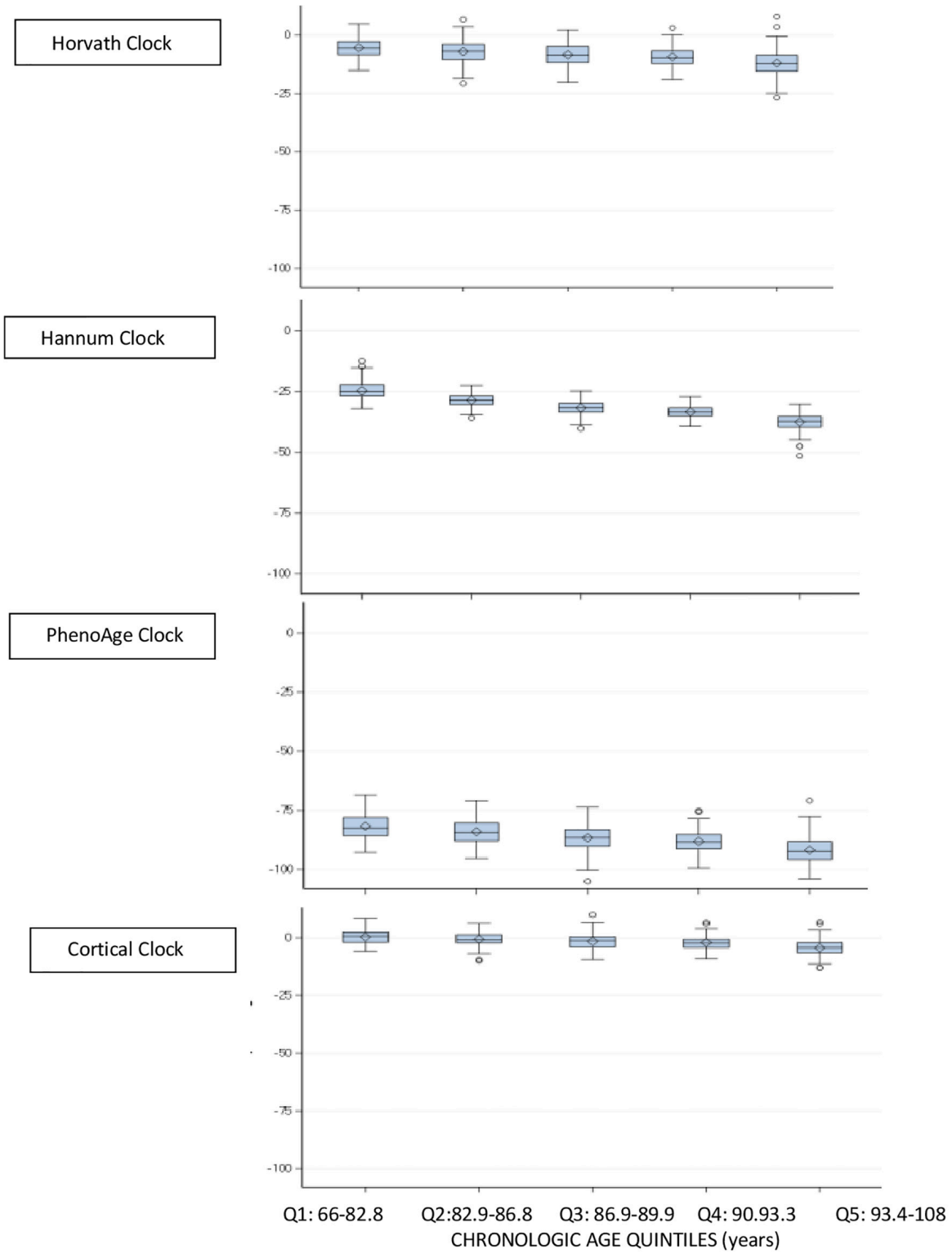

[a] Each boxplot represents the distribution of "delta age" (on the y-axis), or epigenetic minus chronologic age; thus negative values indicate that epigenetic age is younger than chronologic age. N=730 for Horvath, Hannum, PhenoAge clocks, n=642 for Cortical clock.

FIGURE 1 | Difference between epigenetic clock age and chronologic age[a], within quintiles of chronologic age, in dorsolateral prefrontal cortex.

PhenoAge and Cortical clocks, respectively. That is, all clocks underestimated chronologic age by greater amounts with older age of the participants.

These findings were all generally consistent in the PCC (data not shown), although Cortical age in the PCC was greater than chronologic age in virtually all samples.

Next, we directly examined correlations of clock age to chronologic age within the blood samples (**Figure 2**), correlations were generally reasonable for the Horvath, Hannum, PhenoAge and Cortical clocks, ranging from a low of 0.31 (Horvath clock in the blood proximate to death) to a high of 0.66 (Horvath and Hannum clocks in the baseline blood). Across the clocks, correlations tended to be lowest in the blood samples proximate to death (range 0.31–0.43), and correlations tended to be lower for the Cortical clock than the others; for example, the correlation of Cortical to chronologic age was 0.47 in the baseline blood (the lowest of all four clocks).

In brain specimens (**Figure 3**), correlations of epigenetic to chronologic age for the Horvath, Hannum, and PhenoAge clocks largely ranged from approximately 0.5–0.7. The PhenoAge clock consistently performed worst of the four clocks, with a correlation of 0.51 in DLPFC and 0.37 in PCC. The Horvath clock, the only multi-tissue clock, had higher correlations than either the Hannum or PhenoAge clocks in brain specimens. However, the Cortical clock performed best in both the DLPFC and PCC ($r = 0.83$ in DLPFC, $r = 0.74$ in PCC).

For each clock, we also correlated epigenetic ages across paired specimens (**Table 2**), including the two blood samples over time ($n = 41$), the matched blood and DLPFC specimens ($n = 41$), and the two cortical regions ($n = 90$). For the two blood samples, collected an average of 7.5 years apart, correlations were 0.32 for the PhenoAge clock over two timepoints, 0.42 for the Horvath clock, 0.51 for the Hannum clock, and 0.53 for the Cortical clock. When comparing clock ages in blood vs. brain specimens, we found fairly low correlations of the baseline blood sample or the blood sample proximate to death with the postmortem DLPFC; the Horvath and Hannum clocks tended to have better correlations than the other clocks (e.g., $r = 0.31$ and 0.30, respectively, for baseline blood sample). However, we found the highest correlations across specimen types when we compared epigenetic age across the two cortical regions (Horvath: $r = 0.61$; Hannum $r = 0.40$; PhenoAge $r = 0.37$); this correlation was particularly high for the Cortical clock ($r = 0.82$). In additional analyses to explore whether there may be better correlations when considering the extent of epigenetic age acceleration across specimens than the extent of epigenetic aging, we found that results were generally similar for clock age acceleration (data not shown in table) as for clock age.

Within each specimen, when we compared the various clocks to each other (**Table 3**), overall, correlations were 0.65 or greater for over half of the comparisons. The lowest correlations tended to be for the PhenoAge vs. other clocks, perhaps since the PhenoAge clock was the only clock designed to predict biomarkers of aging rather than chronologic age.

Finally, we examined how clock performance may differ in men vs. women, or in those with differing health status (**Figure 4**), in the DLPFC and PCC specimens. Most importantly, the correlations of epigenetic to clock age remained similar across men and women, those with and without pathologic diagnosis of AD, and those with and without clinical diagnosis of dementia. However, there were suggestions of somewhat higher correlations of epigenetic to chronologic age in men than in women, and somewhat lower correlations in those with pathologic AD than without pathologic AD; for example, the correlation of Cortical age to chronologic age in DLFPC was 0.78 among men and 0.69 among women, and was 0.78 in those without pathologic AD compared to 0.68 in those with pathologic AD.

DISCUSSION

In this investigation of characteristics of epigenetic clocks across blood and brain specimens in older adults, we confirmed previous reports (Armstrong et al., 2017; El Khoury et al., 2019; Shireby et al., 2020), that epigenetic age was generally lower than chronologic age, across specimen types. Specifically, for the Horvath, Hannum, and PhenoAge clocks, median epigenetic age was lower than chronologic age from the youngest through the oldest quintiles of age in our sample. By contrast, as may be expected, the Cortical clock demonstrated the smallest differences between epigenetic and chronologic age in DLPFC and in PCC. Indeed, the Cortical clock was not only designed in brain tissue, but the training set included much larger samples of older participants than the other clocks, which certainly further enhances its accuracy in estimating brain aging. We also extended published findings (Lu et al., 2017; Shireby et al., 2020), using varying clocks than previously examined, that correlations of chronologic to epigenetic ages in brain specimens (i.e., DLPFC and PCC) were generally reasonable for blood-based and multi-tissue clocks. In our specimens, these correlations largely ranged from 0.5 to 0.7 for the Horvath, Hannum and PhenoAge clocks—despite none being designed expressly in brain tissue. We further confirmed a previous report (Shireby et al., 2020) that the new Cortical clock—the first designed in post-mortem brain tissue—performed substantially better in brain specimens than the other clocks, with a correlation of epigenetic vs. chronologic age over 0.8 in our DLPFC. Thus, our findings both provide broad support for the value of epigenetic clocks in research on brain aging, as well as specific support for "bespoke" clocks (Bell et al., 2019) designed in target tissues of interest. Finally, however, epigenetic age was only quite modestly correlated across paired blood and DLPFC, indicating that broader research in biologic aging and neurodegeneration may benefit from epigenetic clocks focused in CpG sites better conserved across blood and brain specimens.

Numerous large-scale studies have reported good correlations of chronologic to epigenetic age in peripheral blood, similar to our findings (Chen et al., 2016). However, less is known regarding epigenetic aging specifically in blood samples proximate to death. In our study of 41 blood samples collected a mean of 0.9 years prior to death, we found that the correlation of chronologic to epigenetic age appeared worse than in the baseline samples collected years earlier. Specifically, these correlations

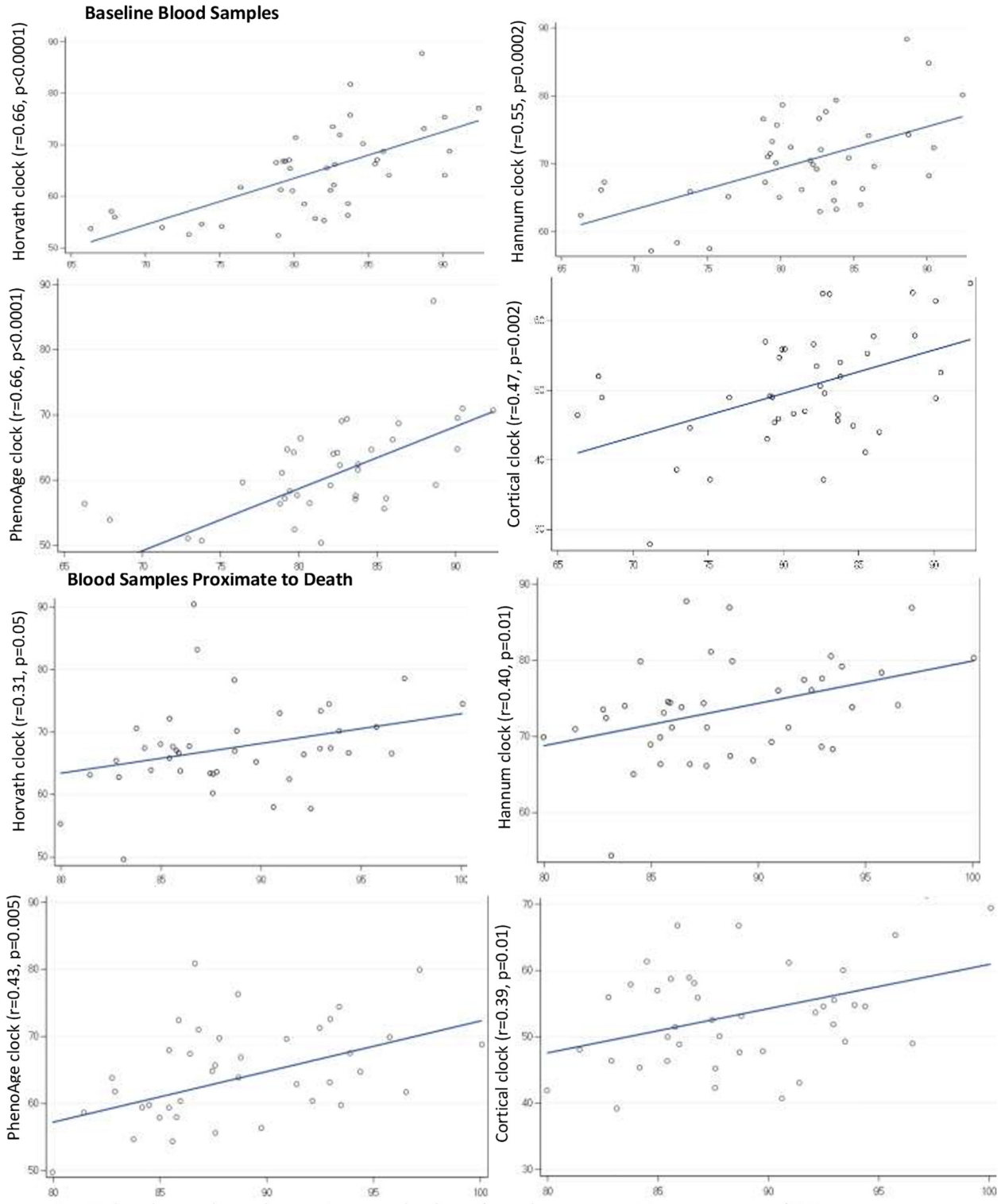

FIGURE 2 | Pearson correlations of epigenetic age to chronologic age in blood samples[a].

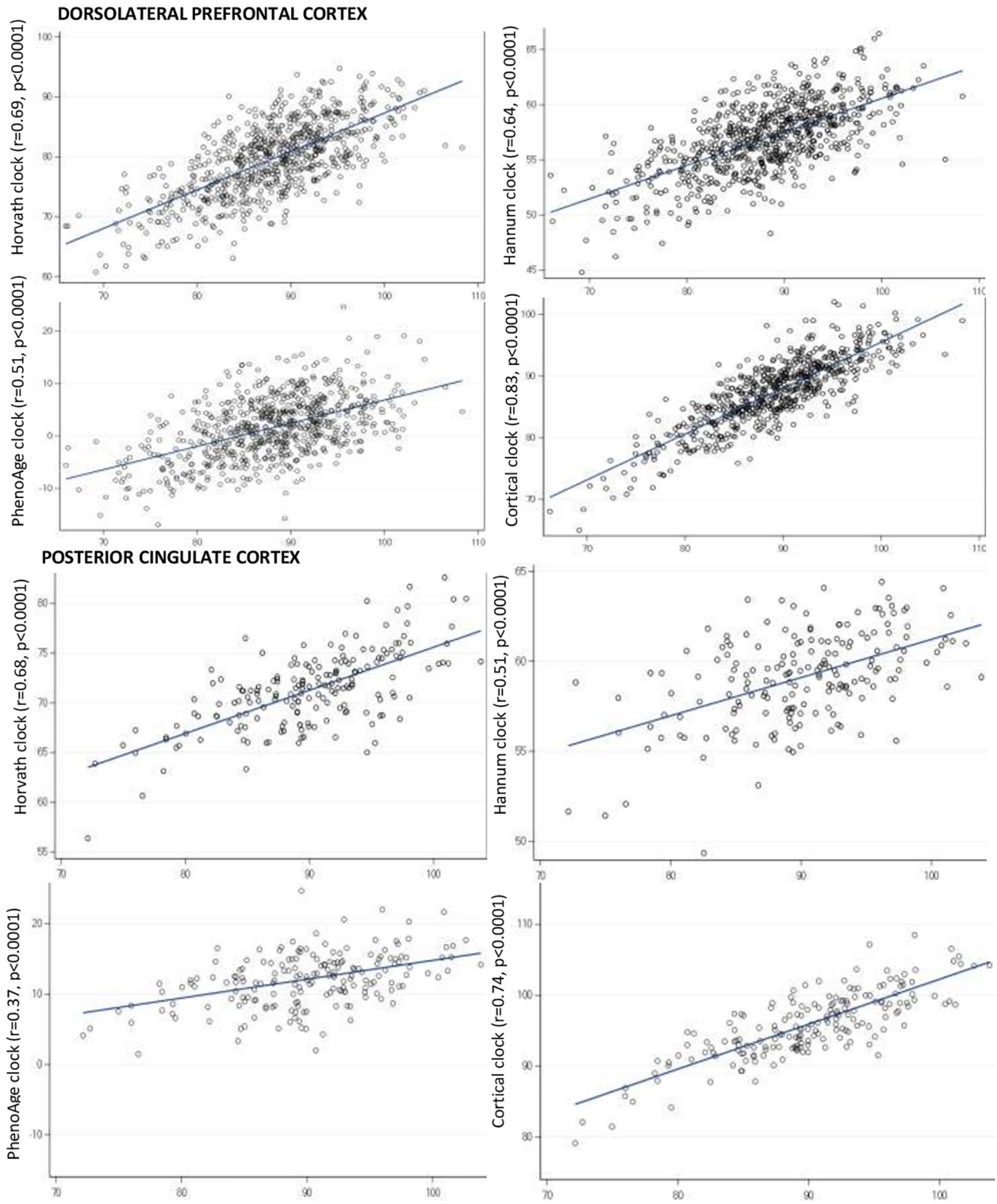

FIGURE 3 | Pearson correlations of epigenetic age to chronologic age in brain specimens[a].

TABLE 2 | Pearson correlations of epigenetic clocks across blood samples and brain regions.

		Correlation across specimen types, for each epigenetic clock (r, *p*-value)			
Sets of biospecimens	***N***	**Horvath clock**	**Hannum clock**	**PhenoAge clock**	**Cortical clock**
Baseline blood/blood proximate to death	41	0.42 ($p = 0.007$)	0.51 ($p = 0.0007$)	0.32 ($p = 0.03$)	0.53 ($p = 0.0003$)
Baseline blood/DLPFC	41	0.31 ($p = 0.05$)	0.30 ($p = 0.05$)	0.08 ($p = 0.6$)	0.24 ($p = 0.1$)
Blood proximate to death/DLPFC	41	0.32 ($p = 0.04$)	0.31 ($p = 0.05$)	0.21 ($p = 0.2$)	0.19 ($p = 0.2$)
DLPFC/PCC	90	0.61 ($p = 0.0001$)	0.40 ($p = 0.0001$)	0.37 ($p = 0.0003$)	0.82 ($p < 0.0001$)

TABLE 3 | Pearson correlations of epigenetic clocks to each other, by specimen type.

		Correlation of epigenetic clocks to each other (r, *p*-value)					
Biospecimen type	***N***	**Horvath vs. Hannum clock**	**Horvath vs. PhenoAge clock**	**Horvath vs. Cortical clock**	**Hannum vs. PhenoAge clock**	**Hannum vs. Cortical clock**	**PhenoAge vs. Cortical clock**
Baseline blood	41	0.74 ($p < 0.0001$)	0.69 ($p < 0.0001$)	0.67 ($p < 0.0001$)	0.68 ($p < 0.0001$)	0.80 ($p < 0.0001$)	0.58 ($p < 0.0001$)
Blood proximate to death	41	0.59 ($p < 0.0001$)	0.74 ($p < 0.0001$)	0.65 ($p < 0.0001$)	0.70 ($p < 0.0001$)	0.71 ($p < 0.0001$)	0.67 ($p < 0.0001$)
DLPFC	730	0.71 ($p < 0.0001$)	0.57 ($p < 0.0001$)	0.79 ($p < 0.0001$)	0.44 ($p < 0.0001$)	0.71 ($p < 0.0001$)	0.50 ($p < 0.0001$)
PCC	186	0.65 ($p < 0.0001$)	0.44 ($p < 0.0001$)	0.75 ($p < 0.0001$)	0.18 ($p = 0.01$)	0.56 ($p < 0.0001$)	0.46 ($p < 0.0001$)

ranged from 0.3 to 0.4. At the same time, from the baseline to the final blood collection, the correlations of epigenetic ages over these 7 years in our study (0.32–0.53) were similar to those reported in other studies with repeated measures of blood DNAm, including studies which did not focus on blood collected proximate to death (Marioni et al., 2019). For example, over approximately 7 years, in two other studies (Marioni et al., 2019) (n = 172 and 175), they found correlations of 0.33–0.64 for the Horvath and for the Hannum clock over time, suggesting that DNAm levels in our study changed in at least somewhat expected ways. Ultimately, our sample size for the peripheral blood was not large, thus it is difficult to ascertain a cause of the observed lower correlations in the blood samples proximate to death. However, our findings indicate that further specific investigations of peripheral blood proximate to death may provide new understanding of DNA methylation in health and mortality.

Considerably less is known regarding epigenetic age in brain tissue. In one publication reporting data only on the Horvath clock, using seven smaller cohorts (n = 37–302, including a subset of the ROS and MAP DLPFC here), Lu et al. (2017) observed correlations of chronologic age to clock age ranging from 0.61 to 0.99 within 6 brain regions. In more recent research of PhenoAge, Levine et al. (2018) reported correlations with chronologic age of 0.51–0.92 across varying brain regions (including DLPFC in ROSMAP). Thus, both of these publications found largely similar correlations as we report here, supporting the relevance of epigenetic clocks to brain aging. Moreover, we found especially high correlations of Cortical age to chronologic age in the DLPFC and PCC—and excellent correlation of Cortical age across the DLPFC and PCC. Further, in limited existing clinical research in brain tissue, the Horvath clock in ROSMAP DLPFC was related to some neuropathologic measures, with significant correlations of DNAm age to amyloid load, neuritic plaques, and diffuse plaques, but not to tangles, pathologic AD or to clinical measures of cognitive function (Levine et al., 2015). Interestingly, although we found that the PhenoAge clock had the lowest correlation with chronologic age in brain tissue, initial analyses by Levine et al. (2018) suggested that PhenoAge in the ROSMAP DLPFC was also significantly related to amyloid load, to neurofibrillary tangles, as well as to pathologic AD diagnosis. It will clearly be important in future research to extensively explore each of the clocks, assessed in brain tissue, in association with neuropathologic and clinical neurologic outcomes. In particular, while the Cortical clock here was best correlated to chronologic age in the brain tissue, and had the smallest absolute difference between epigenetic and chronologic age, it will be interesting and important to evaluate whether this also translates into higher predictive ability for neuropathologic and clinical neurologic outcomes above and beyond the effect of chronologic age.

Notably, we also found that correlations of epigenetic age in blood vs. brain samples were low, largely 0.3 or lower across the clocks. While research focused in brain specimens remains central to understanding neurodegeneration, epigenetic clocks that could allow direct translation across brain and blood, will have the greatest research potential, given the accessibility of blood samples. Future development of epigenetic clocks for translational research in neurodegenerative diseases might benefit from focusing on CpG sites which are conserved across blood and brain tissue, as an approach to explore for improved relevance in both tissue types.

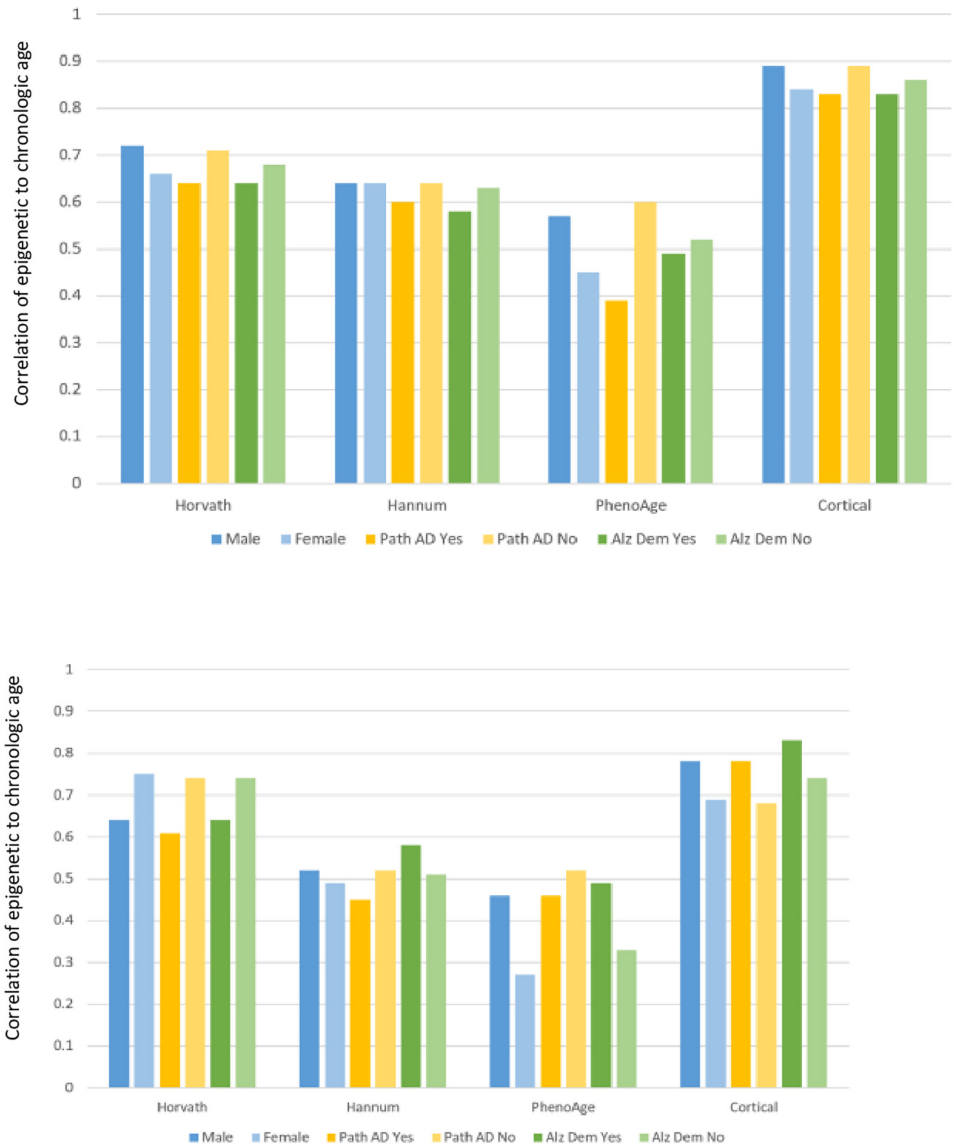

[a] In dorsolateral prefrontal cortex, n=264 men and 466 women; n=440 with pathologic Alzheimer disease (path AD) and 290 without; n=308 with clinical Alzheimer dementia (Alz Dem) and 403 without (n=19 missing). For Cortical clock, 88 participants were excluded who were in the original training set. In posterior cingulate cortex, n=64 men and 122 women; n=112 with pathologic Alzheimer disease and 74 without; n=62 with clinical Alzheimer dementia and 121 without (n=3 missing). All p-values for Pearson correlations <0.05.

FIGURE 4 | Pearson correlations of epigenetic age to chronologic age, according to characteristics of participants[a].

Finally, when we specifically examined brain specimens from participants according to sex or to health profiles, we found that the clocks consistently performed well in males and females, and in those with or without either pathologic diagnosis of AD or clinical diagnosis of dementia. This is reassuring evidence that underlying characteristics of participants do not appear to have material influence on basic functioning of the epigenetic clocks. Interestingly, the Cortical clock is the only clock trained in a sample which excluded Alzheimer disease cases, due to concerns that underlying disease could potentially influence results (Shireby et al., 2020). However, in comparison to the other clocks, the Cortical clock did not demonstrate correlations with chronologic age that were consistently better or worse in our participants with vs. without pathologic AD, or clinical dementia; this may further support the ability of epigenetic clocks to estimate broad biologic aging across and within specific underlying disease states.

Strengths of our study include the unique availability of paired blood samples and brain specimens, enabling investigation of epigenetic clocks across these tissues. Further, our large sample of older persons permitted detailed examination of epigenetic clocks from brain tissue at older ages. There are limitations as well. The proportion of neurons and other cell types in the gray matter may confound DNAm states, which we did not consider here; however, in previous analyses in ROSMAP DLPFC, control for neuron count when broadly examining DNAm profiles or specifically examining epigenetic clocks, did not meaningfully change results (Horvath et al., 2015; Levine et al., 2018). The blood samples were limited to $CD4^+$ cells, whereas prior studies examined clocks built from a wide variety of cell types (Fransquet et al., 2019); however, our findings largely mirror those of studies using varying blood cells. Nonetheless, it is possible that specific findings here (e.g., the generally low correlations between clocks in blood vs. brain tissue), might be different in other blood cell types, a topic meriting additional research. Further, the sample size of blood specimens, including matched blood and brain specimens, was small, limiting our analyses and interpretations. Finally, we did not consider how the epigenetic clocks may predict the span of neuropathologic or clinical neurologic outcomes. Instead, we chose to focus here on extensive consideration of basic characteristics of epigenetic clocks in blood and brain specimens—a crucial step prior to broader neurologic research. In future investigations, we will more directly address relations of these clocks to brain pathology and to cognition.

DATA AVAILABILITY STATEMENT

Publicly available datasets were analyzed in this study. The ROSMAP datasets analyzed here can be requested at https://www.radc.rush.edu/.

ETHICS STATEMENT

The studies involving human participants were reviewed and approved by the Rush University Medical Center IRB. The patients/participants provided their written informed consent to participate in this study.

AUTHOR CONTRIBUTIONS

FG and BL drafted the manuscript and contributed to conception, design, and analysis and interpretation of data. LY revised the manuscript, and contributed to conception and design of the research, and data acquisition, analysis, and interpretation. AI revised the manuscript and contributed to data acquisition and interpretation. PD revised the manuscript, and contributed to conception and design of the research, and data acquisition and interpretation. DB revised the manuscript, and contributed to conception and design of the research, and data acquisition, analysis and interpretation. All authors contributed to the article and approved the submitted version.

FUNDING

This work was supported by NIH grants P30AG10161, R01AG15819, R01AG17917, R01AG36042, RC2AG36547, and U01AG61356. The funding agencies had no role in study design, data collection and analysis, decision to publish, or preparation of the manuscript.

ACKNOWLEDGMENTS

We thank the participants of ROS and MAP for their essential contributions and the gift of their brain to these projects.

REFERENCES

Alzheimer's Association (2019). 2019 Alzheimer's disease facts and figures. *Alzheimers Dement* 15, 321–387. doi: 10.1016/j.jalz.2019.01.010

Armstrong, N. J., Mather, K. A., Thalamuthu, A., Wright, M. J., Trollor, J. N., Ames, D., et al. (2017). Aging, exceptional longevity and comparisons of the Hannum and Horvath epigenetic clocks. *Epigenomics* 9, 689–700. doi: 10.2217/epi-2016-0179

Bell, C. G., Lowe, R., Adams, P. D., Baccarelli, A. A., Beck, S., Bell, J. T., et al. (2019). DNA methylation aging clocks: challenges and recommendations. *Genome Biol.* 20:249.

Bennett, D. A., Buchman, A. S., Boyle, P. A., Barnes, L. L., Wilson, R. S., and Schneider, J. A. (2018). Religious orders study and rush memory and aging project. *J. Alzheimers Dis.* 64(Suppl. 1), S161–S189.

Bennett, D. A., Schneider, J. A., Aggarwal, N. T., Arvanitakis, Z., Shah, R. C., Kelly, J. F., et al. (2006). Decision rules guiding the clinical diagnosis of Alzheimer's disease in two community-based cohort studies compared to standard practice in a clinic-based cohort study. *Neuroepidemiology* 27, 169–176. doi: 10.1159/000096129

Chen, B. H., Marioni, R. E., Colicino, E., Peters, M. J., Ward-Caviness, C. K., Tsai, P. C., et al. (2016). DNA methylation-based measures of biological age: meta-analysis predicting time to death. *Aging (Albany N.Y.)* 8, 1844–1865.

Chuang, Y. H., Paul, K. C., Bronstein, J. M., Bordelon, Y., Horvath, S., and Ritz, B. (2017). Parkinson's disease is associated with DNA methylation levels in human blood and saliva. *Genome Med.* 9:76.

De Jager, P. L., Srivastava, G., Lunnon, K., Burgess, J., Schalkwyk, L. C., Yu, L., et al. (2014). Alzheimer's disease: early alterations in brain DNA methylation at ANK1, BIN1, RHBDF2 and other loci. *Nat. Neurosci.* 17, 1156–1163. doi: 10.1038/nn.3786

El Khoury, L. Y., Gorrie-Stone, T., Smart, M., Hughes, A., Bao, Y., Andrayas, A., et al. (2019). Systematic underestimation of the epigenetic clock and age acceleration in older subjects. *Genome Biol.* 20:283.

Fransquet, P. D., Wrigglesworth, J., Woods, R. L., Ernst, M. E., and Ryan, J. (2019). The epigenetic clock as a predictor of disease and mortality risk: a systematic review and meta-analysis. *Clin. Epigenetics* 11:62.

Hannum, G., Guinney, J., Zhao, L., Zhang, L., Hughes, G., Sadda, S., et al. (2013). Genome-wide methylation profiles reveal quantitative views of aging rates. *Mol. Cell* 49, 359–367. doi: 10.1016/j.molcel.2012.10.016

Horvath, S. (2013). DNA methylation age of human tissues and cell types. *Genome Biol.* 14:R115.

Horvath, S., Langfelder, P., Kwak, S., Aaronson, J., Rosinski, J., Vogt, T. F., et al. (2016). Huntington's disease accelerates epigenetic aging of human brain and disrupts DNA methylation levels. *Aging (Albany N.Y.)* 8, 1485–1512. doi: 10.18632/aging.101005

Horvath, S., Pirazzini, C., Bacalini, M. G., Gentilini, D., Di Blasio, A. M., Delledonne, M., et al. (2015). Decreased epigenetic age of PBMCs from Italian semi-supercentenarians and their offspring. *Aging (Albany N.Y.)* 7, 1159–1170. doi: 10.18632/aging.100861

Jylhava, J., Pedersen, N. L., and Hagg, S. (2017). Biological age predictors. *EBioMedicine* 21, 29–36. doi: 10.1016/j.ebiom.2017.03.046

Klein, H. U., Bennett, D. A., and De Jager, P. L. (2016). The epigenome in Alzheimer's disease: current state and approaches for a new path to gene discovery and understanding disease mechanism. *Acta Neuropathol.* 132, 503–514. doi: 10.1007/s00401-016-1612-7

Levine, M. E., Lu, A. T., Bennett, D. A., and Horvath, S. (2015). Epigenetic age of the pre-frontal cortex is associated with neuritic plaques, amyloid load, and Alzheimer's disease related cognitive functioning. *Aging (Albany N.Y.)* 7, 1198–1211. doi: 10.18632/aging.100864

Levine, M. E., Lu, A. T., Quach, A., Chen, B. H., Assimes, T. L., Bandinelli, S., et al. (2018). An epigenetic biomarker of aging for lifespan and healthspan. *Aging (Albany N.Y.)* 10, 573–591. doi: 10.18632/aging.101414

Lu, A. T., Hannon, E., Levine, M. E., Crimmins, E. M., Lunnon, K., Mill, J., et al. (2017). Genetic architecture of epigenetic and neuronal ageing rates in human brain regions. *Nat. Commun.* 8:15353.

Lunnon, K., Smith, R., Hannon, E., De Jager, P. L., Srivastava, G., Volta, M., et al. (2014). Methylomic profiling implicates cortical deregulation of ANK1 in Alzheimer's disease. *Nat. Neurosci.* 17, 1164–1170. doi: 10.1038/nn.3782

Marioni, R. E., Shah, S., McRae, A. F., Ritchie, S. J., Muniz-Terrera, G., Harris, S. E., et al. (2015). The epigenetic clock is correlated with physical and cognitive fitness in the Lothian Birth Cohort 1936. *Int. J. Epidemiol.* 44, 1388–1396. doi: 10.1093/ije/dyu277

Marioni, R. E., Suderman, M., Chen, B. H., Horvath, S., Bandinelli, S., Morris, T., et al. (2019). Tracking the epigenetic clock across the human life course: a meta-analysis of human cohort data. *J. Gerontol. A Biol. Sci. Med. Sci.* 74, 57–61. doi: 10.1093/gerona/gly060

Marras, C., Beck, J. C., Bower, J. H., Roberts, E., Ritz, B., Ross, G. W., et al. (2018). Prevalence of Parkinson's disease across North America. *NPJ Parkinsons Dis.* 4:21.

McKhann, G., Drachman, D., Folstein, M., Katzman, R., Price, D., and Stadlan, E. M. (1984). Clinical diagnosis of Alzheimer's disease: report of the NINCDS-ADRDA work group under the auspices of Department of Health and Human Services task force on Alzheimer's disease. *Neurology* 34, 939–944. doi: 10.1212/wnl.34.7.939

National Institute on Aging and Reagan Institute Working Group on Diagnostic Criteria for the Neuropathological Assessment of Alzheimer's Disease (1997). Consensus recommendations for the postmortem diagnosis of Alzheimer's disease. *Neurobiol. Aging* 18(4 Suppl.), S1–S2.

Raina, A., Zhao, X., Grove, M. L., Bressler, J., Gottesman, R. F., Guan, W., et al. (2017). Cerebral white matter hyperintensities on MRI and acceleration of epigenetic aging: the atherosclerosis risk in communities study. *Clin. Epigenetics* 9:21.

Shah, N. S., Lloyd-Jones, D. M., O'Flaherty, M., Capewell, S., Kershaw, K. N., Carnethon, M., et al. (2019). Trends in cardiometabolic mortality in the United States, 1999-2017. *JAMA* 322, 780–782. doi: 10.1001/jama.2019.9161

Shireby, G. L., Davies, J. P., Francis, P. T., Burrage, J., Walker, E. M., Neilson, G. W. A., et al. (2020). Recalibrating the epigenetic clock: implications for assessing biological age in the human cortex. *Brain* awaa334. doi: 10.1093/brain/awaa334

Siegel, R. L., Miller, K. D., and Jemal, A. (2018). Cancer statistics, 2018. *CA Cancer J. Clin.* 68, 7–30. doi: 10.3322/caac.21442

Yu, L., Chibnik, L. B., Yang, J., McCabe, C., Xu, J., Schneider, J. A., et al. (2016). Methylation profiles in peripheral blood CD4+ lymphocytes versus brain: the relation to Alzheimer's disease pathology. *Alzheimers Dement* 12, 942–951. doi: 10.1016/j.jalz.2016.02.009

Conflict of Interest: The authors declare that the research was conducted in the absence of any commercial or financial relationships that could be construed as a potential conflict of interest.

frontiers in Neuroscience

REVIEW
published: 03 February 2021
doi: 10.3389/fnins.2021.614251

Advances of Mechanisms-Related Metabolomics in Parkinson's Disease

*Yanyan Zhang, Jie Li, Xiao Zhang, Dongdong Song and Tian Tian**

Department of Neurology, The First Affiliated Hospital of Zhengzhou University, Zhengzhou, China

Parkinson's disease (PD) is a multifactorial disorder characterized by progressively debilitating dopaminergic neurodegeneration in the substantia nigra and the striatum, along with various metabolic dysfunctions and molecular abnormalities. Metabolomics is an emerging study and has been demonstrated to play important roles in describing complex human diseases by integrating endogenous and exogenous sources of alterations. Recently, an increasing amount of research has shown that metabolomics profiling holds great promise in providing unique insights into molecular pathogenesis and could be helpful in identifying candidate biomarkers for clinical detection and therapies of PD. In this review, we briefly summarize recent findings and analyze the application of molecular metabolomics in familial and sporadic PD from genetic mutations, mitochondrial dysfunction, and dysbacteriosis. We also review metabolic biomarkers to assess the functional stage and improve therapeutic strategies to postpone or hinder the disease progression.

Keywords: Parkinson disease, metabolomics, genetic mutations, mitochondrial dysfunction, dysbacteriosis

OPEN ACCESS

Edited by:
Deepti Lall,
Cedars Sinai Medical Center, United States

Reviewed by:
Maria Shadrina, Institute of Molecular Genetics (RAS), Russia
Anandhan Annadurai, University of Arizona, United States

****Correspondence:***
Tian Tian
fcctiant@zzu.edu.cn

Specialty section:
This article was submitted to Neurodegeneration, a section of the journal Frontiers in Neuroscience

Received: *05 October 2020*
Accepted: *11 January 2021*
Published: *03 February 2021*

Citation:
Zhang Y, Li J, Zhang X, Song D and Tian T (2021) Advances of Mechanisms-Related Metabolomics in Parkinson's Disease. Front. Neurosci. 15:614251. doi: 10.3389/fnins.2021.614251

INTRODUCTION

As the second most common chronic neurodegenerative disorder after Alzheimer's disease, Parkinson's disease (PD) is a multisystemic disease with multiple mechanisms and neurochemical features, affecting around >2% of all persons above 65 years of age and >4% of all persons over the age of 80 (GBD 2015 Neurological Disorders Collaborator Group, 2017; Santos Garcia et al., 2019; Xu et al., 2019). E Ray Dorsey et al. make an important point about the global burden of PD, with the number of affected individuals having risen from 2.5 million in 1990 to 6.1 million in 2016, with projections that by 2050 the number of PD patients will be at 12 million (GBD 2016 Parkinson's Disease Collaborators, 2018). From an etiological perspective, the two hallmarks and indicators of a definite diagnosis of PD are the deterioration of dopaminergic neurons and the accumulation of intracytoplasmic protein α-Synuclein (α-Syn), called Lewy bodies, in the substantia nigra region of the brain (Spillantini et al., 1997; Spillantini and Goedert, 2018). They are mainly relevant to various neuropathological insults, such as genetic mutants (Kim and Alcalay, 2017), oxidative stress (Puspita et al., 2017), apoptosis, neuroinflammation (De Virgilio et al., 2016; Rocha et al., 2018), mitochondrial dysfunction (Bose and Beal, 2016), disrupting intercellular communication (Hou et al., 2019), endocrine disorders (De Pablo-Fernández et al., 2017), and inhibition of aberrant protein degradation pathways (Tofaris et al., 2001; Spencer et al., 2014; Sugeno et al., 2014). The α-Syn is linked to PD pathology, which possesses prion-like behavior and presents in various throughout the nervous systems before neuronal death and classical symptoms (Grassi et al., 2018; Ma et al., 2019). However, as a multifactorial disease, PD is also influenced by dietary factors (Tufi et al., 2014; Fitzgerald et al., 2017; Lehmann et al., 2017; Zhao et al., 2019), microorganisms (Keshavarzian et al., 2015; Scheperjans et al., 2015), and different

environmental elements, such as metal (Kim et al., 2018), neurotoxins (Bove and Perier, 2012), light exposure (Willis et al., 2018), and infection. The disease has complex etiopathogenesis that has still not been fully elucidated. Though four categories of biomarkers have been recommended to confer accurate diagnosis and assess the condition of patients, including clinical symptoms, genetic mutation, pathological, and neuroimaging changes (Delenclos et al., 2016), markers for an early diagnosis and effective treatments of PD are still lacking. Clinically, there is a high rate of misdiagnosis of the disease and clinical accuracy of PD diagnosis is only 76–84%. Therefore, a better understanding of the etiology and pathogenesis, as well as molecular events associated with clinical symptoms, will be significant for early diagnosis and therapeutic strategies.

Metabolomics is an emerging and effective approach used in the identification and discovery of metabolic biomarkers; it relies on the assessment of various biological samples and provides a series of metabolic signatures involving molecular processes that elucidate pathological changes of diseases. The technology links various metabolic molecular mechanisms to neuronal activity alterations, protein changes or genetic mutations, mitochondrial dysfunction, or dysbacteriosis. As an advanced technique of omics, metabolomics can integrate endogenous and exogenous cellular metabolic activities, holding great promise in its ability to probe biochemical details about the pathological status, progression, and treatment of many chronic metabolic diseases, such as cancer, neurodegenerative disease, and kidney disease (Kalim and Rhee, 2017; Willis et al., 2018). Interestingly, an increasing number of scholars devoted to PD research have indicated that metabolomics can be considered as a powerful tool to define biochemical information, detect metabolomic status, and speculate on underlying mechanisms in the disease (Koeth et al., 2013; Pannkuk et al., 2015). Metabolomics' high-sensitivity and high-throughput properties might support detailed information of the end-product abnormalities arising from interactions between genes, chemicals, protein structure, and various environmental factors. In this respect, metabolomics could be more applicable than other "omics" techniques, including genomics, pharmacogenomics, and transcriptomics, in the qualitative and quantitative analysis of metabolites from cell or biologic specimens to effectively reflect subtle changes of metabolites (Stoessel et al., 2018). Therefore, the introduction of metabolomics in PD research would provide a new solution for seeking underlying metabolic biomarkers for the predication and treatment of the disease.

Considering clinical and experimental findings in pathological mechanisms, we know that multiple mechanisms may contribute to PD pathogenesis. Specially, most studies about the metabolomics of PD mainly focus on gene alterations, energy homeostasis, and redox reactions resulting from mitochondrial dysfunction. Meanwhile, declined antioxidation systems and mitochondrial disorders are also important causes of neuron inflammation and senescence associated with neuropathology (Boland et al., 2018). Updated preclinical evidence indicated that the bidirectional communication between the gut community patterns and the nervous system of the brain, hereto dysbacteriosis, was identified and plays an important role in both the metabolism and pathology of patients with PD. So, in-depth research on the metabolomics regarding potential metabolic indicators and pathways of PD should focus on its effects on pathogenesis and the pathological process.

In this review article, we provide a concise overview on technical methods and related operative procedures in the field of metabolomics. We review recent research on the relationship between metabolomics and neuropathological changes of PD in terms of genetic mutation, mitochondrial dysfunctions, and dysbacteriosis, and also summarize the molecular mechanisms and metabolites underlying pathological signs as promising biomarkers of pathogenesis in both sporadic and familial PD.

METABOLOMICS

The metabolome is the entire collection of a wide range of small molecules that participate in body metabolic responses, such as saccharides, amino acids, nucleotides, lipids, and acylcarnitines. Metabolomics, as an analytical technique to investigate disorders in the metabolome of an organism, possess substantial sensitivity, selectivity, and identification capabilities of analyzing diverse varieties of molecular species in biofluids, ranging from ionic compounds in cell lysates to various organic compounds/composition in plasma, cerebrospinal fluid (CSF), urine, and tissue (**Figure 1**). Compared with traditional targeted approaches, the new untargeted metabolomics have great potential to identify some novel biomarkers and help in indicating the metabolite levels of body fluids, seeking different disease biomarkers to provide useful information about metabolic pathways, metabolites, and pathological mechanisms.

In the past decade, many analytical technologies have been introduced and applied in various metabolomic research fields and thus have furthered the understanding of neurodegenerative diseases on the basis of relevant metabolites as biomarkers. In general, the methodologies used for metabolic identification mainly include proton nuclear magnetic resonance (NMR), magnetic resonance spectroscopy (MRS), liquid chromatography mass spectrometry (LCMS), gas chromatography mass spectrometry (GCMS), flourier transform infrared spectrum (FTIR), and high-performance liquid chromatography (HPLC). The first two metrics utilize the magnetic properties of molecular atomic nuclei in metabolic samples to obtain detailed chemical, structural, and quantities information of metabolites in little samples. By contrast, chromatography mass spectrometry (CMS), which combines the efficient separation capability of chromatography with the high detectability of mass spectrometry, has high analytical precision and superior reproducibility and versatility (Kiraly et al., 2016).

With the development of technologies and current research, there are different groups of metabolic biomarkers used in susceptivity, diagnosis, pharmacodynamic response, and prognostic assessment of diseases (Correia et al., 2017). Emerging evidence has revealed that related metabolomics would be a potential tool for screening and monitoring molecular

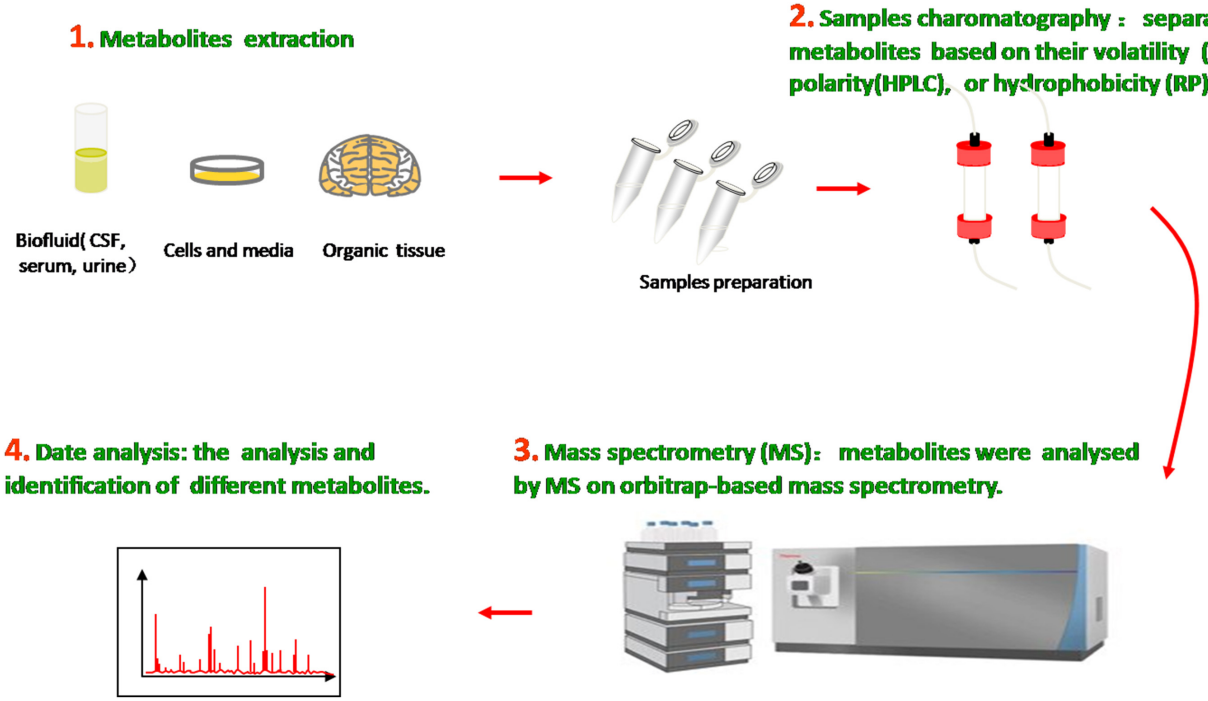

FIGURE 1 | Metabolomics analysis methods. Molecular metabolites were extracted from different samples, ranging from ionic compounds in cell lysates to various organic compositions in plasma, cerebrospinal fluid (CSF), urine, and tissue. Samples chromatography and mass spectrometry were prepared and administrated for analysis and identification.

mechanisms and chemical phenotypes and seeking metabolic signatures as diagnostic and prognostic biomarkers of familial and idiopathic PD. For instance, Bogdanov et al. reported the differences of metabolomic profiling of plasma from idiopathic PD and LRRK2 patients with the G2019S mutation, implicating that the familial PD has unique metabolomic profiles associated with the purine pathway and oxidative processes (Bogdanov et al., 2008; Johansen et al., 2009; Bolner et al., 2011). Similarly, metabolic profiles of blood in idiopathic PD are also different from healthy groups, such as alpha-synuclein, tau protein, urate, and a series of amino acid metabolism (Bolner et al., 2011; Luan et al., 2015; Saiki et al., 2017; Chang et al., 2018; Goldman et al., 2018). These disturbances in the metabolic pathways are related to mitochondrial dysfunctions and the concomitant changes in energy homeostasis and redox reaction, which are thought to be the final common pathways of most endogenous and exogenous factors that are involved in the etiology of PD (Bhinderwala et al., 2019). Recent studies have revealed that there are metabolic differences between treated and drug-naïve PD patients (Bogdanov et al., 2008; Troisi et al., 2019), as well as patients with and without dementia or depression (Hatano et al., 2016; Dong et al., 2018). In addition, biofluids metabolome has potential to distinguish the phenotype of PD. For example, James Roede et al. (2013), used mass spectrometry-based metabolic profiling and showed that polyamine dopamine metabolism was significantly altered in the rapid motor progression of PD compared to both healthy subjects and slow progression PD subjects, which potentially effects of neurodegeneration on neuroinflammation or dopamine metabolism. The metabolomics of animal models demonstrated disturbed metabolic pathways in acylcarnitines, glycerophospholipid, and 4-hydroxypoline in serum, indicating the metabolism influence on the onset and progression of α-Syn pathology (Graham et al., 2018).

GENETIC METABOLOMICS IN PD PATIENTS

Genomics is the upstream regulator of metabolomics and participates in the modulation of differential metabolite concentrations. Since 1977, studies have provided initial insights into molecular genetics and identified the key contributors that give rise to the occurrence and progression of familial PD cases (Polymeropoulos et al., 1997; Kruger et al., 1998; Braak et al., 2003; Zarranz et al., 2004). Until now, 27 PD-associated genes regions have been identified, affecting 20% of all PD patients (Klein and Westenberger, 2012; Correia et al., 2017; Arkinson and Walden, 2018). There are six genes contributing to the clinically classical form of PD, including three autosomal dominant (SNCA, LRRK2, and VPS35) and three autosomal recessively (PINK1, PARK2, and DJ-1). Additionally, some singular gene mutations are associated with an increased risk of developing PD, including autosomal dominant (*PARK3, GIGYF2, HTRA2, EIF4G1,* RAB39B, *TMEM230, CHCHD2, RIC3,* and *GBA*) and autosomal recessive (*ATP13A2, PLA2GB, FBXO7, DNAJC13, SYNJ1,* and *VPS13C*). Previous studies revealed that three

types of metabolic defects mainly play important roles in the progression of PD: a-Syn protein aggregation, mitochondrial dysfunction, and related oxidative damage. From the structural and functional perspectives, these cellular dysfunctions are associated with different sites and types of alterations in these genes (**Figure 2**). Even though most familial monogenic forms of PD are identified, metabolic research mainly focuses on the minority of PD related-genes mutations, including *SNCA, LRRK2, PARK2,* and *GBA*. Therefore, a thorough understanding of these gene-related metabolomics will provide available biomarkers for diagnosing and tracking familial PD.

SNCA

The *SNCA* gene is the first gene to be implicated in PD. Of note, the gene encodes a-Syn protein and its pathogenic mutations were linked with the abnormal accumulation of the presynaptic protein. The initial link between the *SNCA* gene and PD was found by Polymeropoulos et al. (1997) when a missense mutation (A53T) of *SNCA* was implicated in patients with autosomal dominant Parkinsonism from a large Italian family. Shortly thereafter, accumulating evidence has shown the mutations of A30Pro (Kruger et al., 1998), E46K (Zarranz et al., 2004), H50Q, G51D, and A53E in the alpha-synuclein gene (Parajuli et al., 2020). All six-point mutants have been involved in a-Syn overexpression, accumulation, and aggregation, conferring the risk of the disease's onset or causing familial PD (Singleton et al., 2013). In addition, the SNCA duplication or triplication events (*PARK4* variant), as well as the promoter's variation, were also involved in the formation of toxic oligomers, misfolded α-Syn, and nigrostriatal denervation, which are vital causes of the disease (Gatto et al., 2010; Koros et al., 2018).

Apart from protein-encoding, research has suggested the role of the SNCA gene in fatty acid synthesis, lipid metabolism (Golovko et al., 2007), mitochondrial membrane composition (Barcelo-Coblijn et al., 2007), and inflammatory responses in the brain (Castagnet et al., 2005; Golovko et al., 2009). Consistent with previous reports, a current study supports previous findings of the SNCA involvement in substance metabolism of the brain. It is worth noting that the authors identified a range of metabolic changes related to the gene through untargeted metabolomic profiling of the brain, such as glycogen depletion, impaired activity of succinate dehydrogenase, and the abnormality of taurine and glutamine (Musgrove et al., 2014). The metabolic alterations not only reflect impaired mitochondrial function in energy production, but also indicate the pathologies associated with other metabolic pathways. Similar to deteriorating metabolic abnormalities in the brain, the *SNCA* gene-related mutations could affect peripheral tissue metabolism in PD patients, which are useful in understanding the metabolic status of the brain and providing molecular signatures. Demonstrated in a cross-sectional study by Heather et al., the premotor A53T *SNCA* carriers have decreasing serotonin transporter densities and serotonergic pathologies compared with healthy controls (Wilson et al., 2019). In addition, the serotonergic abnormalities preceded dopaminergic neuron loss and clinical symptoms, suggesting the potential role of the serotonergic neurotransmitter system in screening and monitoring the progression of the disease (Qamhawi et al., 2015; Wilson et al., 2018). In a longitudinal study, the comparison between A53T transgenic mice and controls revealed that the A53T mutation could substantially increase guanosine levels as a positive regulation against neurodegeneration (Chen et al., 2015).

LRRK2

LRRK2 (*Leucine-rich repeat kinase 2*) is the most common gene related to PD, with a frequency of 10% in familiar cases (Paisan-Ruiz et al., 2008; Hernandez et al., 2016). Located in a region on chromosome 12, the gene consists of 51 exons which encode a 2,527 amino acid member of the ROCO protein family (Paisan-Ruiz et al., 2008), and relates to mitochondrial functions, cytoskeletal dynamics, and cellular processes (Guaitoli et al., 2016; Bae and Lee, 2019). Based on current research, eight pathogenic substitutions (p.Arg1441Cys/Gly/His, p.Asn1437His, p.Tyr1699Cys, p.Gly2019Ser, p.Ile2020Thr, and p.Ile2012Thr) and two susceptibility variants (p.Arg1628Pro and p.Gly2385Arg) in *LRRK2* have been identified. The G2019S substitution is most frequent *LRRK2*-related mutation. These PD-associated *LRRK2* mutations might increase intracellular ROS production and contribute to oxidative stress and the loss of dopaminergic neurons.

The correlation between the increase of oxidative stress markers and reduced antioxidant capacity and *LRRK* mutation was assessed in the current study (Loeffler et al., 2017). They measured oxidative stress and antioxidant markers in CSF from *LRRK2*-related PD patients, sporadic patients, and control subjects. Two direct indicators of oxidative stress, the 8-hydroxy-2'-deoxyguanosine (8-OHdG) and 8-isoprostane (8-ISO) concentrations, were increased in LRRK2 patients compared with healthy groups, while antioxidant capacity might decrease during the progression of the disease. Similar to the *SNCA* gene, the metabolomic profiles of low molecular weight substances in PD patients with LRRK2 mutations are also different from idiopathic PD and healthy controls (Johansen et al., 2009). In this study, the *LRRK2* mutation patients showed significantly decreased hypoxanthine, Xanthine, and uric acid in plasma, suggesting the reduction of related antioxidant activities. In addition, several studies have provided evidence that blood levels of uric acid appeared to correlate negatively with the risk for developing PD (Annanmaki et al., 2007; Ascherio et al., 2009; Ou et al., 2017). These suggest that metabolites of the purine pathway play a potential role in elucidating pathogenesis and biomarkers of PD. Like uric acid, *LRRK2* mutation was associated with impaired serine metabolism, showing decreased serine racemase expression and increased serine levels (Nickels et al., 2019). *LRRK2* genes also took part in other metabolic responses, such as Akt signaling, glucose metabolism, or immunity, contributing to the identification of metabolism in *LRRK*-PD (Infante et al., 2015; Wile et al., 2017).

PINK1 and PARK2

In autosomal recessively PD, *PINK1*, and *PARK2* are associated with the neurodegenerative disorder, which encode the E3 ubiquitin ligase Parkin and the mitochondrial serine/threonine kinase PINK1 that play important roles in mitochondrial quality

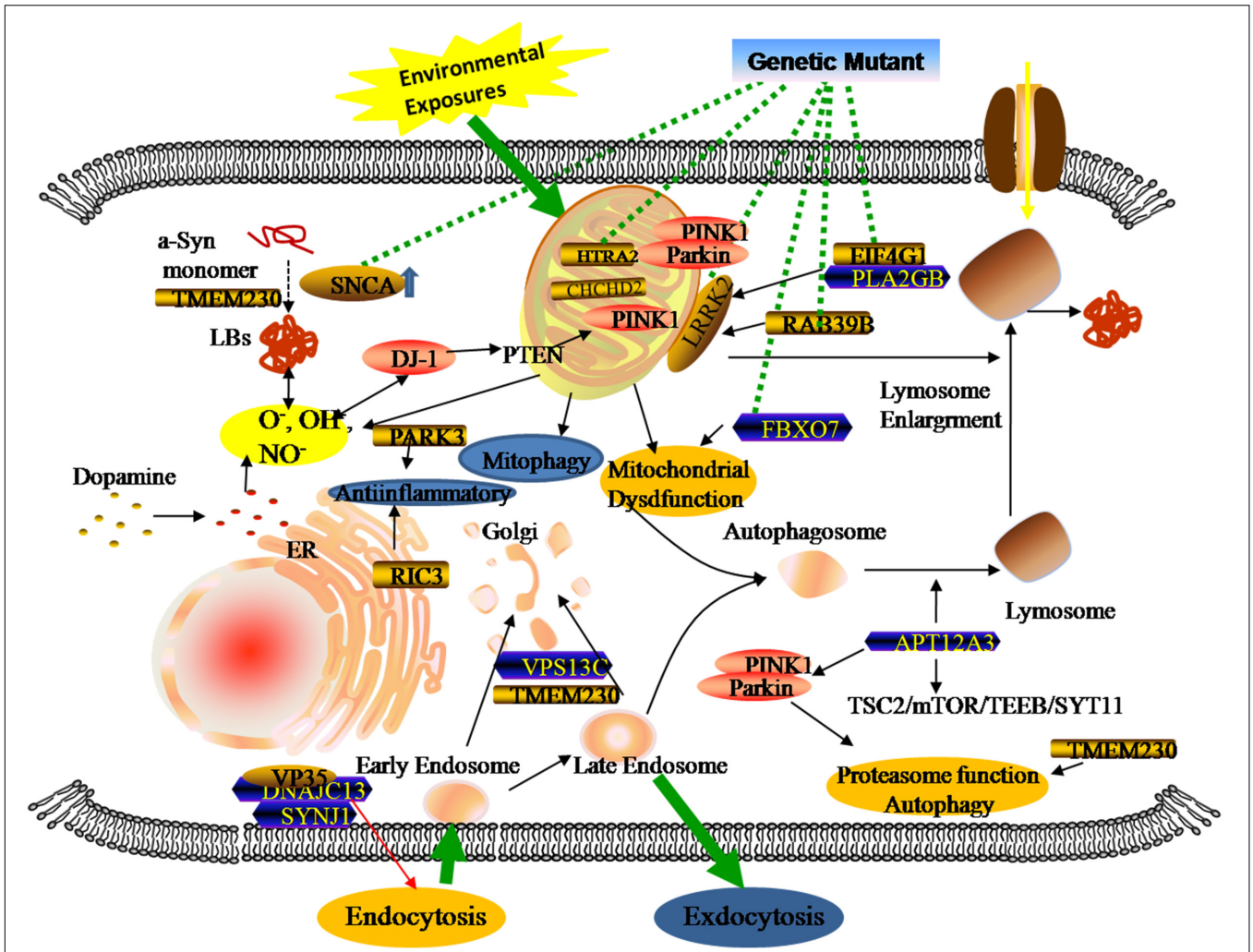

FIGURE 2 | Genetic metabolomics in PD. The complexity of the pathology of PD stemming from the overlap of multiple gene mutants and complex environmental factors. Both locally and systemically, these hazards contribute to a series of responses associated with mitochondrial dysfunction, neuroinflammation, and the failure of clearance mechanisms.

control and turnover (Arkinson and Walden, 2018). Under normal conditions, PINK1 can phosphorylate and recruit Parkin proteins from the cytoplasm to depolarized mitochondria, then meditate the ubiquitination of mitochondrial outer membrane proteins and activate mitophagy to degrade the ubiquitin mitochondrial proteins mitofusin 1 and 2 (Pickrell and Youle, 2015; Matheoud et al., 2016; Barodia et al., 2017). Similar to autosomal dominant genes, *PINK1 and PARK2* mutations induce metabolomic changes in PD patients. Okuzumi et al. (2019) analyzed serum metabolomics from *Parkin* patients and age-matched controls, and revealed higher levels of oxidized lipids and fatty acid metabolites and lower levels of antioxidant markers in PARK2 patients, suggesting the relationship between the serum/plasma metabolomics and gene dysfunction. Additionally, as a way of ensuring mitochondrial quality control, the mutation effects the elimination of dysfunctional mitochondria that was associated with an increase of mitochondrial stress, manifesting a systemic oxidative stress markers for the pathomechanisms of *Parkin*-mutation patients (Ueno et al., 2020).

GBA

The most common genetic risk factor for PD is the glucocerebrosidase (GBA) gene, which is located on chromosome 1q21 and contains 11 exons that encode the lysosomal enzyme glucocerebrosidase. In normal cells, the metabolism of glucocerebroside attributes to the efficacy of the glucocerebrosidase (GCase). Reports indicated that GCase not only increases the breakdown of glucocerebroside into glucose and ceramide, but also plays a role in α-Syn degradation (Sidransky and Lopez, 2012; Migdalska-Richards and Schapira, 2016). By contrast, previous studies have shown that the variants of p.E365K and p.T408M in the GBA gene are associated with PD (Liu et al., 2016; Mallett et al., 2016). The *GBA* mutations disturb the function of related lysosomal enzymes, which provoke a-Syn accumulation (Sidransky and Lopez, 2012), disrupt

autophagy-lysosome and molecular homeostasis (Uemura et al., 2015), and impair the functional mitochondria by inhibiting mitophagy (Zampieri et al., 2017). For understanding metabolic consequences associated with the *GBA* gene alterations, recent research has detected the CSF of patients with glucocerebrosidase dysfunction, and observed impairments in mitochondrial function and the urea cycle that increased the abundance of several metabolites, such as 1,5-anhydro-D-glucitol, asparagine, ornithine, glutamine, and glycine (Greuel et al., 2020).

METABOLOMICS ASSOCIATED WITH IDIOPATHIC PD PATIENTS

Most patients are diagnosed as sporadic idiopathic PD as opposed to familial patients, in which environmental hazards play an important role in the pathogenesis of neurodegeneration diseases. The pathogenesis of PD involves complex interactions among multifarious pathomechanisms that include oxidative stress, mitochondrial alterations, inflammatory response, and dysbacteriosis. These pathological changes usually accelerate the truncation (Kahle et al., 2001; Auluck et al., 2002; Liu et al., 2005) and multimerization of misfolding proteins through phospholipid binding, membrane compound altering, and change in the function of molecular chaperones (Tuttle et al., 2016; Gerez et al., 2019). The identification of aberrant biochemistry underlying neuronal degeneration could be an important step toward discovering mechanisms and accurate markers for the diagnosis and therapy of PD. Based on previous studies and updated evidence exploring the metabolomics profiling of biofluids in PD patients, most existing knowledge shows the alteration of different molecular species that mainly focus on genes alterations, energy homeostasis, and redox reaction resulting from mitochondrial dysfunction. Hence, we summarize the progress on metabolomics in idiopathic PD cases and focus on the metabolic biomarkers associated with mitochondrial dysfunction and dysbacteriosis.

MITOCHONDRIAL DYSFUNCTION

As the dynamic powerhouse of a cell, the mitochondrion plays a major role in metabolic activity and generates over 90% of the ATP in a cell. Mitochondria contain their own genomes (mtDNA) and encode vital components associated with mitochondrial function. There is increasing evidence that the mitochondrial function extends well beyond the production of energy in carbohydrate, fatty acid, amino acid, and nucleotide metabolism, it aids in the stabilization of cytosolic calcium, and relates to metabolic pathways, such as the pyruvate oxidation, the Krebs cycle, and various immune responses (Luan et al., 2015; Di Maio et al., 2016). To date, diverse gene mutations and environmental factors have been identified as the cause of mitochondrial dysfunction; it likely to be a key contributor to PD pathogenesis by damaging the transport of mitochondrial proteins, inhibiting respiratory chain function, actuating the generation of reactive oxygen species (ROS), and increasing α-Syn aggregation. As shown in previous studies, the complex I function of the electron transport chain in mitochondrion is impaired because of exposure to environmental toxins such as paraquat, rotenone, and metals (Muthukumaran et al., 2014; Stauch et al., 2016; Thellung et al., 2019). Patients with sporadic PD not only present metabolic changes about abnormal mitochondrial activity in energy homeostasis and redox reaction (Krige et al., 1992; Haas et al., 1995; Penn et al., 1995), but have the presence of mitochondrial oxidative metabolism and insulin resistance (Marcovina et al., 2013; Gonzalez-Casacuberta et al., 2019; Djordjevic et al., 2020). As can be seen in **Figure 3**, these impaired mitochondrial protein import reduced mitochondrial dynamics, increase ROS, and create mitophagy abnormalities or bioenergetic defects that would deteriorate α-Syn protein misfolding and aggregation.

These mitochondrial changes disturb a series of energy metabolism systems (pentose phosphate pathway, glycolysis, mitochondrial oxidative phosphorylation, glycolysis, acylcarnitines, and the tricarboxylic cycle) (Roede et al., 2013; Trupp et al., 2014; Willkommen et al., 2018), and are also involved in the upregulation or downregulation of amino acids, lipids, and antioxidant substances in PD (Bazinet and Laye, 2014; Lei et al., 2014; Tyurina et al., 2015). Like the correlation between mitochondrial function and gene alterations (**Figure 3**), comprehensive metabolic analysis of mitochondrial defects arising from environmental factors, such as oxidative stress and energy substance metabolism, might promote the discovery of some discern biomarkers for PD. For example, Younes-Mhenni et al. (2007) and Lewitt et al. (2013) found significantly higher activity of oxidized glutathione, superoxide dismutase (SOD), and catalase in PD patients compared with healthy people. Similarly, increasing 8-hydroxy-2-deoxyguanosine (8-OHdG), an oxidative product of damaged DNA, has also been detected in the blood and urine of PD patients (Roede et al., 2013). On the contrary, the high levels of antioxidants could lower the occurrence and slow the progression of the neurodegenerative disease (Ascherio et al., 2006). Except for metabolic alteration related to mitochondrial oxidation, recent research about metabolomic analysis of cell lysates showed that PD patients present with an increase of lactic acid and a depletion of pyruvic acid and aberrant choline metabolism in extracellular fluid (Amo et al., 2019). Reports have shown that acylcarnitine, as the essential amino acid for fatty acid transport into mitochondria for energy metabolism, was definite in upregulative stages and potentially effected the structure and function of substantia nigra (Mallah et al., 2019).

Notably, some alterations of oxidative stress metabolites might be used to evaluate different subtypes and stages of the disease. Based on CSF and blood samples from patients with PD, Karsten et al. observed specific increases of mannose and fructose, as well as increased threonic acid and reduced dehydroascorbic acid in early-stage PD patients (Trezzi et al., 2017). These changes in oxidation products could reflect the activation of antioxidative stress responses as a resistance mechanism against neuronal injury, in contrast to which, the failure in antioxidant reserve could aggregate the neurodegeneration (Dunn et al., 2014). Significant increases

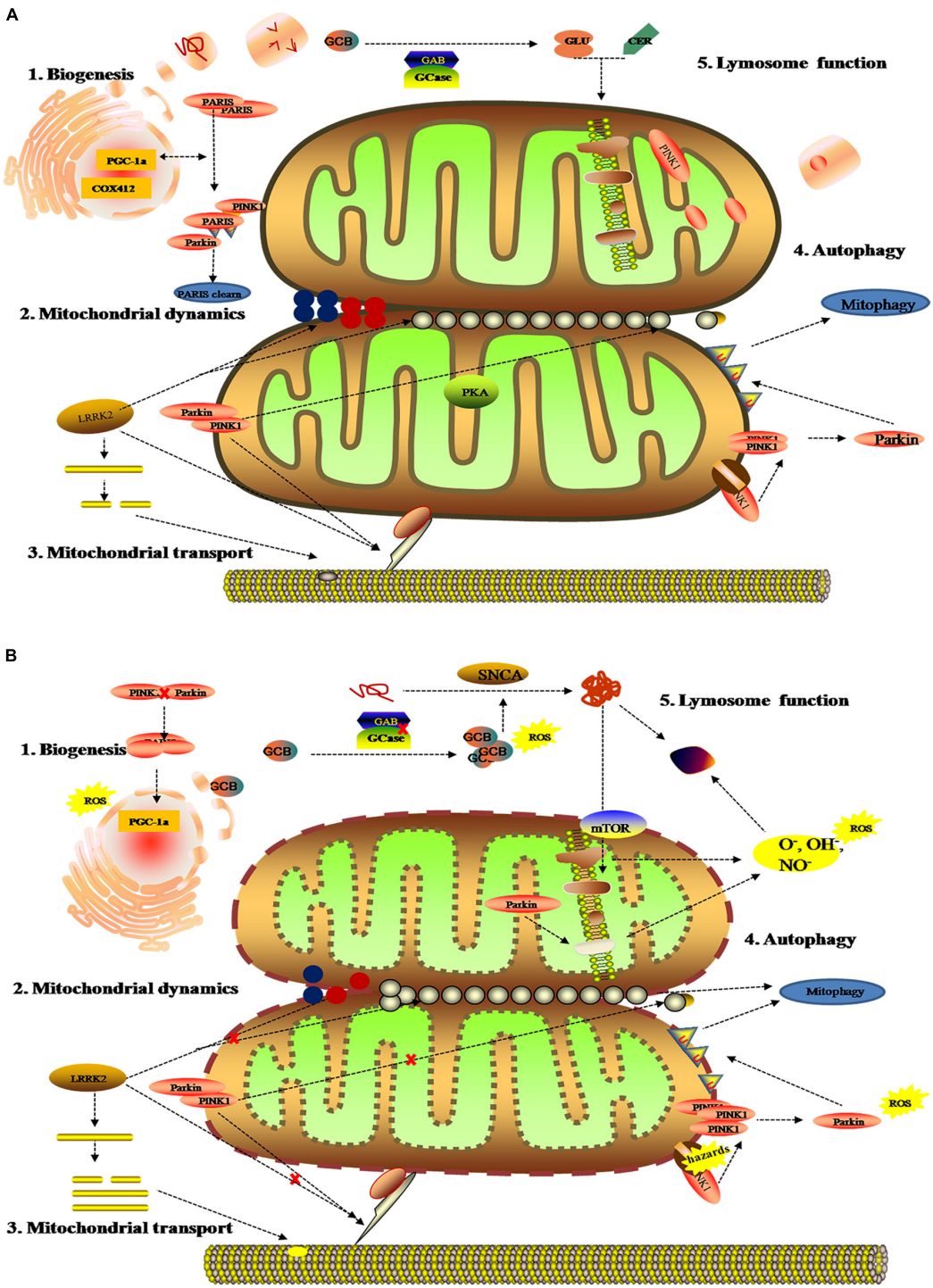

FIGURE 3 | Mitochondrial metabolomics in PD patients. **(A)** Under normal status: 1. mitochondrial complex IV subunit 4 isoform (COX4I2) and proliferator-activated receptor gamma coactivator 1-α (PGC1α) facilitate mitochondrial biogenesis. Additionally, PINK1 and Parkin alleviates PARIS toxicity by phosphorylation and ubiquitination, respectively. 2. PINK1 acts on dynamin-related protein 1 (DRP1) to regulate mitochondrial fission and PKA (PINK1 inhibits protein kinase) inhibits the progress. As such, LRRK2 is also involved in mitochondrial dynamic by MFNs and OPA1 (two mitochondrial fusion proteins) as well as DRP1 (a mitochondrial fission protein). 3. PINK1, Parkin, and LRRK2 mediate mitochondrial transport. 4. PINK1/Parkin clears damaged mitochondria by mitophagy **(B)**. Under gene mutant: 1. mitochondrial biogenesis is inhibited by upregulating PGC1α, which is vulnerable to ROS. 2. The imbalance of mitochondrial dynamics. 3. The mutation of PINK1, Parkin, or LRRK2 halt mitochondrial transportation via Miro, Milton, and motor protein Kinesin-1. In addition, altering LRRK2 expression can stabilize filamentous actin (F-actin) and promote tau neurotoxicity. 4. Hazards causes PINK1 to accumulate when Parkin is impaired, followed by failure in the mitophagy and production of ROS. 5. Deposition of GCB and misfolding a-Syn disrupt mitochondrial respiration, leading to the production of ROS and dysfunction of lysosomes.

TABLE 1 | Summary of gut microbiota and their changes in the fecal samples of PD.

Phylum	Family	Genus	Metabolite	Alteration	References
Firmicutes				Down/Up	GBD 2015 Neurological Disorders Collaborator Group, 2017; Xu et al., 2019
	Clostridiaceae	Clostridium	–	Up	Santos Garcia et al., 2019
	Eubacteriaceae	Acetobacterium	–	Up	GBD 2015 Neurological Disorders Collaborator Group, 2017
	Veillonellaceae	Veillonella	–	Up	Xu et al., 2019
	Lachnospiraceae	Anaerostipes	–	Up	GBD 2016 Parkinson's Disease Collaborators, 2018
		Dorea	–	Down	
		Blautia	–	Down	Spillantini et al., 1997; Xu et al., 2019
		Roseburia	–	Down	Spillantini et al., 1997; Xu et al., 2019
		Coprococcus	–	Down	
		Fusicatenibacter	–	Down	Spillantini et al., 1997
		Faecalibacterium	–	Down	Spillantini and Goedert, 2018
		Lachnospira	Nicotinic acid Pantothenic acid	Down/Up	Spillantini et al., 1997; Kim and Alcalay, 2017; Xu et al., 2019
		Pseudobutyrivibrio	–	Down	Spillantini et al., 1997
	Lactobacillaceae	Lactobacter	–	Up	Kim and Alcalay, 2017; Puspita et al., 2017
	Streptococcaceae	Streptococcus	Cadaverine	Down/Up	Santos Garcia et al., 2019
	Ruminococcaceae	Anaerotruncus	–	Up	GBD 2015 Neurological Disorders Collaborator Group, 2017
Bacteroidetes				Down/Up	Kim and Alcalay, 2017; Santos Garcia et al., 2019
	Bacteroidaceae	Bacteroides	–	Down/Up	Rocha et al., 2018; Santos Garcia et al., 2019
	Odoribacteriaceae	Odoribacter	–	Down	Spillantini et al., 1997; De Virgilio et al., 2016
	Rikenellaceae		–	Down	
	Prevotellaceae	Prevotella	–	Down/Up	Bose and Beal, 2016; Rocha et al., 2018
	Porphyromonas		–	Up	Spillantini et al., 1997
Proteobacteria				Up	De Virgilio et al., 2016; Santos Garcia et al., 2019
	Alcaligenaceae		–	Down	
	Comamonadaceae		–	Down	
	Desulfovibrionaceae	Desulfovibrio	–	Up	
	Desulfohalobiaceae	Desulfonauticus	–	Up	
	Enterobacteriaceae			Down/Up	De Virgilio et al., 2016; Rocha et al., 2018
		Enterobacter	–	Up	
		Escherichia	–	Up	
		Serratia	Nicotinic acid	Up	
		Oscillospira	–	Down/Up	Spillantini et al., 1997; Santos Garcia et al., 2019
		Corynebacterium	–	Up	Spillantini et al., 1997
	Sutterellaceae	Sutterella	–	Down	
	Comamonadaceae	Comamonas	–	Up	
Actinobacteria				Up	Hou et al., 2019
	Bifidobacteriaceae	Bifidobacterium	Pantothenic acid Pyroglutamic acid	Up	GBD 2015 Neurological Disorders Collaborator Group, 2017; Kim and Alcalay, 2017
	Coriobacteriaceae	Slackia	–	Up	
	Microbacteriaceae		–	Up	GBD 2015 Neurological Disorders Collaborator Group, 2017
	Brevibacteriaceae	Brevibacterium	–	Down	Spillantini and Goedert, 2018
Verrucomicrobia				Up	De Virgilio et al., 2016; Santos Garcia et al., 2019; Xu et al., 2019
	Verrucomicrobiaceae	Akkermansia	–	Up	Kim and Alcalay, 2017; Santos Garcia et al., 2019
		Prosthecobacter	–	Up	
Cyanobacteria				Down	Hou et al., 2019
	Aphanizomenonaceae	Dolichospermum	–	Down	

TABLE 2 | Summary of microbiota cluster and their features in gut.

Cluster		Features	Alteration	References
Opportunistic pathogens	Porphyromonas Prevotella Corynebacterium	NLRP3 inflammasome LPS	Up	Spillantini et al., 1997
SCFA-producing bacteria	Blautia, Roseburia, Coprococcus Dorea Lachnospira Faecalibacterium Oscillospira Corynebacterium	SCFAs-producing Butyrate-producing Vagal activation	Down	Spillantini and Goedert, 2018; Xu et al., 2019
Probiotic bacteria	Lactobacillus Bifidobacteriaceae	Cellulose metabolism	Up	Kim and Alcalay, 2017
Cohesive bacteria	Clostridium Oscillospira Akkermansia Ruminococcaceae	–	Up	Spillantini and Goedert, 2018

were seen in pyroglutamate and 2-oxoisocaproate and decreases in 3-hydroxyisovalerate, tryptophan, and creatinine, which supported an increase of marks in oxidative responses in preclinical PD (Liu and Wang, 2014). Additionally, some metabolites have also been identified as indicators of the severity of Parkinson's disease, including uric acid and taurine (Engelborghs et al., 2003).

GASTROINTESTINAL DYSFUNCTION AND DYSBACTERIOSIS

As we all know, gastrointestinal microbes and host usually remain in a mutualistic relationship, in which the microbes keep its diversification and function via the gut to absorb nutrition. In turn, the parasitic microbiota parasitize in the digestive tract and produce a series of biochemical compounds to contribute physical and bioactive barriers or trigger protective immune responses to withstand the effect of exogenous factors (Reza et al., 2019; Parker et al., 2020). Accumulating evidence suggests that many diseases have specific microbiome profiles and potentially communicate mechanisms between the gastrointestinal and the nervous systems, so alterations in gut microbiota have been linked to neurodegeneration, including AD, PD, and Multiple Sclerosis (Sasmita, 2019).

Over the last two decades, neurologists have begun to explore in detail the relationship between the gastrointestinal tract, gut microbiota, and the central nerve systems (CNS). In the last several years, the gut and related microbiome have gained increasing attention because of its close relationship with the etiology of PD. Clinical evidence revealed that neuropathological changes in PD are accompanied by varying symptoms of gastrointestinal dysfunction (indigestion, constipation, bloating, and dysbacteriosis) before the onset of motor symptoms. Experimental evidence showed that bacterial abnormalities and intestinal pathology may play a role in PD symptoms (Fasano et al., 2013; Tan et al., 2015; Van Laar et al., 2019; Mertsalmi et al., 2020). In recent reports, the gut and relevant metabolic products have been given increasing attention because of their importance in the disease pathogenesis (Sampson et al., 2016; Kim et al., 2019), showing that PD patients usually show significant changes in microbiotal abundance and diversity, as well as distinctive profiles of microbiota composition and intestinal metabolites (Keshavarzian et al., 2015; Vascellari et al., 2020; Wallen et al., 2020; **Table 1**). Although these microbiota composition alterations are heterogeneous, both microbiota disorders and intestinal damage could act as triggering events that lead to dopaminergic loss and pathological a-Syn (Matheoud et al., 2019). Further, numerous experimental and clinical reports indicated that the a-Syn could gather and spread from the gastrointestine to the deep brain (Braak et al., 2003; Kim et al., 2019; Van Den Berge et al., 2019). Notably, the alteration in microbiota abundance was noted in different subtypes and stages of the disease. A study has demonstrated that the abundancy of some microbial compositions, such as Lactococcus, Faecalibacterium, and Leptotrichia, was increased in early-stages of PD, while Comamonas was common in patients with late-onset symptoms. The abundance of Bacteroidetes and Firmicutes were significantly increased in patients with motor-symptoms (Keshavarzian et al., 2015; Lin et al., 2018). Likewise, decreased Prevotellaceae abundance and increased Enterobacteriaceae may have a positive association with intestinal dysfunction in PD patients. Keeping this point in mind, we know that the dysbacteriosis and microbiota metabolomics have potential relevance to the existence of gastrointestinal a-Syn and pathology. The understanding of microbiota metabolomics is essential for exploring the pathogenesis of PD and seeking specific biomarkers that support a more accurate assessment, earlier diagnosis, and better monitoring of the disease progression.

To our knowledge, gut microbiota contributes to host metabolism in the regulation of organic energy metabolism (e.g., lipids, amino acids, and vitamins), as well as to the differentiation and function of immune cells (Cani, 2018). The specific microbial metabolites are disordered when gut microbes are out of balance in abundance and diversity (**Table 2**). Based on previous studies, the PD-related dysbacteriosis could induce changes in carbohydrate fermentation, protein, and lipid metabolism which could generate SCFA, p-cresol and phenylacetylglutamine, protocatechuic acid, secondary bile acids, and other metabolites (Wahlstrom et al., 2016; Murota et al., 2018; Cirstea et al., 2020). Specifically, the concentration of short chain fatty acids (SCFA) have largely implicated a significant correlation between gut microbiota and PD, and has been implicated as a driver of the onset and progression of PD (Qiao et al., 2020). The SCFA is a metabolic product that possesses anti-inflammatory and anti-microbial function qualities and protects from intestinal permeability, oxidative stress, and immune injury (Donohoe et al., 2011; Sanchez-Guajardo et al., 2015). Further, the SCFA contain a functional composition—Butyrate—that not only supplies

the main source of energy for the gut epithelium, but also strengthens the gastrointestinal barrier function (Volf et al., 2016; Agusti et al., 2018). Therefore, the lower abundance of the microbes that produce SCFA could have negative effects for the intestinal barrier and immune function to induce gastrointestinal symptoms of PD, including constipation, intestinal inflammation, and intestinal barrier leakiness (Segain et al., 2000). From what has been discussed above, the metabolic changes of SCFA caused by gut microbial dysbiosis may be a biomarker for better evaluation of PD conditions.

FUTURE PERSPECTIVES

Collectively, these findings may mark a new step on the path toward the metabolomics of PD. Paralleling with the availability of test samples and advances in identification technology, metabolomics has been considerably applied as a tool in PD research (Koeth et al., 2013; Pannkuk et al., 2015). However, due to the heterogeneity of humans in regards to genetic expression, dietary habit, environmental exposure, and physical behaviors, only a few specific biomarkers can currently be recommended in clinical practice. Hence, further works on the correlation between metabolomics and the neurodegenerative disease would be valuable. It is of great clinical significance to discover specific biological markers of PD, so as to early screen high-risk populations and facilitate timely diagnosis and reasonable therapeutics.

AUTHOR CONTRIBUTIONS

YZ drafted the manuscript. TT was responsible for the design and conception of the work. JL, XZ, and DS participated in the discussion about article writing and revision. All authors read and approved the final manuscript.

FUNDING

This study was supported by funds from the National Natural Science Foundation of China (Grant No: U1804171).

REFERENCES

Agusti, A., Garcia-Pardo, M. P., Lopez-Almela, I., Campillo, I., Maes, M., Romani-Perez, M., et al. (2018). Interplay between the gut-brain axis, obesity and cognitive function. *Front. Neurosci.* 12:155. doi: 10.3389/fnins.2018.00155

Amo, T., Oji, Y., Saiki, S., and Hattori, N. J. B. (2019). Metabolomic analysis revealed mitochondrial dysfunction and aberrant choline metabolism in MPP-exposed SH-SY5Y cells. *Biochem. Biophys. Res. Commun.* 519, 540–546. doi: 10.1016/j.bbrc.2019.09.031

Annanmaki, T., Muuronen, A., and Murros, K. (2007). Low plasma uric acid level in Parkinson's disease. *Mov. Disord.* 22, 1133–1137. doi: 10.1002/mds.21502

Arkinson, C., and Walden, H. (2018). Parkin function in Parkinson's disease. *Science* 360, 267–268.

Ascherio, A., LeWitt, P., Watts, A., Kieburtz, K., Rudolph, A., Schwid, S., et al. (2006). "CSF as well as serum urate are predictors of Parkinson's disease progression," in *Proceedings of the 10th International Conference of Parkinson's Disease and Movement Disorders*, Kyoto.

Ascherio, A., LeWitt, P. A., Xu, K., Eberly, S., Watts, A., Matson, W. R., et al. (2009). Urate as a predictor of the rate of clinical decline in Parkinson disease. *Arch. Neurol.* 66, 1460–1468. doi: 10.1001/archneurol.2009.247

Auluck, P. K., Chan, H. Y., Trojanowski, J. Q., Lee, V. M., and Bonini, N. M. (2002). Chaperone suppression of alpha-synuclein toxicity in a *Drosophila* model for Parkinson's disease. *Science* 295, 865–868. doi: 10.1126/science.1067389

Bae, E. J., and Lee, S. J. (2019). The LRRK2-RAB axis in regulation of vesicle trafficking and alpha-synuclein propagation. *Biochim. Biophys. Acta Mol. Basis Dis.* 1866:165632. doi: 10.1016/j.bbadis.2019.165632

Barcelo-Coblijn, G., Golovko, M. Y., Weinhofer, I., Berger, J., and Murphy, E. J. (2007). Brain neutral lipids mass is increased in alpha-synuclein gene-ablated mice. *J. Neurochem.* 101, 132–141. doi: 10.1111/j.1471-4159.2006.04348.x

Barodia, S. K., Creed, R. B., and Goldberg, M. S. (2017). Parkin and PINK1 functions in oxidative stress and neurodegeneration. *Brain Res. Bull.* 133, 51–59. doi: 10.1016/j.brainresbull.2016.12.004

Bazinet, R. P., and Laye, S. (2014). Polyunsaturated fatty acids and their metabolites in brain function and disease. *Nat. Rev. Neurosci.* 15, 771–785. doi: 10.1038/nrn3820

Bhinderwala, F., Lei, S., Woods, J., Rose, J., Marshall, D. D., Riekeberg, E., et al. (2019). Metabolomics analyses from tissues in Parkinson's disease. *Methods Mol. Biol.* 1996, 217–257. doi: 10.1007/978-1-4939-9488-5_19

Bogdanov, M., Matson, W. R., Wang, L., Matson, T., Saunders-Pullman, R., Bressman, S. S., et al. (2008). Metabolomic profiling to develop blood biomarkers for Parkinson's disease. *Brain* 131, 389–396. doi: 10.1093/brain/awm304

Boland, B., Yu, W., Corti, O., Mollereau, B., Henriques, A., Bezard, E., et al. (2018). Promoting the clearance of neurotoxic proteins in neurodegenerative disorders of ageing. *Nat. Rev. Drug Discov.* 17, 660–688. doi: 10.1038/nrd.2018.109

Bolner, A., Pilleri, M., De Riva, V., and Nordera, G. P. (2011). Plasma and urinary HPLC-ED determination of the ratio of 8-OHdG/2-dG in Parkinson's disease. *Clin. Lab.* 57, 859–866.

Bose, A., and Beal, M. F. (2016). Mitochondrial dysfunction in Parkinson's disease. *J. Neurochem.* 139 (Suppl. 1), 216–231. doi: 10.1111/jnc.13731

Bove, J., and Perier, C. (2012). Neurotoxin-based models of Parkinson's disease. *Neuroscience* 211, 51–76. doi: 10.1016/j.neuroscience.2011.10.057

Braak, H., Del Tredici, K., Rub, U., de Vos, R. A., Jansen Steur, E. N., and Braak, E. (2003). Staging of brain pathology related to sporadic Parkinson's disease. *Neurobiol. Aging* 24, 197–211. doi: 10.1016/s0197-4580(02)00065-9

Cani, P. D. (2018). Human gut microbiome: hopes, threats and promises. *Gut* 67, 1716–1725. doi: 10.1136/gutjnl-2018-316723

Castagnet, P. I., Golovko, M. Y., Barcelo-Coblijn, G. C., Nussbaum, R. L., and Murphy, E. J. (2005). Fatty acid incorporation is decreased in astrocytes cultured from alpha-synuclein gene-ablated mice. *J. Neurochem.* 94, 839–849. doi: 10.1111/j.1471-4159.2005.03247.x

Chang, K. H., Cheng, M. L., Tang, H. Y., Huang, C. Y., Wu, Y. R., and Chen, C. M. (2018). Alternations of metabolic profile and kynurenine metabolism in the plasma of Parkinson's Disease. *Mol. Neurobiol.* 55, 6319–6328. doi: 10.1007/s12035-017-0845-3

Chen, X., Xie, C., Sun, L., and Cai, H. (2015). Longitudinal metabolomics profiling of Parkinson's disease-related alpha-synuclein A53T transgenic mice. *PLoS One* 10:e0136612. doi: 10.1371/journal.pone.0136612

Cirstea, M., Yu, A., Golz, E., Sundvick, K., Kliger, D., Radisavljevic, N., et al. (2020). Microbiota composition and metabolism are associated with gut function in Parkinson's disease. *Mov. Disord.* 35, 1208–1217. doi: 10.1002/mds.28052

Correia, C. N., Nalpas, N. C., McLoughlin, K. E., Browne, J. A., Gordon, S. V., MacHugh, D. E., et al. (2017). Circulating microRNAs as potential biomarkers of infectious disease. *Front. Immunol.* 8:118. doi: 10.3389/fimmu.2017.00118

De Pablo-Fernández, E., Breen, D. P., Bouloux, P., Barker, R., Foltynie, T., Warner, T., et al. (2017). Neuroendocrine abnormalities in Parkinson's disease. *J. Neurol. Neurosurg. Psychiatry* 88, 176–185. doi: 10.1136/jnnp-2016-314601

De Virgilio, A., Greco, A., Fabbrini, G., Inghilleri, M., Rizzo, M. I., Gallo, A., et al. (2016). Parkinson's disease: autoimmunity and neuroinflammation. *Autoimmun. Rev.* 15, 1005–1011. doi: 10.1016/j.autrev.2016.07.022

Delenclos, M., Jones, D. R., McLean, P. J., and Uitti, R. J. (2016). Biomarkers in Parkinson's disease: advances and strategies. *Parkinsonism Relat. Disord.* 22(Suppl. 1), S106–S110. doi: 10.1016/j.parkreldis.2015.09.048

Di Maio, R., Barrett, P. J., Hoffman, E. K., Barrett, C. W., Zharikov, A., Borah, A., et al. (2016). Alpha-synuclein binds to TOM20 and inhibits mitochondrial protein import in Parkinson's disease. *Sci. Transl. Med.* 8:342ra78. doi: 10.1126/scitranslmed.aaf3634

Djordjevic, J., Roy Chowdhury, S., Snow, W. M., Perez, C., Cadonic, C., Fernyhough, P., et al. (2020). Early onset of sex-dependent mitochondrial deficits in the cortex of 3xTg Alzheimer's mice. *Cells* 9:1541. doi: 10.3390/cells9061541

Dong, M. X., Feng, X., Xu, X. M., Hu, L., Liu, Y., Jia, S. Y., et al. (2018). Integrated analysis reveals altered lipid and glucose metabolism and identifies NOTCH2 as a biomarker for Parkinson's disease related depression. *Front. Mol. Neurosci.* 11:257. doi: 10.3389/fnmol.2018.00257

Donohoe, D., Garge, N., Zhang, X., Sun, W., O'Connell, T., Bunger, M., et al. (2011). The microbiome and butyrate regulate energy metabolism and autophagy in the mammalian colon. *Cell Metab.* 13, 517–526. doi: 10.1016/j.cmet.2011.02.018

Dunn, L., Allen, G., Mamais, A., Ling, H., Li, A., Duberley, K., et al. (2014). Dysregulation of glucose metabolism is an early event in sporadic Parkinson's disease. *Neurobiol. Aging* 35, 1111–1115. doi: 10.1016/j.neurobiolaging.2013.11.001

Engelborghs, S., Marescau, B., and De Deyn, P. P. (2003). Amino acids and biogenic amines in cerebrospinal fluid of patients with Parkinson's disease. *Neurochem. Res.* 28, 1145–1150. doi: 10.1023/a:1024255208563

Fasano, A., Bove, F., Gabrielli, M., Petracca, M., Zocco, M., Ragazzoni, E., et al. (2013). The role of small intestinal bacterial overgrowth in Parkinson's disease. *Mov. Disord.* 28, 1241–1249. doi: 10.1002/mds.25522

Fitzgerald, J. C., Zimprich, A., Carvajal Berrio, D. A., Schindler, K. M., Maurer, B., Schulte, C., et al. (2017). Metformin reverses TRAP1 mutation-associated alterations in mitochondrial function in Parkinson's disease. *Brain* 140, 2444–2459. doi: 10.1093/brain/awx202

Gatto, N. M., Rhodes, S. L., Manthripragada, A. D., Bronstein, J., Cockburn, M., Farrer, M., et al. (2010). Alpha-synuclein gene may interact with environmental factors in increasing risk of Parkinson's disease. *Neuroepidemiology* 35, 191–195. doi: 10.1159/000315157

GBD 2015 Neurological Disorders Collaborator Group (2017). Global, regional, and national burden of neurological disorders during 1990-2015: a systematic analysis for the Global Burden of Disease Study 2015. *Lancet Neurol.* 16, 877–897. doi: 10.1016/S1474-4422(17)30299-5

GBD 2016 Parkinson's Disease Collaborators (2018). Global, regional, and national burden of Parkinson's disease, 1990-2016: a systematic analysis for the Global Burden of Disease Study 2016. *Lancet Neurol.* 17, 939–953. doi: 10.1016/S1474-4422(18)30295-3

Gerez, J. A., Prymaczok, N. C., Rockenstein, E., Herrmann, U. S., Schwarz, P., Adame, A., et al. (2019). A cullin-RING ubiquitin ligase targets exogenous alpha-synuclein and inhibits Lewy body-like pathology. *Sci. Transl. Med.* 11:eaau6722. doi: 10.1126/scitranslmed.aau6722

Goldman, J. G., Andrews, H., Amara, A., Naito, A., Alcalay, R. N., Shaw, L. M., et al. (2018). Cerebrospinal fluid, plasma, and saliva in the BioFIND study: relationships among biomarkers and Parkinson's disease features. *Mov. Disord.* 33, 282–288. doi: 10.1002/mds.27232

Golovko, M. Y., Barceló-Coblijn, G., Castagnet, P. I., Austin, S., Combs, C. K., and Murphy, E. J. (2009). The role of α-synuclein in brain lipid metabolism: a downstream impact on brain inflammatory response. *Mol. Cell. Biochem.* 326, 55–66. doi: 10.1007/s11010-008-0008-y

Golovko, M. Y., Rosenberger, T. A., Feddersen, S., Faergeman, N. J., and Murphy, E. J. (2007). Alpha-synuclein gene ablation increases docosahexaenoic acid incorporation and turnover in brain phospholipids. *J. Neurochem.* 101, 201–211. doi: 10.1111/j.1471-4159.2006.04357.x

Gonzalez-Casacuberta, I., Juarez-Flores, D. L., Moren, C., and Garrabou, G. (2019). Bioenergetics and autophagic imbalance in patients-derived cell models of Parkinson disease supports systemic dysfunction in neurodegeneration. *Front. Neurosci.* 13:894. doi: 10.3389/fnins.2019.00894

Graham, S. F., Rey, N. L., Yilmaz, A., Kumar, P., Madaj, Z., Maddens, M., et al. (2018). Biochemical profiling of the brain and blood metabolome in a mouse model of prodromal Parkinson's disease reveals distinct metabolic profiles. *J. Proteome Res.* 17, 2460–2469. doi: 10.1021/acs.jproteome.8b00224

Grassi, D., Howard, S., Zhou, M., Diaz-Perez, N., Urban, N. T., Guerrero-Given, D., et al. (2018). Identification of a highly neurotoxic alpha-synuclein species inducing mitochondrial damage and mitophagy in Parkinson's disease. *Proc. Natl. Acad. Sci. U.S.A.* 115, E2634–E2643. doi: 10.1073/pnas.1713849115

Greuel, A., Trezzi, J., Glaab, E., Ruppert, M., Maier, F., Jäger, C., et al. (2020). GBA variants in Parkinson's disease: clinical, metabolomic, and multimodal neuroimaging phenotypes. *Mov. Disord.* 35, 2201–2210. doi: 10.1002/mds.28225

Guaitoli, G., Raimondi, F., Gilsbach, B. K., Gomez-Llorente, Y., Deyaert, E., Renzi, F., et al. (2016). Structural model of the dimeric Parkinson's protein LRRK2 reveals a compact architecture involving distant interdomain contacts. *Proc. Natl. Acad. Sci. U.S.A.* 113, E4357–E4366. doi: 10.1073/pnas.1523708113

Haas, R. H., Nasirian, F., Nakano, K., Ward, D., Pay, M., Hill, R., et al. (1995). Low platelet mitochondrial complex I and complex II/III activity in early untreated Parkinson's disease. *Ann. Neurol.* 37, 714–722.

Hatano, T., Saiki, S., Okuzumi, A., Mohney, R. P., and Hattori, N. (2016). Identification of novel biomarkers for Parkinson's disease by metabolomic technologies. *J. Neurol. Neurosurg. Psychiatry* 87, 295–301. doi: 10.1136/jnnp-2014-309676

Hernandez, D. G., Reed, X., and Singleton, A. B. (2016). Genetics in Parkinson disease: mendelian versus non-mendelian inheritance. *J. Neurochem.* 139(Suppl. 1), 59–74. doi: 10.1111/jnc.13593

Hou, Y., Dan, X., Babbar, M., Wei, Y., Hasselbalch, S. G., Croteau, D. L., et al. (2019). Ageing as a risk factor for neurodegenerative disease. *Nat. Rev. Neurol.* 15, 565–581. doi: 10.1038/s41582-019-0244-7

Infante, J., Prieto, C., Sierra, M., Sanchez-Juan, P., Gonzalez-Aramburu, I., Sanchez-Quintana, C., et al. (2015). Identification of candidate genes for Parkinson's disease through blood transcriptome analysis in LRRK2-G2019S carriers, idiopathic cases, and controls. *Neurobiol. Aging* 36, 1105–1109. doi: 10.1016/j.neurobiolaging.2014.10.039

Johansen, K. K., Wang, L., Aasly, J. O., White, L. R., Matson, W. R., Henchcliffe, C., et al. (2009). Metabolomic profiling in LRRK2-related Parkinson's disease. *PLoS One* 4:e7551. doi: 10.1371/journal.pone.0007551

Kahle, P. J., Neumann, M., Ozmen, L., Muller, V., Odoy, S., Okamoto, N., et al. (2001). Selective insolubility of alpha-synuclein in human Lewy body diseases is recapitulated in a transgenic mouse model. *Am. J. Pathol.* 159, 2215–2225. doi: 10.1016/s0002-9440(10)63072-6

Kalim, S., and Rhee, E. P. (2017). An overview of renal metabolomics. *Kidney Int.* 91, 61–69. doi: 10.1016/j.kint.2016.08.021

Keshavarzian, A., Green, S. J., Engen, P. A., Voigt, R. M., Naqib, A., Forsyth, C. B., et al. (2015). Colonic bacterial composition in Parkinson's disease. *Mov. Disord.* 30, 1351–1360. doi: 10.1002/mds.26307

Kim, C. Y., and Alcalay, R. N. (2017). Genetic forms of Parkinson's disease. *Semin. Neurol.* 37, 135–146. doi: 10.1055/s-0037-1601567

Kim, M. J., Oh, S. B., Kim, J., Kim, K., Ryu, H. S., Kim, M. S., et al. (2018). Association of metals with the risk and clinical characteristics of Parkinson's disease. *Parkinsonism Relat. Disord.* 55, 117–121. doi: 10.1016/j.parkreldis.2018.05.022

Kim, S., Kwon, S.-H., Kam, T.-I., Panicker, N., Karuppagounder, S. S., Lee, S., et al. (2019). Transneuronal propagation of pathologic α-synuclein from the gut to the brain models Parkinson's disease. *Neuron* 103, 627–641.e7.

Kiraly, M., Dalmadine Kiss, B., Vekey, K., Antal, I., and Ludanyi, K. (2016). [Mass spectrometry: past and present]. *Acta Pharm. Hung.* 86, 3–11.

Klein, C., and Westenberger, A. (2012). Genetics of Parkinson's disease. *Cold Spring Harb. Perspect Med.* 2:a008888. doi: 10.1101/cshperspect.a008888

Koeth, R. A., Wang, Z., Levison, B. S., Buffa, J. A., Org, E., Sheehy, B. T., et al. (2013). Intestinal microbiota metabolism of L-carnitine, a nutrient in red meat, promotes atherosclerosis. *Nat. Med.* 19, 576–585. doi: 10.1038/nm.3145

Koros, C., Simitsi, A., Prentakis, A., Beratis, I., Papadimitriou, D., Kontaxopoulou, D., et al. (2018). 123I-FP-CIT SPECT [(123) I-2beta-carbomethoxy-3beta-(4-iodophenyl)-N-(3-fluoropropyl) nortropane single photon emission computed tomography] imaging in a p.A53T alpha-synuclein Parkinson's disease cohort versus Parkinson's disease. *Mov. Disord.* 33, 1734–1739. doi: 10.1002/mds.27451

Krige, D., Carroll, M. T., Cooper, J. M., Marsden, C. D., and Schapira, A. H. (1992). Platelet mitochondria function in Parkinson's disease. *Ann. Neurol.* 32, 782–788.

Kruger, R., Kuhn, W., Muller, T., Woitalla, D., Graeber, M., Kosel, S., et al. (1998). Ala30Pro mutation in the gene encoding alpha-synuclein in Parkinson's disease. *Nat. Genet.* 18, 106–108. doi: 10.1038/ng0298-106

Lehmann, S., Loh, S. H., and Martins, L. M. (2017). Enhancing NAD(+) salvage metabolism is neuroprotective in a PINK1 model of Parkinson's disease. *Biol. Open* 6, 141–147. doi: 10.1242/bio.022186

Lei, S., Zavala-Flores, L., Garcia-Garcia, A., Nandakumar, R., Huang, Y., Madayiputhiya, N., et al. (2014). Alterations in energy/redox metabolism induced by mitochondrial and environmental toxins: a specific role for glucose-6-phosphate-dehydrogenase and the pentose phosphate pathway in paraquat toxicity. *ACS Chem. Biol.* 9, 2032–2048. doi: 10.1021/cb400894a

Lewitt, P., Li, J., Lu, M., Beach, T., Adler, C., Guo, L., et al. (2013). 3-hydroxykynurenine and other Parkinson's disease biomarkers discovered by metabolomic analysis. *Mov. Disord.* 28, 1653–1660. doi: 10.1002/mds.25555

Lin, A., Zheng, W., He, Y., Tang, W., Wei, X., He, R., et al. (2018). Gut microbiota in patients with Parkinson's disease in southern China. *Parkinsonism Relat. Disord.* 53, 82–88. doi: 10.1016/j.parkreldis.2018.05.007

Liu, C. W., Giasson, B. I., Lewis, K. A., Lee, V. M., Demartino, G. N., and Thomas, P. J. (2005). A precipitating role for truncated alpha-synuclein and the proteasome in alpha-synuclein aggregation: implications for pathogenesis of Parkinson disease. *J. Biol. Chem.* 280, 22670–22678. doi: 10.1074/jbc.M501508200

Liu, G., Boot, B., Locascio, J. J. I, Jansen, E., Winder-Rhodes, S., Eberly, S., et al. (2016). Specifically neuropathic Gaucher's mutations accelerate cognitive decline in Parkinson's. *Ann. Neurol.* 80, 674–685. doi: 10.1002/ana.24781

Liu, J., and Wang, L. N. (2014). Mitochondrial enhancement for neurodegenerative movement disorders: a systematic review of trials involving creatine, coenzyme Q10, idebenone and mitoquinone. *CNS Drugs* 28, 63–68. doi: 10.1007/s40263-013-0124-4

Loeffler, D. A., Klaver, A. C., Coffey, M. P., Aasly, J. O., and LeWitt, P. A. (2017). Increased oxidative stress markers in cerebrospinal fluid from healthy subjects with Parkinson's disease-associated LRRK2 gene mutations. *Front. Aging Neurosci.* 9:89. doi: 10.3389/fnagi.2017.00089

Luan, H., Liu, L. F., Tang, Z., Zhang, M., Chua, K. K., Song, J. X., et al. (2015). Comprehensive urinary metabolomic profiling and identification of potential noninvasive marker for idiopathic Parkinson's disease. *Sci. Rep.* 5:13888. doi: 10.1038/srep13888

Ma, J., Gao, J., Wang, J., and Xie, A. (2019). Prion-like mechanisms in Parkinson's disease. *Front. Neurosci.* 13:552. doi: 10.3389/fnins.2019.00552

Mallah, K., Quanico, J., Raffo-Romero, A., Cardon, T., Aboulouard, S., Devos, D., et al. (2019). Matrix-assisted laser desorption/ionization-mass spectrometry imaging of lipids in experimental model of traumatic brain injury detecting acylcarnitines as injury related markers. *Anal. Chem.* 91, 11879–11887. doi: 10.1021/acs.analchem.9b02633

Mallett, V., Ross, J. P., Alcalay, R. N., Ambalavanan, A., Sidransky, E., Dion, P. A., et al. (2016). GBA p.T369M substitution in Parkinson disease: polymorphism or association? A meta-analysis. *Neurol. Genet.* 2:e104. doi: 10.1212/NXG.0000000000000104

Marcovina, S. M., Sirtori, C., Peracino, A., Gheorghiade, M., Borum, P., Remuzzi, G., et al. (2013). Translating the basic knowledge of mitochondrial functions to metabolic therapy: role of L-carnitine. *Transl. Res.* 161, 73–84. doi: 10.1016/j.trsl.2012.10.006

Matheoud, D., Cannon, T., Voisin, A., Penttinen, A. M., Ramet, L., Fahmy, A. M., et al. (2019). Intestinal infection triggers Parkinson's disease-like symptoms in Pink1(-/-) mice. *Nature* 571, 565–569. doi: 10.1038/s41586-019-1405-y

Matheoud, D., Sugiura, A., Bellemare-Pelletier, A., Laplante, A., Rondeau, C., Chemali, M., et al. (2016). Parkinson's disease-related proteins PINK1 and Parkin repress mitochondrial antigen presentation. *Cell* 166, 314–327.

Mertsalmi, T., Pekkonen, E., and Scheperjans, F. (2020). Antibiotic exposure and risk of Parkinson's disease in Finland: a nationwide case-control study. *Mov. Disord.* 35, 431–442. doi: 10.1002/mds.27924

Migdalska-Richards, A., and Schapira, A. H. (2016). The relationship between glucocerebrosidase mutations and Parkinson disease. *J. Neurochem.* 139(Suppl. 1), 77–90. doi: 10.1111/jnc.13385

Murota, K., Nakamura, Y., and Uehara, M. (2018). Flavonoid metabolism: the interaction of metabolites and gut microbiota. *Biosci. Biotechnol. Biochem.* 82, 600–610. doi: 10.1080/09168451.2018.1444467

Musgrove, R. E., Horne, J., Wilson, R., King, A. E., Edwards, L. M., and Dickson, T. C. (2014). The metabolomics of alpha-synuclein (SNCA) gene deletion and mutation in mouse brain. *Metabolomics* 10, 114–122. doi: 10.1007/s11306-013-0561-6

Muthukumaran, K., Leahy, S., Harrison, K., Sikorska, M., Sandhu, J. K., Cohen, J., et al. (2014). Orally delivered water soluble coenzyme Q10 (Ubisol-Q10) blocks on-going neurodegeneration in rats exposed to paraquat: potential for therapeutic application in Parkinson's disease. *BMC Neurosci.* 15:21. doi: 10.1186/1471-2202-15-21

Nickels, S. L., Walter, J., Bolognin, S., Gérard, D., Jaeger, C., Qing, X., et al. (2019). Impaired serine metabolism complements LRRK2-G2019S pathogenicity in PD patients. *Parkinsonism Relat. Disord.* 67, 48–55. doi: 10.1016/j.parkreldis.2019.09.018

Okuzumi, A., Hatano, T., Ueno, S. I., Ogawa, T., Saiki, S., Mori, A., et al. (2019). Metabolomics-based identification of metabolic alterations in PARK2. *Ann. Clin. Transl. Neurol.* 6, 525–536. doi: 10.1002/acn3.724

Ou, R., Cao, B., Wei, Q., Hou, Y., Xu, Y., Song, W., et al. (2017). Serum uric acid levels and freezing of gait in Parkinson's disease. *Neurol. Sci.* 38, 955–960. doi: 10.1007/s10072-017-2871-3

Paisan-Ruiz, C., Nath, P., Washecka, N., Gibbs, J. R., and Singleton, A. B. (2008). Comprehensive analysis of LRRK2 in publicly available Parkinson's disease cases and neurologically normal controls. *Hum. Mutat.* 29, 485–490. doi: 10.1002/humu.20668

Pannkuk, E. L., Laiakis, E. C., Authier, S., Wong, K., and Fornace, A. J. Jr. (2015). Global metabolomic identification of long-term dose-dependent urinary biomarkers in nonhuman primates exposed to ionizing radiation. *Radiat. Res.* 184, 121–133. doi: 10.1667/rr14091.1

Parajuli, L. K., Wako, K., Maruo, S., Kakuta, S., Taguchi, T., Ikuno, M., et al. (2020). Developmental changes in dendritic spine morphology in the striatum and their alteration in an A53T alpha-synuclein transgenic mouse model of Parkinson's disease. *eNeuro* 7:ENEURO.0072-20.2020. doi: 10.1523/ENEURO.0072-20.2020

Parker, A., Fonseca, S., and Carding, S. R. (2020). Gut microbes and metabolites as modulators of blood-brain barrier integrity and brain health. *Gut Microbes* 11, 135–157. doi: 10.1080/19490976.2019.1638722

Penn, A., Roberts, T., Hodder, J., Allen, P., Zhu, G., and Martin, W. J. N. (1995). Generalized mitochondrial dysfunction in Parkinson's disease detected by magnetic resonance spectroscopy of muscle. *Neurology* 45, 2097–2099.

Pickrell, A. M., and Youle, R. J. (2015). The roles of PINK1, parkin, and mitochondrial fidelity in Parkinson's disease. *Neuron* 85, 257–273. doi: 10.1016/j.neuron.2014.12.007

Polymeropoulos, M. H., Lavedan, C., Leroy, E., Ide, S. E., Dehejia, A., Dutra, A., et al. (1997). Mutation in the alpha-synuclein gene identified in families with Parkinson's disease. *Science* 276, 2045–2047. doi: 10.1126/science.276.5321.2045

Puspita, L., Chung, S. Y., and Shim, J. W. (2017). Oxidative stress and cellular pathologies in Parkinson's disease. *Mol. Brain* 10:53. doi: 10.1186/s13041-017-0340-9

Qamhawi, Z., Towey, D., Shah, B., Pagano, G., Seibyl, J., Marek, K., et al. (2015). Clinical correlates of raphe serotonergic dysfunction in early Parkinson's disease. *Brain* 138, 2964–2973. doi: 10.1093/brain/awv215

Qiao, C., Sun, M., Jia, X., Shi, Y., Zhang, B., Zhou, Z., et al. (2020). Sodium butyrate causes α-synuclein degradation by an Atg5-dependent and PI3K/Akt/mTOR-related autophagy pathway. *Exp. Cell Res.* 387:111772. doi: 10.1016/j.yexcr.2019.111772

Reza, M., Finlay, B., and Pettersson, S. (2019). Gut microbes, ageing & organ function: a chameleon in modern biology? *EMBO Mol. Med.* 11:e9872. doi: 10.15252/emmm.201809872

Rocha, E. M., De Miranda, B., and Sanders, L. H. (2018). Alpha-synuclein: pathology, mitochondrial dysfunction and neuroinflammation in

Parkinson's disease. *Neurobiol. Dis.* 109, 249–257. doi: 10.1016/j.nbd.2017.04.004

Roede, J., Uppal, K., Park, Y., Lee, K., Tran, V., Walker, D., et al. (2013). Serum metabolomics of slow vs. rapid motor progression Parkinson's disease: a pilot study. *PLoS One* 8:e77629. doi: 10.1371/journal.pone.0077629

Saiki, S., Hatano, T., Fujimaki, M., Ishikawa, K. I., Mori, A., Oji, Y., et al. (2017). Decreased long-chain acylcarnitines from insufficient beta-oxidation as potential early diagnostic markers for Parkinson's disease. *Sci. Rep.* 7:7328. doi: 10.1038/s41598-017-06767-y

Sampson, T. R., Debelius, J. W., Thron, T., Janssen, S., Shastri, G. G., Ilhan, Z. E., et al. (2016). Gut microbiota regulate motor deficits and neuroinflammation in a model of Parkinson's disease. *Cell* 167, 1469–1480.e12.

Sanchez-Guajardo, V., Tentillier, N., and Romero-Ramos, M. J. N. (2015). The relation between α-synuclein and microglia in Parkinson's disease: recent developments. *Neuroscience* 302, 47–58. doi: 10.1016/j.neuroscience.2015.02.008

Santos Garcia, D., de Deus Fonticoba, T., Suarez Castro, E., Borrue, C., Mata, M., Solano Vila, B., et al. (2019). Non-motor symptoms burden, mood, and gait problems are the most significant factors contributing to a poor quality of life in non-demented Parkinson's disease patients: results from the COPPADIS study cohort. *Parkinsonism Relat. Disord.* 66, 151–157. doi: 10.1016/j.parkreldis.2019.07.031

Sasmita, A. O. (2019). Modification of the gut microbiome to combat neurodegeneration. *Rev. Neurosci.* 30, 795–805. doi: 10.1515/revneuro-2019-0005

Scheperjans, F., Aho, V., Pereira, P. A., Koskinen, K., Paulin, L., Pekkonen, E., et al. (2015). Gut microbiota are related to Parkinson's disease and clinical phenotype. *Mov. Disord.* 30, 350–358. doi: 10.1002/mds.26069

Segain, J., Raingeard de la Blétière, D., Bourreille, A., Leray, V., Gervois, N., Rosales, C., et al. (2000). Butyrate inhibits inflammatory responses through NFkappaB inhibition: implications for Crohn's disease. *Gut* 47, 397–403. doi: 10.1136/gut.47.3.397

Sidransky, E., and Lopez, G. (2012). The link between the GBA gene and parkinsonism. *Lancet Neurol.* 11, 986–998. doi: 10.1016/S1474-4422(12)70190-4

Singleton, A. B., Farrer, M. J., and Bonifati, V. (2013). The genetics of Parkinson's disease: progress and therapeutic implications. *Mov. Disord.* 28, 14–23.

Spencer, B., Emadi, S., Desplats, P., Eleuteri, S., Michael, S., Kosberg, K., et al. (2014). ESCRT-mediated uptake and degradation of brain-targeted α-synuclein single chain antibody attenuates neuronal degeneration in vivo. *Mol. Ther.* 22, 1753–1767. doi: 10.1038/mt.2014.129

Spillantini, M. G., and Goedert, M. (2018). Neurodegeneration and the ordered assembly of α-synuclein. *Cell Tissue Res.* 373, 137–148.

Spillantini, M. G., Schmidt, M. L., Lee, V. M.-Y., Trojanowski, J. Q., Jakes, R., and Goedert, M. J. N. (1997). α-Synuclein in Lewy bodies. *Nature* 388, 839–840.

Stauch, K. L., Villeneuve, L. M., Purnell, P. R., Ottemann, B. M., Emanuel, K., and Fox, H. S. (2016). Loss of Pink1 modulates synaptic mitochondrial bioenergetics in the rat striatum prior to motor symptoms: concomitant complex I respiratory defects and increased complex II-mediated respiration. *Proteomics Clin. Appl.* 10, 1205–1217. doi: 10.1002/prca.201600005

Stoessel, D., Schulte, C., Teixeira Dos Santos, M. C., Scheller, D., Rebollo-Mesa, I., Deuschle, C., et al. (2018). Promising metabolite profiles in the plasma and CSF of early clinical Parkinson's disease. *Front. Aging Neurosci.* 10:51. doi: 10.3389/fnagi.2018.00051

Sugeno, N., Hasegawa, T., Tanaka, N., Fukuda, M., Wakabayashi, K., Oshima, R., et al. (2014). Lys-63-linked ubiquitination by E3 ubiquitin ligase Nedd4-1 facilitates endosomal sequestration of internalized α-synuclein. *J. Biol. Chem.* 289, 18137–18151. doi: 10.1074/jbc.M113.529461

Tan, A., Mahadeva, S., Marras, C., Thalha, A., Kiew, C., Yeat, C., et al. (2015). *Helicobacter* pylori infection is associated with worse severity of Parkinson's disease. *Parkinsonism Relat. Disord.* 21, 221–225. doi: 10.1016/j.parkreldis.2014.12.009

Thellung, S., Corsaro, A., Nizzari, M., Barbieri, F., and Florio, T. (2019). Autophagy activator drugs: a new opportunity in neuroprotection from misfolded protein toxicity. *Int. J. Mol. Sci.* 20:901. doi: 10.3390/ijms20040901

Tofaris, G., Layfield, R., and Spillantini, M. (2001). Alpha-synuclein metabolism and aggregation is linked to ubiquitin-independent degradation by the proteasome. *FEBS Lett.* 509, 22–26. doi: 10.1016/s0014-5793(01)03115-5

Trezzi, J. P., Galozzi, S., Jaeger, C., Barkovits, K., Brockmann, K., Maetzler, W., et al. (2017). Distinct metabolomic signature in cerebrospinal fluid in early Parkinson's disease. *Mov. Disord.* 32, 1401–1408. doi: 10.1002/mds.27132

Troisi, J., Landolfi, A., Vitale, C., Longo, K., Cozzolino, A., Squillante, M., et al. (2019). A metabolomic signature of treated and drug-naive patients with Parkinson's disease: a pilot study. *Metabolomics* 15:90. doi: 10.1007/s11306-019-1554-x

Trupp, M., Jonsson, P., Ohrfelt, A., Zetterberg, H., Obudulu, O., Malm, L., et al. (2014). Metabolite and peptide levels in plasma and CSF differentiating healthy controls from patients with newly diagnosed Parkinson's disease. *J. Parkinsons Dis.* 4, 549–560. doi: 10.3233/JPD-140389

Tufi, R., Gandhi, S., de Castro, I. P., Lehmann, S., Angelova, P. R., Dinsdale, D., et al. (2014). Enhancing nucleotide metabolism protects against mitochondrial dysfunction and neurodegeneration in a PINK1 model of Parkinson's disease. *Nat. Cell Biol.* 16, 157–166. doi: 10.1038/ncb2901

Tuttle, M. D., Comellas, G., Nieuwkoop, A. J., Covell, D. J., Berthold, D. A., Kloepper, K. D., et al. (2016). Solid-state NMR structure of a pathogenic fibril of full-length human α-synuclein. *Nat. Struct. Mol. Biol.* 23, 409–415.

Tyurina, Y. Y., Polimova, A. M., Maciel, E., Tyurin, V. A., Kapralova, V. I., Winnica, D. E., et al. (2015). LC/MS analysis of cardiolipins in substantia nigra and plasma of rotenone-treated rats: implication for mitochondrial dysfunction in Parkinson's disease. *Free Radic. Res.* 49, 681–691. doi: 10.3109/10715762.2015.1005085

Uemura, N., Koike, M., Ansai, S., Kinoshita, M., Ishikawa-Fujiwara, T., Matsui, H., et al. (2015). Viable neuronopathic Gaucher disease model in medaka (*Oryzias latipes*) displays axonal accumulation of alpha-synuclein. *PLoS Genet.* 11:e1005065. doi: 10.1371/journal.pgen.1005065

Ueno, S. I., Hatano, T., Okuzumi, A., Saiki, S., Oji, Y., Mori, A., et al. (2020). Nonmercaptalbumin as an oxidative stress marker in Parkinson's and PARK2 disease. *Ann. Clin. Transl. Neurol.* 7, 307–317. doi: 10.1002/acn3.50990

Van Den Berge, N., Ferreira, N., Gram, H., Mikkelsen, T. W., Alstrup, A. K. O., Casadei, N., et al. (2019). Evidence for bidirectional and trans-synaptic parasympathetic and sympathetic propagation of alpha-synuclein in rats. *Acta Neuropathol.* 138, 535–550. doi: 10.1007/s00401-019-02040-w

Van Laar, T., Boertien, J., and Herranz, A. H. (2019). Faecal transplantation, pro- and prebiotics in Parkinson's disease; hope or hype? *J. Parkinsons Dis.* 9, S371–S379. doi: 10.3233/jpd-191802

Vascellari, S., Palmas, V., Melis, M., Pisanu, S., Cusano, R., Uva, P., et al. (2020). Gut microbiota and metabolome alterations associated with Parkinson's disease. *mSystems* 5:e00561-20.

Volf, J., Polansky, O., Varmuzova, K., Gerzova, L., Sekelova, Z., Faldynova, M., et al. (2016). Transient and prolonged response of chicken cecum mucosa to colonization with different gut microbiota. *PLoS One* 11:e0163932. doi: 10.1371/journal.pone.0163932

Wahlstrom, A., Sayin, S. I., Marschall, H. U., and Backhed, F. (2016). Intestinal crosstalk between bile acids and microbiota and its impact on host metabolism. *Cell Metab.* 24, 41–50. doi: 10.1016/j.cmet.2016.05.005

Wallen, Z., Appah, M., Dean, M., Sesler, C., Factor, S., Molho, E., et al. (2020). Characterizing dysbiosis of gut microbiome in PD: evidence for overabundance of opportunistic pathogens. *NPJ Parkinsons Dis.* 6:11. doi: 10.1038/s41531-020-0112-6

Wile, D. J., Agarwal, P. A., Schulzer, M., Mak, E., Dinelle, K., Shahinfard, E., et al. (2017). Serotonin and dopamine transporter PET changes in the premotor phase of LRRK2 parkinsonism: cross-sectional studies. *Lancet Neurol.* 16, 351–359. doi: 10.1016/S1474-4422(17)30056-X

Willis, G. L., Boda, J., and Freelance, C. B. (2018). Polychromatic light exposure as a therapeutic in the treatment and management of Parkinson's disease: a controlled exploratory trial. *Front. Neurol.* 9:741. doi: 10.3389/fneur.2018.00741

Willkommen, D., Lucio, M., Moritz, F., Forcisi, S., Kanawati, B., Smirnov, K. S., et al. (2018). Metabolomic investigations in cerebrospinal fluid of Parkinson's disease. *PLoS One* 13:e0208752. doi: 10.1371/journal.pone.0208752

Wilson, H., Dervenoulas, G., Pagano, G., Koros, C., Yousaf, T., Picillo, M., et al. (2019). Serotonergic pathology and disease burden in the premotor and motor phase of A53T alpha-synuclein parkinsonism: a cross-sectional study. *Lancet Neurol.* 18, 748–759. doi: 10.1016/S1474-4422(19)30140-1

Wilson, H., Giordano, B., Turkheimer, F. E., Chaudhuri, K. R., and Politis, M. (2018). Serotonergic dysregulation is linked to sleep problems in Parkinson's disease. *Neuroimage Clin.* 18, 630–637. doi: 10.1016/j.nicl.2018.03.001

Xu, L., Lee, J. R., Hao, S., Ling, X. B., Brooks, J. D., Wang, S. X., et al. (2019). Improved detection of prostate cancer using a magneto-nanosensor assay for serum circulating autoantibodies. *PLoS One* 14:e0221051. doi: 10.1371/journal.pone.0221051

Younes-Mhenni, S., Frih-Ayed, M., Kerkeni, A., Bost, M., and Chazot, G. (2007). Peripheral blood markers of oxidative stress in Parkinson's disease. *Eur. Neurol.* 58, 78–83.

Zampieri, S., Cattarossi, S., Bembi, B., and Dardis, A. (2017). GBA analysis in next-generation era: pitfalls, challenges, and possible solutions. *J. Mol. Diagn.* 19, 733–741. doi: 10.1016/j.jmoldx.2017.05.005

Zarranz, J. J., Alegre, J., Gomez-Esteban, J. C., Lezcano, E., Ros, R., Ampuero, I., et al. (2004). The new mutation, E46K, of alpha-synuclein causes Parkinson and Lewy body dementia. *Ann. Neurol.* 55, 164–173. doi: 10.1002/ana.10795

Zhao, X., Zhang, M., Li, C., Jiang, X., Su, Y., and Zhang, Y. (2019). Benefits of vitamins in the treatment of Parkinson's disease. *Oxid. Med. Cell. Longev.* 2019:9426867. doi: 10.1155/2019/9426867

Conflict of Interest: The authors declare that the research was conducted in the absence of any commercial or financial relationships that could be construed as a potential conflict of interest.

frontiers in Neuroscience

ORIGINAL RESEARCH
published: 17 March 2021
doi: 10.3389/fnins.2021.642324

Network Analysis of the CSF Proteome Characterizes Convergent Pathways of Cellular Dysfunction in ALS

Alexander G. Thompson[1], Elizabeth Gray[1], Philip D. Charles[2], Michele T. M. Hu[1], Kevin Talbot[1], Roman Fischer[2], Benedikt M. Kessler[2] and Martin R. Turner[1]**

[1] Nuffield Department of Clinical Neurosciences, University of Oxford, Oxford, United Kingdom, [2] Target Discovery Institute, Centre for Medicines Discovery, Nuffield Department of Medicine, University of Oxford, Oxford, United Kingdom

Background: Amyotrophic lateral sclerosis is a clinical syndrome with complex biological determinants, but which in most cases is characterized by TDP-43 pathology. The identification in CSF of a protein signature of TDP-43 network dysfunction would have the potential to inform the identification of new biomarkers and therapeutic targets.

Methods: We compared CSF proteomic data from patients with ALS (n = 41), Parkinson's disease (n = 19) and healthy control participants (n = 20). Weighted correlation network analysis was used to identify modules within the CSF protein network and combined with gene ontology enrichment analysis to functionally annotate module proteins. Analysis of module eigenproteins and differential correlation analysis of the CSF protein network was used to compare ALS and Parkinson's disease protein co-correlation with healthy controls. In order to monitor temporal changes in the CSF proteome, we performed longitudinal analysis of the CSF proteome in a subset of ALS patients.

Results: Weighted correlation network analysis identified 10 modules, including those enriched for terms involved in gene expression including nucleic acid binding, RNA metabolism and translation; humoral immune system function, including complement pathways; membrane proteins, axonal outgrowth and adherence; and glutamatergic synapses. Immune system module eigenproteins were increased in ALS, whilst axonal module eigenproteins were decreased in ALS. The 19 altered protein correlations in ALS were enriched for gene expression (OR 3.05, p = 0.017) and membrane protein modules (OR 17.48, p = 0.011), including intramodular hub proteins previously identified as TDP-43 interactors. Proteins decreasing over longitudinal analysis ALS were enriched in glutamatergic synapse and axonal outgrowth modules. Protein correlation network disruptions in Parkinson's disease showed no module enrichment.

Conclusions: Alterations in the co-correlation network in CSF samples identified a set of pathways known to be associated with TDP-43 dysfunction in the pathogenesis of ALS, with important implications for therapeutic targeting and biomarker development.

Keywords: cerebrospinal fluid, amyotrophic lateral sclerosis, motor neuron disease, biomarker, proteomics, proteomics & bioinformatics, WGCNA, network analysis

OPEN ACCESS

Edited by:
Manoj Kumar Jaiswal, Icahn School of Medicine at Mount Sinai, United States

Reviewed by:
Paul Roy Heath, The University of Sheffield, United Kingdom
Erik Johnson, Emory University, United States
Nicholas T. Seyfried, Emory University, United States

****Correspondence:***
Benedikt M. Kessler
benedikt.kessler@ndm.ox.ac.uk
Martin R. Turner
martin.turner@ndcn.ox.ac.uk

Specialty section:
This article was submitted to Neurodegeneration, a section of the journal Frontiers in Neuroscience

Received: *15 December 2020*
Accepted: *18 February 2021*
Published: *17 March 2021*

Citation:
Thompson AG, Gray E, Charles PD, Hu MTM, Talbot K, Fischer R, Kessler BM and Turner MR (2021) Network Analysis of the CSF Proteome Characterizes Convergent Pathways of Cellular Dysfunction in ALS. Front. Neurosci. 15:642324. doi: 10.3389/fnins.2021.642324

INTRODUCTION

Amyotrophic lateral sclerosis (ALS) is a fatal neurodegenerative disease, associated with selective loss of motor neurons in the spinal cord and brain. Alterations in multiple cellular pathways have been implicated in the pathogenesis of ALS, including excitotoxicity, cellular energy metabolism, protein degradation and non-cell autonomous glial mechanisms, representing multiple overlapping tributaries into the final common pathway of motor neuron degeneration (Talbot et al., 2018). Since the discovery of mislocalized cytoplasmic aggregates of 43 kDa trans-active response DNA-binding protein (TDP-43) as the neuropathological hallmark of nearly all ALS cases (Neumann et al., 2006), focus has fallen on mechanisms related to alterations in the function and behavior of TDP-43, particularly its roles in RNA splicing, the stress response and its propensity for aggregation (Taylor et al., 2016).

Evidence of perturbations in many pathways implicated in ALS have been identified in biofluid samples from ALS patients. Alterations in markers of oxidative stress, glial and immune activation, axonal degeneration and protein degradation mechanisms have been detected in patient samples using candidate-driven and untargeted studies of cerebrospinal fluid (CSF) proteins and metabolites (Turner et al., 2009).

A major advantage of the high-dimensional data produced by untargeted approaches is the capability to explore co-ordinated network alterations, engendering broader understanding of the pathophysiological changes associated with a disease or phenotype. Analytical techniques based on co-correlation, such as weighted gene correlation network analysis (WGCNA) (Langfelder and Horvath, 2008) and differential gene correlation analysis (McKenzie et al., 2016) have been applied widely in genomics and proteomics to derive regulatory networks, understand disease-associated alterations in protein networks and identify candidate therapeutic targets. Here, we apply this approach to CSF, comparing network changes in patients with ALS with healthy controls and, in order to distinguish disease-specific changes from neurodegeneration-associated changes, patients with Parkinson's disease (PD) aiming to identify network disruption overlooked by conventional analysis.

MATERIALS AND METHODS

Participants and Sampling

Ethical approval for this study was obtained from South Central Oxford Ethics Committee B (08/H0605/85) NRES Central Committee South Central – Berkshire (14/SC/0083 and 10/H0505/71). All participants provided written consent (or gave permission for a carer to sign on their behalf). The study included 43 patients with ALS, 20 patients with Parkinson's disease, and 20 healthy control subjects. Patients with ALS were recruited from the Oxford ALS Centre, Oxford, United Kingdom and patients with Parkinson's disease were recruited through the Oxford Parkinson's Disease Centre, Oxford, United Kingdom.

CSF was collected at baseline and, in ALS patients, every 6 months when available. Clinical data was ascertained on the same day. CSF samples were processed in accordance with consensus guidelines for biomarker development within 1 h of sampling and stored at −80°C until use. Symptom onset was defined as first weakness reported by patients. Disease progression rate was calculated per-visit using the revised ALS functional rating scale (ALSFRS-R) by [48 – ALSFRS-R]/[months from symptom onset].

Proteomic Analysis

The raw data used in this analysis has been previously published (Thompson et al., 2018b). In brief, samples of CSF were thawed on ice and digested using heat stable immobilized trypsin as per the manufacturer's instructions (SMART digest, Thermo Fisher Scientific, United Kingdom). 50 μL of CSF was mixed with 150 μL SMART digest buffer and added to SMART digest plates. Samples were incubated at 70°C with shaking at 1,400 rpm for 60 min. Digested samples were desalted using SOLAμ plates and dried by vacuum centrifugation. Samples were resuspended in 20 μL buffer A (2% acetonitrile, 0.1% formic acid in water) and kept at −20°C until analysis. Peptide concentrations were assayed using a Pierce quantitative colorimetric peptide assay (Thermo Fisher Scientific, United Kingdom) according to the manufacturer's instructions. A pooled sample was produced by combining equal quantities of digested peptide from each individual sample and injected after every tenth sample for use in quality control analysis.

Peptides were analyzed by nano ultra-high performance liquid chromatography tandem mass spectrometry (nUHPLC LC-MS/MS) using a Dionex Ultimate 3000 UHPLC (Thermo Fisher Scientific, Germany) coupled to a Q Exactive HF tandem mass spectrometer (Thermo Fisher Scientific, Germany). 500 nL of peptides from each sample were injected and analyzed using a 60-min linear gradient at a 250 nL/min flow rate. The gradient used to elute the peptides started at 3 min with 2% buffer B (0.1% TFA and 5% DMSO in CH_3CN) increasing to 5% by 6 min followed by an increase up to 35% by 63 min. The data were acquired with a resolution of 60,000 full-width at half maximum ion intensity with a mass/charge ratio of 400 and a lock mass enabled at 445.120025 m/z. The 12 most abundant precursor ions in each MS1 scan were selected for fragmentation by higher-energy collisional dissociation (HCD) at a normalized collision energy of 28 followed by exclusion for 27 s.

Raw MS data were analyzed using Progenesis QI for Proteomics software v3.0 (Non-linear Dynamics). MS/MS spectra were searched against the UniProt Homo Sapiens Reference proteome (retrieved 01/06/2017) using Mascot v2.5.1 (Matrix Science) allowing for a precursor mass tolerance of 10 ppm and a fragment ion tolerance of 0.05 Da. Deamidation on asparagine and glutamine and oxidation on methionine were included as variable modifications. The peptide false discovery rate (FDR) was set at 1% and all peptides with an ion score higher than 20 into were imported into Progenesis QIP. Proteins that were defined with at least one unique peptide were included in the protein data set for further analysis (289 proteins had one unique peptide; **Supplementary Figure 1**). Protein abundance values were centered to a background median (similar to the Progenesis QIP 'robust mean' used for normalization within the

software), where the background was taken as the 90% of proteins with the lowest variance across all runs (Keilhauer et al., 2015). Values were then scaled by median absolute deviation.

Statistical Analysis

Statistical and bioinformatic analysis was performed in R version 4.0.2. Correction for multiple comparisons was performed using the Benjamini-Hochberg step-up procedure, with adjusted $p < 0.1$ taken to indicate statistical significance. Raw, uncorrected p-values were reported where fewer than 20 hypothesis tests were carried out, using $p < 0.05$ to denote statistical significance.

Weighted Correlation Network Analysis

Weighted correlation network analysis was performed with the weighted gene correlation network analysis (WGCNA) package in R. Three outlying samples (two ALS and one Parkinson's disease) were identified using hierarchical clustering and were excluded from subsequent analysis (**Supplementary Figure 2**; participant demographics including longitudinal sampling **Table 1**). Eighteen proteins were excluded due to an excessive degree of missing data (>50% from any group). Only baseline samples visits for longitudinal participants were included in network analysis. A signed, weighted network was constructed using soft thresholding power = 7 using Pearson correlation as the dissimilarity measure, minimum module size 5 and cut height 0.05. The most highly connected 10% of proteins within each module (highest k_{in}) were denoted intramodular hub proteins. Module stability was assessed by iterating network construction using the same settings, randomly excluding one sample from each run and comparing the proportion of shared protein module assignments between with the reference network. Network graphs were produced in R using the igraph package.

Module-phenotype associations were analyzed by comparing module eigenprotein expression between conditions with a pairwise Mann-Whitney U test, comparing healthy controls with ALS or PD samples.

TABLE 1 | Baseline demographic features of participants included in WGCNA analysis.

	ALS	HC	PD	*p*
n, visit 1	41	20	19	–
n, visit 2	20	–	–	–
n, visit 3	12	–	–	–
n, visit 4	10	–	–	–
n, visit 5	2	–	–	–
Age at sampling, years (mean ± SD)	62.62 ± 9.99	58.53 ± 8.57	62.87 ± 3.95	0.263*
Age at symptom onset, years (mean ± SD)	59.95 ± 10.75	–	61.12 ± 3.87	0.925*
Male participants, *n* (%)	30 (73.2)	11 (55)	10 (52.6)	0.193+
Baseline disease progression rate, points/month (median [IQR])	0.5 [0.27–1.00]	–	–	–

**Kruskal-Wallis H test.*
+Fisher Exact test.
ALS, amyotrophic lateral sclerosis; HC, healthy control; PD, Parkinson's disease; SD, standard deviation; IQR, interquartile range.

Comparisons With ALS-FTD Cortical Networks

The CSF protein network was compared with a previously published frontal cortex proteomic dataset from control, ALS, FTD and ALS-FTD patients using a cross-tabulation approach (Umoh et al., 2018). Individual module protein and gene assignments were compared between CSF and frontal cortex module allocations for each module pair using a hypergeometric test.

Differential Correlation Analysis

Analysis of differential correlation were performed by within-group pairwise Pearson correlation of protein abundance in healthy control, ALS and PD samples and correlations compared using Fisher's r-to-z transformation. Resulting p-values were corrected for multiple comparisons using the Benjamini-Hochberg step-up procedure.

Enrichment Analysis

Proteins were abstracted to genes for gene ontology (GO) and module enrichment analysis. GO enrichment analysis was performed in R with TopGo using the "weight" algorithm. Foreground lists comprised genes within each module or differentially correlated proteins, the background list comprised all genes identified in the proteomic analysis. Module enrichment analysis was performed using a hypergeometric test.

Longitudinal Analysis

Longitudinal analysis was performed in R using the nlme package. Models were constructed using log_transformed longitudinal data, including only participants for whom longitudinal samples were available. Individual participants were specified as random effects and anchored to the date of the initial visit using linear mixed effects modeling with a random intercept, fixed slope model, uncorrelated covariance structure and degrees of freedom as calculated by Pinheiro and Bates (Pinehiro and Bates, 2000).

RESULTS

The CSF Protein Correlation Network

WGCNA of the CSF proteome yielded a protein network comprising 776 proteins in 10 modules ranging from 7 to 183 proteins (**Figure 1**). 107 proteins were not allocated to a module. To understand the biological relevance of the protein correlation network modules, Gene Ontology (GO) enrichment analysis was performed (**Figure 2** and **Supplementary Table 1**).

Two large modules demonstrated significant enrichment for distinct groups of GO terms. Module 1, the largest comprising 183 proteins, was enriched in intracellular proteins annotated to cytoplasmic and nuclear intracellular compartments. Concordant with this, module one proteins were enriched

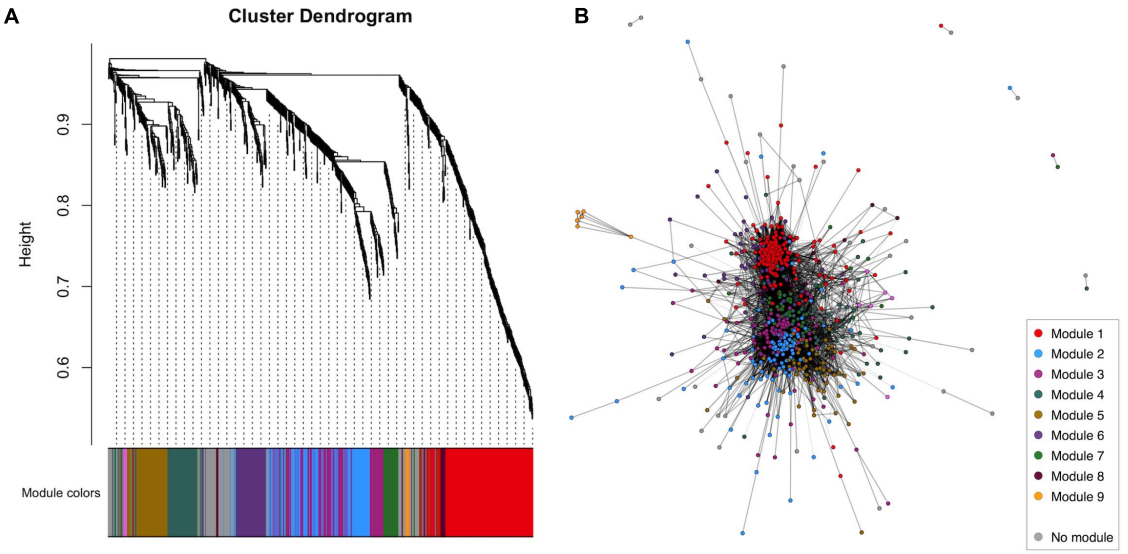

FIGURE 1 | WGCNA of the healthy control CSF proteome. **(A)** Cluster dendrogram indicating module allocation. **(B)** Network graph indicating modules. For ease of visualization, pairwise correlations with FDR-adjusted $p > 0.01$ have been excluded from this graph. CSF, cerebrospinal fluid; WGCNA, weighted gene correlation network analysis.

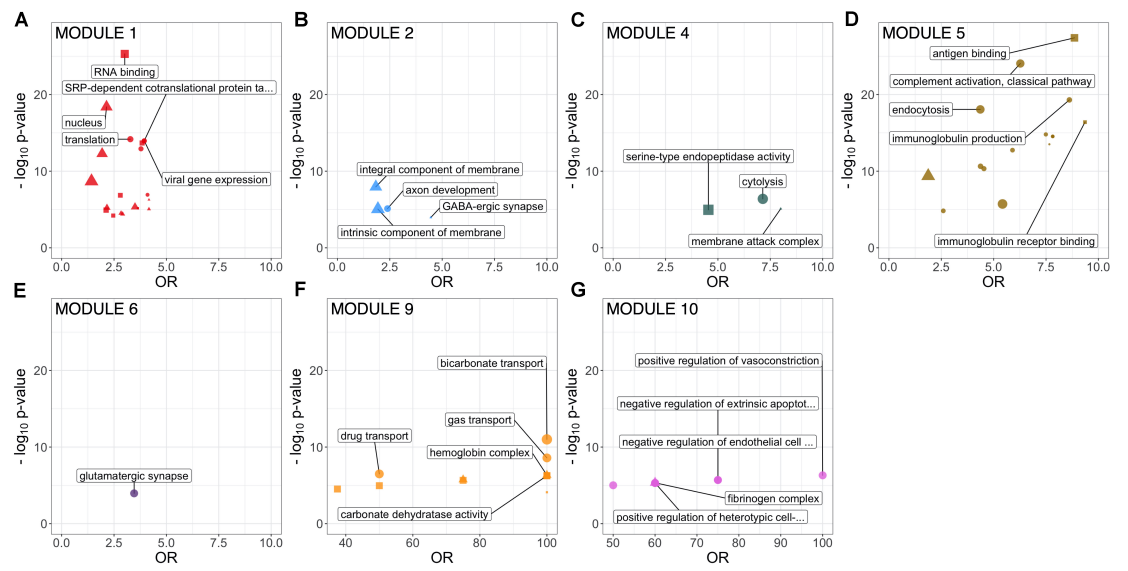

FIGURE 2 | GO term enrichment of identified CSF protein network modules (FDR-adjusted $p < 0.1$). Size proportional to number of annotated proteins within a GO term in that module. Top 5 GO terms by *p*-value are labeled. All significantly enriched GO terms are detailed in **Supplementary Table 1**. CSF, cerebrospinal fluid; GO, Gene Ontology.

for functions involved in gene expression including nucleic acid binding, RNA metabolism and translation (**Figure 2** and **Supplementary Table 1**). Module 2, comprising 115 proteins was enriched in GO terms relating to axon development, neurons, GABAergic synapses and the cell membrane. Module 4 (75 proteins) was enriched for cytolysis and the membrane attack complex. Module 5 (67 proteins) was enriched in immune system proteins relating primarily to the humoral immune system including immunoglobulins and complement, B-cell signaling and fibrinolysis. Smaller modules were enriched in glutamatergic synapse proteins (module 6, 58 proteins); blood proteins involved in gas transport (module 9, 7 proteins); fibrinogen complex, peptide hormone secretion and vasoconstriction (module 10, 7 proteins). Module stability analysis indicated reproducible protein-module assignment for >75% of proteins in over 50% of iterations for modules 1, 2, 4, 5, and 6, and >50% for module 3 (**Supplementary Figure 3**).

Differences in module protein expression as measured by module eigenproteins were observed between ALS and healthy control samples for module 2 (healthy control median 0.054, ALS median 0.001, $p = 0.031$), module 4 (healthy control median −0.036, ALS median 0.036, $p = 0.016$), and module 9 (healthy control median −0.052, ALS median −0.036, $p = 0.015$) and between PD and healthy control samples for module 9 (healthy control median −0.052, PD median 0.053, $p < 0.001$; **Figure 3**).

Differential Protein Correlation Analysis Reveals Altered Cellular Processes in ALS

To examine disease-related disruptions in the protein correlation network at a more granular level, differential correlation analysis was performed, comparing pairwise protein correlations in CSF from ALS and PD patients with those in healthy control CSF. This identified 11 significantly altered correlations between 19 proteins (19 genes) in ALS (**Supplementary Table 2**). There was no significant GO term enrichment (false discovery rate (FDR)-adjusted $p < 0.1$) amongst differentially correlated proteins, likely attributable to the small number of proteins in the foreground list. There was enrichment of proteins in module 1 (9/19 proteins, OR 3.05, $p = 0.017$) and module 9 (2/19 proteins, OR 17.48, $p = 0.011$; **Figure 4A**).

Module 1 proteins with altered correlation in ALS included RNA and DNA binding proteins and proteins involved in transcription and translation: Putative elongation factor 1-alpha 1 (EEF1A1), Histone H2B type 1-N (H2BC11), Acidic leucine-rich nuclear phosphoprotein 32 family member A (ANP32A) and Y-box-binding protein 1 (YBX1); the microtubule protein Tubulin beta chain (TUBB); the glycolytic enzymes Glyceraldehyde-3-phosphate dehydrogenase (GAPDH) and lactate dehydrogenase (LDHA); and Macrophage migration inhibitory factor (MIF). Three of the Module 1 proteins with altered correlation in ALS were intramodular hub proteins (EEF1A1, H2BC11 and GAPDH).

There were three altered correlations in which both proteins were within module 1: H2BC11 with TUBB ($r = 0.97$ HC, 0.56 ALS, FDR-adjusted $p = 0.035$), EEFA1A with TUBB ($r = 0.97$ HC, 0.57 ALS, $p = 0.057$), and GAPDH with MIF ($r = 0.93$ HC, 0.25 ALS, $p = 0.057$).

Differential correlation analysis comparing PD and healthy controls identified 27 significant altered correlations between 36 proteins (36 genes). No significant GO enrichment was identified. Dyscorrelated proteins were enriched in module 7 (5/36 proteins, OR 3.98, $p = 0.016$) and module 9 proteins (3/36 proteins, OR 18.31, $p = 0.002$) including blood proteins and proteins involved in adhesion and carbohydrate metabolism (**Figure 4B** and **Supplementary Table 2**).

Longitudinal Analysis Indicates Modulation in Axon Guidance and Neurodevelopment Pathways in ALS

Linear mixed-model analysis identified 10 longitudinally increasing and 15 longitudinally decreasing proteins in ALS patients (FDR-adjusted $p < 0.1$; **Supplementary Table 3**). The proteins with longitudinally increasing abundance comprised proteins present at high levels in plasma including complement components C7 and C1S, Thyroxine-binding globulin, and immunoglobulins; and extracellular matrix proteins Laminin subunit alpha-2 and Galectin-3-binding protein. There was no significant GO or module enrichment of increasing proteins (**Figure 4C**).

Proteins with longitudinally decreasing abundance were enriched in module 2 proteins (**Figure 4D**, enriched for membrane, neuronal cell body and axon development

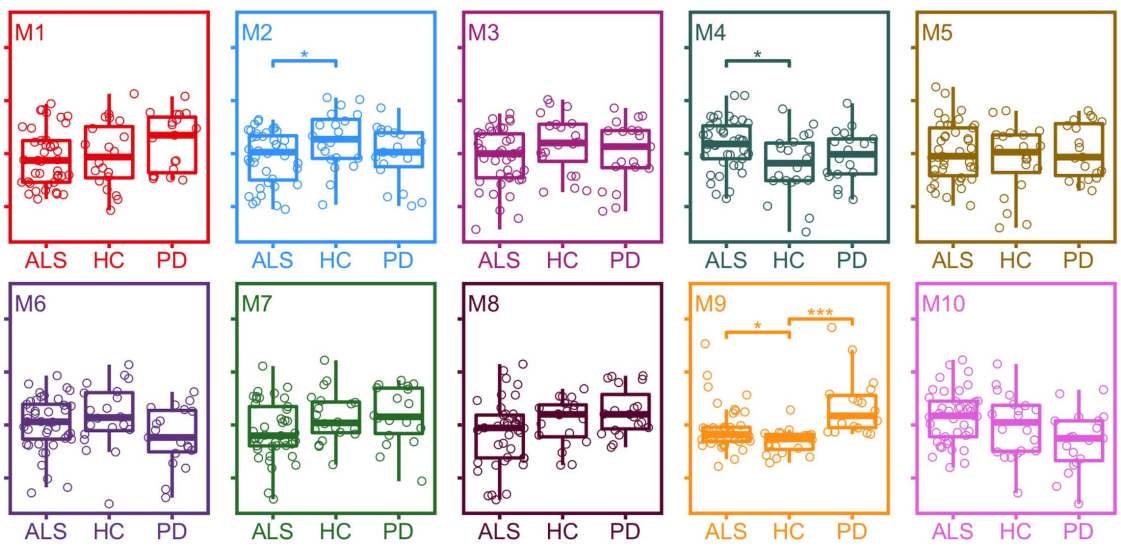

FIGURE 3 | Expression of module eigenproteins between conditions. *$p < 0.05$, **$p < 0.01$, ***$p < 0.001$. ALS, amyotrophic lateral sclerosis; HC, healthy control; PD, Parkinson's disease.

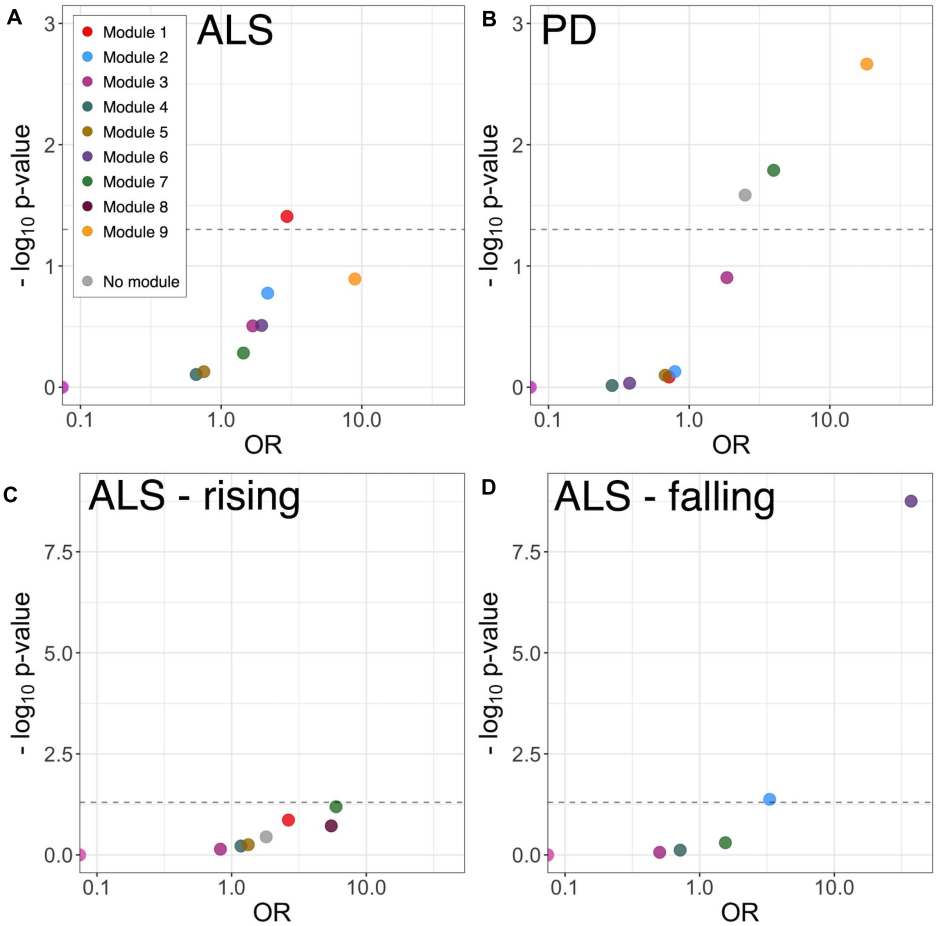

FIGURE 4 | Module enrichment of differentially correlated proteins in ALS **(A)** and PD **(B)**, and longitudinally falling **(C)** or rising **(D)** proteins in ALS. ALS, amyotrophic lateral sclerosis; PD, Parkinson's disease.

5/15 proteins; OR 3.31, $p = 0.042$) and module 6 proteins (glutamatergic synapse; 10/15 proteins OR 37.21, $p < 0.001$). Though lacking significant GO term enrichment, they were annotated to concordant, disease-relevant GO terms. These included axonal guidance and neurodevelopment (Neurofascin, Semaphorin-7A, Ciliary neurotrophic factor receptor subunit alpha, Peptidyl-glycine alpha-amidating monooxygenase, Neuritin, Disintegrin and metalloproteinase domain-containing protein 22), synapse assembly and function (Calsyntenin-3, Receptor-type tyrosine-protein phosphatase-like N, Neurofascin), neuropeptide signaling [Neuroendocrine protein 7B2, identified as a candidate ALS biomarker in a previous CSF proteomic study (Ranganathan et al., 2005)] and RNA processing (ATP-dependent RNA helicase DHX8). Of the longitudinally decreasing proteins, Neuritin and Neurofascin were intramodular hubs.

Frontal Cortex and CSF Protein Networks Show Major Differences

The CSF protein network was compared with that of a previously published frontal cortex protein network derived from shotgun proteomic analysis of control, ALS, FTD and ALS-FTD patient tissue. The overlap between proteins and genes between the two datasets was limited (intersect 107 proteins of 776 CSF and 2612 cortex; intersect 283 genes of 684 CSF and 2487 cortex genes). Module preservation analysis by cross tabulation (pairwise enrichment analysis of CSF and frontal cortex modules) demonstrated no evidence of preservation of any modules. When abstracted to genes, there was significant, albeit modest, overlap of frontal cortex module 9 (midnight blue) with CSF module 1 (9/170, OR 10.52, $p < 0.001$) and CSF module 10 (3/6, OR 135.95, $p < 0.001$; **Figure 5**).

DISCUSSION

This study analyzed a large CSF proteomic dataset to delineate the overall protein network structure in healthy controls, ALS and PD. The analysis identified several major protein modules, the first enriched in intracellular compartment proteins and functions involved in gene expression and regulation. The second large module, was enriched with proteins involved in axonal development, inhibitory synapses and membrane proteins.

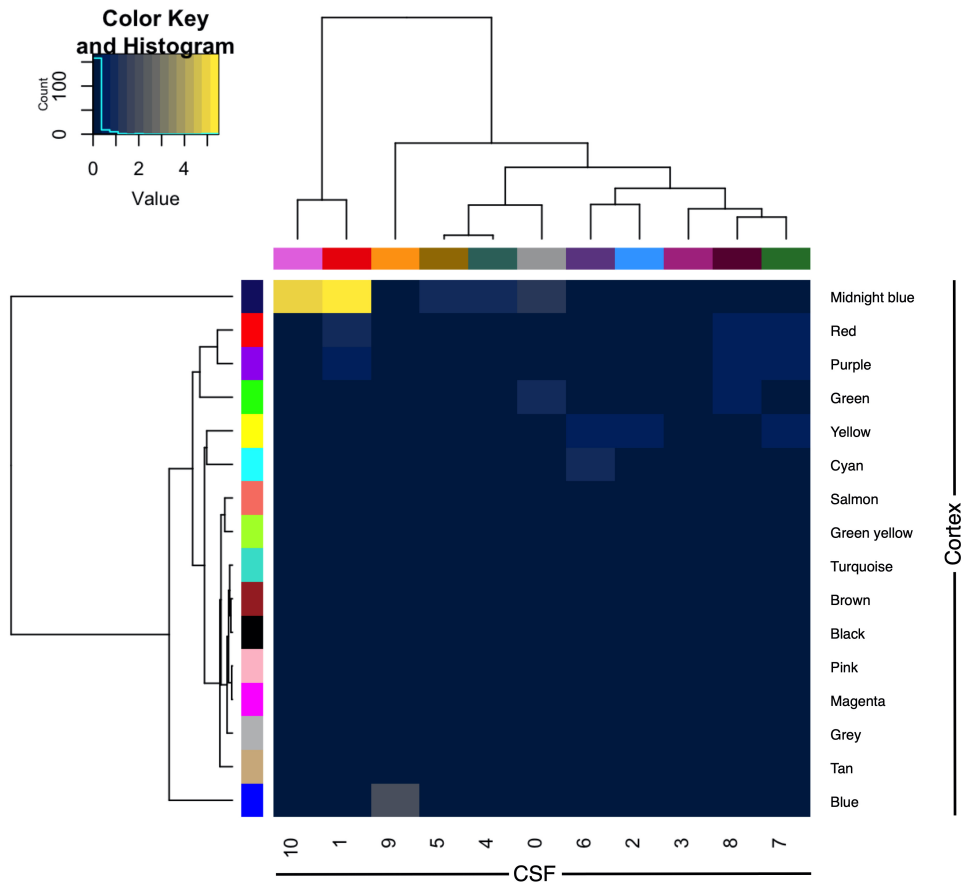

FIGURE 5 | Module preservation of CSF (columns) and frontal cortex (rows) by cross-tabulation. Significant overlaps were observed between CSF modules 1 and 10 with frontal cortex module 9 (midnight blue). Color indicates $-\log_{10}$ *p*-value for enrichment. CSF, cerebrospinal fluid.

Smaller, less stable, modules were enriched for immune system proteins (modules 4 and 5), glutamatergic synapse proteins (module 6) and blood proteins involved in gas transport (module 9), endothelial and clotting pathways (module 10).

Module eigenprotein-phenotype relationships identified decreased expression of module 2 and increased expression of modules 4 and 9 in ALS, and of module 9 in PD. Module 2 proteins include neural growth factors, guidance proteins and cell adhesion molecules, many of which have been studied in ALS and FTD as biomarker candidates. The module 2 intramodular hub protein Ephrin type A receptor 4 has been identified as a modifier of ALS severity, with lower levels associated with later onset and more rapid disease progression (Van Hoecke et al., 2012). Missense mutations in CDH13, encoding Cadherin 13 precursor, another module 2 intramodular hub protein, have been identified in sporadic ALS patients, though this finding has not been replicated (Daoud et al., 2011). Altered regulation of synaptic adhesion proteins in module 2 Neurexin 1 and Neurexin 3 (of which Neurexin 1 is a module 2 intramodular hub protein) have also been identified as a consequence of TDP-43 depletion (Polymenidou et al., 2011).

The finding of decreases in module 2 synaptic proteins in ALS is consistent with previous work in ALS, but differs from Alzheimer's disease, in which increases in levels of synaptic proteins in CSF have been observed (Dayon et al., 2018; Portelius et al., 2018; Higginbotham et al., 2020). It is possible that the low levels observed in ALS reflect synaptic loss, whilst in Alzheimer's they indicate an active process within synapses and alterations in synaptic protein turnover (Hark et al., 2021).

Module 4 contains proteins involved in the innate immune response including the ALS microglial activity marker Chitotriosidase 1 (Steinacker et al., 2018; Thompson et al., 2018b, 2019; Vu et al., 2020), as well as complement components and apolipoproteins. Marked inflammatory change, particularly involving microglia and involving complement, is a well-described feature of ALS neuropathology (Brettschneider et al., 2012; Bahia El Idrissi et al., 2016), whilst alterations in apolipoprotein metabolism have been implicated in the development of ALS and as a modulator of disease progression (Mariosa et al., 2017; Ingre et al., 2020). Alterations in module 9 may be a reflection of altered blood-brain or blood-CSF barrier function (Garbuzova-Davis and Sanberg, 2014), though this is less well-recognized as a feature of PD (Desai et al., 2007).

Differential protein correlation analysis provided evidence of disease-specific alterations in relevant network modules. Several of the proteins with altered correlation derive from pathways

strongly implicated in ALS pathogenesis. In particular, alterations in gene expression pathways have been demonstrated in disease models and *post mortem* tissue from ALS patients (Polymenidou et al., 2011; Krach et al., 2018). Differential correlations in ALS were identified in H2BC11, a histone protein, YBX1, a transcription factor implicated in ALS through model and *post mortem* tissue analysis, identified as an interactor of TDP-43 and stress granule component (Anders et al., 2018; Nijssen et al., 2018; Feneberg et al., 2020; La Cognata et al., 2020), and EEF1A1, a translational elongation factor and, like YBX1, stress granule component and TDP-43 interactor (Kim et al., 2010; Anders et al., 2018). EEF1A1 and YBX1 are also components of the synaptic protein expression machinery, potentially linking alterations in module 2 protein levels with loss of correlation in module 1 (Holt et al., 2019). TUBB, again a TDP-43 interactor (Freibaum et al., 2010), dimerizes with Tubulin alpha to form microtubules; mutations in genes encoding cytoskeletal proteins including Tubulin alpha (though not TUBB) have been identified as a rare cause of ALS (Smith et al., 2014). Alterations were also observed in the relationship of several enzymes, such as GAPDH, involved in carbohydrate metabolism, implicated through disease models and epidemiological studies (Kioumourtzoglou et al., 2015; Szelechowski et al., 2018).

The main signal emerging from longitudinal analysis indicated striking progressive downregulation of proteins in the module enriched for glutamatergic synapse proteins as well as axonal and neuronal proteins. This is in keeping with the progressive loss of axons, neurons and synapses that are a core pathological feature of ALS (Sasaki and Maruyama, 1994).

Analysis incorporating comparing the CSF protein network with a previously published frontal cortex protein correlation network indicated limited topological overlap between this CSF protein network and that of frontal cortex (Umoh et al., 2018).

Despite the lack of topological overlap, there was similarity in the functional annotation of identified modules in frontal cortex and CSF, notably between CSF module 1 and frontal cortex module 2, both enriched in transcription and translation-related ontological terms. CSF module 5 and cortex module 15 were enriched in antigen binding and immune system terms, whilst synaptic, membrane and axons terms were identified in cortex module 1 overlapping with CSF module 2 and module 6 (specifically glutamatergic synapse in the latter).

Although the CSF proteome receives a significant contribution from the brain, much of this arises from the white matter and gray matter regions beyond the frontal cortex. In addition, a large proportion of the CSF protein constitution arises through filtration of blood and secretion from the choroid plexus and includes a large proportion of classically secreted and non-classically secreted proteins (Thompson et al., 2018a). Furthermore, many neuronal and glial intracellular proteins might not be translocated into the extracellular space and hence the CSF in normal conditions, and the egress of proteins from CSF if determined by additional physiological processes (such as CSF flow rate) that would not necessarily affect all proteins proportionately (Reiber, 2001). The relatively limited overlap in the protein identifications, likely attributable to differences in methodological approach and the challenges of achieving proteomic depth in biological fluids, is also a consideration.

There are several limitations to this study. Genotype data, including presence of the ALS-causing *C9orf72* hexanucleotide repeat expansion, was not included since testing was not widely available at the time of sampling of participants in the study. Though sharing the main pathological features of sporadic ALS, *C9orf72* genotype could influence CSF network structure, but in this sporadic cohort it would not be expected to assert major effects, though would potentially have provided insights into the molecular divergence of genetic and non-genetic ALS. A significant proportion of proteins were identified based on one unique peptide (289/776), which might influence the accuracy of identification in some cases. Lower abundance proteins with higher variance will tend to have lower correlation, hence lower connectivity, potentially obscuring important relationships and excluding lower abundance proteins from modules and impacting power to detect differential correlations.

Conclusions

This analysis found changes within the CSF protein network in modules and pathways of established relevance to the pathogenesis of ALS, including those linked to the known functions of TDP-43. The diversity of alterations suggests that successful treatment of ALS will require targeting multiple pathways. Restoration of alterations in the CSF protein network might be a useful group-level outcome measure to detect disease modifying effects in therapeutic trials targeting a broad range of potentially pathogenic pathways in ALS.

DATA AVAILABILITY STATEMENT

Publicly available datasets were analyzed in this study. This data can be found here: https://www.ebi.ac.uk/pride/archive PRIDE archive Accession: PXD024219, DOI: 10.6019/PXD024219.

ETHICS STATEMENT

The studies involving human participants were reviewed and approved by South Central Oxford Ethics Committee B (08/H0605/85) and NRES Central Committee South Central – Berkshire (14/SC/0083 and 10/H0505/71). The participants provided their written informed consent to participate in this study.

AUTHOR CONTRIBUTIONS

All authors contributed to study design. AT prepared the manuscript and figures. All authors read and approved the final manuscript.

FUNDING

AT receives funding from the Medical Research Council and Motor Neurone Disease Association Lady Edith Wolfson

Fellowship (MR/T006927/1). MH receives support from Parkinson's UK, Oxford NIHR BRC, University of Oxford, CPT, Lab10X, NIHR, Michael J Fox Foundation, H2020 European Union, GE Healthcare and the PSP Association. MT receives funding from the Motor Neurone Disease Association.

SUPPLEMENTARY MATERIAL

The Supplementary Material for this article can be found online at: https://www.frontiersin.org/articles/10.3389/fnins.2021.642324/full#supplementary-material

REFERENCES

Anders, M., Chelysheva, I., Goebel, I., Trenkner, T., Zhou, J., Mao, Y., et al. (2018). Dynamic m6a methylation facilitates mRNA triaging to stress granules. *Life Sci. Alliance* 1:e201800113. doi: 10.26508/lsa.201800113

Bahia El Idrissi, N., Bosch, S., Ramaglia, V., Aronica, E., Baas, F., and Troost, D. (2016). Complement activation at the motor end-plates in amyotrophic lateral sclerosis. *J. Neuroinflammation* 13:72. doi: 10.1186/s12974-016-0538-2

Brettschneider, J., Toledo, J. B., Van Deerlin, V. M., Elman, L., McCluskey, L., Lee, V. M., et al. (2012). Microglial activation correlates with disease progression and upper motor neuron clinical symptoms in amyotrophic lateral sclerosis. *PLoS One* 7:e39216. doi: 10.1371/journal.pone.0039216

Daoud, H., Valdmanis, P. N., Gros-Louis, F., Belzil, V., Spiegelman, D., Henrion, E., et al. (2011). Resequencing of 29 candidate genes in patients with familial and sporadic amyotrophic lateral sclerosis. *Arch. Neurol.* 68, 587–593. doi: 10.1001/archneurol.2010.351

Dayon, L., Núñez Galindo, A., Wojcik, J., Cominetti, O., Corthésy, J., Oikonomidi, A., et al. (2018). Alzheimer disease pathology and the cerebrospinal fluid proteome. *Alzheimers Res. Ther.* 10:66. doi: 10.1186/s13195-018-0397-4

Desai, B. S., Monahan, A. J., Carvey, P. M., and Hendey, B. (2007). Blood-brain barrier pathology in Alzheimer's and Parkinson's disease: implications for drug therapy. *Cell Transplant.* 16, 285–299. doi: 10.3727/000000007783464731

Feneberg, E., Gordon, D., Thompson, A. G., Finelli, M. J., Dafinca, R., Candalija, A., et al. (2020). An ALS-linked mutation in TDP-43 disrupts normal protein interactions in the motor neuron response to oxidative stress. *Neurobiol. Dis.* 144:105050. doi: 10.1016/j.nbd.2020.105050

Freibaum, B. D., Chitta, R. K., High, A. A., and Taylor, J. P. (2010). Global analysis of TDP-43 interacting proteins reveals strong association with RNA splicing and translation machinery. *J. Proteome Res.* 9, 1104–1120. doi: 10.1021/pr901076y

Garbuzova-Davis, S., and Sanberg, P. R. (2014). Blood-CNS barrier impairment in ALS patients versus an animal model. *Front. Cell. Neurosci.* 8:21. doi: 10.3389/fncel.2014.00021

Hark, T. J., Rao, N. R., Castillon, C., Basta, T., Smukowski, S., Bao, H., et al. (2021). Pulse-chase proteomics of the app knockin mouse models of Alzheimer's disease reveals that synaptic dysfunction originates in presynaptic terminals. *Cell Syst.* 12, 141–158. doi: 10.1016/j.cels.2020.11.007

Higginbotham, L., Ping, L., Dammer, E. B., Duong, D. M., Zhou, M., Gearing, M., et al. (2020). Integrated proteomics reveals brain-based cerebrospinal fluid biomarkers in asymptomatic and symptomatic Alzheimer's disease. *Sci. Adv.* 6:eaaz9360. doi: 10.1126/sciadv.aaz9360

Holt, C. E., Martin, K. C., and Schuman, E. M. (2019). Local translation in neurons: visualization and function. *Nat. Struct. Mol. Biol.* 26, 557–566. doi: 10.1038/s41594-019-0263-5

Ingre, C., Chen, L., Zhan, Y., Termorshuizen, J., Yin, L., and Fang, F. (2020). Lipids, apolipoproteins, and prognosis of amyotrophic lateral sclerosis. *Neurology* 94, E1835–E1844. doi: 10.1212/WNL.0000000000009322

Keilhauer, E. C., Hein, M. Y., and Mann, M. (2015). Accurate protein complex retrieval by affinity enrichment mass spectrometry (AE-MS) rather than affinity purification mass spectrometry (AP-MS). *Mol. Cell. Proteomics* 14, 120–135. doi: 10.1074/mcp.M114.041012

Kim, S. H., Shanware, N. P., Bowler, M. J., and Tibbetts, R. S. (2010). Amyotrophic lateral sclerosis-associated proteins TDP-43 and FUS/TLS function in a common biochemical complex to co-regulate HDAC6 mRNA. *J. Biol. Chem.* 285, 34097–34105. doi: 10.1074/jbc.M110.154831

Kioumourtzoglou, M. A., Rotem, R. S., Seals, R. M., Gredal, O., Hansen, J., and Weisskopf, M. G. (2015). Diabetes mellitus, obesity, and diagnosis of amyotrophic lateral sclerosis a population-based study. *JAMA Neurol.* 72, 905–911. doi: 10.1001/jamaneurol.2015.0910

Krach, F., Batra, R., Wheeler, E. C., Vu, A. Q., Wang, R., Hutt, K., et al. (2018). Transcriptome–pathology correlation identifies interplay between TDP-43 and the expression of its kinase CK1E in sporadic ALS. *Acta Neuropathol.* 136, 405–423. doi: 10.1007/s00401-018-1870-7

La Cognata, V., Gentile, G., Aronica, E., and Cavallaro, S. (2020). Splicing players are differently expressed in sporadic amyotrophic lateral sclerosis molecular clusters and brain regions. *Cells* 9:159. doi: 10.3390/cells9010159

Langfelder, P., and Horvath, S. (2008). WGCNA: an R package for weighted correlation network analysis. *BMC Bioinformatics* 9:559. doi: 10.1186/1471-2105-9-559

Mariosa, D., Hammar, N., Malmström, H., Ingre, C., Jungner, I., Ye, W., et al. (2017). Blood biomarkers of carbohydrate, lipid, and apolipoprotein metabolisms and risk of amyotrophic lateral sclerosis: a more than 20-year follow-up of the Swedish AMORIS cohort. *Ann. Neurol.* 81, 718–728. doi: 10.1002/ana.24936

McKenzie, A. T., Katsyv, I., Song, W. M., Wang, M., and Zhang, B. (2016). DGCA: a comprehensive r package for differential gene correlation analysis. *BMC Syst. Biol.* 10:106. doi: 10.1186/s12918-016-0349-1

Neumann, M., Sampathu, D. M., Kwong, L. K., Truax, A. C., Micsenyi, M. C., Chou, T. T., et al. (2006). Ubiquitinated TDP-43 in frontotemporal lobar degeneration and amyotrophic lateral sclerosis. *Science* 314, 130–133. doi: 10.1126/science.1134108

Nijssen, J., Aguila, J., Hoogstraaten, R., Kee, N., and Hedlund, E. (2018). Axon-Seq decodes the motor axon transcriptome and its modulation in response to ALS. *Stem Cell Rep.* 11, 1565–1578. doi: 10.1016/j.stemcr.2018.11.005

Pinehiro, J. C., and Bates, D. M. (eds) (2000). *Mixed-Effects Models in S and S-PLUS*. Berlin: Springer.

Polymenidou, M., Lagier-Tourenne, C., Hutt, K. R., Huelga, S. C., Moran, J., Liang, T. Y., et al. (2011). Long pre-mRNA depletion and RNA missplicing contribute to neuronal vulnerability from loss of TDP-43. *Nat. Neurosci.* 14, 459–468. doi: 10.1038/nn.2779

Portelius, E., Olsson, B., Höglund, K., Cullen, N. C., Kvartsberg, H., Andreasson, U., et al. (2018). Cerebrospinal fluid neurogranin concentration in neurodegeneration: relation to clinical phenotypes and neuropathology. *Acta Neuropathol.* 136, 363–376. doi: 10.1007/s00401-018-1851-x

Ranganathan, S., Williams, E., Ganchev, P., Gopalakrishnan, V., Lacomis, D., Urbinelli, L., et al. (2005). Proteomic profiling of cerebrospinal fluid identifies biomarkers for amyotrophic lateral sclerosis. *J. Neurochem.* 95, 1461–1471. doi: 10.1111/j.1471-4159.2005.03478.x

Reiber, H. (2001). Dynamics of brain-derived proteins in cerebrospinal fluid. *Clin. Chim. Acta* 310, 173–186. doi: 10.1016/S0009-8981(01)00573-3

Sasaki, S., and Maruyama, S. (1994). Synapse loss in anterior horn neurons in amyotrophic lateral sclerosis. *Acta Neuropathol.* 88, 222–227. doi: 10.1007/BF00293397

Smith, B. N., Ticozzi, N., Fallini, C., Gkazi, A. S., Topp, S., Kenna, K. P., et al. (2014). Exome-wide rare variant analysis identifies TUBA4A mutations associated with familial ALS. *Neuron* 84, 324–331. doi: 10.1016/j.neuron.2014.09.027

Steinacker, P., Verde, F., Fang, L., Feneberg, E., Oeckl, P., Roeber, S., et al. (2018). Chitotriosidase (CHIT1) is increased in microglia and macrophages in spinal cord of amyotrophic lateral sclerosis and cerebrospinal fluid levels correlate with disease severity and progression. *J. Neurol. Neurosurg. Psychiatry* 89, 239–247. doi: 10.1136/jnnp-2017-317138

Szelechowski, M., Amoedo, N., Obre, E., Léger, C., Allard, L., Bonneu, M., et al. (2018). Metabolic reprogramming in amyotrophic lateral sclerosis. *Sci. Rep.* 8:3953. doi: 10.1038/s41598-018-22318-5

Talbot, K., Feneberg, E., Scaber, J., Thompson, A. G., and Turner, M. R. (2018). Amyotrophic lateral sclerosis: the complex path to precision medicine. *J. Neurol.* 265, 2454–2462. doi: 10.1007/s00415-018-8983-8

Taylor, J. P., Brown, R. H. J., and Cleveland, D. W. (2016). Decoding ALS: from genes to mechanism. *Nature* 539, 197–206. doi: 10.1038/nature20413

Thompson, A. G., Gray, E., Bampton, A., Raciborska, D., Talbot, K., and Turner, M. R. (2019). CSF chitinase proteins in amyotrophic lateral sclerosis.

J. Neurol. Neurosurg. Psychiatry 90, 1215–1220. doi: 10.1136/jnnp-2019-320442

Thompson, A. G., Gray, E., Mager, I., Fischer, R., Thézénas, M. L., Charles, P. D., et al. (2018a). UFLC-derived CSF extracellular vesicle origin and proteome. *Proteomics* 18:1800257. doi: 10.1002/pmic.201800257

Thompson, A. G., Gray, E., Thézénas, M. L., Charles, P. D., Evetts, S., Hu, M. T., et al. (2018b). Cerebrospinal fluid macrophage biomarkers in amyotrophic lateral sclerosis. *Ann. Neurol.* 83, 258–268. doi: 10.1002/ana.25143

Turner, M. R., Kiernan, M. C., Leigh, P. N., and Talbot, K. (2009). Biomarkers in amyotrophic lateral sclerosis. *Lancet Neurol.* 8, 94–109. doi: 10.1016/S1474-4422(08)70293-X

Umoh, M. E., Dammer, E. B., Dai, J., Duong, D. M., Lah, J. J., Levey, A. I., et al. (2018). A proteomic network approach across the ALS - FTD disease spectrum resolves clinical phenotypes and genetic vulnerability in human brain. *EMBO Mol. Med.* 10, 48–62. doi: 10.15252/emmm.201708202

Van Hoecke, A., Schoonaert, L., Lemmens, R., Timmers, M., Staats, K. A., Laird, A. S., et al. (2012). EPHA4 is a disease modifier of amyotrophic lateral sclerosis in animal models and in humans. *Nat. Med.* 18, 1418–1422.

Vu, L., An, J., Kovalik, T., Gendron, T., Petrucelli, L., and Bowser, R. (2020). Cross-sectional and longitudinal measures of chitinase proteins in amyotrophic lateral sclerosis and expression of CHI3L1 in activated astrocytes. *J. Neurol. Neurosurg. Psychiatry* 91, 350–358. doi: 10.1136/jnnp-2019-321916

Conflict of Interest: MH has received payment for Advisory Board attendance/consultancy for Biogen, Roche, CuraSen Therapeutics, Evidera, Manus Neurodynamica and the MJFF Digital Health Assessment Board. MH is a co-applicant on a patent application related to smartphone predictions in Parkinson's (PCT/GB2019/052522) pending.

The remaining authors declare that the research was conducted in the absence of any commercial or financial relationships that could be construed as a potential conflict of interest.

frontiers in Neuroscience

ORIGINAL RESEARCH
published: 16 June 2021
doi: 10.3389/fnins.2021.682247

Decreased MEF2A Expression Regulated by Its Enhancer Methylation Inhibits Autophagy and May Play an Important Role in the Progression of Alzheimer's Disease

*Hui Li, Feng Wang, Xuqi Guo and Yugang Jiang**

Tianjin Institute of Environmental and Operational Medicine, Tianjin, China

Alzheimer's disease (AD) is a neurodegenerative disease characterized by amyloid plaques and neurofibrillary tangles which significantly affects people's life quality. Recently, AD has been found to be closely related to autophagy. The aim of this study was to identify autophagy-related genes associated with the pathogenesis of AD from multiple types of microarray and sequencing datasets using bioinformatics methods and to investigate their role in the pathogenesis of AD in order to identify novel strategies to prevent and treat AD. Our results showed that the autophagy-related genes were significantly downregulated in AD and correlated with the pathological progression. Furthermore, enrichment analysis showed that these autophagy-related genes were regulated by the transcription factor myocyte enhancer factor 2A (MEF2A), which had been confirmed using si-MEF2A. Moreover, the single-cell sequencing data suggested that MEF2A was highly expressed in microglia. Methylation microarray analysis showed that the methylation level of the enhancer region of MEF2A in AD was significantly increased. In conclusion, our results suggest that AD related to the increased methylation level of MEF2A enhancer reduces the expression of MEF2A and downregulates the expression of autophagy-related genes which are closely associated with AD pathogenesis, thereby inhibiting autophagy.

Keywords: Alzheimer's disease, autophagy, MEF2A, microglia, enhancer, methylation

OPEN ACCESS

Edited by:
Manoj Kumar Jaiswal,
Icahn School of Medicine at Mount Sinai, United States

Reviewed by:
Rocío Ruiz,
Seville University, Spain
Adele Woodhouse,
University of Tasmania, Australia
Johannes Schlachetzki,
University of California, San Diego, United States
Serge Rivest,
Laval University, Canada

***Correspondence:**
Yugang Jiang
jyg1967@126.com

Specialty section:
This article was submitted to Neurodegeneration, a section of the journal Frontiers in Neuroscience

Received: *18 March 2021*
Accepted: *12 May 2021*
Published: *16 June 2021*

Citation:
Li H, Wang F, Guo X and Jiang Y (2021) Decreased MEF2A Expression Regulated by Its Enhancer Methylation Inhibits Autophagy and May Play an Important Role in the Progression of Alzheimer's Disease. Front. Neurosci. 15:682247. doi: 10.3389/fnins.2021.682247

INTRODUCTION

With an increasing aging population, the prevalence of cognitive impairment and neurodegenerative disease has increased. Alzheimer's disease (AD), the most common form of dementia, is characterized by progressive cognitive impairment and behavioral disorders. The main pathological features of AD are amyloid plaque deposition and neurofibrillary tangles (NFTs),

Abbreviations: AD, Alzheimer's disease; NFT, neurofibrillary tangle; CDR, clinical dementia rating; PLQ_Mn, average of neuritic plaque counts; NPrSum, sum of scores for all cortical regions examined neuropathologically; snRNA-seq, single-nucleus RNA-seq; NTrSum, sum of semiquantitative NFT density ratings for all cortical regions examined; PPI, protein-protein interaction; ANOVA, analysis of variance; LSD, least significant difference; WGCNA, weighted correlation network analysis; SEs, super enhancers; DMPs, differentially methylated positions; DEGs, differentially expressed genes; MEF2A, myocyte enhancer factor 2A.

which are neurotoxic and cause neuronal loss, synapse reduction, neurological degeneration, and brain atrophy. Pathological studies have demonstrated that NFTs and amyloid plaque deposition initially occurred in the cortical and hippocampal tissues of AD and subsequently spread to the whole brain (Braak and Braak, 1995). Inhibiting neurotoxicity by reducing amyloid plaque deposition and NFTs has been unsuccessfully attempted (Doody et al., 2013; Ostrowitzki et al., 2017).

Autophagy consists of a series of complex physiological processes in cells, which can eliminate misfolded proteins and damaged organelles, promote the synthesis of biofilms and transport of vesicles, and thus play a key role in reshaping the cell structure and regulating energy metabolism, resisting adverse external stimuli and stabilizing cell homeostasis. Autophagy disorders are closely related to AD (Nixon et al., 2005). Inhibiting lysosomal proteolysis produces similar neuropathological manifestations in wild-type mice and exacerbates amyloid plaque deposition and autophagy pathology in mouse models of AD (Nixon and Yang, 2011). Presenilin 1 mutations, associated with familial AD, result in decreased maturation of the lysosomal v-ATPase and, thus, directly increased lysosomal pH and impaired lysosome function, which would be predicted to reduce autophagosome clearance (Lee et al., 2010). Another genetic risk factor for AD is mutations in apolipoprotein E 4 (ApoE4). ApoE4 destabilizes lysosomal membranes in an allele-specific manner. Other factors include reactive oxygen species and amyloid plaque and oxidized lipids and lipoproteins, which also contribute to AD by impeding lysosomal proteolysis, damaging lysosomal membranes, and disrupting lysosomal integrity, thereby releasing proteases that can mediate neuronal cell death (Boya and Kroemer, 2008; Nixon, 2013). Moreover, a study found that autophagy inducers such as rapamycin in 3xTg-AD mice can effectively reduce the deposition of amyloid plaques in the brain and improve cognitive performance (Majumder et al., 2011). However, the relationships between the pathological progression of AD and autophagy-related genes remain unclear, and the mechanisms have not been elucidated.

Systems biology concepts and methods provide multivariate approaches to holistically analyze the larger interactive network of biological pathways and identify important players in AD onset and progression. In this study, multiple datasets were downloaded, and bioinformatics methods were used to analyze the correlation between autophagy-related genes and pathological progression of AD, assessing the reasons for their differential expression, thereby providing new clues for elucidating the mechanism of AD.

MATERIALS AND METHODS

Data Sources

Five gene expression profiles of mRNA, one DNA methylation profile, and related clinical data of AD were downloaded from the Gene Expression Omnibus database[1] (**Table 1**). The workflow is represented in **Figure 1**.

[1]http://www.ncbi.nlm.nih.gov/geo/

TABLE 1 | Data sources.

Series ID	Platform ID	Samples	Groups	Regions	Species	Cell types	Reference	Type
GSE84422	GPL96/97/570	1,053	Definite AD (328) Healthy controls (214) Possible AD (229) Probable AD (180)	19 cortical regions	*Homo sapiens*	Mixed cells	PMID: 27799057	Expression profiling by array
GSE122063	GPL16699	31	AD (12) Vascular dementia (8) Healthy controls (11)	Frontal and temporal cortex	*Homo sapiens*	Mixed cells	PMID: 30990880	Expression profiling by array
GSE118553	GPL10558	401	AD (167) AsymAD (134) Healthy controls (100)	Entorhinal cortex, temporal cortex, frontal cortex, and cerebellum brain region	*Homo sapiens*	Mixed cells	PMID: 31063847	Expression profiling by array
GSE132903	GPL10558	195	AD (97) Healthy controls (98)	Middle temporal gyrus	*Homo sapiens*	Mixed cells	PMID: 31256118	Expression profiling by array
GSE80970	GPL13534	147	AD (74) Healthy controls (69)	Superior temporal gyrus and prefrontal cortex	*Homo sapiens*	Mixed cells	PMID: 29550519	Methylation profiling by genome tiling array
GSE62420	GPL11180	56	4 months (24) 12 months (16) 22 months (16)	Cerebellum, cortex, hippocampus, and striatum	*Mus musculus*	Microglia	PMID: 26780511	Expression profiling by array
GSE138852	GPL18573	16	AD (8) Healthy controls (8)	Entorhinal cortex	*Homo sapiens*	Mixed cells	PMID: 31768052	Single nuclei RNA sequencing

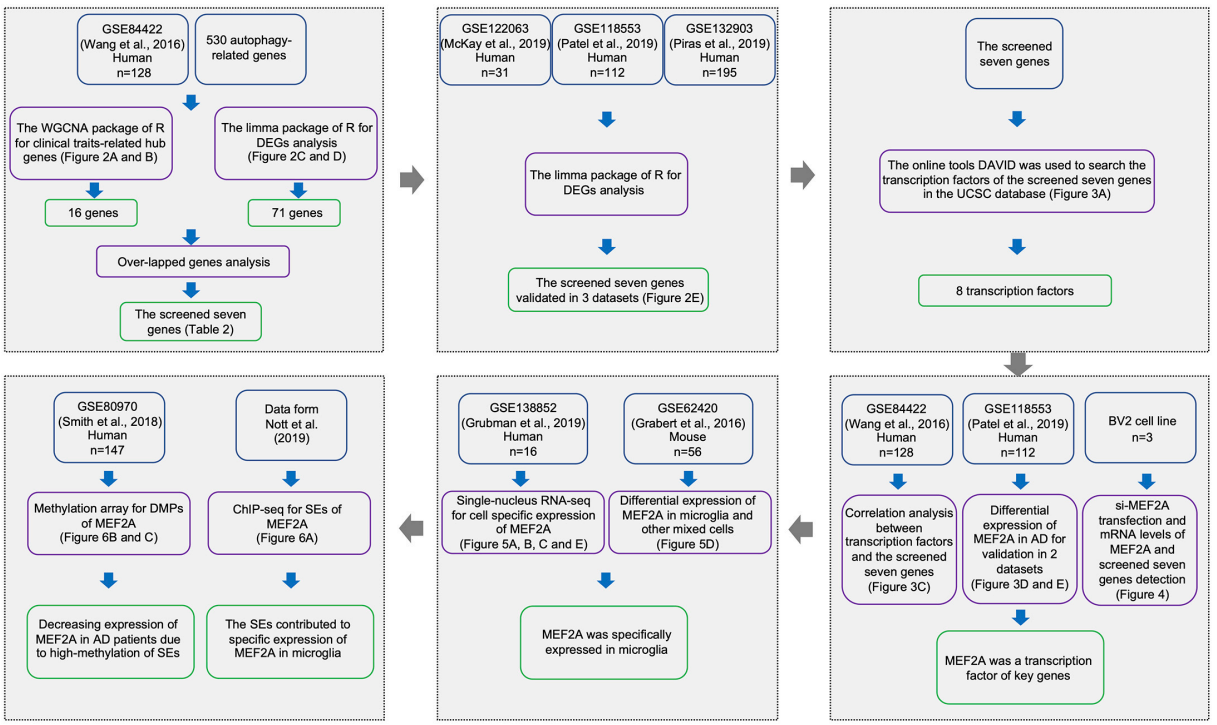

FIGURE 1 | Workflow of sample procedures. The samples and data sources are shown in blue boxes, methods for data processing are shown in purple boxes, and results are shown in green boxes.

GSE84422 (Wang et al., 2016) was used to perform a weighted correlation network analysis (WGCNA), which consisted of 1,053 postmortem brain samples across 19 brain regions from 125 participants dying of varying severities of dementia and variable AD-neuropathology severities, including clinical dementia rating (CDR), Braak NFT score (Braak), CERAD diagnoses and ratings of pathology (CERAD), average of neuritic plaque counts in five cardinal cortical regions (PLQ_Mn), sum of CERAD semiquantitative rating scores for all cortical regions examined neuropathologically (NPrSum), and sum of semiquantitative NFT density ratings for all cortical regions examined (NTrSum). GSE84422, GSE122063 (McKay et al., 2019), GSE118553 (Patel et al., 2019), and GSE132903 (Piras et al., 2019) were used to screen and validate differentially expressed genes (DEGs). GSE122063 includes frontal and temporal cortical samples from vascular dementia (n = 8), AD (n = 12), and healthy controls (n = 11). GSE118553 includes 401 human brain samples (entorhinal cortex, temporal cortex, frontal cortex, and cerebellum brain region) from 100 healthy controls, 134 asymptomatic AD (AsymAD), and 167 AD participants. Samples of GSE132903 consisted of middle temporal gyrus between AD (n = 97) and healthy controls (n = 98). GSE62420 (Grabert et al., 2016) was used to validate differentially expressed myocyte enhancer factor 2A (MEF2A).

The mRNA expression levels in GSE84422, GSE118553, GSE132903, and GSE62420 were measured using Illumina HumanHT-12 V4.0 expression beadchip, and the mRNA expression levels in GSE122063 were measured using Agilent-039494 SurePrint G3 Human GE v2 8 × 60K Microarray 039381.

GSE80970 (Smith et al., 2018) contained prefrontal cortex and superior temporal gyrus tissue from 147 participants with varying levels of AD pathology. DNA modifications for these samples were quantified using the Illumina Infinium Human 450K Methylation Array.

Single-nucleus RNA-seq (snRNA-seq), GSE138852 (Grubman et al., 2019), on the entorhinal cortex from control and AD brains of 16 participants, yielding a total of 13,214 high-quality nuclei, were used to check the gene expression distributions across cells in Alzheimer's disease brains.

In GSE62420, brains of 4-, 12-, and 22-month-old C57Bl/6J mice were collected and dissected into four regions: cerebellum, cortex, hippocampus, and striatum. Microglia were extracted from each region using a magnetic bead-based approach. Total RNA was immediately isolated for purified microglia and stored (−80°C) until performing microarray analysis of purified microglia and regional brain homogenates (n = 56).

The autophagy gene list with a total of 530 autophagy-related genes was derived from the Gene Ontology with the term "autophagy" (GO: 0006914) in the Homo sapiens organism.

Weighted Gene Coexpression Network Analysis

We extracted the autophagy genes to perform WGCNA with expression data retrieved from GSE84422 (Wang et al., 2016)

microarray data. The R package "WGCNA" was applied to find clinical trait-related modules and hub genes among them as previously described (Zhang et al., 2014). The adjacency matrix was transformed into topological overlap matrix. According to the topological overlap matrix-based dissimilarity measure, genes were divided into different gene modules. Herein, we set soft-thresholding power as 6 (scale free $R^2 = 0.85$), cut height as 0.25, and minimal module size as 10 to identify key modules. The module with the highest correlation with clinical traits (age, sex, race, PIM, pH, CDR, Braak, CERAD, PLQ_Mn, NPrSum, and NTrSum) was selected to explore its biological function through gene ontology (GO) analyses and to screen hub genes. Hub genes were defined as those with gene significance > 0.3 and module membership > 0.8.

Differential Expression Analysis

For the microarray differential expression analyses of GSE84422 (Wang et al., 2016), robust multichip average (RMA) was used for background correction of raw gene expression matrixes, then $\log_2$ transformation of expression matrixes. The "affy" R package was used for quantile normalization and median polish algorithm summarization. Next, all gene probes were mapped into gene symbols by the affymetrix annotation files. The "limma" (linear models for microarray data) R package was performed for identifying DEGs between definite AD samples and healthy controls, and the results were visualized using the volcano plot and heat map. Cutoff criteria for screening DEGs were $p < 0.05$ and $|\log2\text{fold change}| \geq 1.3$. The screened seven genes were obtained by taking the intersection of the DEGs of GSE84422 and hub genes related to pathological progression of AD from WGCNA. The differential expression analyses were performed in GSE84422, GSE122063 (McKay et al., 2019), GSE118553 (Patel et al., 2019), and GSE132903 (Piras et al., 2019) datasets and log2fold changes in the screened seven genes and significantly differences (AD versus control expression levels) were represented with the corresponding bar plot.

Transcription Factors Enrichment

To shed further light on the functions of the candidate genes, DAVID online tools (Huang et al., 2009; Wishart et al., 2009) in the UCSC database were used for transcription factor annotations. The motif matrix profile MA0052.4 of MEF2A was downloaded from JASPAR Fornes et al. (2020), and Find Individual Motif Occurrences (FIMO, Grant et al., 2011) of motif-based sequence analysis tools (MEME suite 5.3.3, Bailey et al., 2009) was used to scan sequences of candidate genes for individual matches to the motif of MEF2A. The positions and sequences of the screened seven genes were inquired in UCSC, and promoters were defined as the 2,000-bp window centered on the transcript start site of genes.

Correlation Analysis

Correlations between each transcription factor and the expression of downstream genes were analyzed (Pearson's correlation) in GSE84422 (Wang et al., 2016), and result was represented with a heatmap. The correlation between MEF2A and the screened seven genes was validated (Pearson's correlation) in GSE118553 (Patel et al., 2019), and result was represented with scatter plots. MEF2A mRNA expression levels (signal intensity) in different groups in GSE84422 and GSE118553 were shown, and p-values were calculated using GraphPad. In GSE84422, three groups (control, definite AD, possible AD) were classified according to neuropathology category as measured by CERAD (to unify the results, we combined the diagnosis of possible AD and probe AD into possible AD). In GSE118553, participants in the control group were classified as showing no clinical sign of any form of dementia and no neuropathological evidence of neurodegeneration. Participants in the AsymAD group were defined as clinically dementia free at the time of death, but neuropathological assessment at autopsy revealed hallmark AD pathology. Participants in the AD group had both a clinical diagnosis of AD at death and received confirmation of this diagnosis through neuropathological evaluation at autopsy. A one-way analysis of variance (ANOVA) followed by a least significant difference (LSD) test was used for comparison among groups.

snRNA-Seq Data Analysis

Single-nucleus RNA-seq data were downloaded from the website[2] as described by Grubman et al. (2019). We then analyzed the expression of MEF2A in different cell types and different groups. The MEF2A mRNA expression levels (logCounts) in different cell types were represented and significant differences (compared with microglia) were calculated using GraphPad. The expression of MEF2A and screened seven genes (logCounts) in different groups were represented using the ggplot2 package in the R software and significant differences (AD versus control expression levels) were calculated using GraphPad. Following the standardization of GSE62420 (Grabert et al., 2016) microarray data, the signal intensity of MEF2A in microglia and other mixed cell types were shown and significant differences (compared with microglia) were calculated using GraphPad.

Methylation Array Data Analysis

The ChAMP package in R software (Tian et al., 2017) was used to analyze the differentially methylated positions (DMPs), and the screening condition yielded a value of $p < 0.05$. The DMPs range around MEF2A (from the last gene to the next gene) was approximately 99,676,703–100,882,647 bp of chromosome 15, and the coMET package of the R software (Martin et al., 2015) was used to create a Manhattan plot with a threshold value of $p = 0.05$. These DMPs were annotated by UCSC, and the means of CpG methylation levels in different groups were represented in a violin plot in the enhancers.

Super Enhancers and Chromatin Interaction Analysis

The super enhancer (SE) analyses, as Nott et al. (2019) described, were performed in UCSC. The ATAC-seq, H3K27ac

[2]http://adsn.ddnetbio.com

and H3K4me3 ChIP-seq, and PLAC-seq in all types of cells in the 99,950,000–100,200,000-bp section of chromosome 15 were queried, and the original images were downloaded.

Cell Culture

The mouse microglia cells (BV2), obtained from the Cell Resource Center, Peking Union Medical College (China), were cultured in Dulbecco's modified Eagle's medium (DMEM, Gibco, United States) with 10% fetal bovine serum (Gibco, United States) in 5% CO_2 at 37°C. For *in vitro* transfection ($n = 3$), the target and control siRNA (GenePharma Co., Ltd., China) were transfected into BV2 cells using Lipofectamine 2000 (Invitrogen, United States) according to the manufacturer's guidelines. Cells were collected 48 h after transfection. The siRNA sequences were listed (**Table 2**).

Quantitative Real-Time PCR

Total RNA was extracted using TRIzol® Reagent (Life Technologies, Grand Island, NY, United States) and reverse transcribed into cDNA using PrimeScript™ II 1st Strand cDNA Synthesis Kit for qPCR (TaKaRa, Tokyo, Japan) according to the manufacturer's instructions. Quantitative real-time PCR was performed to detect the gene mRNA levels using 2 × Universal SYBR Green Fast qPCR Mix (ABclonal, Wuhan, China). Primers were synthesized by Sangon (Sangon Biotech Co., Ltd., Shanghai, China). The qPCR conditions were as follows: 95°C for 3 min and 40 cycles of 95°C for 5 s and 60°C for 30 s. Melting curves were tested to assess the accuracy of the PCR analysis. The $2^{-\Delta\Delta Ct}$ was calculated to analyze the gene expression levels: ΔCt = Ct (target gene) - Ct (β-actin gene), ΔΔCt = ΔCt (treatment) - ΔCt (control). The primer sequences were listed (**Table 3**).

TABLE 2 | The siRNA sequences of MEF2A.

siRNA	Sequences	
	Sense (5′-3′)	Antisense (5′-3′)
si-MEF2A-1	GUGGCAGUCUUGGAAUGAATT	UUCAUUCCAAGACUGCCACTT
si-MEF2A-2	CAGCCACGCUACAUAGAAATT	UUUCUAUGUAGCGUGGCUGTT
si-MEF2A-3	GCUCUAAUAAGCUGUUUCATT	UGAAACAGCUUAUUAGAGCTT
Negative control	UUCUCCGAACGUGUCACGUTT	ACGUGACACGUUCGGAGAATT

TABLE 3 | The primer sequences of MEF2A and the screened seven genes.

Genes	Sequences	
	Forward	Reverse
MEF2A	CAGGTGGTGGCAGTCTTGG	TGCTTATCCTTTGGGCATTCAA
BNIP3	TCCTGGGTAGAACTGCACTTC	GCTGGGCATCCAACAGTATTT
CDK5R1-F	CTGTCCCTATCCCCCAGCTAT	GGCAGCACCGAGATGATGG
HERC1-F	TATAACCTGGAACCCTGTGAACC	TCATGTCGCTTGATGCTCTGT
ITPR1-F	CGTTTTGAGTTTGAAGGCGTTT	CATCTTGCGCCAATTCCCG
OPTN-F	TCACAGGTGGCTACAGGTATC	CCGGAGTTGAGTTTGAGCTG
UBQLN2-F	GCCGAGCCCAAAATCATCAAA	ATCTTTCCGGCGAAAATCAGC
USP33-F	GAGGTTTGTTGTCTCATGTGTCC	GTTCATCTCTGGCGAAGAAGG

Statistical Analysis Software

RStudio (version 3.6.2) was used for data processing, GraphPad (version 8.0) was used for the calculation of significance and means of the differences, and Adobe Illustrator 2020 (version 24.0.1) was used for image processing.

RESULTS

WGCNA and Differential Expression Analysis Were Used to Determine Hub Genes Related to AD Clinical Phenotypes

To assess the relationship between gene expression and clinical phenotypes of AD, dataset GSE84422 (Wang et al., 2016) were downloaded and the WGCNA package, which can cluster genes and divide them into different modules and associate the genes of each module with the clinical phenotypes, was used to cluster autophagy genes and divide them into 11 hub gene modules with different module colors, according to the gene expression correlation patterns (**Figure 2B**). The correlation between each module and clinical phenotypes was calculated (**Figure 2A**). In the MEblack module, 16 genes included were negatively correlated with CDR, CERAD, PLQ_Mn, NPrSum, and NTrSum ($p < 0.05$), especially, the correlation with the CERAD was the most significant. The MEgreen module was negatively correlated with CDR, Braak, CERAD, PLQ_Mn, and NTrSum ($p < 0.05$); the MEturquoise module was negatively correlated with CDR, CERAD, and NTrSum ($p < 0.05$); the MEred module was negatively correlated with NTrSum ($p < 0.05$); the MEblue module was negatively correlated with CDR, CERAD, PLQ_Mn, and NPrSum ($p < 0.05$); besides, gene expression levels in the MEgrey module were positively correlated with age ($p < 0.05$).

To investigate whether the expression levels of autophagy-related genes were different between healthy controls and AD, we used the limma package to analyze differential expression of autophagy-related genes in definite AD and healthy controls in dataset GSE84422, and then screened 71 DEGs shown in a heatmap (**Figure 2C**). Compared with healthy controls, the expression of autophagy genes in AD was mostly reduced (69 genes) and only two genes were increased (**Figure 2D**). The autophagy-related genes of AD were inhibited, suggesting that their autophagy function was lower than that of healthy controls.

Seven genes were screened by taking the intersection of the autophagy-related genes with significant differences and the black module hub genes with strong correlation with pathological progression of AD screened by WGCNA (**Table 4**). Validating the multiple differences of the screened seven genes (**Figure 2E**), we found that compared with the control group, all screened seven genes showed a significant decrease in the AD group in GSE118553 (Patel et al., 2019; $p < 0.05$); six genes showed a significant decrease in the AD group in GSE132903 (Piras et al., 2019; $p < 0.05$); four genes showed a significant decrease in the AD group in GSE122063 (McKay et al., 2019; $p < 0.05$).

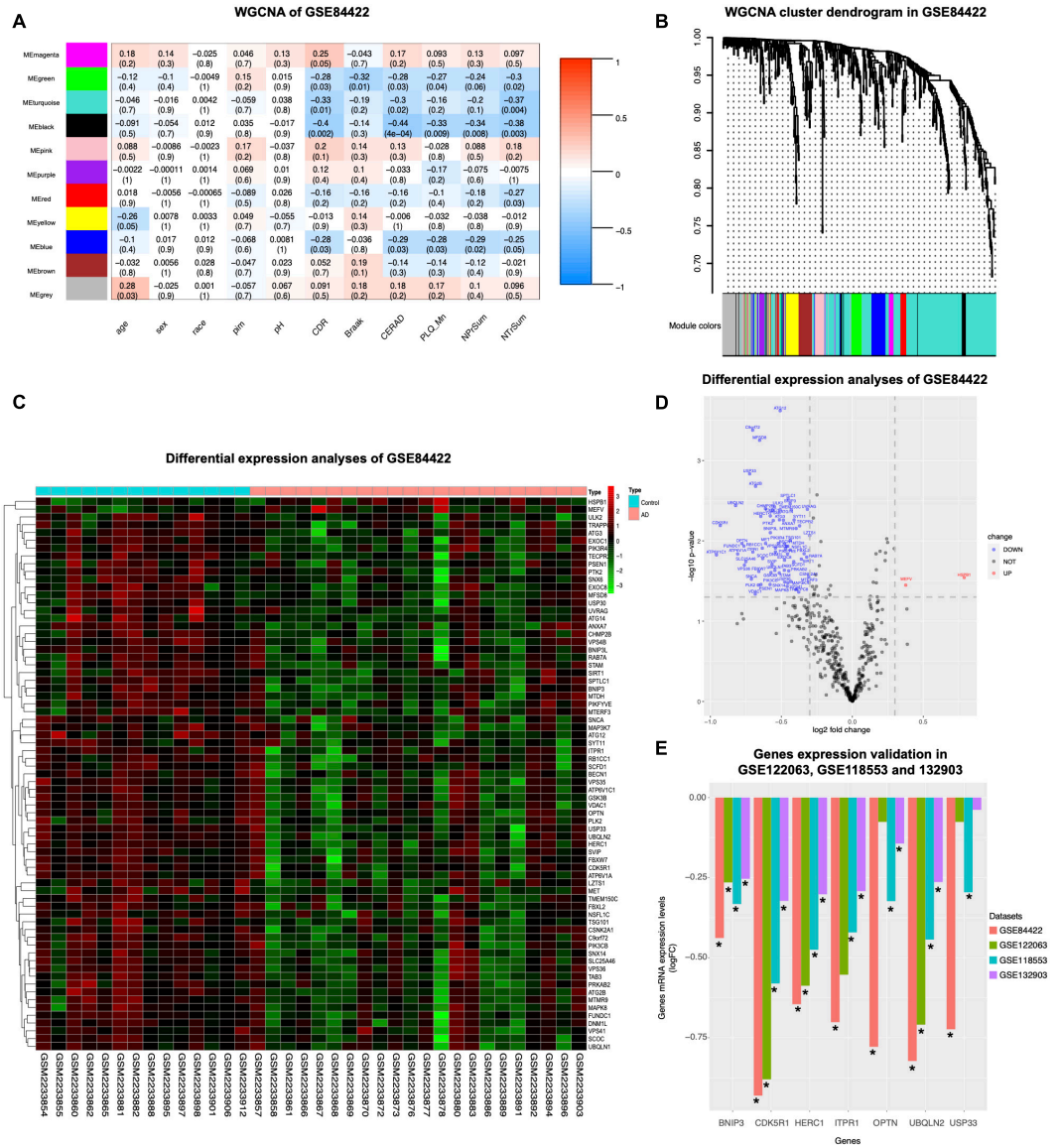

FIGURE 2 | WGCNA coexpression analysis and differential expression analysis. GSE84422 (Wang et al., 2016) was used to perform WGCNA. **(A)** The correlation between each module and clinical phenotypes is shown, including 11 modules and 11 clinical phenotypes. In each unit, the numbers above show the correlation, and the numbers below show the *p*-value. Abbreviations: CDR, clinical dementia rating; Braak, Braak NFT score; CERAD, CERAD diagnoses and ratings of pathology; PLQ_Mn, average of neuritic plaque counts in five cardinal cortical regions; NPrSum, sum of CERAD semiquantitative rating scores for all cortical regions examined neuropathologically; NTrSum, sum of semiquantitative NFT density ratings for all cortical regions examined. **(B)** Cluster dendrogram of the coexpression network modules was produced based on the autophagy genes, including 11 modules. **(C)** DEGs in healthy control and AD in GSE84422 were shown in the heatmap. Cut-off criteria for screening DEGs were $p < 0.05$ and $|\log2\text{fold change}| \geq 1.3$. **(D)** Autophagy genes with significantly different expression in GSE84422 were shown in the volcano plot. Red spots indicate upregulated genes, and blue spots indicate downregulated genes. Cut-off criteria for screening DEGs were $p < 0.05$ and $|\log2\text{fold change}| \geq 1.3$. **(E)** Validation of the gene expression levels of BNIP3, CDK5R1, HERC1, ITPR1, OPTN, UBQLN2, and USP33 between healthy control and AD was shown in three other datasets, GSE122063 (McKay et al., 2019), GSE118553 (Patel et al., 2019), and GSE132903 (Piras et al., 2019). Y-axes in the left indicate log2fold change of the screened seven genes in each dataset. Significant differences (AD versus control expression levels) were performed, $^*p < 0.05$ compared with the control group.

MEF2A Expression Is Related to the Screened Seven Genes and AD Neuropathological Category

The online annotation website DAVID was used to perform transcription factor analysis for 71 DEGs and 16 genes in the black module (total 80 genes) in the UCSC database. The result showed that 18 transcription factors were identified by enrichment analysis of 80 genes ($p < 0.05$), including 73 genes enriched in organic cation transporter 1 (OCT1), 66 genes enriched in Ecotropic Virus Integration Site 1 (EVI1),

TABLE 4 | The expression of autophagy-related genes with significant differences in black module.

Gene symbol	Entrez ID	Gene name	logFC	*p*-value
CDK5R1	8851	Cyclin-dependent kinase 5 regulatory subunit 1	−0.9307557	0.0064305
UBQLN2	29978	Ubiquilin 2	−0.8225799	0.0036374
OPTN	10133	Optineurin	−0.7782243	0.0107843
USP33	23032	Ubiquitin-specific peptidase 33	−0.7235492	0.0014619
ITPR1	3708	Inositol 1,4,5-trisphosphate receptor type 1	−0.7013134	0.0137605
HERC1	8925	HECT and RLD domain containing E3 ubiquitin protein ligase family member 1	−0.6453281	0.0049519
BNIP3	664	BCL2 interacting protein 3	−0.4385456	0.0034525

and 65 genes enriched in MEF2 (**Supplementary Figure 1**). This data suggested that these 18 transcription factors were likely to play important roles in the regulation of autophagy genes in AD. To further investigate the autophagy genes with differences and related to pathological progression of AD, the screened seven genes were annotated by DAVID, revealing that the screened seven genes were regulated by transcription factors MEF2A and CUX1 (**Figure 3A**). Transcription factors can specifically bind to target motifs to regulate the expression of downstream genes; therefore, the expression of transcription factors was consistent with the expression of downstream genes. We analyzed the correlation between transcription factors and the expression of the screened seven genes obtained from the query of the UCSC database in GSE84422 (Wang et al., 2016; **Figure 3C**). Among them, the expression of MEF2A was most correlated to the screened seven genes. The motifs of the screened seven genes matched to MEF2A ($p < 0.001$) were scanned by MEME tools (described in Methods section "Transcription Factors Enrichment") and were shown in UCSC (**Figure 3B**). The correlation between transcription factors and the expression of the screened seven genes were validated in GSE118553 (Patel et al., 2019; **Supplementary Figure 2**). These results showed that MEF2A had the strongest correlation with the screened seven genes, so that we selected MEF2A for further study.

We downloaded dataset GSE84422 and extracted the mRNA expression data of MEF2A, and then compared different neuropathological categories of the sample (**Figure 3D**) and found no significant difference in the possible AD group compared with the control group; in addition, the definite AD group showed a significant difference ($p < 0.05$). The expression of MEF2A in the control group was the highest, followed by the possible AD group, and finally the definite AD group. To validate our results, another dataset GSE118553 was used (**Figure 3E**). The MEF2A expression levels were significantly lower in the AD group than in the control group ($p < 0.05$) in different brain regions (entorhinal cortex, frontal cortex, and temporal cortex), except for the cerebellum, while AsymAD revealed no significant difference ($p > 0.05$) compared with control.

In our experiment, to verify the relationship between MEF2A and the screened seven genes, three siRNA were transfected into BV2 cells to knock down the expression of MEF2A, and the mRNA levels of the seven autophagy-related genes were detected using qPCR (**Figure 4**). These results showed that most of the screened seven genes were significantly decreased following siRNA transfection ($p < 0.05$), suggesting that the expression of the screened seven genes was influenced by MEF2A.

MEF2A Expression Is Cell Type Specific and Mainly Concentrated in Microglia

The brain contains different cell types, which are responsible for different physiological processes. Therefore, transcriptome sequencing of different subgroups of cells can reflect the functions of different types of cells. Grubman et al. (2019) performed single-cell sequencing on the entorhinal cortex of participants with AD and healthy controls, and the cells with different types of markers were clearly divided into eight subgroups (**Figure 5A**). The expression levels of MEF2A detected in microglia were significantly higher than those in other subgroups (**Figure 5B**). The single-cell sequencing dataset, GSE138852 (Grubman et al., 2019), showed that the expression of MEF2A in microglia was significantly ($p < 0.05$) higher than that in other subgroups (**Figure 5C**), validating the above results. Furthermore, the expression levels of MEF2A in AD were significantly ($p < 0.05$) higher than that in healthy controls in microglia, doublet, oligodendrocyte, and oligodendrocyte progenitor cells (OPC, **Figure 5E**). Besides, there were no significant difference between AD and healthy controls of the screened seven genes in microglia ($p > 0.05$, **Supplementary Figure 3**).

In another dataset, GSE62420 (Grabert et al., 2016), microglia from mouse brain tissue were purified according to specific markers, and gene expression was measured. We downloaded the expression matrix and screened the expression levels of MEF2A in each tissue and found that MEF2A was significantly ($p < 0.05$) upregulated in microglia compared with mixed brain cells across different brain regions (**Figure 5D**). These results suggested that the expression of MEF2A in brain tissue was cell type specific, and the expression of MEF2A in microglia was significantly higher than that in other cells.

Enhancer Region Methylation Regulates MEF2A Expression

We then assessed whether epigenetic regulation could alter the expression of MEF2A because both the pathological progression of AD and tissue specificity could change it. SEs are important gene control elements composed of a series of enhancers. We analyzed datasets involved in the interactions between SEs and promoters of different cell types in brain tissue previously

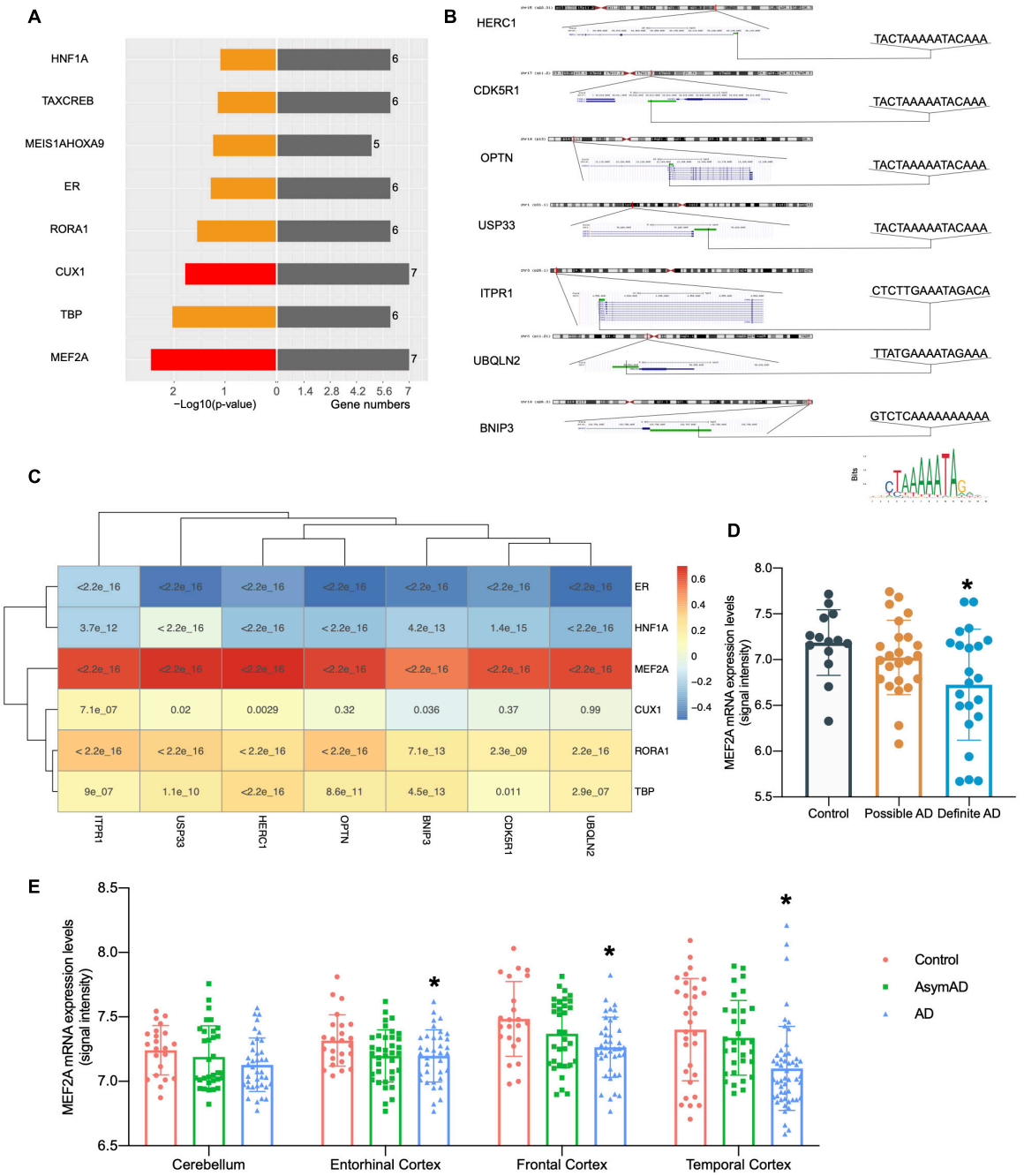

FIGURE 3 | Relationship between MEF2A expression and the screened seven genes. **(A)** Transcription factors were investigated from the UCSC database with online annotation website DAVID; transcription factors correlated with all the screened seven genes are indicated in red. In the left section, -log10(*p*-value) values are shown, and gene numbers enriched are shown in the right section. **(B)** The motifs of the screened seven genes matched to MEF2A ($p < 0.001$) were scanned by MEME tools (described in Methods section "Transcription Factors Enrichment") and were shown in UCSC. The positions and sequences of the screened seven genes were inquired in UCSC, and promoters (shown as green bar) were defined as the 2,000 bp window centered on the transcript start site of genes. The motif of MEF2A downloaded from JASPAR 2020 is shown on the bottom right. **(C)** Correlations between transcription factors and the expression levels of BNIP3, CDK5R1, HERC1, ITPR1, OPTN, UBQLN2, and USP33 were analyzed (Pearson's correlation) in the dataset GSE84422 (Wang et al., 2016) and was shown as the heatmap. **(D)** The dataset GSE84422 (Wang et al., 2016) was downloaded, and the mRNA expression (signal intensity) of MEF2A in different neuropathological category of sample (possible AD group, control group, and the definite AD group) were shown using GraphPad. ANOVA followed by LSD test was used for comparison among groups. *$p < 0.05$ compared with the control group. **(E)** The dataset GSE118553 (Patel et al., 2019) was downloaded and the mRNA expression (signal intensity) of MEF2A in different groups (AD, AsymAD, and control group) and brain regions of sample (cerebellum, entorhinal cortex, the frontal cortex and temporal cortex) were shown using GraphPad. An ANOVA followed by an LSD test was used for comparison among groups. *$p < 0.05$ compared with the control group.

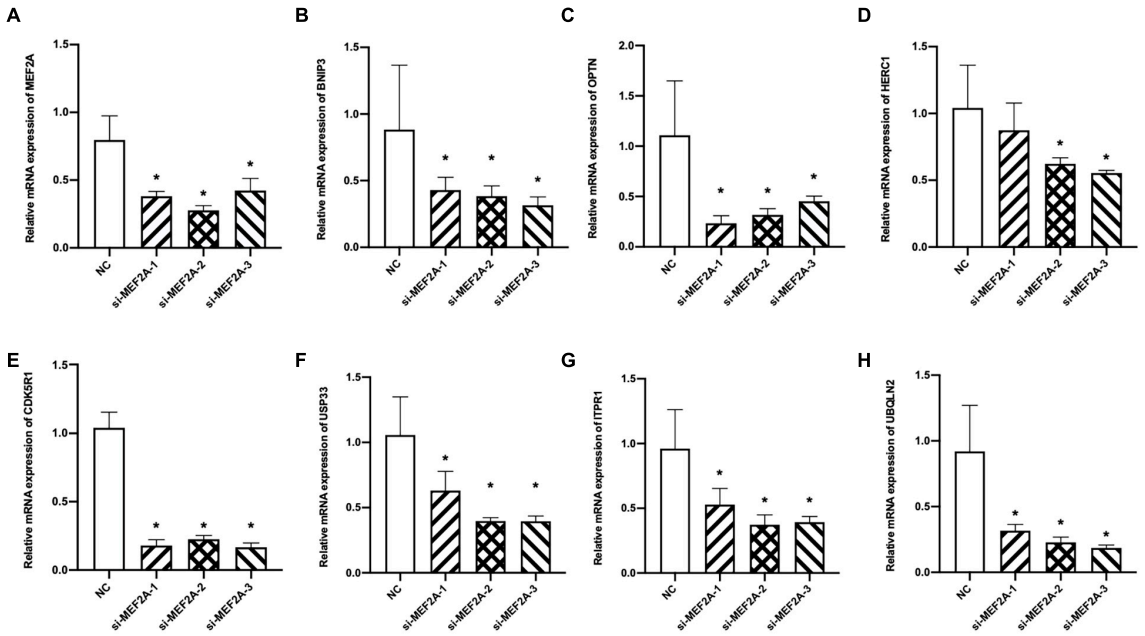

FIGURE 4 | Expression levels of the screened seven genes after si-MEF2A transfection. **(A–H)** After BV2 cells transfected with three si-MEF2A for 48 h to knock down the expression of MEF2A, the expression levels of MEF2A, BNIP3, CDK5R1, HERC1, ITPR1, OPTN, UBQLN2, and USP33 were detected using qPCR. ANOVA followed by LSD test was used for comparison among groups. *$p < 0.05$ compared with the control group.

published in Nott et al. (2019). We found that ATAC-seq, H3K27ac, and H3K4me3 ChIP-seq showed significant peaks in the MEF2A promoter, with no cell type specificity. The H3K27ac ChIP-seq (a characteristic marker of enhancers and promoters) in microglia showed significant peaks in the MEF2A enhancers, but no significant peaks were observed in neurons or astrocytes. The PLAC-seq revealed a series of regions, mainly concentrated in microglia, which had a high degree of interaction with the promoter of MEF2A, suggesting only microglia had SEs (**Figure 6A**). Therefore, this suggested that the specific expression of MEF2A in microglia was due to the SEs, which promoted the expression of MEF2A.

We analyzed the DMPs in the dataset GSE80970 (Smith et al., 2018), and the results were shown in a Manhattan plot (**Figure 6B**). In the SEs region between MEF2A and LRRC28, there were eight DMPs which had methylation differences ($p < 0.05$) in AD compared with healthy controls. The methylation levels of SEs in participants with AD were significantly higher than that in healthy controls (**Figure 6C**, $p < 0.05$). This suggested that AD may lead to an increase in the methylation of the SE region of MEF2A, thereby reducing the mutual binding with the MEF2A promoter, leading to a decrease in the expression of MEF2A.

DISCUSSION

In this study, we used bioinformatics methods to investigate the relationship between autophagy-related genes and pathological progression of AD. We downloaded the datasets and identified the seven autophagy-related genes to be correlated with pathological progression of AD using WGCNA. A correlation analysis showed that MEF2A, a transcription factor enriched in UCSC database, was closely related to the screened seven genes. Furthermore, MEF2A was highly expressed in microglia due to the existence of SEs, and the decreased expression of MEF2A in AD was caused by the increased methylation of the SEs.

As a chronic neurodegenerative disease, AD has been found to be closely related to autophagy, given that autophagy-related pathology including accumulated autophagic vacuoles (AVs) were found in a number of dystrophic neurites in AD (Nixon and Yang, 2011). Through live-imaging studies of cortical neurons, this study showed that the inhibition of lysosomal proteolysis could selectively disrupt the axonal transport of autophagy-related compartments, causing an AD-like axonal dystrophy. Our analysis of the array dataset showed that many genes related to autophagy were significantly decreased in AD and closely related to the pathological progression of AD. Among them, gene expression in MEblack module was most strongly associated with CDR, CERAD, PLQ_Mn, NPrSum, and NTrSum, which can reflect the pathology of AD. Thus, genes in MEblack module, including BNIP3, OPTN, CDK5R1, UBQLN2, ITPR1, USP33, and HERC1, were selected for further analysis.

Currently, many studies showed that age-related declines in cognitive fitness were associated with a reduction in autophagy (Hou et al., 2019). However, according to our results, age was positively related to autophagy gene expression in MEgrey module. This may be related to the fact that participants were all over the age of 60. This was consistent with the

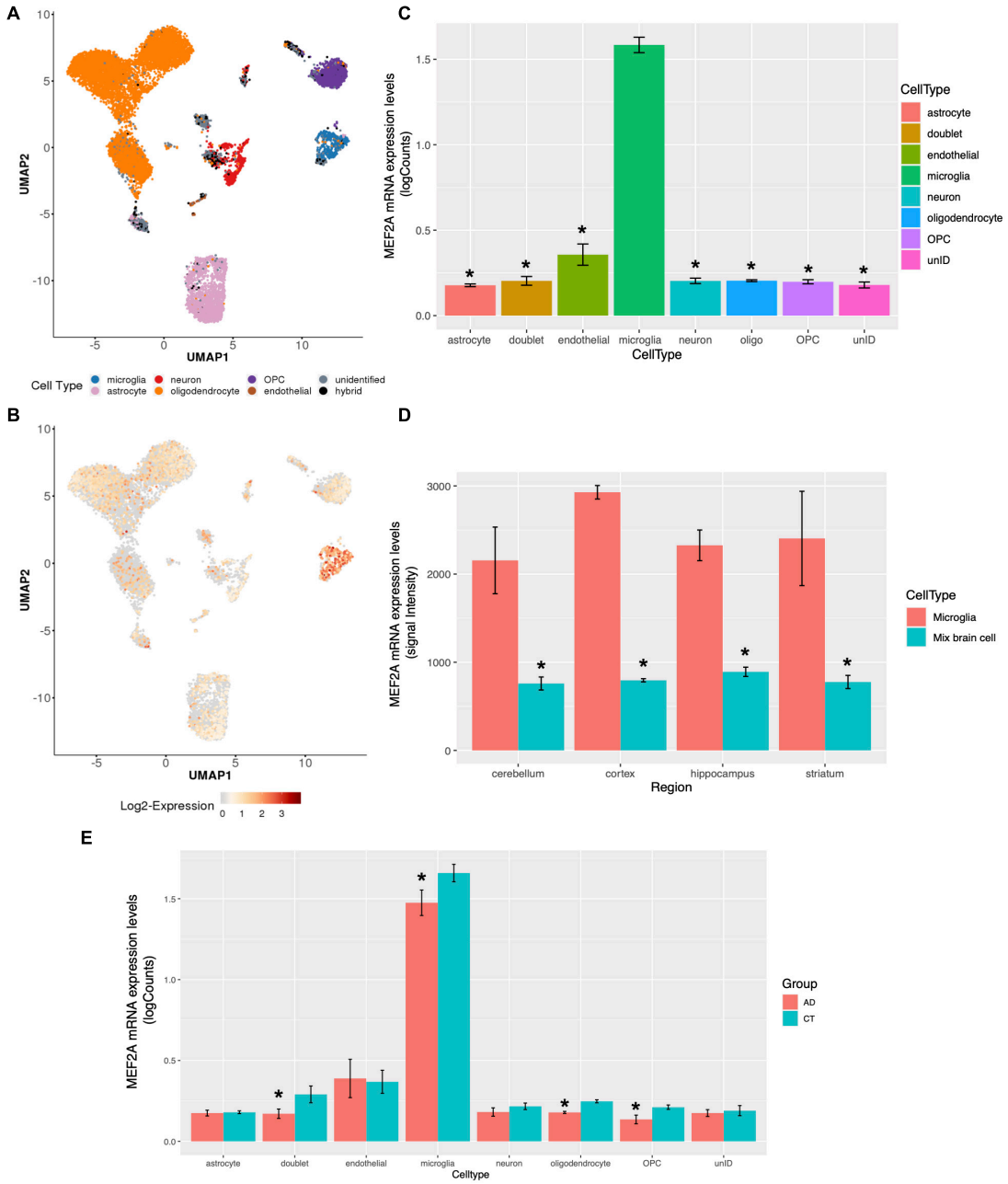

FIGURE 5 | MEF2A expression in brain tissue for different cell types. The snRNA-seq data of GSE138852 (Grubman et al., 2019) were downloaded, and the expression of MEF2A in different cell types were analyzed (A, B, C, E). **(A)** The PCA analysis for cells with different types of markers and cells were clearly divided into eight clusters. **(B)** The differential mRNA expression of MEF2A in each cell types are shown, and the red color indicates high expression. **(C)** The mRNA expression of MEF2A in different cell types was performed using GraphPad. An ANOVA followed by an LSD test were used for comparison among groups. *$p < 0.05$ compared with the microglia group. **(D)** The mRNA expression of MEF2A in microglia and in mixed brain cell from different brain regions in dataset GSE62420 (Grabert et al., 2016) were performed using GraphPad. An ANOVA followed by an LSD test was used for comparison among groups. *$p < 0.05$ compared with the microglia group. **(E)** The mRNA expression levels of MEF2A in AD and in healthy controls are shown. *t*-Test was performed for comparison between groups. *$p < 0.05$ compared with the control group.

report of Glatigny et al. (2019) which stated that autophagy was increased in many long-lived model organisms and contributed significantly to their longevity. The relationship between autophagy and longevity warrants further study.

For the genes in MEblack module, the functions of BNIP3, OPTN, and UBQLN2 are related to LC3 on the lysosomal membrane and participate in the fusion process between lysosomes and autophagosomes. BNIP3, a BH3-domain protein

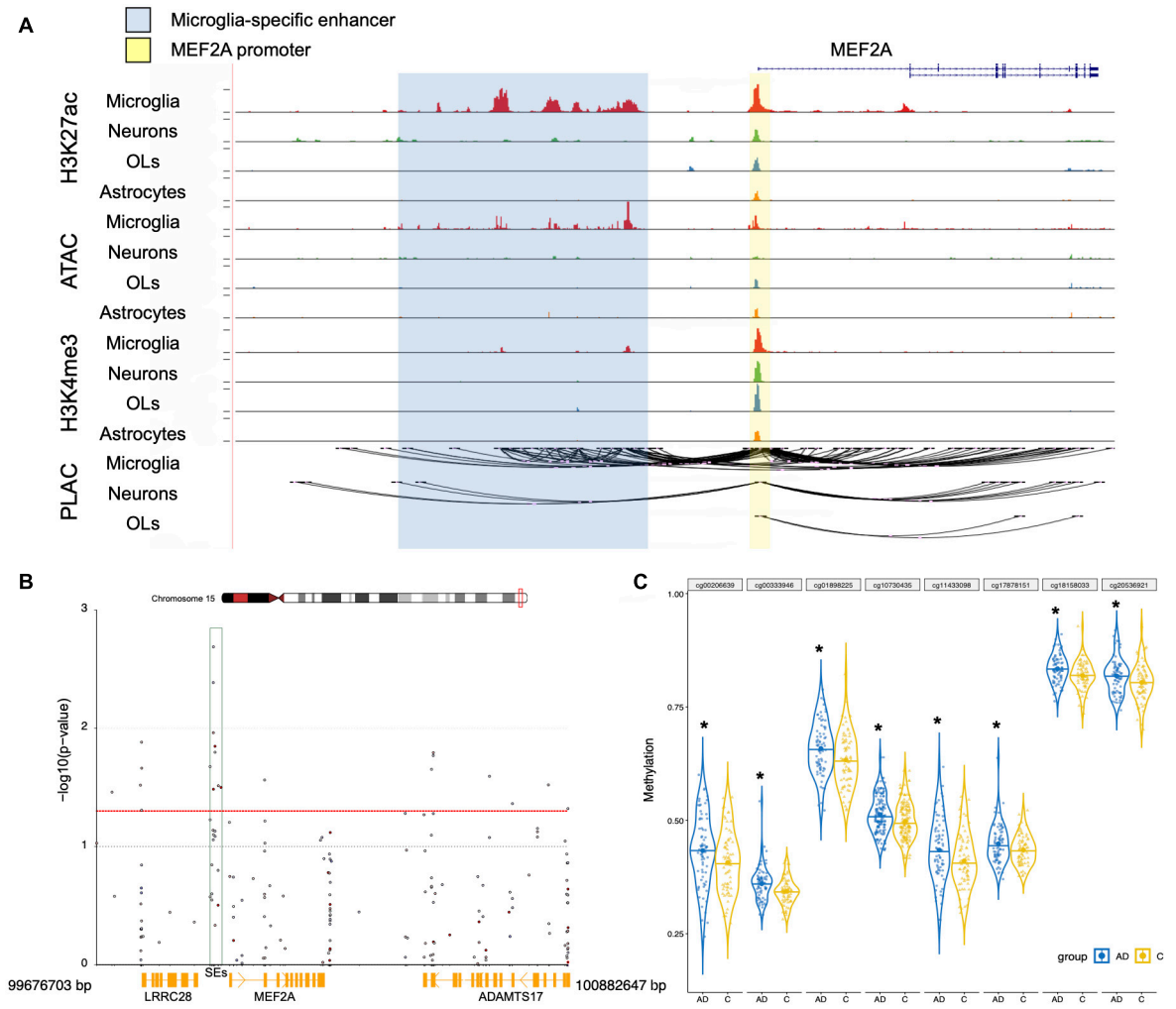

FIGURE 6 | Epigenetic regulation analysis of MEF2A expression. **(A)** UCSC browser of the MEF2A locus showed ATAC-seq, H3K27ac and H3K4me3 ChIP-seq, and PLAC-seq in brain cell types, including neurons, microglia, astrocytes, and oligodendrocytes (OLs). Shared active promoter region is indicated in yellow; microglia-specific enhancer region is indicated in blue. **(B)** The DMPs range around MEF2A, approximately 99,676,703–100,882,647 bp of chromosome 15, was used to create a Manhattan plot by coMET package of the R software with a threshold *p*-value of 0.05 (shown as red dotted line). The -log10(*p*-value) of DMPs for MEF2A in dataset GSE80970 (Smith et al., 2018) were shown in the Manhattan plot. The SEs region is shown as a green box. **(C)** The methylation levels for eight DMPs of the enhancer region in AD and healthy people were shown using GraphPad, and a Student's *t*-test was used for comparisons across groups. $^{*}p < 0.05$ compared with the control group.

of the Bcl-2 family located mainly on the outer membrane of mitochondria, is an important mitochondrial autophagy receptor that can specifically bind to LC3 on the lysosomal membrane to promote the fusion of autophagosomes containing mitochondria with lysosomes to induce autophagy (Chourasia and Macleod, 2015; Tang et al., 2019). OPTN is a ubiquitin-bound autophagy receptor involved in pathogen autophagy and mitochondrial autophagy (Bussi et al., 2018). In aged APP-PSEN1-SREBF2 mice, chronic cholesterol accumulation results in an age-dependent impairment of OPTN translocation to mitochondria, inhibiting mitophagosome formation (Roca-Agujetas et al., 2021). APP/PS1 mice had enhanced Aβ clearance, improved cognition and mobility when treated with miR-331-3p and miR-9-5p, two microRNAs targeting autophagy receptors SQSTM1 and OPTN, respectively, and antagomirs at a late stage (Chen et al., 2021). The function of UBQLN2 in the ubiquitin protease system was to direct misfolded or redundant proteins to the proteasome for degradation. Several studies have shown that UBQLN2 was involved in the process of autophagy and directly combined with LC3 to promote the fusion of lysosomes and autophagosomes (Osaka et al., 2015; Hjerpe et al., 2016; Chen et al., 2018). UBQLN2(P497H) transgenic mice, causes amyotrophic lateral sclerosis (ALS) and frontotemporal type of dementia, had the feature of a dendritic spinopathy with protein aggregation in the dendritic spines and an associated decrease in dendritic spine density and synaptic dysfunction, related to impaired protein degradation (Gorrie et al., 2014).

The other four genes were also closely related to autophagy. CDK5, a serine/threonine kinase, is essential for neuronal migration and synaptic plasticity. CDK5 activation depends on the protein p35 encoded by the CDK5R1 gene, which forms a complex with CDK5 to perform its biological functions (Roufayel and Murshid, 2019). CDK5 genetically interacts with Acinus (Acn), a primarily nuclear protein, which promotes starvation-independent, basal autophagy. Downregulation of CDK5 influences pathologic processes of AD, including the formation of amyloid plaques and tau hyperphosphorylation (Nandi et al., 2017; Nandi and Krämer, 2018). CDK5R1 determines the risk for AD, with a 12.5-fold decrease in AD risk associated with both homozygosity for CDK5R1 (3′-UTR, rs735555) A allele and homozygosity for GSK-3β (-50, rs334558) C allele (Mateo et al., 2009). Moncini et al. (2017) demonstrated that two microRNAs, miR-103 and miR-107, regulate CDK5R1 expression and affect the levels of p35. As the autophagy receptor of cells, ITPR1, a member of the IP3 receptor family, encodes the endoplasmic reticulum (ER) receptor and mediates the release of ER calcium to induce autophagy (Messai et al., 2015; Ren et al., 2017; Xu et al., 2019). Recently, Seo et al. (2020) found ITPR1 displayed associations with the neuroimaging features of AD pathologies through a targeted sequencing analysis of the coding and UTR regions of 132 AD susceptibility genes including 557 participants. USP33 is a deubiquitination enzyme associated with the regulation of lysosomal activity and cell membrane surface receptors (Kommaddi et al., 2015). HERC1, a giant protein belonging to the HERC family, is involved in regulating the ubiquitination of intracellular proteins and can interact with mTOR to regulate the autophagy process (Mashimo et al., 2009; Ruiz et al., 2016; Bachiller et al., 2018).

MEF2A, a member of the MEF2 family, belongs to the MADS-box superfamily and is involved in the transcription of many important genes in the cell life cycle in the form of dimers, including the growth, differentiation and apoptosis of neurons (Zhu et al., 2018). Vargas et al. (2018) used the transcription regulatory network and master regulator analyses on transcriptomic data of human hippocampus from GEO to identify transcription factors that can potentially act as master regulators in AD, and then 34 master regulator candidates were identified including MEF2A. Our results showed that MEF2A, a transcription factor for the seven autophagy-related genes, was significantly decreased in AD. González-Velasco et al. (2020) also reported that 158 genes were regulated by transcription factors MEF2A among the transcriptional changes in the cerebral cortex and hippocampus caused by aging. Genome-wide association studies (GWAS) were performed to assess the significance of the overlap between genome-wide significant AD risk variants and sites of open chromatin from data sets representing diverse tissue types (Tansey et al., 2018). AD risk variants of MEF2A were significantly enriched both in macrophage and microglia. González et al. (2007) stated that variation in the MEF2A gene could be involved in the risk of developing late-onset AD. Besides, MEF2C, another member of the MEF2 transcription factor family, identified by GWAS as also having effects on AD risk, was inferred as a MEF2A target. Moreover, using rapid time-lapse two-photon calcium imaging of network activity and single-neuron growth within the unanesthetized developing brain, Chen et al. (2012) found that MEF2A was the major regulator of neuronal response to plasticity-inducing visual stimulation directing both structural and functional changes.

Microglia, accounting for 10-15% of the total number of brain cells, are an innate immune cell in the central nervous system that uses phagocytosis to engulf apoptotic cells and cellular debris (Plaza-Zabala et al., 2017). Microglia participates in the regulation of tissue repair, synaptic plasticity and synaptogenesis, resist invasion of foreign pathogens, and maintaining the stability of central nervous system tissues. In our study, we found that MEF2A, as a transcription factor to regulate BNIP3, OPTN, and UBQLN2, was highly expressed in microglia. Phagocytosis is very similar to autophagy in vacuole formation and lysosomal digestion. However, unlike autophagy, which is present in all cells, phagocytosis is a unique function of innate immune cells such as microglia. The dysregulation of microglia is closely related to the pathological process of AD, in particular in the context of its role in the phagocytosis of amyloid plaques (Condello et al., 2015; Sacks et al., 2018). The potential regulatory effect of autophagy on phagocytosis may occur in different phases of the phagocytosis cascade, including phagocytosis of substrates, maturation of phagocytes, and fusion with lysosomes, thereby affecting the degradation of phagocytes. For examples, in the LC3-related phagocytosis process, autophagy is partially transferred to phagocytosis to promote the effective intracellular degradation of phagocytic extracellular substances (Martinez et al., 2016). Heckmann et al. (2019) found that the clearance of Aβ in microglia cells correlated with LC3-related phagocytosis, which can promote the phagocytosis efficiency of cells and reuse the membrane receptors related to Aβ phagocytosis, such as CD36, TERM2, and TLR4, to improve cognitive levels.

In the past, microglial phenotypes were characterized by cell surface molecules and were classified as M0, M1 like (exhibiting proinflammatory signaling and neurotoxicity), or M2 like (participating in the resolution of inflammation). However, with the help of newly developed technologies, including single cell RNA sequencing, quantitative proteomics, and epigenetic studies, the characterization of microglial diversity in health and disease has therefore been redefined (Ransohoff, 2016). Recent genome−wide transcriptomic analyses of microglial cells under different disease conditions have uncovered a new subpopulation named disease−associated microglia (MGnD, Verheijen and Sleegers, 2018; García-Revilla et al., 2019). Krasemann et al. (2017) found that MEF2A was significantly decreased in microglia of EAE (multiple sclerosis models), SOD1 (ALS models), and APP/PS1 (AD models) mice. The aggregation of amyloid β (Aβ) changed the M0-homeostatic microglial phenotype to the neurodegenerative phenotype MGnD identified by two major gene clusters, after which the expression of MEF2A was significantly decreased. TREM2 induced APOE signaling and targeting the TREM2-APOE pathway restored the homeostatic signature of microglia in ALS and AD mouse models and prevented neuronal loss in an acute model of neurodegeneration. Our results may explain

that the changes in microglia homeostasis in AD were related to autophagy regulated by MEF2A. A genome-wide analysis of gene expression in microglia from different brain regions across the adult lifespan of the mouse was performed, revealing that there were region-specific transcriptional profiles and age-dependent regional variability in gene expression (Grabert et al., 2016). The presence of microglial heterogeneity may underly the different expression patterns of MEF2A in the different brain regions.

The relationship between AD and methylation has been well investigated. Wu et al. (2008) assessed AD-related gene methylation in peripheral blood leucocytes of diagnosed AD, which revealed decreased DNA methylation at the amyloid precursor protein (APP) promoter regions accompanied by upregulated APP transcripts. The methylation of other genes, including BACE1, PSEN1, SORL1, and NEP, involved in amyloidogenic pathway, was also shown to be related to AD (Poon et al., 2020). The epigenetic mechanisms, including the methylation of GSK3β, BDNF, ANK1, BIN1, and RELN, have been consistently reported to play critical roles in neurochemical processes including long-term potentiation (LTP) and synaptic plasticity (Jager et al., 2014; Poon et al., 2020). We found that the MEF2A in AD had significantly higher levels of methylation in the SE region than in healthy controls. SEs are composed of a series of enhancers and are gene control elements with tissue specificity. The significant peaks of H3K27ac ChIP-seq (a characteristic marker of enhancers and promoters) in MEF2A enhancers and promoters in microglia illustrated the reason for which MEF2A is highly expressed in microglia. Changing the methylation levels of SEs can regulate their interaction with gene promoters and thus regulate the expression of related genes (Flam et al., 2019). This suggests that SEs play a key regulatory role in the expression of the MEF2A.

Currently, there is no direct evidence that the screened seven genes are significantly reduced in microglia from the snRNA-seq dataset of GSE138852 (Grubman et al., 2019). However, this does not mean that the screened seven genes are not altered in microglia in AD. We speculate that the expression of these genes may be too low to be accurately detected in microglia, especially OPTN, CDK5R1, and BNIP3, based on the report of Li et al. (2019). Similarly, the low expression levels of these genes do not mean that they are dispensable to microglia. Indeed, these genes are crucial to the function of microglia. Bussi et al. (2018) found that autophagy induced by exogenous fibrillar in microglia correlated with lysosomal damage and was characterized by the recruitment of the selective autophagy-associated proteins TANK-binding kinase 1 (TBK1) and OPTN to ubiquitinated lysosomes. Ma et al. (2013) found that enhanced CDK5 activity by increasing p35-to-p25 conversion promoted Aβ phagocytosis in microglia, whereas the inhibition of CDK5 reduced Aβ internalization. Gong et al. (2020) reported that pinocembrin protected microglial cells against intermittent hypoxia (IH)-induced cytotoxicity by activating BNIP3-dependent mitophagy through the JNK-ERK signaling pathway. In addition, another reason may be linked to the fact that the MGnD was not captured accurately; it was found mainly concentrated around the amyloid plaques and was not evenly distributed throughout AD brain tissue (Krasemann et al., 2017). Besides, whether the reduced expression of these genes in microglia was influenced by epigenetics mechanisms warrants further investigation.

CONCLUSION

In summary, our results indicated that AD is associated with the increased methylation levels of MEF2A enhancer, reducing the expression of MEF2A and downregulating the expression of autophagy-related genes which were closely related to AD pathogenesis, thereby inhibiting autophagy. Although further conformational studies are warranted, our findings provide further insights into the role of MEF2A in the prevention and treatment of AD. The association between the reduction of MEF2A expression and autophagy-related genes in AD warrants further investigations.

DATA AVAILABILITY STATEMENT

The original contributions presented in the study are included in the article/**Supplementary Material**, further inquiries can be directed to the corresponding author/s.

AUTHOR CONTRIBUTIONS

YJ contributed to the perception and finally approved the version to be published. HL participated the whole work, drafted the article, and did the data analysis. FW and XG collected and downloaded the data. All authors contributed to the article and approved the submitted version.

FUNDING

This research was supported by the National Natural Science Foundation of China (No. 81872606).

SUPPLEMENTARY MATERIAL

The Supplementary Material for this article can be found online at: https://www.frontiersin.org/articles/10.3389/fnins.2021.682247/full#supplementary-material

Supplementary Figure 1 | Transcription factor analysis in UCSC database. The online annotation website DAVID was used to performed transcription factor analysis for 71 DEGs and 16 genes in the black module (total 80 genes) in the UCSC database.

Supplementary Figure 2 | The correlation between MEF2A and the expression of the screened seven genes. The correlation between MEF2A and the expression of the screened seven genes were validated in GSE118553 (Pearson's correlation).

Supplementary Figure 3 | The mRNA expression levels of the screened seven genes in microglia. In GSE138852, the mRNA expression levels (logCounts) of BNIP3, CDK5R1, HERC1, ITPR1, OPTN, UBQLN2, and USP33 in AD and in healthy controls were shown. A *t*-test was performed for comparison between groups. $^{*}p < 0.05$ compared with the control group.

REFERENCES

Bachiller, S., Roca-Ceballos, M. A., García-Domínguez, I., Pérez-Villegas, E. M., Martos-Carmona, D., Pérez-Castro, M. Á, et al. (2018). HERC1 ubiquitin ligase is required for normal axonal myelination in the peripheral nervous system. *Mol. Neurobiol.* 55, 8856–8868. doi: 10.1007/s12035-018-1021-0

Bailey, T. L., Boden, M., Buske, F. A., Frith, M., Grant, C. E., Clementi, L., et al. (2009). MEME SUITE: tools for motif discovery and searching. *Nucleic Acids Res.* 37, W202–W208. doi: 10.1093/nar/gkp335

Boya, P., and Kroemer, G. (2008). Lysosomal membrane permeabilization in cell death. *Oncogene* 27, 6434–6451. doi: 10.1038/onc.2008.310

Braak, H., and Braak, E. (1995). Staging of Alzheimer's disease-related neurofibrillary changes. *Neurobiol. Aging* 16, 271–278. doi: 10.1016/0197-4580(95)00021-6

Bussi, C., Ramos, J. M. P., Arroyo, D. S., Gallea, J. I., Ronchi, P., Kolovou, A., et al. (2018). Alpha-synuclein fibrils recruit TBK1 and OPTN to lysosomal damage sites and induce autophagy in microglial cells. *J. Cell Sci.* 131:jcs226241. doi: 10.1242/jcs.226241

Chen, M., Hong, C., Yue, T., Li, H., Duan, R., Hu, W., et al. (2021). Inhibition of miR-331-3p and miR-9-5p ameliorates Alzheimer's disease by enhancing autophagy. *Theranostics* 11, 2395–2409. doi: 10.7150/thno.47408

Chen, S. X., Cherry, A., Tari, P. K., Podgorski, K., Kwong, Y. K. K., Haas, K., et al. (2012). The transcription factor MEF2 directs developmental visually driven functional and structural metaplasticity. *Cell* 151, 41–55. doi: 10.1016/j.cell.2012.08.028

Chen, T., Huang, B., Shi, X., Gao, L., and Huang, C. (2018). Mutant UBQLN2(P497H) in motor neurons leads to ALS-like phenotypes and defective autophagy in rats. *Acta Neuropathol. Commun.* 6:122. doi: 10.1186/s40478-018-0627-9

Chourasia, A. H., and Macleod, K. F. (2015). Tumor suppressor functions of BNIP3 and mitophagy. *Autophagy* 11, 1937–1938. doi: 10.1080/15548627.2015.1085136

Condello, C., Yuan, P., Schain, A., and Grutzendler, J. (2015). Microglia constitute a barrier that prevents neurotoxic protofibrillar Aβ42 hotspots around plaques. *Nat. Commun.* 6:6176. doi: 10.1038/ncomms7176

Doody, R. S., Raman, R., Farlow, M., Iwatsubo, T., Vellas, B., Joffe, S., et al. (2013). A phase 3 trial of semagacestat for treatment of Alzheimer's disease. *N. Engl. J. Med.* 369, 341–350. doi: 10.1056/NEJMoa1210951

Flam, E. L., Danilova, L., Kelley, D. Z., Stavrovskaya, E., Guo, T., Considine, M., et al. (2019). Differentially methylated super-enhancers regulate target gene expression in human cancer. *Sci. Rep.* 9:15034. doi: 10.1038/s41598-019-51018-x

Fornes, O., Castro-Mondragon, J. A., Khan, A., Lee, R. V. D., Zhang, X., Richmond, P. A., et al. (2020). JASPAR 2020: update of the open-access database of transcription factor binding profiles. *Nucleic Acids Res.* 48, D87–D92. doi: 10.1093/nar/gkz1001

García-Revilla, J., Alonso-Bellido, I. M., Burguillos, M. A., Herrera, A. J., Espinosa-Oliva, A. M., Ruiz, R., et al. (2019). Reformulating pro-oxidant microglia in neurodegeneration. *J. Clin. Med.* 8:1719. doi: 10.3390/jcm8101719

Glatigny, M., Moriceau, S., Rivagorda, M., Ramos-Brossier, M., Nascimbeni, A. C., Lante, F., et al. (2019). Autophagy is required for memory formation and reverses age-related memory decline. *Curr. Biol.* 29, 435–448.e8. doi: 10.1016/j.cub.2018.12.021

Gong, L., Wang, X., Gu, W., and Wu, X. (2020). Pinocembrin ameliorates intermittent hypoxia-induced neuroinflammation through $BNIP_3$-dependent mitophagy in a murine model of sleep apnea. *J. Neuroinflammation.* 17:337. doi: 10.1186/s12974-020-02014-w

González, P., Alvarez, V., Menéndez, M., Lahoz, C. H., Martínez, C., Corao, A. I., et al. (2007). Myocyte enhancing factor-2A in Alzheimer's disease: genetic analysis and association with MEF2A-polymorphisms. *Neurosci. Lett.* 411, 47–51. doi: 10.1016/j.neulet.2006.09.055

González-Velasco, O., Papy-García, D., Douaron, G. L., Sánchez-Santos, J. M., and Rivas, J. D. L. (2020). Transcriptomic landscape, gene signatures and regulatory profile of aging in the human brain. *Biochim. Biophys. Acta. Gene Regul. Mech.* 1863, 194491–194508. doi: 10.1016/j.bbagrm.2020.194491

Gorrie, G. H., Fecto, F., Radzicki, D., Weiss, C., Shi, Y., Dong, H., et al. (2014). Dendritic spinopathy in transgenic mice expressing ALS/dementia-linked mutant UBQLN2. *Proc. Natl. Acad. Sci. U. S. A.* 111, 14524–14529. doi: 10.1073/pnas.1405741111

Grabert, K., Michoel, T., Karavolos, M. H., Clohisey, S., Baillie, J. K., Stevens, M. P., et al. (2016). Microglial brain region-dependent diversity and selective regional sensitivities to aging. *Nat. Neurosci.* 19, 504–516. doi: 10.1038/nn.4222

Grant, C. E., Bailey, T. L., and Noble, W. S. (2011). FIMO: scanning for occurrences of a given motif. *Bioinformatics* 27, 1017–1018. doi: 10.1093/bioinformatics/btr064

Grubman, A., Chew, G., Ouyang, J. F., Sun, G., Choo, X. Y., McLean, C., et al. (2019). A single-cell atlas of entorhinal cortex from individuals with Alzheimer's disease reveals cell-type-specific gene expression regulation. *Nat. Neurosci.* 22, 2087–2097. doi: 10.1038/s41593-019-0539-4

Heckmann, B. L., Teubner, B. J. W., Tummers, B., Boada-Romero, E., Harris, L., Yang, M., et al. (2019). LC3-associated endocytosis facilitates b-amyloid clearance and mitigates neurodegeneration in murine Alzheimer's disease. *Cell* 178, 536–551.e14. doi: 10.1016/j.cell.2019.05.056

Hjerpe, R., Bett, J. S., Keuss, M. J., Solovyova, A., McWilliams, T. G., Johnson, C., et al. (2016). UBQLN2 mediates autophagy-independent protein aggregate clearance by the proteasome. *Cell* 166, 935–949. doi: 10.1016/j.cell.2016.07.001

Hou, Y., Dan, X., Babbar, M., Wei, Y., Hasselbalch, S. G., Croteau, D. L., et al. (2019). Ageing as a risk factor for neurodegenerative disease. *Nat. Rev. Neurol.* 15, 565–581. doi: 10.1038/s41582-019-0244-7

Huang, D. W., Sherman, B. T., and Lempicki, R. A. (2009). Systematic and integrative analysis of large gene lists using DAVID bioinformatics resources. *Nat. Protoc.* 4, 44–57. doi: 10.1038/nprot.2008.211

Jager, P. L. D., Srivastava, G., Lunnon, K., Burgess, J., Schalkwyk, L. C., Yu, L., et al. (2014). Alzheimer's disease: early alterations in brain DNA methylation at ANK1, BIN1, RHBDF2 and other loci. *Nat. Neurosci.* 17, 1156–1163. doi: 10.1038/nn.3786

Kommaddi, R. P., Jean-Charles, P. Y., and Shenoy, S. K. (2015). Phosphorylation of the deubiquitinase USP20 by protein kinase A regulates post-endocytic trafficking of β2 adrenergic receptors to autophagosomes during physiological stress. *J. Biol. Chem.* 290, 8888–8903. doi: 10.1074/jbc.M114.630541

Krasemann, S., Madore, C., Cialic, R., Baufeld, C., Calcagno, N., Fatimy, R. E., et al. (2017). The TREM2-APOE pathway drives the transcriptional phenotype of dysfunctional microglia in neurodegenerative diseases. *Immunity* 47, 566–581.e9. doi: 10.1016/j.immuni.2017.08.008

Lee, J., Yu, W. H., Kumar, A., Lee, S., Mohan, P. S., Peterhoff, C. M., et al. (2010). Lysosomal proteolysis and autophagy require presenilin 1 and are disrupted by Alzheimer-related PS1 mutations. *Cell* 141, 1146–1158. doi: 10.1016/j.cell.2010.05.008

Li, Q., Cheng, Z., Zhou, L., Darmanis, S., Neff, N. F., Okamoto, J., et al. (2019). Developmental heterogeneity of microglia and brain myeloid cells revealed by deep single-cell RNA sequencing. *Neuron* 101, 207–223. doi: 10.1016/j.neuron.2018.12.006

Ma, Y., Bao, J., Zhao, X., Shen, H., Lv, J., Ma, S., et al. (2013). Activated cyclin-dependent kinase 5 promotes microglial phagocytosis of fibrillar β-amyloid by up-regulating lipoprotein lipase expression. *Mol. Cell Proteomics* 12, 2833–2844. doi: 10.1074/mcp.M112.026864

Majumder, S., Richardson, A., Strong, R., and Oddo, S. (2011). Inducing autophagy by rapamycin before, but not after, the formation of plaques and tangles ameliorates cognitive deficits. *PLoS One* 6:e25416. doi: 10.1371/journal.pone.0025416

Martin, T. C., Yet, I., Tsai, P. C., and Bell, J. T. (2015). coMET: visualisation of regional epigenome-wide association scan results and DNA co-methylation patterns. *BMC Bioinformatics* 16:131. doi: 10.1186/s12859-015-0568-2

Martinez, J., Cunha, L. D., Park, S., Yang, M., Lu, Q., Orchard, R., et al. (2016). Noncanonical autophagy inhibits the auto-inflammatory, lupus-like response to dying cells. *Nature* 533, 115–119. doi: 10.1038/nature17950

Mashimo, T., Hadjebi, O., Amair-Pinedo, F., Tsurumi, T., Langa, F., Serikawa, T., et al. (2009). Progressive Purkinje cell degeneration in tambaleante mutant mice is a consequence of a missense mutation in HERC1 E3 ubiquitin ligase. *PLoS Genet.* 5:e1000784. doi: 10.1371/journal.pgen.1000784

Mateo, I., Vázquez-Higuera, J. L., Sánchez-Juan, P., Rodríguez-Rodríguez, E., Infante, J., García-Gorostiaga, I., et al. (2009). Epistasis between tau phosphorylation regulating genes (CDK5R1 and GSK-3beta) and Alzheimer's

disease risk. *Acta. Neurol. Scand.* 120, 130–133. doi: 10.1111/j.1600-0404.2008.01128.x

McKay, E. C., Beck, J. S., Khoo, S. K., Dykema, K. J., Cottingham, S. L., Winn, M. E., et al. (2019). Peri-infarct upregulation of the oxytocin receptor in vascular dementia. *J. Neuropathol. Exp. Neurol.* 78, 436–452. doi: 10.1093/jnen/nlz023

Messai, Y., Noman, M. Z., Janji, B., Hasmim, M., Escudier, B., and Chouaib, S. (2015). The autophagy sensor ITPR1 protects renal carcinoma cells from NK-mediated killing. *Autophagy* doi: 10.1080/15548627.2015.1017194 [Epub ahead of print]

Moncini, S., Lunghi, M., Valmadre, A., Grasso, M., Vescovo, V. D., Riva, P., et al. (2017). The miR-15/107 family of microRNA genes regulates CDK5R1/p35 with implications for Alzheimer's disease pathogenesis. *Mol. Neurobiol.* 54, 4329–4342. doi: 10.1007/s12035-016-0002-4

Nandi, N., and Krämer, H. (2018). Cdk5-mediated Acn/Acinus phosphorylation regulates basal autophagy independently of metabolic stress. *Autophagy* 14, 1271–1272. doi: 10.1080/15548627.2018.1441472

Nandi, N., Tyra, L. K., Stenesen, D., and Krämer, H. (2017). Stress-induced Cdk5 activity enhances cytoprotective basal autophagy in Drosophila melanogaster by phosphorylating acinus at serine 437. *Elife* 6:e30760. doi: 10.7554/eLife.30760

Nixon, R. A. (2013). The role of autophagy in neurodegenerative disease. *Nat. Med.* 19, 983–997. doi: 10.1038/nm.3232

Nixon, R. A., Wegiel, J., Kumar, A., Yu, W. H., Peterhoff, C., Cataldo, A., et al. (2005). Extensive involvement of autophagy in Alzheimer disease: an immuno-electron microscopy study. *J. Neuropathol. Exp. Neurol.* 64, 113–122. doi: 10.1093/jnen/64.2.113

Nixon, R. A., and Yang, D. (2011). Autophagy failure in Alzheimer's disease–locating the primary defect. *Neurobiol. Dis.* 43, 38–45. doi: 10.1016/j.nbd.2011.01.021

Nott, A., Holtman, I. R., Coufal, N. G., Schlachetzki, J. C. M., Yu, M., Hu, R., et al. (2019). Brain cell type–specific enhancer–promoter interactome maps and disease risk association. *Science* 366, 1134–1139. doi: 10.1126/science aay0793

Osaka, M., Ito, D., Yagi, T., Nihei, Y., and Suzuki, N. (2015). Evidence of a link between ubiquilin 2 and optineurin in amyotrophic lateral sclerosis. *Hum. Mol. Genet.* 24, 1617–1629. doi: 10.1093/hmg/ddu575

Ostrowitzki, S., Lasser, R. A., Dorflinger, E., Scheltens, P., Barkhof, F., Nikolcheva, T., et al. (2017). A phase III randomized trial of gantenerumab in prodromal Alzheimer's disease. *Alzheimers Res. Ther.* 9:95. doi: 10.1186/s13195-017-0318-y

Patel, H., Hodges, A. K., Curtis, C., Lee, S. H., Troakes, C., Dobson, R. J. B., et al. (2019). Transcriptomic analysis of probable asymptomatic and symptomatic alzheimer brains. *Brain Behav. Immun.* 80, 644–656. doi: 10.1016/j.bbi.2019.05.009

Piras, I. S., Krate, J., Delvaux, E., Nolz, J., Mastroeni, D. F., Persico, A. M., et al. (2019). Transcriptome changes in the Alzheimer's disease middle temporal gyrus: importance of RNA metabolism and mitochondria-associated membrane genes. *J. Alzheimers Dis.* 70, 691–713. doi: 10.3233/JAD-181113

Plaza-Zabala, A., Sierra-Torre, V., and Sierra, A. (2017). Autophagy and microglia: novel partners in neurodegeneration and aging. *Int. J. Mol. Sci.* 18:598. doi: 10.3390/ijms18030598

Poon, C. H., Tse, L. S. R., and Lim, L. W. (2020). DNA methylation in the pathology of Alzheimer's disease: from gene to cognition. *Ann. N Y Acad. Sci.* 1475, 15–33. doi: 10.1111/nyas.14373

Ransohoff, R. M. (2016). A polarizing question: do M1 and M2 microglia exist? *Nat. Neurosci.* 19, 987–991. doi: 10.1038/nn.4338

Ren, G., Zhou, Y., Liang, G., Yang, B., Yang, M., King, A., et al. (2017). General anesthetics regulate autophagy via modulating the inositol 1,4,5-trisphosphate receptor: implications for dual effects of cytoprotection and cytotoxicity. *Sci. Rep.* 7:12378. doi: 10.1038/s41598-017-11607-0

Roca-Agujetas, V., Barbero-Camps, E., Dios, C. D., Podlesniy, P., Abadin, X., Morales, A., et al. (2021). Cholesterol alters mitophagy by impairing optineurin recruitment and lysosomal clearance in Alzheimer's disease. *Mol. Neurodegener.* 16:15. doi: 10.1186/s13024-021-00435-6

Roufayel, R., and Murshid, N. (2019). CDK5: key regulator of apoptosis and cell survival. *Biomedicines* 7:88. doi: 10.3390/biomedicines7040088

Ruiz, R., Pérez-Villegas, E. M., Bachiller, S., Rosa, J. L., and Armengol, J. A. (2016). HERC 1 ubiquitin ligase mutation affects neocortical, CA3 hippocampal and spinal cord projection neurons: an ultrastructural study. *Front. Neuroanat.* 10:42. doi: 10.3389/fnana.2016.00042

Sacks, D., Baxter, B., Campbell, B. C. V., Carpenter, J. S., Cognard, C., Dippel, D., et al. (2018). Multisociety consensus quality improvement revised consensus statement for endovascular therapy of acute ischemic stroke. *Int. J. Stroke* 13, 612–632. doi: 10.1177/1747493018778713

Seo, J., Byun, M. S., Yi, D., Lee, J. H., Jeon, S. Y., Shin, S. A., et al. (2020). Genetic associations of in vivo pathology influence Alzheimer's disease susceptibility. *Alzheimers Res. Ther.* 12:156. doi: 10.1186/s13195-020-00722-2

Smith, R. G., Hannon, E., Jager, P. L. D., Chibnik, L., Lott, S. J., Condliffe, D., et al. (2018). Elevated DNA methylation across a 48-kb region spanning the HOXA gene cluster is associated with Alzheimer's disease neuropathology. *Alzheimers Dement.* 14, 1580–1588. doi: 10.1016/j.jalz.2018.01.017

Tang, C., Han, H., Liu, Z., Liu, Y., Yin, L., Cai, J., et al. (2019). Activation of BNIP3-mediated mitophagy protects against renal ischemia–reperfusion injury. *Cell Death Dis.* 10:677. doi: 10.1038/s41419-019-1899-0

Tansey, K. E., Cameron, D., and Hill, M. J. (2018). Genetic risk for Alzheimer's disease is concentrated in specific macrophage and microglial transcriptional networks. *Genome Med.* 10:14. doi: 10.1186/s13073-018-0523-8

Tian, Y., Morris, T. J., Webster, A. P., Yang, Z., Beck, S., Feber, A., et al. (2017). ChAMP: updated methylation analysis pipeline for Illumina BeadChips. *Bioinformatics* 33, 3982–3984. doi: 10.1093/bioinformatics/btx513

Vargas, D. M., Bastiani, M. A. D., Zimmer, E. R., and Klamt, F. (2018). Alzheimer's disease master regulators analysis: search for potential molecular targets and drug repositioning candidates. *Alzheimers Res. Ther.* 10:59. doi: 10.1186/s13195-018-0394-7

Verheijen, J., and Sleegers, K. (2018). Understanding Alzheimer disease at the interface between genetics and transcriptomics. *Trends Genet.* 34, 434–447. doi: 10.1016/j.tig.2018.02.007

Wang, M., Roussos, P., McKenzie, A., Zhou, X., Kajiwara, Y., Brennand, K. J., et al. (2016). Integrative network analysis of nineteen brain regions identifies molecular signatures and networks underlying selective regional vulnerability to Alzheimer's disease. *Genome Med.* 8:104. doi: 10.1186/s13073-016-0355-3

Wishart, D. S., Knox, C., Guo, A. C., Eisner, R., Young, N., Gautam, B., et al. (2009). HMDB: a knowledgebase for the human metabolome. *Nucleic Acids Res.* 37, D603–D610. doi: 10.1093/nar/gkn810

Wu, J., Basha, M. R., Brock, B., Cox, D. P., Cardozo-Pelaez, F., McPherson, C. A., et al. (2008). Alzheimer's dis- ease (AD)-like pathology in aged monkeys after infantile exposure to environmental metal lead (Pb): evidence for a developmental origin and environmental link for AD. *J. Neurosci.* 28, 3–9. doi: 10.1523/jneurosci.4405-07.2008

Xu, S., Wang, P., Zhang, J., Wu, H., Sui, S., Zhang, J., et al. (2019). Ai-lncRNA EGOT enhancing autophagy sensitizes paclitaxel cytotoxicity via upregulation of ITPR1 expression by RNA-RNA and RNA-protein interactions in human cancer. *Mol. Cancer* 18:89. doi: 10.1186/s12943-019-1017-z

Zhang, L., Sun, Y., Fei, M., Tan, C., Wu, J., Zheng, J., et al. (2014). Disruption of chaperone-mediated autophagydependent degradation of MEF2A by oxidative stress-induced lysosome destabilization. *Autophagy* 10, 1015–1035. doi: 10.4161/auto.28477

Zhu, B., Carmichael, R. E., Valois, L. S., Wilkinson, K. A., and Henley, J. M. (2018). The transcription factor MEF2A plays a key role in the differentiation/maturation of rat neural stem cells into neurons. *Biochem. Biophys. Res. Commun.* 500, 645–649. doi: 10.1016/j.bbrc.2018.04.125

Conflict of Interest: The authors declare that the research was conducted in the absence of any commercial or financial relationships that could be construed as a potential conflict of interest.

frontiers in Neuroscience

ORIGINAL RESEARCH
published: 21 March 2022
doi: 10.3389/fnins.2022.739201

Downregulation of m6A Methyltransferase in the Hippocampus of *Tyrobp*$^{-/-}$ Mice and Implications for Learning and Memory Deficits

*Zhanyun Lv[1,2], Tongxiao Xu[3], Ran Li[4], Dejie Zheng[5], Yanxin Li[6], Wei Li[3], Yan Yang[3,7] and Yanlei Hao[3,7]**

[1] Zhejiang University Medical Center, Hangzhou, China, [2] School of Brain Science and Brain Medicine, Zhejiang University, Hangzhou, China, [3] College of Clinical Medicine, Jining Medical University, Jining, China, [4] Cheeloo College of Medicine, Shandong University, Jinan, China, [5] Health Management Center, Weifang People's Hospital, Weifang, China, [6] Department of Neurology, Pingdu People's Hospital, Qingdao, China, [7] Department of Neurology, The Affiliated Hospital of Jining Medical University, Jining, China

OPEN ACCESS

Edited by:
Manoj Kumar Jaiswal,
Icahn School of Medicine at Mount Sinai, United States

Reviewed by:
Benjamin Wolozin,
Boston University, United States
Esko Kankuri,
University of Helsinki, Finland
Aaron M. Johnson,
University of Colorado, United States
Manoj Kandpal,
Northwestern University, United States

***Correspondence:**
Yanlei Hao
yhao@mail.jnmc.edu.cn

Specialty section:
This article was submitted to Neurodegeneration, a section of the journal Frontiers in Neuroscience

Received: 10 July 2021
Accepted: 10 February 2022
Published: 21 March 2022

Citation:
Lv Z, Xu T, Li R, Zheng D, Li Y, Li W, Yang Y and Hao Y (2022) Downregulation of m6A Methyltransferase in the Hippocampus of Tyrobp$^{-/-}$ Mice and Implications for Learning and Memory Deficits. Front. Neurosci. 16:739201. doi: 10.3389/fnins.2022.739201

Loss-of-function mutations in the gene that encodes TYRO protein kinase-binding protein (*TYROBP*) cause Nasu-Hakola disease, a heritable disease resembling Alzheimer's disease (AD). Methylation of N6 methyl-adenosine (m6A) in mRNA plays essential roles in learning and memory. Aberrant m6A methylation has been detected in AD patients and animal models. In the present study, *Tyrobp*$^{-/-}$ mice showed learning and memory deficits in the Morris water maze, which worsened with age. *Tyrobp*$^{-/-}$ mice also showed elevated levels of total tau, Ser202/Thr205-phosphorylated tau and amyloid β in the hippocampus and cerebrocortex, which worsened with aging. The m6A methyltransferase components METTL3, METTL14, and WTAP were downregulated in *Tyrobp*$^{-/-}$ mice, while expression of demethylases that remove the m6A modification (e.g., FTO and ALKBH5) were unaltered. Methylated RNA immunoprecipitation sequencing identified 498 m6A peaks that were upregulated in *Tyrobp*$^{-/-}$ mice, and 312 m6A peaks that were downregulated. Bioinformatic analysis suggested that most of these m6A peaks occur in sequences near stop codons and 3′-untranslated regions. These findings suggest an association between m6A RNA methylation and pathological TYROBP deficiency.

Keywords: ***Tyrobp***$^{-/-}$ **mice, m6A methylation, METTL3, METTL14, WTAP, ALKBH5, FTO, MeRIP-seq**

INTRODUCTION

In the brain, TYRO protein kinase-binding protein (TYROBP) is expressed mainly by microglia (Ma et al., 2015). A *TYROBP*-centered pathway has been identified in microglia of healthy adult and aged mice, and 44 of the 100 genes interact directly or indirectly with *TYROBP* (Hickman et al., 2013). Loss-of-function mutations in the *TYROBP* gene cause Nasu-Hakola disease (NHD), also known as polycystic lipomembranous osteodysplasia with sclerosing leukoencephalopathy

(MIM 221770) (Paloneva et al., 2000). NHD patients typically experience frequent bone fractures starting in their 30s, progressive memory deficits and personality changes starting from their 40s, and eventually dementia and death (Xing et al., 2015). *TYROBP* mutations have also been detected in patients with Alzheimer's disease (AD) (Pottier et al., 2016). A study of 1,647 AD patients *post mortem* revealed upregulation of TYROBP and suggested that it is a key regulator of AD-related processes (Zhang et al., 2013).

NHD and AD overlap significantly in clinical presentations as well as in pathological features. The pathologic hallmark of AD is the accumulation of insoluble neurotoxic aggregates, including amyloid β (Aβ) plaques and intracellular tau neurofibrillary tangles. Aβ deposition and neurofibrillary changes have been reported in the brains of NHD patients bearing homozygous Q33X mutations in the *TREM2* gene (Maderna et al., 2021). NHD patients have been found to contain Aβ deposits in the frontal cortex and phosphorylated tau in hippocampal neurons (Satoh et al., 2018).

N6-methyladenosine (m6A) methylation in RNA is a post-transcriptional modification that attaches a methyl group at the N6 position of adenosine (Zaccara et al., 2019), which helps regulate the localization, transport and translation of mRNAs involved in memory and learning (Zhang et al., 2018). Transgenic *APP/PS1* mice show elevated m6A methylation in the cerebrocortex and hippocampus; upregulation of methyltransferase-like protein 3 (METTL3), which helps generate m6A (Liu et al., 2014); as well as downregulation of fat mass- and obesity-associated protein (FTO), a demethylase that removes the m6A modification (Jia et al., 2011; Han et al., 2020).

Given the similarities between AD and NHD, we compared hippocampal m6A methylation between *Tyrobp*$^{-/-}$ and wild-type (WT) mice. The function of differentially expressed RNAs was predicted based on enrichment in Gene Ontology (GO) terms and Kyoto Encyclopedia of Genes and Genomes (KEGG) pathways.

MATERIALS AND METHODS

Animal Subjects

F0 *Tyrobp*$^{+/-}$ mice were obtained from Cyagen Biosciences (Guangzhou, China). The mouse strain was constructed by microinjecting into fertilized eggs a transcription activator-like effector nuclease (TALEN) that removes 10 bases (GTACAGGCCC) from exon 2 of the *TYROBP* gene. F0 mice were bred with C57/BL6 mice to produce the F1 generation, and the mutant F1 generation was inbred to generate the F2 generation. Gene knockout was confirmed using Sanger sequencing and western blotting.

All experiments were carried out using male mice. Age-matched WT littermates were used as controls. *APP*$^{KM670/671NL}$/*PSEN1*$^{\Delta exon9}$ *(APP/PS1)* mice and C57/BL6J WT mice were purchased from Huafukang Bioscience Co., Ltd. (Beijing, China). Mice were housed in groups of four with *ad libitum* access to standard food pellets and water on a 12/12h light/dark cycle. Experiments were approved by the Ethics Committee for Animal Experiments at The Affiliated Hospital of Jining Medical University.

Morris Water Maze

Each group in this test contained six mice aged 2, 6, and 9 months. Testing was conducted using a standard 5-day regimen with a circular pool filled with opaque water by handlers who were blinded to grouping. During training sessions, which were conducted once a day for the first 5 days, a platform was placed 1 cm below the surface, and the mice were placed into the water in different quadrants facing the pool wall. If the mouse failed to locate the platform within 60 s, it was guided to the platform and allowed to stay on the platform for 15 s. Animal trajectories were recorded using a video-based image tracking system and ANY maze software (Global Biotech, Mount Laurel, NJ, United States).

Immunofluorescence Analysis

At 24 h after the Morris water maze testing, three mice per group were deeply anesthetized with 1% carbrital and perfused transcardially with 0.9% saline, followed by cold 4% paraformaldehyde in 0.1 M phosphate-buffered saline (PBS, pH 7.4). Brains were dissected out and maintained overnight in 4% paraformaldehyde, cryopreserved in PBS containing 30% sucrose, then stored at −70°C until use. Brain sections (10 μm) were prepared and incubated for 12 h with one of the following antibodies: mouse monoclonal antibody against TYROBP (B-2, 1:100, cat# sc-166086, Santa Cruz Biotechnology, Dallas, TX, United States), mouse monoclonal antibody against tau (Tau5, 1:100, cat# ab80579, Abcam, Cambridge, MA, United States), mouse monoclonal antibody against Ser202/Thr205-phosphorylated tau (AT8, 1:100, cat# MN1020, Thermo Fisher Scientific, Waltham, MA, United States), mouse antibody against Aβ(1-16) (6E10, 1:100, cat# SIG-39320, Biolegend, San Diego, CA, United States), rabbit antibody against m6A (1:200, cat# A17924, ABclonal, Wuhan, Hubei, China) mixed with 2% BSA, 1 × DNase I Buffer (10 mM Tris-HCl, 2.5 mM MgCl2, 0.5 mM CaCl2), 25 U/mL DNase I (cat# 79254, Qiagen, Beverly, MA, United States), mouse monoclonal antibody against Iba1 (1:100, cat# ab283319, Abcam), rabbit monoclonal antibody against Iba1 (1:100, cat# ab178846, Abcam), mouse monoclonal antibody against GFAP (1:200, cat# CL488-60190, Proteintech Group, Chicago, IL, United States) and mouse monoclonal antibody against NeuN (1:200, cat# 66836-1-Ig, Proteintech Group). The sections were then incubated for 1 h with either Alexa Flour 488-conjugated goat anti-rabbit IgG (1:50, cat# SA00013-2, Proteintech Group) or Alexa Flour 568-conjugated goat anti-mouse IgG (1:1,000, cat# ab175473, Abcam). Images were acquired using an upright Zeiss microscope (Axio Imager.Z2, Carl Zeiss, Oberkochen, Germany), and analyzed using Image J (National Institutes of Health, Bethesda, MD, United States) (Schneider et al., 2012).

RNA Isolation and Quantitative Real-Time PCR

Total RNA was isolated from each group of nine mice aged 6 months, then purified using TRIzol reagent (cat# 15596018, Invitrogen, Carlsbad, CA, United States). The amount and quality of the purified RNA were examined using the ND-1000 system (NanoDrop, Wilmington, DE, United States). Only RNA giving an absorbance ratio A_{260}/A_{280} of 1.8–2.0 was used in further experiments. An aliquot of mRNA (1 μg per sample) was reverse-transcribed into cDNA using the SuperScript III First-StrandKit (cat# 18080051, Invitrogen), and 1 μL of cDNA (diluted 1:2) was used as template in quantitative PCR in the ChamQ^{TM} Universal SYBR qPCR Master Mix (cat# Q711-02, Vazyme, Nanjing, Jiangsu, China). β-actin served as the internal control. Primer sequences were designed using the online Primer Blast tool ([1]**Supplementary Table 1**). Levels of mRNA were expressed using the $2^{-\Delta\Delta Ct}$ method (Lv et al., 2016). Only genes associated with transcript Ct ≤ 30 were considered to be expressed.

Western Blotting

Total protein was isolated from frozen hippocampi from groups of six mice aged 6 months using RIPA lysis buffer (Beyotime Biotechnology, Nanjing, China) containing PMSF (Beyotime Biotechnology). Lysates were left standing for 30 min, then centrifuged at 12,000 × *g* for 20 min at 4°C. Protein concentration was estimated using bicinchoninic acid (Beyotime Biotechnology), and equal amounts (30 μg) were separated by electrophoresis on precast 10% Bis-Tris gels (Bio-Rad Laboratories, Hercules, CA, United States), transferred to polyvinylidene difluoride membranes, and incubated with one of the following primary antibodies: rabbit antibody against TYROBP (B-2, 1:200, cat# sc-166086, Santa Cruz Biotechnology), rabbit antibody against METTL3 (1:1,000, cat# ab195352, Abcam), rabbit antibody against METTL14 (1:1,000, cat# A8530, ABclonal), rabbit antibody against WTAP (1:1,000, cat# 56501, Cell Signaling Technology, Danvers, MA, United States) and mouse antibody against GAPDH (1:50,000, cat# AC033, ABclonal). Secondary antibodies included horseradish peroxidase-conjugated goat anti-rabbit secondary IgG (1:5,000, cat# AS014, ABclonal) and goat anti-mouse IgG (1:5,000, cat# AS003, ABclonal). Antibody binding was visualized using enhanced chemiluminescence (cat# 32106, Thermo Fisher Scientific) and a Tanon 5200 imaging analysis system (Tanon Technology, Shanghai, China). Band intensities were analyzed using Image J.

Enzyme-Linked Immunosorbent Assay

RIPA-soluble protein was isolated from the brains of groups of three to six mice aged 2, 6, and 9 months. Aβ levels were quantified using commercial ELISAs against Aβ40 (cat# MU30299, BIOSWAMP, Wuhan, Hubei, China) and Aβ42 (cat# MU30114, BIOSWAMP) according to the manufacturer's protocols.

[1]https://www.ncbi.nlm.nih.gov/tools/primer-blast

Quantification of m6A Methylation

Levels of m6A methylation in total hippocampal RNA from groups of six mice aged 6 months were measured using a commercial kit (cat# ab185912, Abcam) according to the manufacturer's instructions. Each sample contained 1,000 ng of total RNA. Absorbance was measured at 450 nm and converted to m6A levels using a standard curve.

Methylated RNA Immunoprecipitation Sequencing

The MeRIP-Seq required at least 100 μg RNA in each sample; therefore, the RNAs of three mouse hippocampi (either WT or *Tyrobp*$^{-/-}$) were pooled as one sample for MeRIP-Seq. The RNA was isolated as described above, and its integrity was assessed using a Bioanalyzer 2100 (Agilent, CA, United States) and denaturing agarose gel electrophoresis. RNA was used only if the RNA integrity number > 7.0. Poly(A) RNA was purified from 50 μg total RNA using oligo$(dT)_{25}$ Dynabeads (cat# 61005, Thermo Fisher Scientific), and fragmented into small pieces at 86°C for 7 min using a Magnesium RNA Fragmentation Module (cat# e6150, New England Biolabs, Ipswich, MA, United States). The cleaved RNA fragments were incubated at 4°C for 2 h with an antibody against m6A (cat# 202003, Synaptic Systems, Göttingen, Niedersachsen, Germany) in 50 mM Tris-HCl, 750 mM NaCl and 0.5% Igepal CA-630. Immunoprecipitated RNA was reverse-transcribed into cDNA using SuperScript^{TM} II Reverse Transcriptase (cat# 1896649, Invitrogen), which was then used as template to synthesize U-labeled second-strand DNA using *E. coli* DNA polymerase I (cat# m0209, New England Biolabs), RNase H (cat# m0297, New England Biolabs) and dUTP (cat# R0133, Thermo Fisher Scientific). The blunt ends of strands were extended with A bases for ligation to indexed adapters. Each adapter contained a T-base overhang to allow it to be ligated to the A-tailed DNA. Single- or dual-index adapters were ligated to the fragments, which were selected by size using AMPureXP beads. The ligated products were treated with a heat-labile UDG enzyme (cat# m0280, New England Biolabs), then amplified by PCR under the following conditions: initial denaturation at 95°C for 3 min; eight cycles of denaturation at 98°C for 15 s, annealing at 60°C for 15 s, and extension at 72°C for 30 s; then final extension at 72°C for 5 min. The average insert size for the final cDNA library was 300 ± 50 bp. The library was subjected to 2 × 150-bp paired-end sequencing (PE 150) on an illumineNovaseq^{TM} 6000 (Illumina, San Diego, CA, United States).

Bioinformatic Analysis

Fastp software[2] (Chen et al., 2018), with its default parameters, was used to remove adapter contamination and low-quality reads, defined as Q ≤ 10. Fastp was also used to verify sequence quality of the input and immunoprecipitated samples. We used HISAT2[3] (Kim et al., 2015) to map the reads to the *Mus musculus* genome (version: v96). Mapped reads of immunoprecipitated

[2]https://github.com/OpenGene/fastp

[3]http://daehwankimlab.github.io/hisat2

and input libraries were analyzed using the exomePeak package in R[4] (Meng et al., 2014), which identified m6A peaks using the bed or bigwig format. Output was visualized using IGV software[5] (Robinson et al., 2011). MEME[6] (Bailey et al., 2009) and HOMER[7] were used to identify *de novo* and known motifs, followed by localization of the motif with respect to the peak summit.

Peaks were annotated based on intersection with gene architecture using the ChIPseeker package in R[8] (Yu et al., 2015). The expression levels of all mRNAs in input libraries were assessed using StringTie[9]. FPKM was calculated as total exon fragments/mapped reads (millions) × exon length (kB). The mRNAs differentially expressed between *Tyrobp*$^{-/-}$ and WT mice were defined as those showing fold change ≥ 2 or ≤ -2 and $P < 0.05$ based on the edgeR package in R[10] (Robinson et al., 2010).

Statistical Analysis

All statistical analyses were conducted using GraphPad Prism (version 8.0, Graphpad, San Diego, CA, United States). Data were presented as mean ± SEM. Pairwise comparisons were assessed for significance using Student's *t* test for independent samples. Differences in the Morris water maze test were assessed using two-way ANOVA for repeated measures, followed by Tukey's *post hoc* test. Differences in gene expression profiles were assessed in terms of fold change. $P < 0.05$ were considered statistically significant.

[4]https://bioconductor.org/packages/exomePeak

[5]https://www.igv.org

[6]https://meme-suite.org

[7]http://homer.ucsd.edu/homer/motif

[8]https://bioconductor.org/packages/ChIPseeker

[9]https://ccb.jhu.edu/software/stringtie

[10]https://bioconductor.org/packages/edgeR

RESULTS

Learning and Memory Deficits in *Tyrobp*$^{-/-}$ Mice

Tyrobp$^{-/-}$ mice showed extremely low expression of TYROBP, whereas WT animals showed abundant protein, especially in microglia (**Figures 1A–C**).

On day 1 in the Morris water maze, escape latency was higher for *Tyrobp*$^{-/-}$ mice than for WT animals aged 2 months (20.95 ± 3.31 vs. 10.51 ± 3.21 s, $P = 0.008$), 6 months (24.27 ± 4.80 vs. 12.54 ± 2.78 s, $P = 0.019$) or 9 months (39.63 ± 9.33 vs. 23.90 ± 3.86 s, $P = 0.036$; **Figures 2A–C**). Similar results were observed on day 5 among animals aged 2 months (10.65 ± 0.61 vs. 8.97 ± 0.81 s, $P = 0.032$), 6 months (22.38 ± 0.77 vs. 13.27 ± 0.99 s, $P = 0.0001$) or 9 months (33.39 ± 1.93 vs. 16.58 ± 1.02 s, $P = 0.002$; **Figures 2A–C**). In contrast, *Tyrobp*$^{-/-}$ and WT mice did not differ significantly in swimming speed (data not shown). *Tyrobp*$^{-/-}$ mice at all three ages showed higher levels of soluble Aβ40 and Aβ42 than WT mice in the hippocampus, cortex and cerebellum (**Figures 2D–I**).

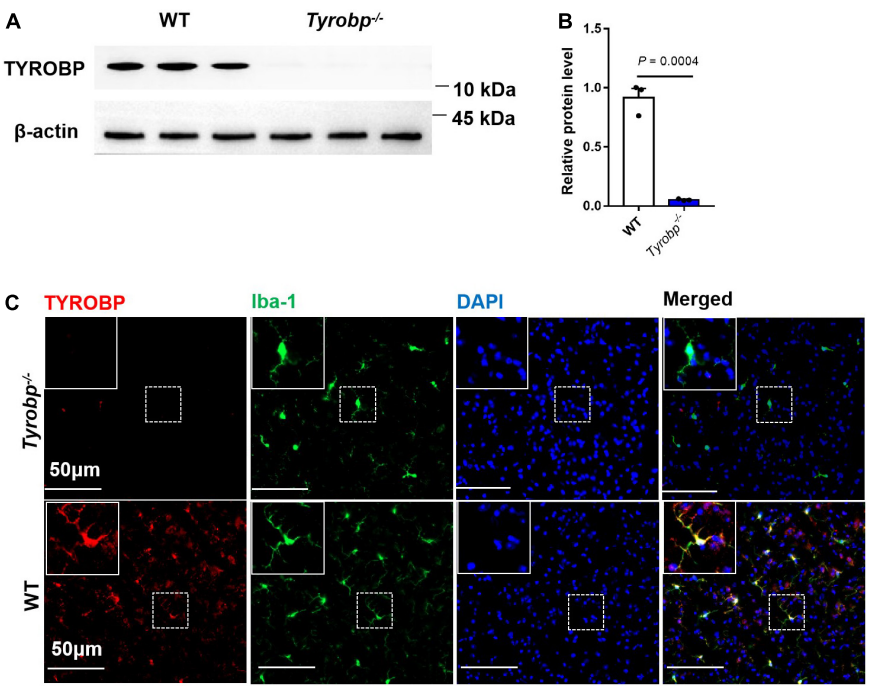

FIGURE 1 | Western blotting and immunofluorescence analysis of wild-type (WT) and *Tyrobp*$^{-/-}$ mice. **(A,B)** Western blotting and quantification of TYROBP in WT and *Tyrobp*$^{-/-}$ mice. **(C)** Immunofluorescence analysis of WT and *Tyrobp*$^{-/-}$ mice. Data in panel **(B)** are mean ± SEM. Statistical significance was calculated using Student's *t* test.

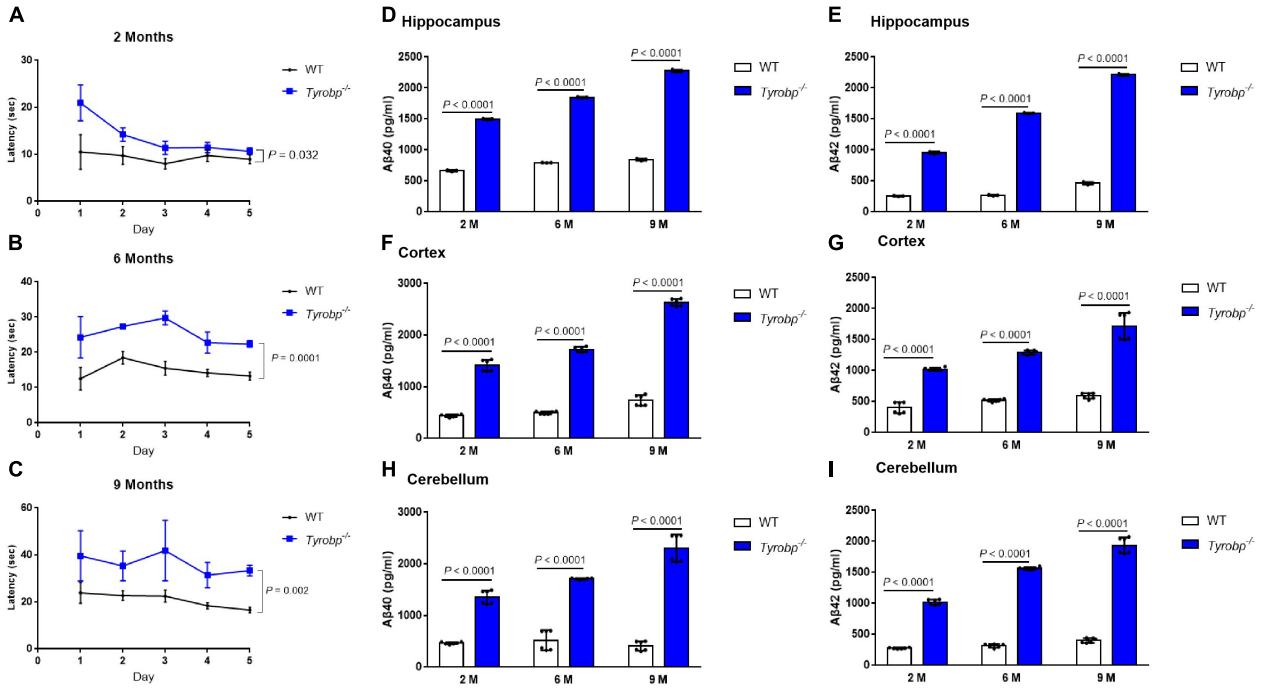

FIGURE 2 | Performance in the Morris water maze and levels of soluble Aβ40 and Aβ42 in WT and *Tyrobp*$^{-/-}$ mice. **(A–C)** Escape latency of WT and *Tyrobp*$^{-/-}$ mice aged 2, 6, or 9 months. **(D,E)** Levels of soluble Aβ40 and Aβ42 in hippocampus of WT and *Tyrobp*$^{-/-}$ mice aged 2, 6, or 9 months (M), as detected by ELISA. **(F,G)** Levels of soluble Aβ40 and Aβ42 in cortex of WT and *Tyrobp*$^{-/-}$ mice aged 2, 6, or 9 months (M), as detected by ELISA. **(H,I)** Levels of soluble Aβ40 and Aβ42 in cerebellum of WT and *Tyrobp*$^{-/-}$ mice aged 2, 6, or 9 months (M), as detected by ELISA. Data are mean ± SEM (six mice per group). Differences were assessed for significance using two-way ANOVA for repeated measures, followed by Tukey's *post hoc* test.

Higher Levels of Total Tau, Ser202/Thr205-Phosphorylated Tau and Aβ in *Tyrobp*$^{-/-}$ Mice

Given that *Tyrobp*$^{-/-}$ mice showed abnormal behavior and elevated levels of soluble Aβ40 and Aβ42 at 2, 6, and 9 months, we used six-month-old animals in subsequent experiments. *Tyrobp*$^{-/-}$ mice showed significantly higher hippocampal levels of total tau (5.23 ± 0.24 vs. 3.06 ± 0.20%, $P < 0.0001$), Ser202/Thr205-phosphorylated tau (13.82 ± 0.64 vs. 6.20 ± 0.37%, $P < 0.0001$) and Aβ (17.40 ± 0.56 vs. 5.24 ± 0.28%, $P < 0.0001$; **Figure 3**). Similar results were observed in the cortex: total tau, 8.82 ± 0.45 vs. 4.82 ± 0.32%, $P < 0.0001$; Ser202/Thr205-phosphorylated tau, 12.75 ± 0.48 vs. 3.71 ± 0.45%, $P < 0.0001$; and Aβ, 15.39 ± 1.92 vs. 5.09 ± 1.10%, $P < 0.0001$ (**Supplementary Figure 1**). Similar results were also observed in the cerebellum: total tau, 7.91 ± 0.31 vs. 4.76 ± 0.27%, $P < 0.0001$; Ser202/Thr205-phosphorylated tau, 7.98 ± 0.53 vs. 3.68 ± 0.28%, $P < 0.0001$; and Aβ, 7.27 ± 0.43 vs. 3.32 ± 0.24%, $P < 0.0001$ (**Supplementary Figure 2**).

To benchmark the phenotype of *Tyrobp*$^{-/-}$ mice against an AD phenotype, we compared hippocampal levels of total tau and Ser202/Thr205-phosphorylated tau between *Tyrobp*$^{-/-}$ and *APP/PS1* mice, all 15 months old. *Tyrobp*$^{-/-}$ mice showed higher levels of Ser202/Thr205-phosphorylated tau (0.45 ± 0.10 vs. 0.88 ± 0.07, $P = 0.043$) and total tau (0.79 ± 0.22 vs. 1.51 ± 0.07, $P = 0.047$) than WT animals. However, *Tyrobp*$^{-/-}$ mice showed lower levels of Ser202/Thr205-phosphorylated tau (0.79 ± 0.22 vs. 1.49 ± 0.10, $P = 0.015$) and total tau (1.51 ± 0.07 vs. 1.81 ± 0.02, $P = 0.012$) than the *APP/PS1* mice (**Figure 4**).

Reduced m6A Methyltransferases in the Hippocampus of *Tyrobp*$^{-/-}$ Mice

Tyrobp$^{-/-}$ mice contained significantly lower hippocampal levels of *Mettl3*, *Mettl14*, and *Wtap* mRNAs, which encode methyltransferases ($P < 0.001$, **Figure 5A**). These mRNA results were verified at the protein level by western blotting (**Figures 5B,C**). In contrast, the two types of animals did not differ significantly in expression of the *Fto* or *Alkbh5* genes encoding demethylases.

The global m6A RNA methylation level in hippocampal was significantly lower in six-month-old *Tyrobp*$^{-/-}$ mice than in age-matched WT animals (0.0357 ± 0.00008 vs. 0.0529 ± 0.00005%, $P = 0.005$), (**Supplementary Figure 3A**). Similarly, based on immunofluorescence staining, the m6A RNA methylation were significantly lower in six-month-old *Tyrobp*$^{-/-}$ mice than in age-matched WT animals (12.12 ± 1.69 vs. 5.54 ± 0.81, $P = 0.024$) (**Supplementary Figure 3B**), and the decrease in m6A methylation occurred in microglia (1.14 ± 0.12 vs. 0.63 ± 0.06, $P = 0.020$) (**Supplementary Figures 3C,D**), astrocytes (4.27 ± 0.39 vs. 2.76 ± 0.30, $P = 0.037$) (**Supplementary Figures 3E,F**) and neurons (10.17 ± 1.20 vs. 4.78 ± 0.55, $P = 0.015$) (**Supplementary Figures 3G,H**).

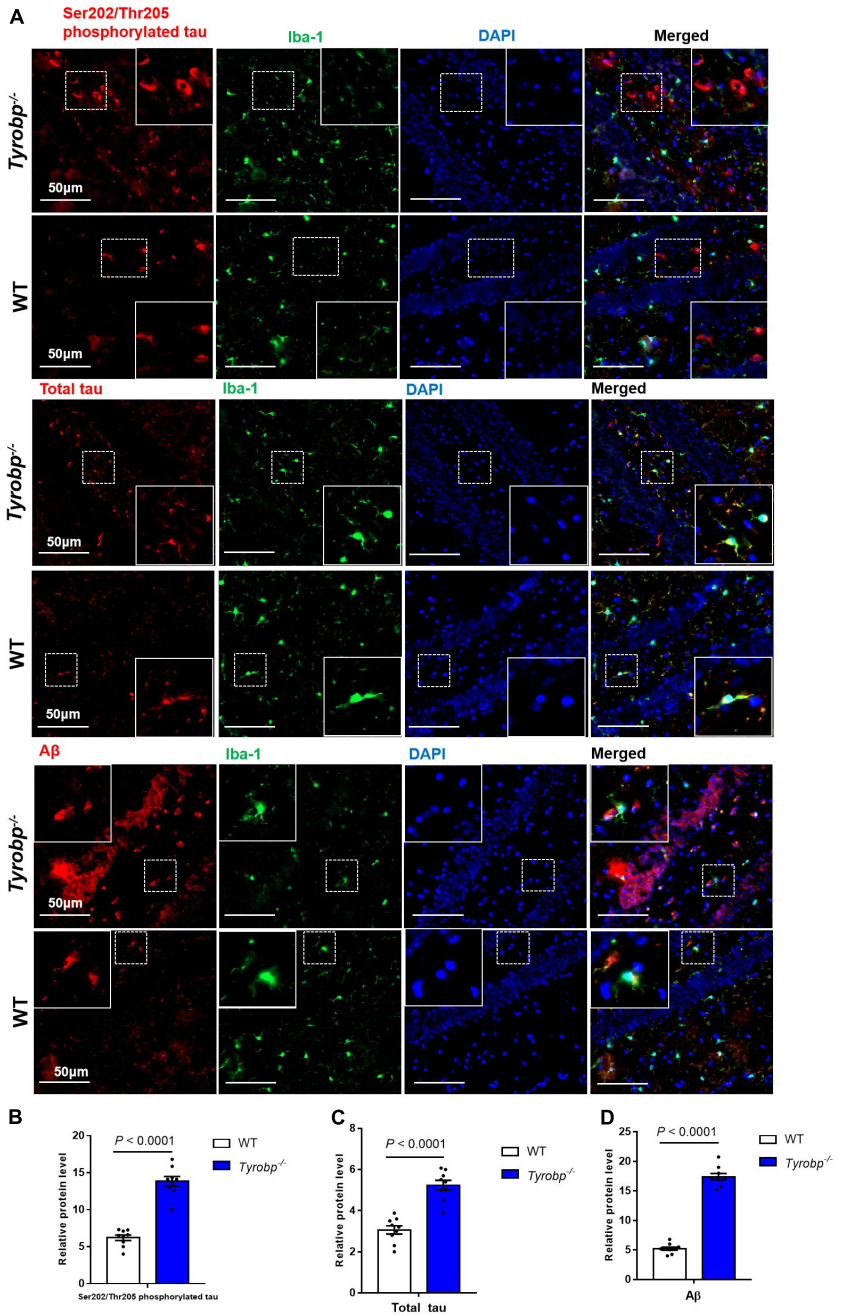

FIGURE 3 | Numbers of hippocampal cells immunopositive for total tau, Ser202/Thr205-phosphorylated tau, and Aβ. Tissues from hippocampus of wild-type (WT) and *Tyrobp*$^{-/-}$ mice aged 6 months were immunostained for total tau (tau-5), Ser202/Thr205-phosphorylated tau (AT8), and Aβ (6E10). **(A)** Representative micrographs. **(B–D)** Quantification of total tau, Ser202/Thr205-phosphorylated tau, and Aβ. Data are mean ± SEM from three independent experiments (three mice per group). Differences were assessed for significance using Student's *t* test.

Altered m6A RNA Methylation Patterns in *Tyrobp*$^{-/-}$ Mice

The original data, which were deposited in the GEO database under accession number GSE179827, were of generally high quality, with > 97% of reads meeting the Q20 criterion and > 92% of reads exceeding the Q30 criterion (**Supplementary Table 2**). *Tyrobp*$^{-/-}$ mice showed 810 m6A peaks differing significantly from WT animals (**Supplementary Table 3**), of which 498 peaks were significantly higher and 312 significantly lower in *Tyrobp*$^{-/-}$ mice (**Figure 6A**). In *Tyrobp*$^{-/-}$ and WT mice, the m6A peaks were enriched mainly near stop codons and 3′-untranslated regions (**Figure 6B**), and the peaks differing

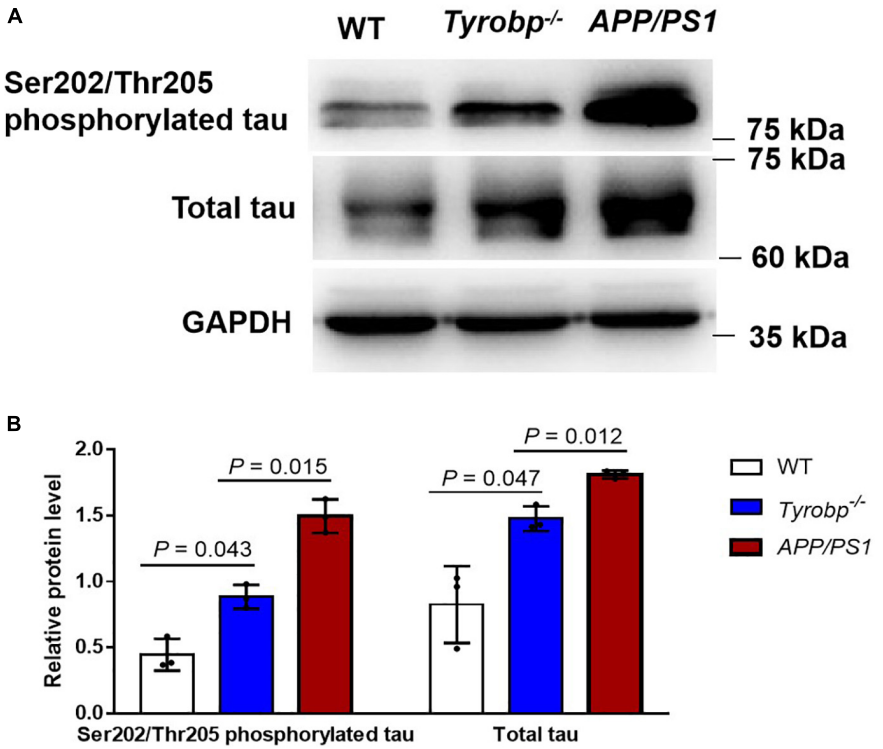

FIGURE 4 | Levels of total tau and Ser202/Thr205-phosphorylated tau in WT, *Tyrobp*$^{-/-}$ and *APP/PS1* mice. **(A)** Western blot analysis. **(B)** Quantification of total tau and Ser202/Thr205-phosphorylated tau. Data are mean ± SEM from three independent experiments (three mice per group). Differences were assessed for significance using Student's *t* test.

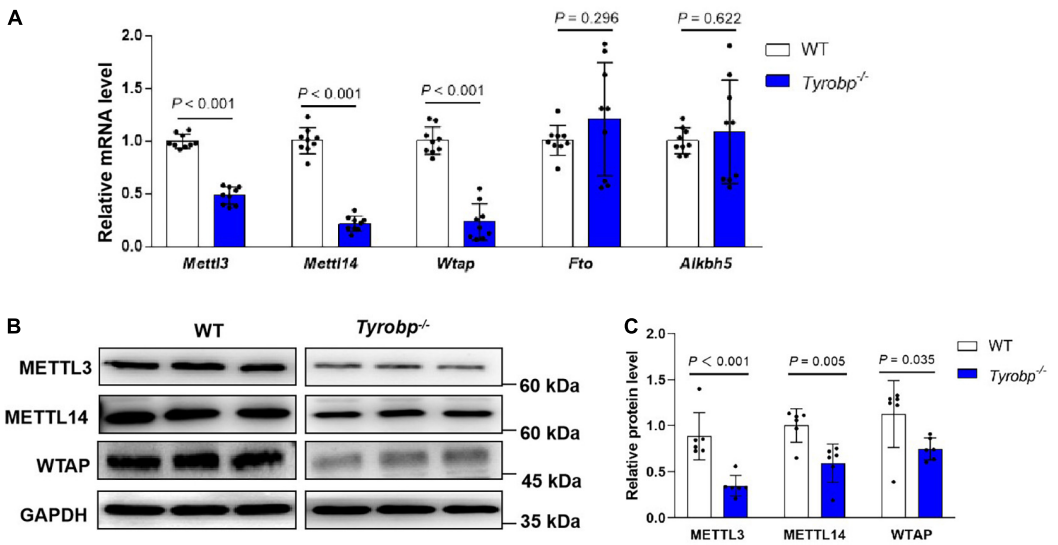

FIGURE 5 | Reduced m6A RNA methyltransferases in the hippocampus of *Tyrobp*$^{-/-}$ mice. **(A)** Relative levels of *Mettl3*, *Mettl14*, and *Wtap* mRNAs encoding methyltransferases and of *Fto* and *Alkbh5* mRNAs encoding demethylases. **(B,C)** Western blotting and quantification of METTL3, METTL14 and WTAP in the hippocampus. Data are mean ± SEM (six or nine mice per group). Differences were assessed for significance using Student's *t* test.

significantly between the two types of mice occurred most often in the 3′-untranslated region (53.26%), followed by other exons (18.62%), 5′-untranslated regions (17.93%), and first exons (10.2%) (**Figure 6C**). Compared to WT animals, *Tyrobp*$^{-/-}$ mice showed higher proportions of m6A peaks in 3′-untranslated regions (49.32 vs. 47.22%) and first exons (11.63 vs. 11.47%), but

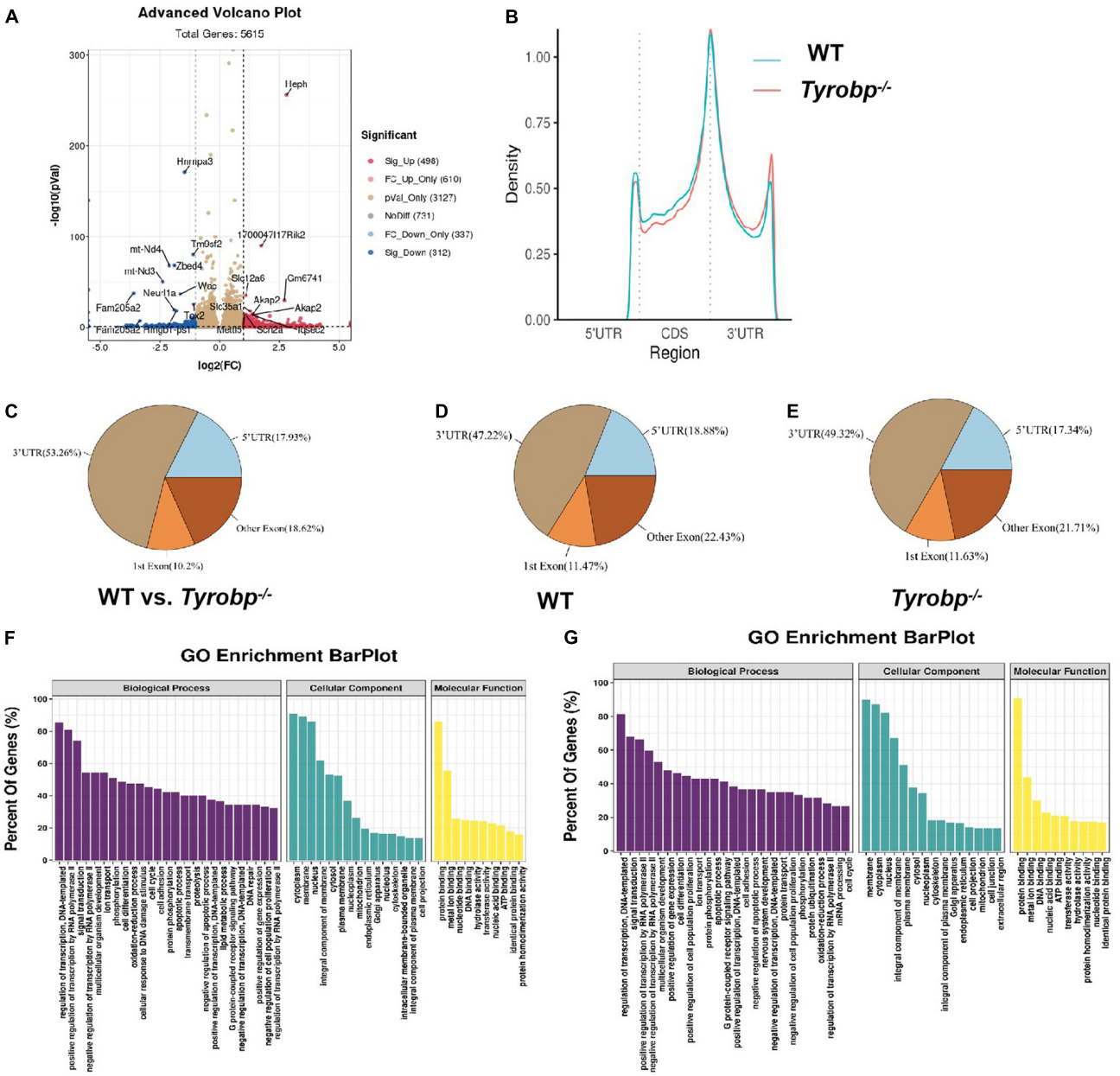

FIGURE 6 | Characteristics of m6A methylation in the hippocampus of 6-month-old *Tyrobp*$^{-/-}$ mice. **(A)** Volcano plots showing m6A peaks differing significantly between *Tyrobp*$^{-/-}$ and wild-type (WT) mice. **(B)** Average distribution of m6A peaks along transcripts in the hippocampus. **(C–E)** Pie charts showing the distribution of m6A peaks. **(F)** Major Gene Ontology terms for transcripts whose m6A methylation was upregulated in *Tyrobp*$^{-/-}$ mice. **(G)** Major Gene Ontology terms for transcripts whose m6A methylation was downregulated in *Tyrobp*$^{-/-}$ mice. Up- or downregulation was defined, respectively, as fold change ≥ 2 or fold change ≤ -2 combined with $P < 0.05$. Nine mice were used in each group.

lower proportions in 5′-untranslated regions (17.34 vs. 18.88%) and other exons (21.71 vs. 22.43%) (**Figures 6D,E**).

In Gene Ontology (GO) analysis, the upregulated peaks were significantly associated with the following biological processes: regulation of DNA-templated transcription, positive regulation of transcription by RNA polymerase II and signal transduction. The upregulated peaks were associated with the cellular components of cytoplasm, membrane and nucleus; and they were associated with the molecular functions of protein binding, metal ion binding and nucleotide binding (**Figure 6F**).

The downregulated peaks, in contrast, were associated mainly with the biological processes of regulation of DNA-templated transcription, signal transduction, and positive regulation of transcription by RNA polymerase II (**Figure 6G**). Downregulated peaks were also associated with the cellular components of membrane, cytoplasm and nucleus; and they were associated with

the molecular functions of protein binding, metal ion binding and DNA binding.

Altered Hippocampal Gene Expression in *Tyrobp*$^{-/-}$ Mice

RNA sequencing data showed that 86 genes were upregulated in *Tyrobp*$^{-/-}$ mice relative to WT controls, while 85 genes were down-regulated (**Supplementary Table 4**). The top five upregulated genes were *Fam177a, Pmch, Pcdhgb4, Hcrt,* and *Tmem181c-ps,* and the top five downregulated genes were *Mgam, Pcdhga2, Gpr176, Pcdhga9,* and *Proz* (**Figures 7A,B**). The altered expression of three upregulated genes (*Fam177a*, *Pcdhgb4* and *Tmem181c-ps*) and three downregulated genes (*Pcdhga2*, *Gpr176* and *Slc16a7*) was verified using quantitative real-time PCR (**Figure 7C**).

The major GO terms and KEGG pathways involving upregulated genes are shown in **Figures 7D,E**. Upregulated KEGG pathways included the cAMP signaling pathway, axon guidance and MAPK signaling pathway (**Figure 7E**). The major GO terms and KEGG pathways involving downregulated genes are shown in **Figures 7F,G**. Downregulated KEGG pathways included the AMPK signaling pathway, PI3K-Akt signaling pathway, and human papillomavirus infection (**Figure 7G**).

Correlation of Altered m6A RNA Methylation With Altered Gene Expression in the Hippocampus of *Tyrobp*$^{-/-}$ Mice

We identified genes whose m6A methylation at the RNA level and whose gene expression were altered (**Supplementary Table 5**), leading to four groups (**Figure 8A**): hypermethylation and upregulation, 38 genes; hypomethylation and downregulation, 16 genes; hypomethylation and upregulation, 43 genes; and hypermethylation and downregulation, 84 genes.

In GO analysis, the top three biological processes were regulation of DNA-templated transcription, negative regulation of ERK1 and ERK2 cascades, and chemical synaptic transmission. The top three cellular components were nucleus, cytoplasm, and membrane, while the top three molecular functions were protein binding, metal ion binding, and nucleic acid binding (**Figure 8B**). The KEGG analysis enriched for the overlap genes were cell adhesion molecules, NOD-like receptor (NLR) signaling and folate biosynthesis (**Figure 8C**).

Cell adhesion molecules of interest included Cldn19, H2-M5 and Alcam. In *Tyrobp*$^{-/-}$ mice, these genes were m6A-hypomethylated and upregulated. The NLR signaling pathway includes *Nlrp6* and *Pstpip1*. In *Tyrobp*$^{-/-}$ mice, the *Nlrp6* gene was m6A-hypermethylated and downregulated, while the *Pstpip1* gene was m6A-hypomethylated and upregulated.

DISCUSSION

Here we demonstrate AD-like histopathology and behavioral deficits in *Tyrobp*$^{-/-}$ mice, which were linked to downregulation of the methyltransferases METTL3, METTL14, and WTAP. These findings suggest that TYROBP deficiency may associate with an altered m6A epitranscriptome in hippocampus as well as altered expression of a variety of genes and signaling pathways involved in cognitive function.

Tyrobp$^{-/-}$ mice mimic central features of NHD and AD, most notably learning and memory deficits (Cui et al., 2021). *Tyrobp*$^{-/-}$ mice in our study showed elevated levels of total tau, Ser202/Thr205-phosphorylated tau and Aβ in the hippocampus, cortex and cerebellum. These elevated hippocampal levels have also been observed in NHD patients (Satoh et al., 2018). NHD patients carrying the Q33X mutation in the *TREM2* gene show AD-like lesions, including Aβ deposition and neurofibrillary changes (Maderna et al., 2021). However, whether deficiency of *TYROBP* contributes to, or protects against neurodegenerative disease, remains controversial. Deleting the *TYROBP* gene from *APP*$^{KM670/671NL}$/*PSEN1*$^{\Delta exon9}$ mice mitigated behavioral and electrophysiological deficits, without affecting the total number of Iba1-positive microglia in cortex or hippocampus (Haure-Mirande et al., 2017, 2019). Deleting the *TYROBP* gene from *MAPT*^{P301S} mice also mitigated clinical and electrophysiological deficits, while paradoxically increasing tau hyperphosphorylation and spreading (Audrain et al., 2019). Overexpression of TYROBP in microglia of mice can decrease amyloid burden but increase tau phosphorylation in an *APP/PSEN1* or *MAPT*^{P301S} background (Audrain et al., 2021). These considerations lead us to speculate that each particular state of microglial activation is associated with an optimal level of TYROBP expression.

The m6A methylation is the most frequent reversible post-transcriptional methylation of mammalian mRNA. The level of m6A methylation increases in the mouse brain during adulthood (Meyer et al., 2012), and it helps regulate long-term memory formation (Zhang et al., 2018), facilitating hippocampus-dependent learning and memory through the YTHDF1 protein (Shi et al., 2018). AD patients show decreased m6A methylation in neurons of the hippocampus and cortex, but higher methylation in GFAP-positive astrocytes and some Iba1-positive microglia (Zhao et al., 2021). The *APP/PS1* mouse model of AD, in contrast, shows elevated m6A methylation, but the immunofluorescence analysis were not done (Han et al., 2020). *Tyrobp*$^{-/-}$ mice in our study showed reduced m6A methylation in microglia, astrocytes and in neurons. However, the immunofluorescence cannot report differentially on ribosomal RNA and mRNA, since they colocalize, an mRNA-enriched ELISA is needed in the future. Further investigation is also needed to clarify whether NHD and AD involve similar changes in m6A methylation, and to explore how these changes correlate with the pathological hallmarks of the two diseases.

In our study, METTL3, METTL14, and WTAP were downregulated in *Tyrobp*$^{-/-}$ mice, and the same proteins were downregulated in hippocampus and cortex of AD patients (Zhao et al., 2021). METTL3 plays a key role in m6A methylation, and depleting METTL3 from the hippocampus of C57BL/6 mice compromises memory consolidation (Zhang et al., 2018) and triggers extensive synaptic loss, neuronal death, oxidative stress and aberrant cell cycling (Zhao et al., 2021). Other studies have linked AD in humans to accumulation of insoluble METTL3 in hippocampus (Huang et al., 2020), or even to

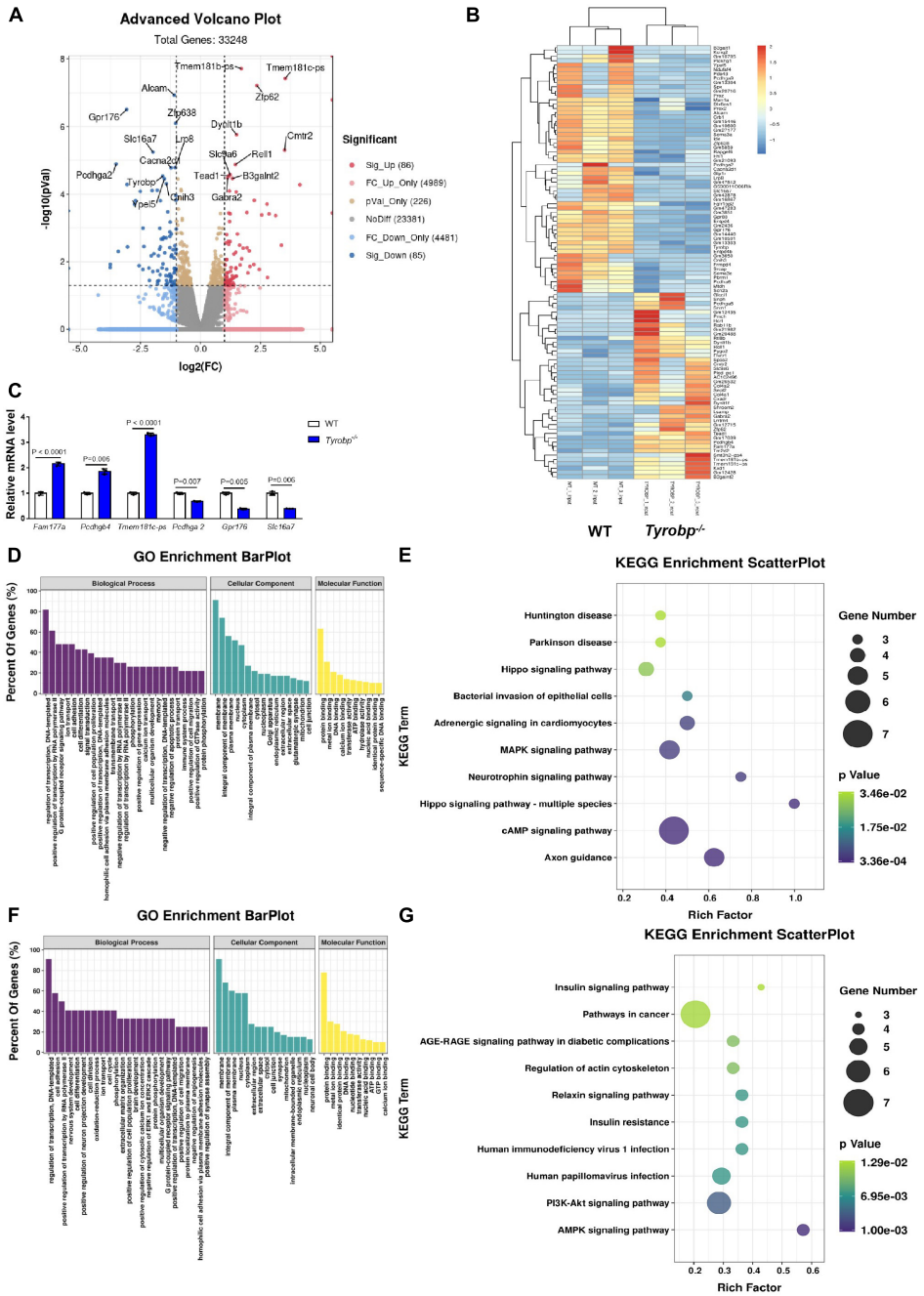

FIGURE 7 | Volcano plots, heatmaps, Gene Ontology (GO) terms and Kyoto Encyclopedia of Genes and Genomes (KEGG) pathways enriched in genes differentially expressed between wild-type (WT) and *Tyrobp*$^{-/-}$ mice. **(A)** Volcano plots and **(B)** heatmap showing genes and transcripts differentially expressed between WT and *Tyrobp*$^{-/-}$ mice. **(C)** Quantitative real-time PCR detection of six genes chosen from the methylated RNA immunoprecipitation sequencing data. **(D,E)** Major GO terms and KEGG pathways were analyzed for genes upregulated by *Tyrobp* knockout. **(F,G)** Major GO terms and KEGG pathways were analyzed for genes downregulated by *Tyrobp* knockout. Up- or downregulation was defined, respectively, as fold change ≥ 2 or fold change ≤ –2 combined with $P < 0.05$. Nine mice were used in each group.

upregulation of METTL3 in the cortex and hippocampus of one mouse model of AD (Han et al., 2020). These conflicting results highlight the need for future studies to clarify how altered m6A methyltransferase activity may contribute to neurological diseases.

Knocking out TYROBP in our mice did not alter expression of FTO or ALKBH5, consistent with a report of normal FTO and ALKBH5 levels in soluble and insoluble hippocampal fractions from AD patients (Huang et al., 2020). Other studies, however, have reported downregulated FTO in the hippocampus of AD

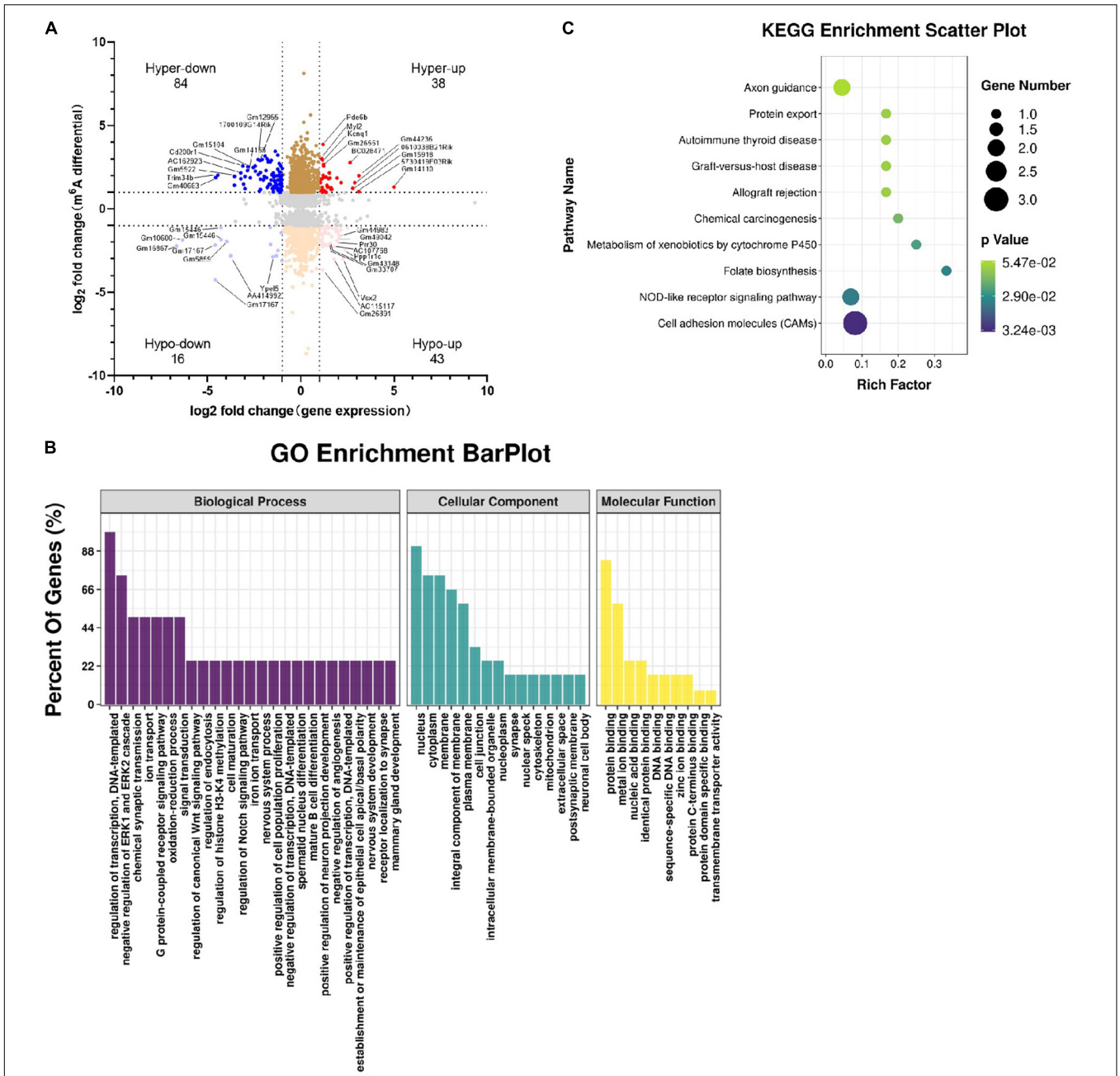

FIGURE 8 | Combined analyses of m6A-RIP-seq and RNA-seq data. Genes whose expression and m6A methylation differed significantly between *Tyrobp*$^{-/-}$ and wild-type mice were analyzed in terms of their **(A)** four-quadrant distribution (see Results), **(B)** major GO terms, and **(C)** top 10 KEGG pathways. Fold change ≥ 2 or fold change ≤ –2 and $P < 0.05$, nine mice were used in each group.

patients and an AD mouse model (Han et al., 2020; Zhao et al., 2021), as well as in the cortex of a rat model for traumatic brain injury (Yu et al., 2020). These discrepancies may depend on the animal species, pathological state, disease stage, and brain fraction (soluble or insoluble) being studied.

Our study appears to report the first analysis of a relationship between differentially expressed m6A peaks and genes in NHD or AD. We found many of the differentially expressed m6A peaks to be related with cancer, including peaks affecting the genes *Trim58*, *Fam83f*, *Whrn*, and *Pde6b*. Among the differentially expressed genes known to be relevant to neuronal functions, the *Pcdhs* cluster, including *Pcdha* and *Pcdhg*, are highly expressed in the brain and help guide neurons during brain development, neuronal differentiation, and synaptogenesis (Shimojima et al., 2011). In *Tyrobp*$^{-/-}$ mice, *Pcdhgb4* and *Pcdhga8* were upregulated, while *Pcdhga2, Pcdhga9* and *Pcdhgb8*

were downregulated, suggesting that *Pcdhg* gene expression might have some relation with TYROBP. *Fam177a* was upregulated in our *Tyrobp*$^{-/-}$ mice, and downregulation of this gene impairs the transduction of TLR4 signaling; inhibits the phosphorylation of NF-κB, Akt, Erk1/2 and JNK; and downregulates TLR4, MyD88, TRAF6, and TRIF (Chen et al., 2021). The potential implication of *Fam177a* in AD requires further investigation.

Our *Tyrobp*$^{-/-}$ mice showed dysregulation of several pathways, including signaling pathways involving cAMP, MAPK, AMPK, and PI3K-Akt. TYROBP may interact with SHIP1 and DOK3 to inhibit Syk, PI3K, and ERK, as well as signaling involving Toll-like receptors in macrophages (Xing et al., 2015; Hamerman et al., 2016). PI3K activates Akt to inhibit mitogen-activated protein kinase kinase kinase, which in turn inhibits Toll-like receptors (Hamerman et al., 2009). Analysis of the overlap between m6A methylation and gene expression identified several pathways, such as the NLR signaling pathway. Unlike Toll-like receptors, NOD-like receptors are intracellular proteins that scan the cytoplasm for the presence of intracellular invaders. Future studies are needed to examine whether NLRs also contribute to NHD.

Our *Tyrobp*$^{-/-}$ mice showed dysregulation of pathways involving cell adhesion molecules. Neural cell adhesion molecules are involved in memory formation and consolidation (Welzl and Stork, 2003), and they also regulate synapse formation, maintenance and function (Thalhammer and Cingolani, 2014). Levels and function of synaptic cell adhesion molecules are altered in brain tissues, cerebrospinal fluid, and sera in AD patients (Leshchyns'ka and Sytnyk, 2016). Our results provide a hint of a relationship between cell adhesion molecules and NHD, so the potential role of these molecules in memory impairment should be explored.

In summary, our study demonstrates that *Tyrobp*$^{-/-}$ mice share behavioral and pathological features of mouse models of AD. Knocking out TYROBP reduced m6A methyltransferases components METTL3, METTL14, and WTAP. These and other observed alterations in m6A methylation profiles may provide clues to the pathogenesis of NHD, AD and other diseases related to the *Tyrobp* gene. Further study is necessary to investigate how decreasing m6A methylation mediates the histopathological and behavioral deficits of *Tyrobp*$^{-/-}$ mice.

DATA AVAILABILITY STATEMENT

The datasets presented in this study can be found in online repositories. The names of the repository/repositories and accession number(s) can be found below: Gene Expression Omnibus accession: GSE179827, available at: https://www.ncbi.nlm.nih.gov/geo/query/acc.cgi?acc=GSE179827.

ETHICS STATEMENT

The animal study was reviewed and approved by Ethical Committee for Animal Experiments at The Affiliated Hospital of Jining Medical University.

AUTHOR CONTRIBUTIONS

ZL and YH designed the study. TX, RL, and YL conducted the experiments. ZL, TX, DZ, WL, RL, and YY analyzed the data. ZL and TX wrote the manuscript. All authors approved the manuscript for publication.

FUNDING

This study was supported by the Natural Science Foundation of China (81401064 and 81771360), the Natural Science Foundation of Shandong Province (ZR2017LH031), and the Shandong Province Medical and Health Science and Technology Development Plan Project (2017WS222).

SUPPLEMENTARY MATERIAL

The Supplementary Material for this article can be found online at: https://www.frontiersin.org/articles/10.3389/fnins.2022.739201/full#supplementary-material

Supplementary Figure 1 | Numbers of cells immunopositive for total tau, Ser202/Thr205-phosphorylated tau, and Aβ in cortex. Cortical tissues were immunostained for total tau (tau-5), Ser202/Thr205-phosphorylated tau (AT8), and Aβ (6E10) in 6-month-old *Tyrobp*$^{-/-}$ and wild-type (WT) mice. **(A)** Representative micrographs. **(B–D)** Quantification of total tau, Ser202/Thr205-phosphorylated tau, and Aβ. Data are mean ± SEM from three independent experiments (three mice per group). Differences were assessed for significance using Student's *t* test.

Supplementary Figure 2 | Numbers of cells immunopositive for total tau, Ser202/Thr205-phosphorylated tau, and Aβ in cerebellum. Cerebellum tissues were immunostained for total tau (tau-5), Ser202/Thr205-phosphorylated tau (AT8), and Aβ (6E10) in 6-month-old *Tyrobp*$^{-/-}$ and wild-type (WT) mice. **(A)** Representative micrographs. **(B–D)** Quantification of total tau, Ser202/Thr205-phosphorylated tau, and Aβ. Data are mean ± SEM from three independent experiments (three mice per group). Differences were assessed for significance using Student's *t* test.

Supplementary Figure 3 | Reduced m6A RNA methylation in hippocampus of *Tyrobp*$^{-/-}$ mice. **(A)** Quantification of total m6A RNA methylation in *Tyrobp*$^{-/-}$ mice and wild-type (WT) mice. **(B)** Quantification of total m6A RNA methylation in *Tyrobp*$^{-/-}$ mice and wild-type (WT) mice, based on immunofluorescence staining. **(C,D)** Immunofluorescence staining and quantification analysis of m6A RNA methylation with microglia marker IBA1 in hippocampal tissues from *Tyrobp*$^{-/-}$ mice and WT mice. **(E,F)** Immunofluorescence staining and quantification analysis of m6A RNA methylation with astrocytes marker GFAP in hippocampal tissues from *Tyrobp*$^{-/-}$ mice and WT mice. **(G,H)** Immunofluorescence staining and quantification analysis of m6A RNA methylation with neuron marker NeuN in hippocampal tissues from *Tyrobp*$^{-/-}$ mice and WT mice. Data are mean ± SEM (three to six mice per group). Differences were assessed for significance using Student's *t* test.

Supplementary Table 1 | Sequences of primers used for RT-qPCR analysis of mRNA levels.

Supplementary Table 2 | Information of quality control of the raw data.

Supplementary Table 3 | Comparison of m6A RNA methylation in *Tyrobp*$^{-/-}$ and wild-type (WT) mice.

Supplementary Table 4 | Genes detected in *Tyrobp*$^{-/-}$ and wild-type (WT) mice.

Supplementary Table 5 | Gene expression and m6A peaks overlapping between *Tyrobp*$^{-/-}$ and wild-type (WT) mice.

REFERENCES

Audrain, M., Haure-Mirande, J. V., Mleczko, J., Wang, M., Griffin, J. K., St George-Hyslop, P. H., et al. (2021). Reactive or transgenic increase in microglial TYROBP reveals a TREM2-independent TYROBP-APOE link in wild-type and Alzheimer's-related mice. *Alzheimers Dement.* 17, 149–163. doi: 10.1002/alz.12256

Audrain, M., Haure-Mirande, J. V., Wang, M., Kim, S. H., Fanutza, T., Chakrabarty, P., et al. (2019). Integrative approach to sporadic Alzheimer's disease: deficiency of TYROBP in a tauopathy mouse model reduces C1q and normalizes clinical phenotype while increasing spread and state of phosphorylation of tau. *Mol. Psychiatry* 24, 1383–1397. doi: 10.1038/s41380-018-0258-3

Bailey, T. L., Boden, M., Buske, F. A., Frith, M., Grant, C. E., Clementi, L., et al. (2009). MEME SUITE: tools for motif discovery and searching. *Nucleic Acids Res.* 37, W202–W208. doi: 10.1093/nar/gkp335

Chen, H., Guo, M., Yue, D., Zhao, J., Zhou, Y., Chen, C., et al. (2021). MicroRNA-7 negatively regulates Toll-like receptor 4 signaling pathway through FAM177A. *Immunology* 162, 44–57. doi: 10.1111/imm.13252

Chen, S., Zhou, Y., Chen, Y., and Gu, J. (2018). fastp: an ultra-fast all-in-one FASTQ preprocessor. *Bioinformatics* 34, i884–i890. doi: 10.1093/bioinformatics/bty560

Cui, X., Qiao, J., Liu, S., Wu, M., and Gu, W. (2021). Mechanism of TREM2/DAP12 complex affecting beta-amyloid plaque deposition in Alzheimer's disease modeled mice through mediating inflammatory response. *Brain Res. Bull.* 166, 21–28. doi: 10.1016/j.brainresbull.2020.10.006

Hamerman, J. A., Ni, M., Killebrew, J. R., Chu, C. L., and Lowell, C. A. (2009). The expanding roles of ITAM adapters FcRgamma and DAP12 in myeloid cells. *Immunol. Rev.* 232, 42–58. doi: 10.1111/j.1600-065X.2009.00841.x

Hamerman, J. A., Pottle, J., Ni, M., He, Y., Zhang, Z. Y., and Buckner, J. H. (2016). Negative regulation of TLR signaling in myeloid cells–implications for autoimmune diseases. *Immunol. Rev.* 269, 212–227. doi: 10.1111/imr.12381

Han, M., Liu, Z., Xu, Y., Liu, X., Wang, D., Li, F., et al. (2020). Abnormality of m6A mRNA methylation is involved in Alzheimer's disease. *Front. Neurosci.* 14:98. doi: 10.3389/fnins.2020.00098

Haure-Mirande, J. V., Audrain, M., Fanutza, T., Kim, S. H., Klein, W. L., Glabe, C., et al. (2017). Deficiency of TYROBP, an adapter protein for TREM2 and CR3 receptors, is neuroprotective in a mouse model of early Alzheimer's pathology. *Acta Neuropathol.* 134, 769–788. doi: 10.1007/s00401-017-1737-3

Haure-Mirande, J. V., Wang, M., Audrain, M., Fanutza, T., Kim, S. H., Heja, S., et al. (2019). Integrative approach to sporadic Alzheimer's disease: deficiency of TYROBP in cerebral Abeta amyloidosis mouse normalizes clinical phenotype and complement subnetwork molecular pathology without reducing Abeta burden. *Mol. Psychiatry* 24, 431–446. doi: 10.1038/s41380-018-0255-6

Hickman, S. E., Kingery, N. D., Ohsumi, T. K., Borowsky, M. L., Wang, L. C., Means, T. K., et al. (2013). The microglial sensome revealed by direct RNA sequencing. *Nat. Neurosci.* 16, 1896–1905. doi: 10.1038/nn.3554

Huang, H., Camats-Perna, J., Medeiros, R., Anggono, V., and Widagdo, J. (2020). Altered expression of the m6A Methyltransferase METTL3 in Alzheimer's disease. *eNeuro* 7, ENEURO.0125–20.2020. doi: 10.1523/ENEURO.0125-20.2020

Jia, G., Fu, Y., Zhao, X., Dai, Q., Zheng, G., Yang, Y., et al. (2011). N6-methyladenosine in nuclear RNA is a major substrate of the obesity-associated FTO. *Nat. Chem. Biol.* 7, 885–887. doi: 10.1038/nchembio.687

Kim, D., Langmead, B., and Salzberg, S. L. (2015). HISAT: a fast spliced aligner with low memory requirements. *Nat. Methods* 12, 357–360. doi: 10.1038/nmeth.3317

Leshchyns'ka, I., and Sytnyk, V. (2016). Synaptic cell adhesion molecules in Alzheimer's disease. *Neural Plast.* 2016:6427537. doi: 10.1155/2016/6427537

Liu, J., Yue, Y., Han, D., Wang, X., Fu, Y., Zhang, L., et al. (2014). A METTL3-METTL14 complex mediates mammalian nuclear RNA N6-adenosine methylation. *Nat. Chem. Biol.* 10, 93–95. doi: 10.1038/nchembio.1432

Lv, Z., Shi, Q., Huang, W., Xing, C., Hao, Y., Feng, X., et al. (2016). MicroRNA expression profiling in Guillain-Barre syndrome. *J. Neuroimmunol.* 301, 12–15. doi: 10.1016/j.jneuroim.2016.10.014

Ma, J., Jiang, T., Tan, L., and Yu, J. T. (2015). TYROBP in Alzheimer's disease. *Mol. Neurobiol.* 51, 820–826. doi: 10.1007/s12035-014-8811-9

Maderna, E., Visona, S., Bolcato, V., Redaelli, V., Caroppo, P., Montalbetti, L., et al. (2021). Neuropathological Alzheimer's disease lesions in Nasu-Hakola disease with TREM2 mutation: atypical distribution of neurofibrillary changes. *J. Alzheimers Dis.* 79, 25–30. doi: 10.3233/JAD-201085

Meng, J., Lu, Z., Liu, H., Zhang, L., Zhang, S., Chen, Y., et al. (2014). A protocol for RNA methylation differential analysis with MeRIP-Seq data and exomePeak R/Bioconductor package. *Methods* 69, 274–281. doi: 10.1016/j.ymeth.2014.06.008

Meyer, K. D., Saletore, Y., Zumbo, P., Elemento, O., Mason, C. E., and Jaffrey, S. R. (2012). Comprehensive analysis of mRNA methylation reveals enrichment in 3′ UTRs and near stop codons. *Cell* 149, 1635–1646. doi: 10.1016/j.cell.2012.05.003

Paloneva, J., Kestila, M., Wu, J., Salminen, A., Bohling, T., Ruotsalainen, V., et al. (2000). Loss-of-function mutations in TYROBP (DAP12) result in a presenile dementia with bone cysts. *Nat. Genet.* 25, 357–361. doi: 10.1038/77153

Pottier, C., Ravenscroft, T. A., Brown, P. H., Finch, N. A., Baker, M., Parsons, M., et al. (2016). TYROBP genetic variants in early-onset Alzheimer's disease. *Neurobiol. Aging* 48, 222.e9–222.e15. doi: 10.1016/j.neurobiolaging.2016.07.028

Robinson, J. T., Thorvaldsdottir, H., Winckler, W., Guttman, M., Lander, E. S., Getz, G., et al. (2011). Integrative genomics viewer. *Nat. Biotechnol.* 29, 24–26. doi: 10.1038/nbt.1754

Robinson, M. D., McCarthy, D. J., and Smyth, G. K. (2010). edgeR: a Bioconductor package for differential expression analysis of digital gene expression data. *Bioinformatics* 26, 139–140. doi: 10.1093/bioinformatics/btp616

Satoh, J. I., Kino, Y., Yanaizu, M., and Saito, Y. (2018). Alzheimer's disease pathology in Nasu-Hakola disease brains. *Intractable Rare Dis. Res.* 7, 32–36. doi: 10.5582/irdr.2017.01088

Schneider, C. A., Rasband, W. S., and Eliceiri, K. W. (2012). NIH Image to ImageJ: 25 years of image analysis. *Nat. Methods* 9, 671–675. doi: 10.1038/nmeth.2089

Shi, H., Zhang, X., Weng, Y. L., Lu, Z., Liu, Y., Lu, Z., et al. (2018). m^{6}A facilitates hippocampus-dependent learning and memory through YTHDF1. *Nature* 563, 249–253. doi: 10.1038/s41586-018-0666-1

Shimojima, K., Isidor, B., Le Caignec, C., Kondo, A., Sakata, S., Ohno, K., et al. (2011). A new microdeletion syndrome of 5q31.3 characterized by severe developmental delays, distinctive facial features, and delayed myelination. *Am. J. Med. Genet. A* 155A, 732–736. doi: 10.1002/ajmg.a.33891

Thalhammer, A., and Cingolani, L. A. (2014). Cell adhesion and homeostatic synaptic plasticity. *Neuropharmacology* 78, 23–30. doi: 10.1016/j.neuropharm.2013.03.015

Welzl, H., and Stork, O. (2003). Cell adhesion molecules: key players in memory consolidation? *News Physiol. Sci.* 18, 147–150. doi: 10.1152/nips.01422.2002

Xing, J., Titus, A. R., and Humphrey, M. B. (2015). The TREM2-DAP12 signaling pathway in Nasu-Hakola disease: a molecular genetics perspective. *Res. Rep. Biochem.* 5, 89–100. doi: 10.2147/RRBC.S58057

Yu, G., Wang, L. G., and He, Q. Y. (2015). ChIPseeker: an R/Bioconductor package for ChIP peak annotation, comparison and visualization. *Bioinformatics* 31, 2382–2383. doi: 10.1093/bioinformatics/btv145

Yu, J., Zhang, Y., Ma, H., Zeng, R., Liu, R., Wang, P., et al. (2020). Epitranscriptomic profiling of N6-methyladenosine-related RNA methylation in rat cerebral cortex following traumatic brain injury. *Mol. Brain* 13:11. doi: 10.1186/s13041-020-0554-0

Zaccara, S., Ries, R. J., and Jaffrey, S. R. (2019). Reading, writing and erasing mRNA methylation. *Nat. Rev. Mol. Cell Biol.* 20, 608–624. doi: 10.1038/s41580-019-0168-5

Zhang, B., Gaiteri, C., Bodea, L. G., Wang, Z., McElwee, J., Podtelezhnikov, A. A., et al. (2013). Integrated systems approach identifies genetic nodes and networks in late-onset Alzheimer's disease. *Cell* 153, 707–720. doi: 10.1016/j.cell.2013.03.030

Zhang, Z., Wang, M., Xie, D., Huang, Z., Zhang, L., Yang, Y., et al. (2018). METTL3-mediated N(6)-methyladenosine mRNA modification enhances long-term memory consolidation. *Cell Res.* 28, 1050–1061. doi: 10.1038/s41422-018-0092-9

Zhao, F., Xu, Y., Gao, S., Qin, L., Austria, Q., Siedlak, S. L., et al. (2021). METTL3-dependent RNA m(6)A dysregulation contributes to neurodegeneration in

Alzheimer's disease through aberrant cell cycle events. *Mol. Neurodegener.* 16, 70–95. doi: 10.1186/s13024-021-00484-x

Conflict of Interest: The authors declare that the research was conducted in the absence of any commercial or financial relationships that could be construed as a potential conflict of interest.

Publisher's Note: All claims expressed in this article are solely those of the authors and do not necessarily represent those of their affiliated organizations, or those of the publisher, the editors and the reviewers. Any product that may be evaluated in this article, or claim that may be made by its manufacturer, is not guaranteed or endorsed by the publisher.

Advantages of publishing in Frontiers

OPEN ACCESS
Articles are free to read for greatest visibility and readership

FAST PUBLICATION
Around 90 days from submission to decision

HIGH QUALITY PEER-REVIEW
Rigorous, collaborative, and constructive peer-review

TRANSPARENT PEER-REVIEW
Editors and reviewers acknowledged by name on published articles

Frontiers
Avenue du Tribunal-Fédéral 34
1005 Lausanne | Switzerland

Visit us: www.frontiersin.org
Contact us: frontiersin.org/about/contact

REPRODUCIBILITY OF RESEARCH
Support open data and methods to enhance research reproducibility

DIGITAL PUBLISHING
Articles designed for optimal readership across devices

FOLLOW US
@frontiersin

IMPACT METRICS
Advanced article metrics track visibility across digital media

EXTENSIVE PROMOTION
Marketing and promotion of impactful research

LOOP RESEARCH NETWORK
Our network increases your article's readership